ABSTRACT

Title of Dissertation: LEVERAGING BIOMATERIAL PROPERTIES TO REPROGRAM IMMUNE FUNCTION IN AUTOIMMUNITY

Emily A. Gosselin, Doctor of Philosophy, 2020

Dissertation directed by: Christopher M. Jewell
Professor
Fischell Department of Bioengineering

Autoimmune diseases occur when immune cells incorrectly identify and attack the body's tissues as foreign. In Multiple Sclerosis (MS), the immune system targets myelin, the protective layer that insulates nerves. Current MS therapies reduce disease severity without treating the cause, requiring frequent treatments to slow disease progression. Further, existing therapies cannot differentiate between dysfunctional myelin-reactive inflammatory cells and normal lymphocytes, leaving patients

vulnerable to infection. To overcome these limitations, this dissertation investigated biodegradable polymeric microparticles (MPs) co-loaded with myelin peptides and rapamycin, an immunomodulatory signal. Directly injecting these tolerogenic MPs into key immune tissues (e.g. lymph nodes, LNs), induces myelin-specific regulatory immune cells that selectively control myelin-specific inflammation. This work aimed to advance pre-clinical studies and motivate clinical research in two ways: investigating the systemic impact of intra-LN tolerogenic MPs in two MS models, and enhancing MP stability using Chemistry, Manufacturing, and Controls (CMC) considerations.

This work showed that across both progressive and relapsing-remitting disease, one tolerogenic intra-LN treatment promoted long-lasting improvements in disease-induced paralysis. Tolerogenic MPs delivered prior to symptom onset promoted tolerance and protected against disease. Treatment at peak disease reversed paralysis and prevented relapse, while treatment during relapse limited disease progression. Strikingly, mice vaccinated against a foreign protein on the same day as intra-LN treatment generated protein-specific T cells and antibodies at similar levels to healthy vaccinated mice, while simultaneously exhibiting significantly reduced paralysis – highlighting the myelin-specific nature of this therapy.

While the low dosage requirements of these studies allowed for on-demand preparation, clinical translation requires investigation into manufacturing, preservation, storage, and stability of this immunotherapy. Thus, this dissertation also tested the impact of lyophilization (freeze-drying) and excipients (stabilizing molecules) on MP stability after storage. Lyophilization with low concentrations of excipients significantly improved MP stability and formulation recovery after reconstitution.

Storage for 5 months at room temperature did not negatively impact cargo loading, MP size, or biofunctionality. MP formulations with excipients could deactivate inflammatory signaling and restrict myelin-specific immune cell proliferation as well as formulations without excipients.

Together, these studies motivate the development of intra-LN delivery of tolerogenic MPs as a potential MS immunotherapy for clinical translation.

LEVERAGING BIOMATERIAL PROPERTIES TO REPROGRAM IMMUNE FUNCTION IN AUTOIMMUNITY

by

Emily A. Gosselin

Dissertation submitted to the Faculty of the Graduate School of the
University of Maryland, College Park, in partial fulfillment
of the requirements for the degree of
Doctor of Philosophy
2020

Advisory Committee:
Professor Christopher M. Jewell, Chair
Professor Jonathan S. Bromberg
Professor Kimberly M. Stroka
Professor Xiaoming "Shawn" He
Professor Roy A. Mariuzza, Dean's Representative

© Copyright by

Emily Anne Gosselin

2020

Acknowledgements

To Chris, thanks for taking a chance on someone who knew absolutely nothing about the immune system when she joined your lab. You've provided me with countless opportunities to grow as a scientist, and I am truly thankful for all the guidance you've provided over the years. To the past and current members of the Jewell lab – thank you so much for all of your advice, your assistance, and your comradery; it's been a privilege to work with you all, and I wish you the best for your futures. To Michelle, Sarah, Mary, Ryan, Helen, Andrew, and Haleigh, thank you for being such a solid support network throughout the highs and lows of graduate school. I couldn't have done this without you. To my parents, Yves and Valerie, and my siblings, Nathan and Livia, thank you for raising a curious and stubborn girl, and for teaching her that the sky is the limit. To Michael, thank you for always believing in me, even when I don't believe in myself. I love you.

Table of Contents

Acknowledgements ii
Table of Contents iii
List of Tables viii
List of Figures ix
List of Abbreviations xiii
Chapter 1: Introduction 1
1.1 Background 1
1.2 Significance 2
1.3 Thesis Goals and Organization 3
Chapter 2: Designing Natural and Synthetic Immune Tissues 6
2.1 Introduction 6
2.2 Engineered immune tissues as tools, vaccines, and immunotherapies 6
2.2.1 Engineered immune tissues as tools 7
2.2.2 Engineered immune tissues as therapeutics 8
2.3 Distinct organs control immune cell development 11
2.4 Immune organoids and organs-on-a-chip 14
2.4.1 Recapitulating organ-level immune function with organoids 15
2.4.2 On-a-chip tools to study immune cell interactions 19
2.5 Reprogramming existing immune tissues in animals 20
2.5.1 Scaffolds to recruit immune cells and direct SLO function 20
2.5.2 Diffusion-limited depots to reprogram the LN environment 24
2.5.3 Using artificial APCs to control T cell expansion in vivo 27
2.6 Designing immune tissues for implantation 28
2.6.1 Mimicking adaptive functions with engineered SLOs 28
2.6.2 Engineered thymus to enable organ transplantation 33
2.6.3 Engineered BM to support hematopoiesis and immunity 34
2.7 New immunological insight informs immune engineering 37
2.7.1 Dynamic stromal cues in SLOs influence cell differentiation 38
2.7.2 Matrix mechanical properties direct immune cell function 38
2.7.3 Peripheral tissues alter immune cell homing and function 39
2.7.4 Vaccine and immunotherapy design informs tissue engineering 41
2.8 Outlook 43

Chapter 3: Using Biomaterials to Promote Immune Tolerance in Autoimmunity 44
3.1 The adaptive immune system allows for potent, antigen-specific responses ... 44
3.1.1 Interactions between DCs and naïve T cells influence T cell differentiation 45
3.1.2 Central and peripheral tolerance fail in cases of autoimmunity 48
3.2 MS is a debilitating disease that impacts more than 2.3 million people worldwide 49
3.2.1 MS symptom severity is influenced by stage of disease..... 50
3.2.2 MS is caused by myelin-specific auto-reactive immune cells 52
3.3 Myelin-specific tolerance would enhance efficacy and selectivity of MS therapies 54
3.3.1 MS therapies aim to slow disease progression, not cure disease..... 54
3.3.2 Generating myelin-specific regulatory T cells could enhance selectivity of MS therapies 56
3.4 Using biomaterials to enhance specificity of immunotherapies 57
3.4.1 Promoting tolerance by targeting APCs 59
3.4.2 Engineering immune tolerance with self-antigens and regulatory molecules 61
3.5 Intra-lymph node delivery of tolerogenic cargo from polymer particles offers a new therapeutic strategy for autoimmune disease 62
Chapter 4: Controlled Release of Second Generation mTOR Inhibitors to Restrain Inflammation in Primary Immune Cells 67
4.1 Introduction..... 67
4.2 Background..... 68
4.3 Materials and Methods..... 72
4.3.1 MP Synthesis 72
4.3.2 MP Characterization. 72
4.3.3 DC Activation 73
4.3.4 Transgenic T Cell Proliferation 74
4.3.5 Cytokine Secretion..... 75
4.3.6 T Cell Phenotypes 75
4.3.7 Statistics 76
4.4 Results..... 76
4.4.1 MPs Allow Tunable Loading and Controlled Release of Rapalogs 76
4.4.2 Drug-Loaded MPs Reduce Expression of Key Markers of DC Activation78

4.4.3 Rapalog MPs Restrain CD4+ T Cell Proliferation in a Transgenic Co-Culture Model 81
4.4.4 Drug-Loaded MPs Reduce Inflammatory Cytokine Secretion in a Transgenic Co-Culture Model 83
4.4.5 Drug-Loaded MPs Reduce Inflammatory T_H1 Phenotypes in a Transgenic Co-Culture Model 85
4.5 Discussion 86
4.6 Conclusion 90
Chapter 5: Intra-Lymph Node Delivery of Tolerogenic Microparticles Promotes Immune Tolerance, Reverses Paralysis, and Prevents Relapse in a Model of Multiple Sclerosis 91
5.1 Introduction 91
5.2 Background 92
5.3 Materials and Methods 94
5.3.1 Materials and Reagents 94
5.3.2 MP Synthesis 95
5.3.3 MP Characterization 95
5.3.4 Mouse MS Model Induction and Monitoring 96
5.3.5 Intra-Lymph Node Tolerogenic MP Injections 97
5.3.6 Ovalbumin Vaccination Studies 97
5.3.7 Tissue Processing and Immune Cell Collection 98
5.3.8 Flow Cytometry Studies 98
5.3.9 Ex Vivo Restimulation Assays 99
5.4 Results 100
5.4.1 $PLP_{139-151}$/Rapa tolerogenic MPs can reverse disease and prevent paralysis in RR-EAE 100
5.4.2 MPs can be loaded with peptides and rapa at similar levels and remain similar in size 104
5.4.3 Tolerogenic MPs prevent disease when administered prior to disease onset 106
5.4.4 Tolerogenic MP treatment at peak diseases reverses paralysis and prevents relapse in mice with RR-EAE 112
5.4.5 Tolerogenic MP treatment reduces immune cell infiltration into CNS. .. 116
5.4.6 Tolerogenic MP treatment does not impair healthy immunity 119
5.5 Discussion 128
5.6 Conclusion 132

Chapter 6: Enhancing the Stability of Polymer Microparticles for Autoimmune Therapy 133
6.1 Introduction 133
6.2 Background 134
6.3 Materials and Methods 137
6.3.1 Materials 137
6.3.2 Preparation of Microparticles 138
6.3.2.1 Synthesis of MPs 138
6.3.2.2 Lyophilization of MPs 139
6.3.3 Characterization of Microparticles 139
6.3.3.1 Stability and Reconstitution Studies 139
6.3.3.2 MPs Loading Analysis 140
6.3.3.3 MPs Size and Polydispersity Index 140
6.3.4 In vitro Cargo Functionality Cellular Assays 141
6.3.4.1 Cell Culture 141
6.3.4.2 Flow Cytometry Studies 142
6.3.4.3 In Vitro DC Activation Studies 142
6.3.4.4 In Vitro T Cell Proliferation Studies 143
6.3.4.5 Cytokine Secretion 144
6.4 Results 144
6.4.1 Characterization of Microparticles 144
6.4.1.1 Incorporating Excipients Prior to Lyophilization Allows for Better Lyo Cake Formation and Resuspension 144
6.4.1.2 MPs Loading Efficiency is Influenced by Excipient Encapsulation Levels 149
6.4.1.3 Encapsulating Excipients Increases MPs Size 151
6.4.2 In Vitro Cargo Functionality Cellular Assays 155
6.4.2.1 Rapa-loaded MPs with or without Excipients Reduce Activation Marker Expression on Dendritic Cells 155
6.4.2.2 MPs Containing MOG with or without Excipients Expand MOG-specific T Cells 160
6.4.2.3 MPs Containing MOG/Rapa with or without Excipients can reduce IL-6, IL-17, and IFN- γ inflammatory cytokine secretion 165
6.5 Discussion 168
6.6 Conclusion 174
Chapter 7: Outlook and Future Work 175

7.1 Outlook 175
7.2 Ongoing and Future Studies – Immunohistochemistry in the Central Nervous System 178
7.3 Ongoing and Future Studies – Magnetic Resonance Imaging in the CNS 180
7.4 Ongoing and Future Studies – Evaluating the Safety and Toxicity of Tolerogenic iLN Therapy in Non-Human Primates. 182
Chapter 8: Contributions 184
8.1 Research Publication Contributions 184
8.2 Research Collaborations 186
8.3 Research Conference Presentations 187
8.4 Research Funding Support and Awards 187
8.5 Service and Mentoring 188
Appendix: List of Publications and Intellectual Property 190
Published First Author: 190
Published Contributing Author: 190
In Progress: 190
Intellectual Property Filing: 190
References 191

List of Tables

Table 2.1. Advances in Engineering Immune Tissues 9

Table 4.1 Rapalog-Loaded Microparticle Characterization 77

Table 5.1 Tolerogenic Microparticle Characterization 105

Table 6.1 MOG/Rapa MPs Formulation Information and Abbreviations 146

Table 6.2 MPs Reconstitution Assay 148

Table 6.3 MPs Rapa and MOG_{35-55} Loading 151

Table 6.4 MPs Sizing and Polydispersity Index Pre-Lyo, Post-Lyo, and 5 months Post-Lyo 155

List of Figures

Figure 2.1. Immune tissues play distinct roles in immune cell development. 13

Figure 2.2 Immune organoids allow for the development of germinal-center-like B cells that undergo complex immunological processes..... 16

Figure 2.3 Engineered bone marrow on-a-chip replicates function of bone marrow in vivo 18

Figure 2.4 Engineered scaffolds recruit APCs to access tumor antigen and improve function after migration to LNs 22

Figure 2.5 Local changes in lymph node structure from direct injection of tolerogenic microparticles into the lymph nodes of mice with autoimmune disease drives systemic changes in immune signaling..... 25

Figure 2.6 Engineering secondary lymphoid tissues can restore immune functions in vivo 30

Figure 2.7 Engineering T cell activating reservoirs to promote anti-tumor efficacy.. 31

Figure 2.8 Engineering primary lymphoid tissues to reprogram immune functions in vivo 36

Figure 2.9 New immunological insight informs immune tissue engineering design . 42

Figure 3.1 DC: T cell interactions influence T cell phenotypic fate..... 46

Figure 3.2 MS symptom severity changes throughout disease course. 52

Figure 3.3 Myelin-reactive immune cells initiate inflammation in MS..... 54

Figure 3.4 MS therapies have become increasingly selective with new insight into disease. 55

Figure 3.5 Biomaterials can be used to precisely deliver immunomodulatory cargo. 57

Figure 3.6 Harnessing the potential of biomaterials in targeting APCs to promote immune tolerance. 59

Figure 3.7 MPs can be injected iLN non surgically due to LN visualization following tracer dye injection. 63

Figure 3.8 iLN treatment with MOG/Rapa depots prevents disease onset in a model of progressive MS. 64

Figure 4.1 Structures of rapamycin and the rapalogs everolimus and temsirolimus .. 77

Figure 4.2 Rapalog MPs have similar characteristics when compared to Rapa MPs. 78

Figure 4.3 Rapalog MP treatment reduces DC activation in a primary immune cell culture after stimulation 80

Figure 4.4 Rapalog MPs exhibit lower toxicity compared to free rapalog treatment. 81

Figure 4.5 Rapalog MPs restrain T cell proliferation in a primary immune cell co-culture after stimulation with antigen and adjuvant. 82

Figure 4.6 Rapalog MPs exhibit enhanced anti-inflammatory properties compared to free rapalog treatment 83

Figure 4.7 Rapalog MP treatment decreases inflammatory cytokine secretion in co-culture after stimulation 84

Figure 4.8 Rapalog MPs limit inflammatory T cell phenotypes in co-culture after stimulation 86

Figure 5.1 Tolerogenic MP Synthesis and Lymph Node Injection 101

Figure 5.2 Treatment with tolerogenic MPs reverses disease and prevents relapse in a model relapsing-remitting MS. 103

Figure 5.3 Tolerogenic MPs prevent disease onset when administered prior to disease onset. 107

Figure 5.4 D7 treatment with tolerogenic MPs iLN delays disease onset and reduces severity. 109

Figure 5.5 Tolerogenic iLN treatment 28 days before induction protects against disease onset 111

Figure 5.6 iLN treatment with PLP_{139}/Rapa MPs reverses disease and prevents relapse. 114

Figure 5.7 Treatment with PLP_{139}/Rapa MPs prevents disease worsening. 116

Figure 5.8 Tolerogenic MP iLN therapy does not impact cell counts in inguinal LN or spinal cord. 117

Figure 5.9 Tolerogenic iLN treatment with PLP_{139}/Rapa MP 28 days before induction causes reduced immune cell infiltration in CNS even 54 days after induction. 118

Figure 5.10 Mice treated iLN with tolerogenic MPs mount antibody responses to foreign protein at similar levels to healthy mice. 120

Figure 5.11 Mice given tolerogenic iLN treatment and vaccinated against OVA on the same day mount similar immune responses to healthy vaccinated mice. 123

Figure 5.12 Vaccination does not interfere with tolerogenic iLN treatment efficacy. 125

Figure 5.13 Treatment with tolerogenic MPs reduces inflammatory cytokine response to myelin, regardless of vaccination against OVA. 127

Figure 6.1 MPs synthesis and lyophilization process 145

Figure 6.2 MPs lyophilized with excipients form better lyo cakes and are more easily reconstituted. 147

Figure 6.3 MPs lyophilized with excipients are more completely reconstituted. 148

Figure 6.4 Loading efficiency of aqueous cargo decreases with increasing concentration of encapsulated excipients..... 150

Figure 6.5 Encapsulated excipients increase MP size, and lyophilization does not change MP size. 152

Figure 6.6 Encapsulated excipients increase MP size, and adding excipients protects against aggregation. 153

Figure 6.7 Adding excipients protects against aggregation following long-term storage. 154

Figure 6.8 Rapa MPs with or without excipients reduce dendritic cell activation after stimulation..... 157

Figure 6.9 Rapa MPs with or without excipients reduce dendritic cell activation after stimulation..... 159

Figure 6.10 MPs containing MOG and lyophilized with or without excipients expand MOG-specific T cells..... 162

Figure 6.11 MPs containing MOG and lyophilized with or without excipients expand MOG-specific T cells..... 164

Figure 6.12 Rapa-loaded MPs with or without excipients restrain inflammatory activity of cells in vitro. 168

Figure 7.1 Tolerogenic iLN therapy reduces the number of T cells present in the spinal cord in mouse models of MS..... 179

Figure 7.2 Immunostaining of healthy mouse spinal cord..... 180

Figure 7.3 MRI imaging in a patient with Relapsing-Remitting MS. 181

Figure 7.4 Relative Weights of Non-Human Primates Following iLN therapy. 182

List of Abbreviations

Acute Myeloid Leukemia	AML
Analysis of Variance	ANOVA
Antigen	Ag
Antigen Presenting Cell	APC
Artificial Antigen Presenting Cell	aAPC
Bone Marrow	BM
Central Nervous System	CNS
Chemistry, Manufacturing, and Controls	CMC
Chimeric Antigen Receptor	CAR
Clinically Isolated Syndrome	CIS
Complete Freund's Adjuvant	CFA
Dendritic Cell	DC
Disease Modifying Therapy	DMT
Empty MPs	X MPs
Encapsulated	Enc
Enzyme-linked Immunsorbent Assay	ELISA
Everolimus	Evero
Experimental Autoimmune Encephalomyelitis	EAE
Externally Incorporated	Ext
Extracellular Matrix	ECM
Germinal Center	GC
Hematopoietic Stem Cell	HSC

Intra-lymph node	iLN
Lipopolysaccharide	LPS
Lymph Node	LN
Magnetic Resonance Imaging	MRI
Major Histocompatibility Complex	MHC
Mannitol	Man
Mean (or Median) Fluorescence Intensity	MFI
Micro Bicinchoninic Acid Protein Assay	mBCA
Microparticle	MP
MOG MPs	M MPs
MOG/Rapa MPs	MR MPs
Multiple Sclerosis	MS
Myelin Basic Protein	MBP
Myelin Oligodendrocyte Glycoprotein	MOG
Non-human Primate	NHP
Myelin Proteolipid Protein	PLP
Molecular Target of Rapamycin	mTOR
Ovalbumin	OVA
Pathogen Asscociated Molecular Pattern	PAMP
Phosphate Buffered Saline	PBS
Polydispersity Index	PDI
Poly(lactic-co-glycolic acid)	PLGA
Poly(lactide-co-glycolide)	PLG

Polyvinyl Alcohol	PVA
Primary Lymphoid Organ	PLO
Primary Progressive MS	PPMS
Rapa MPs	R MPs
Rapamycin	Rapa
Regulatory T Cell	T_{REG}
Relapsing-Remitting MS	RR-MS
Secondary Lymphoid Organ	SLO
Secondary Progressive MS	SPMS
Standard Deviation	SD
Standard Error of the Mean	SEM
Sucrose	Suc
T Cell Receptor	TCR
Temsirolimus	Tems
Thymic Epithelial Cell	TEC
Trehalose	Tre

Chapter 1: Introduction

1.1 Background

Autoimmune diseases occur when the body's immune system incorrectly identifies and attacks "self" molecules as foreign. In Multiple Sclerosis (MS), the immune system incorrectly recognizes myelin, the matrix that insulates neurons in the central nervous system (CNS). Current treatments for MS aim to reduce the severity of disease, but do not treat the cause, and require continual, frequent treatments over the lifetime of the patient to maintain disease remission, though the disease ultimately will progress. Unfortunately, these existing therapy options are also non-specific – they cannot differentiate between myelin-specific inflammatory immune cells and other lymphocytes, leaving patients susceptible to opportunistic infections.

Myelin-specific inflammatory cells are activated in lymph nodes (LNs), tissues which coordinate immune cell interactions that control immune cell phenotypes. In the LNs, antigen presenting cells, including dendritic cells (DCs), present antigens – such as myelin in MS – to T and B cells. Depending on the signals present during this interaction, T cells can become either inflammatory effector cells or regulatory cells (T_{REGS}) that control the activity of inflammatory cells. During MS, these myelin-specific effector cells contribute to inflammation and neurodegeneration in the CNS.

World-wide, nearly 2.3 million people have MS. There are two main forms of MS in patients – relapsing-remitting MS and progressive MS. 85% of patients initially present with relapsing-remitting MS, in which patients experience waves of paralysis as they develop reactivity to different sections of myelin over time. This epitope

spreading complicates treatment regimens, as therapies do not consistently work at all stages of disease. Nearly 80% of relapsing-remitting MS patients eventually stop experiencing periods of remission, developing secondary progressive MS in which their symptoms continuously worsen over time. There are very few treatment options available to patients once they reach this progressive phase of MS.

1.2 Significance

To overcome the limitations of current treatments, my doctoral work has focused on developing therapies that promote selective immune tolerance to myelin by inducing myelin-specific T_{REGS} that can selectively control disease. Promoting myelin-specific tolerance would knock down inflammation to myelin without impairing the activity of healthy, normal lymphocytes. In order to enable this therapeutic potential, it is essential to control immune signals present in the lymph nodes during T cell development to ensure T cells develop regulatory functions. By delivering the relevant immune cargo – myelin peptides and regulatory immune signals – to LNs using a direct LN injection, we can ensure polarization to T_{REGS}. However, soluble immune signals rapidly drain from LNs, making this control short-lived.

To prolong the exposure of immune cells in LN to myelin peptides and regulatory immune cues, this project uses biomaterial-based delivery system to enhance signal retention in LN. Biomaterials can be used to ensure co-delivery of cargo, targeted delivery of cargo, cargo protection, and control over rate of cargo release. By loading relevant immune cargo – myelin peptides and regulatory immune signals – into biodegradable polymeric microparticles (MPs) that can be directly

injected into LN, we can ensure that both immune cues remain in LN over longer periods of time. These MPs are designed to increase signal presence in multiple ways: they degrade and release their cargo slowly into the surrounding environment; they are too large to drain from LN, ensuring their cargo is released primarily into the LN environment; and they protect their cargo reservoir from being degraded rapidly by enzymes and cells present in the body. This increased signal presence then in turn allows for prolonged exposure of key immune cells (e.g. DCs and T cells) to this immune cargo; this localization is important in increasing myelin-specific regulatory T cell differentiation in the LN.

1.3 Thesis Goals and Organization

The work in this dissertation used a mix of techniques at the intersection of immunology and biomaterials to work toward the goal of designing myelin-specific MS therapies to improve the lives of patients. To meet this goal, a direct LN injection technique was used to deposit polymer particles co-loaded with myelin self-antigens and rapamycin, an immunomodulator, in LNs of mice induced with a relapsing-remitting model of MS. This work required expertise in immunology, biomaterials, drug delivery, formulation development and characterization, particle stability, and animal models to begin pushing this intra-lymph node (iLN) delivery technology toward clinical translation.

This dissertation work showed that a direct LN injection of microparticles could be used to target immune cell populations of interest in LNs in models of MS. Delivering polymer particles co-loaded with myelin peptides and rapamycin, an

immunomodulatory signal, alters how the disease course progresses in mouse models of MS and allows for the development of regulatory T cells. In particular, we studied disease progression in a model of the most common form of MS, relapsing-remitting MS. This work investigated how treatments at different stages of disease with different myelin epitopes promotes recovery and prevents relapse. To understand the progression of disease and the barriers faced in designing and translating selective therapies, my doctoral work had three main goals:

1. Investigate the role of intra-lymph node treatment timing and epitope composition on the induction of tolerance and disease progression in a relapsing-remitting model of MS
2. Evaluate the impact of intra-lymph node treatment on disease-specific tissues and healthy immunity
3. Identify and investigate sources of risk in clinical translation of intra-lymph node treatment as a myelin-specific MS therapy, including manufacturing, stability, and safety of tolerogenic MP intra-LN treatment

The work completed for these aims supports the overall goal of collecting information and generating insight into the potential of myelin-specific immune therapies for the treatment of MS. This dissertation begins with an overview of the immune tissues and their roles in generating antigen-specific immune responses. In addition, **Chapter 2** discusses the state of the immune engineering field, with specific examples of engineering strategies that highlight biomaterials and techniques that can be used to study and control immune function. **Chapter 3** highlights specific

considerations for the development of therapies aimed for MS. In particular, this chapter discusses current clinical strategies for MS patients, and how specific features of biomaterials can be tuned and leveraged to overcome these limitations in current strategies. **Chapter 4** leverages primary cell co-cultures to lay the groundwork for translational studies in later chapters. In particular, this chapter introduces rapamycin, the immunomodulator used in this work to reprogram immune function in cases of autoimmunity. In addition, this chapter explains many of the biomaterial synthesis techniques and characterization methods used to evaluate microparticle-mediated immune cargo delivery that will be used throughout this work.

Building on the information presented in earlier chapters, **Chapters 5 and 6** focus on advancing pre-clinical knowledge of tolerogenic intra-LN therapy. In **Chapter 5**, we address Aims 1 and 2. In this chapter, intra-LN delivery of degradable microparticles loaded with myelin peptides and rapamycin is used to reverse paralysis and prevent relapse in a relapsing-remitting model of MS. This chapter evaluates the impact of intra-LN treatment on distant sites of disease (the central nervous system), as well as the ability of intra-LN to promote tolerance without hindering healthy immunity. In **Chapter 6**, we evaluate the stability of the microparticles used for intra-lymph node delivery, in an effort to enhance shelf-life and enable clinical translation of this technology. **Chapter 7** details ongoing and future work that supports these aims, including studies to further investigate CNS inflammation following iLN therapy, and safety studies in non-human primates. **Chapter 8** summaries my contributions to the field, and the **Appendix** contains my publications and intellectual property filing. **References** for this thesis are included at the end of this dissertation.

Chapter 2: Designing Natural and Synthetic Immune Tissues[1]

2.1 Introduction

Vaccines and immunotherapies have provided enormous improvements for public health, but there are fundamental disconnects between where most studies are performed—in cell culture and animal models—and the ultimate application in humans. Engineering immune tissues and organs, such as bone marrow, thymus, lymph nodes and spleen, could be instrumental in over-coming these hurdles. Fundamentally, designed immune tissues could serve as in vitro tools to more accurately study human immune function and disease, while immune tissues engineered for implantation as next-generation vaccines or immunotherapies could enable direct, on-demand control over the generation and regulation of immune function. In this Chapter, we discuss recent interdisciplinary strategies that are merging materials science and immunology to create engineered immune tissues in vitro and in vivo. We also highlight the hurdles facing these approaches and the need for comparison to existing clinical options, relevant animal models, and other emerging technologies.

2.2 Engineered immune tissues as tools, vaccines, and immunotherapies

Vaccines have transformed human health by providing specific, long-lasting protection, even enabling widespread eradication of diseases such as smallpox and polio. Recently, immunotherapies have also led to remarkable successes. In cancer, for example, antibody-based checkpoint inhibitors re-engage the immune system,

[1] Adapted with permission from: **E.A. Gosselin**, H.B. Eppler, J.S. Bromberg, and C.M. Jewell, "Designing natural and synthetic immune tissues." *Nature Materials* 2018, 17: 484-498. (cover article)

dramatically improving outcomes for some patients with cancers of the skin, blood, lung, kidney and others[1, 2]. In autoimmune disease – where the immune system mistakenly attacks host tissue – antibodies that reduce inflammatory cues improve the selectivity and effectiveness of treatments for diseases such as multiple sclerosis (MS) and rheumatoid arthritis. Despite these advances, clinical translation still relies on costly, inefficient trial-and-error methodologies. Furthermore, existing animal models are often not predictive of human disease, leading to failure of late stage trials. In infectious disease, Novavax's vaccine for RSV – a respiratory virus impacting children and elderly – lacked efficacy during a phase III trial (NCT02608502). In cancer, Juno's engineered T cell therapy for leukemia was paused twice following patient deaths in phase II trials[3]. Meanwhile, in autoimmunity, Biogen's MS therapy, Opicinumab, missed efficacy endpoints in phase II[4], while Circassia's cat allergy therapy failed in phase III (NCT01620762). Some of these trials failed because of efficacy, while others encountered safety issues that trials with smaller patient cohorts missed. Both shortcomings emphasize that the way vaccines and immunotherapies are developed – first in cells and animals, then in humans – does not provide a complete picture of how these technologies will perform in humans. Engineered immune tissues could help fill in these gaps by serving both as tools to study and diagnose immune disease, and as next-generation vaccines and immunotherapies with new capabilities.

2.2.1 Engineered immune tissues as tools

In this Chapter, we first highlight the major immune tissues, then discuss efforts to build immune organoids or organs-on-a-chip as tools, to reprogram the function of existing immune tissues, and to design immune tissues for implantation as vaccines and

immunotherapies. As tools, these technologies are significant in several ways. First, engineered immune tissues integrating human cells in culture could provide a more accurate research niche compared with 2D human cultures or pre-clinical mouse models that poorly recapitulate human immunity. Second, engineered immune scaffolds could support proliferation and analysis of rare immune populations isolated from patients. Watching these cells develop in a controlled human niche ex vivo might reveal new insights into pathologies that are difficult to study in patients, or enable renewable sources for blood cell production. Last, engineered immune tissues allow control over stromal components and extracellular cues—such as antigens, cytokines and mechanical properties. This control could help isolate links to differentiation and function of specific immune cell subsets.

2.2.2 Engineered immune tissues as therapeutics

Beyond use as tools, engineered immune tissues could serve as next-generation clinical options. A major challenge in the vaccine and immunotherapy field is targeting lymph nodes and the spleen—organs that coordinate and expand immune cells. This challenge could be bypassed by engineering implantable lymph nodes pre-primed against a particular pathogen or seeded with specific immune cell subsets. These designer tissues could be valuable in many translational contexts: generating durable responses against infectious disease, eliminating the requirement of ex vivo expansion before reinfusion of immune cells during adoptive cell cancer therapy, or programming immune cells to develop regulatory functions that control inflammation or autoimmunity. Engineered generative immune tissues or primary lymphoid organs—such as bone marrow (BM) or thymus—could create accurate humanized animal

models. Such hosts could make clinical trials safer and improve understanding of cell behavior in patient samples that are currently only detectable in vivo. For example, 3D structure and defined stromal cues have recently allowed engraftment of tumors from cancer patients in humanized mice that do not engraft using simple cell infusions[5]. As summarized in **Table 2.1**, below we discuss exciting possibilities to leverage engineered immune tissues, highlight key hurdles that remain to be addressed. and provide comparisons to existing clinical options and emerging technologies.

Table 2.1. Advances in Engineering Immune Tissues

Approach	Goal	Tissue	Key Findings or Advance	Ref
Immune organs-on-a-chip	Mimic immune organ function on-a-chip	Lymph node	Germinal center organoids support B cell expansion and antibody class switching	6, 7
		Thymus	Thymic microenvironments on-a-chip depend on biochemical and mechanical cues from matrix and other cells	8-10
		Bone marrow	Engineered bone marrow niches can be designed to ensure cellular diversity	11, 12
	Study immune cell interactions using organ on-a-chip as a tool	Lymph node	Immune cell directionality and velocity depend on ECM adhesion ligand presentation, matrix pore size, and immune cytokine gradients	13-16
			Microfluidic devices can be used to study individual immune cell interactions	17, 18
			LN on-a-chip tools can be used to spatially resolve cues to control or study immune cell function	19
Biomaterials to reprogram the structure and function of existing	Recruit and reprogram immune cells using implantable scaffolds	Lymph node	Implantable scaffolds with inflammatory cytokines, tumor antigens, and danger signals recruit and activate DCs to leave the scaffold to prime efficacious anti-tumor T cells in LN	20, 21
			Injectable, porous scaffolds can be used to recruit and expand DCs *in situ* and promote a	

immune tissues			regulatory environment depending on method of antigen presentation within the scaffold	[22, 23]
	Control local immune tissue function by implanting depots at the tissue site	Lymph node	Reprograming the local LN environment with diffusion-limited particle depots loaded with immune cargo causes changes in composition and function of both local and distal LNs, promoting inflammatory or regulatory systemic responses	[24-26]
	Control T cell development in vivo using artificial antigen presenting cells	Lymph node	Ellipsoidal artificial antigen presenting cells activate antigen-specific T cells more effectively, and have less non-specific uptake and clearance compared to spherical aAPCs	[27, 28]
			Artificial APCs loaded with antigen and co-stimulatory danger signals can be combined with additional molecules to enhance their ability to activate efficacious antigen-specific T cells *in vivo*	[29, 30]
Engineered immune tissues for implantation	Create adaptive immune function using implantable secondary lymphoid organs	Lymph node	Artificial lymph nodes with collagen sponge scaffolds loaded with stromal cells and activated DCs recruit T and B cells, develop LN organizational features, and restore complex immune functions	[31, 32]
			Alginate gels with stimulatory particles and tumor-specific T cells placed near solid tumors or resection sites effectively deliver tumor-specific T cells and promote inflammatory tumor-specific T cells against tumor escape variants better than cell injections	[33, 34]
	Use implantable, engineered thymus to enable transplantation	Thymus	Engineered thymic tissue containing thymic epithelial cells and hematopoietic stem cells promotes tolerance to donor tissue when thymic epithelial cells contain major histocompatibility complexes specific to donor and the recipient	[35]
	Support immune function and hematopoiesis with engineered implantable bone marrow niches	Bone marrow	Engineered humanized bone marrow niches that include human mesenchymal stem cells can replicate the structural and biochemical features of BM to preferentially recruit injected human stromal stem cells and provide models of hematopoietic diseases	[5, 36-38]

2.3 Distinct organs control immune cell development

Immune cells develop in the BM and thymus—the generative or primary lymphoid organs (PLOs), then migrate to lymph nodes (LNs) and the spleen – the secondary lymph organs (SLOs). In SLOs, immune cells are activated against specific pathogens or molecules, then migrate back to the blood and sites of infection, cancer or disease (**Figure 2.1**). These migration patterns reveal that immune cells programmed in a distinct organ – such as LNs or the spleen – can migrate throughout the host to initiate responses that are both systemic and specific.

In the BM, hematopoietic stem cells (HSCs) develop into common precursors that differentiate to the immune cells populating the body. Common myeloid precursors give rise to antigen presenting cells (APCs), including macrophages and dendritic cells (DCs), that survey blood and tissue for foreign molecules[39]. A common lymphoid precursor gives rise to T and B lymphocytes in the BM that display receptors reactive against specific peptide fragments of degraded pathogens ('antigens') (**Figure 2.1a**). T and B cells are key players in adaptive immunity owing to immunological memory that enables these cells to mount potent, highly specific and fast-acting responses against pathogens. The large majority of B cells develop and exit the BM, migrating to LNs and the spleen until activated (**Figure 2.1a**). A small population of B cells that strongly bind self-antigens—which could lead to autoimmune disease, are deleted or undergo receptor editing to reduce self-reactivity (**Figure 2.1a**)[40, 41]. T cell precursors exit the BM and migrate to the thymus for positive and negative selection. These processes ensure T cells display the molecular machinery needed to bind and process immunological signals presented by APCs, without inappropriate binding of self-

antigen that could drive autoimmune disease (**Figure 2.1b**)[42, 43]. Mature T cells then migrate to the LN and the spleen.

Generation of antigen-specific T and B cell responses requires correct presentation of an antigen matching the specificity of the receptors on the T or B cell (that is, a 'cognate' antigen). Antigen is processed and displayed by APCs in LNs and the spleen after free antigen drains from skin or peripheral tissue, or after APCs in the periphery collect antigen and migrate to LNs or the spleen (**Figure 2.1c**). Additionally, the spleen removes foreign material from blood – such as bacteria, providing systemic antigen surveillance (**Figure 2.1c**)[44]. Within the LN and the spleen, B and T cells are trafficked by a dynamic structural network of stromal cells that control local interactions through structural proteins, such as laminins and secreted chemokines. These interactions are also influenced by mechanical tissue properties and specific microanatomic domains within the SLOs that segregate immune cells and functions[45]. In SLOs, T cells are activated upon encountering DCs presenting their cognate peptide antigens in the context of the major histocompatibility complex (MHC), along with required co-stimulatory signals (**Figure 2.1d**). Following activation, the chemokine receptors on T cells change to support migration of T cells back to the periphery to fight infection in sites displaying the antigen to which they have been primed. Cytotoxic T lymphocytes directly destroy infected host cells to prevent viral replication, while helper T cells secrete supportive signals, such as cues that trigger destruction of phagocytosed bacteria (**Figure 2.1c**). B cells produce low-affinity antibodies when B cell receptors are directly crosslinked by the antigen. High-affinity antibody production requires B cells to interact with helper T cells (**Figure 2.1d**). This

step initiates a cascade by which B cells form specialized domains in LNs—germinal centers (GCs)—where they interact with follicular DCs (FDCs) and helper T cells (**Figure 2.1d**)[46, 47]. In GCs, B cells undergo class switching and affinity maturation, processes that result in differentiated B cells called plasma cells. These cells secrete high-affinity antibodies that neutralize and tag pathogens for destruction (**Figure 2.1c**). Some of the B cells developed in GCs become long-lived memory B cells that enable rapid response against future infections[46].

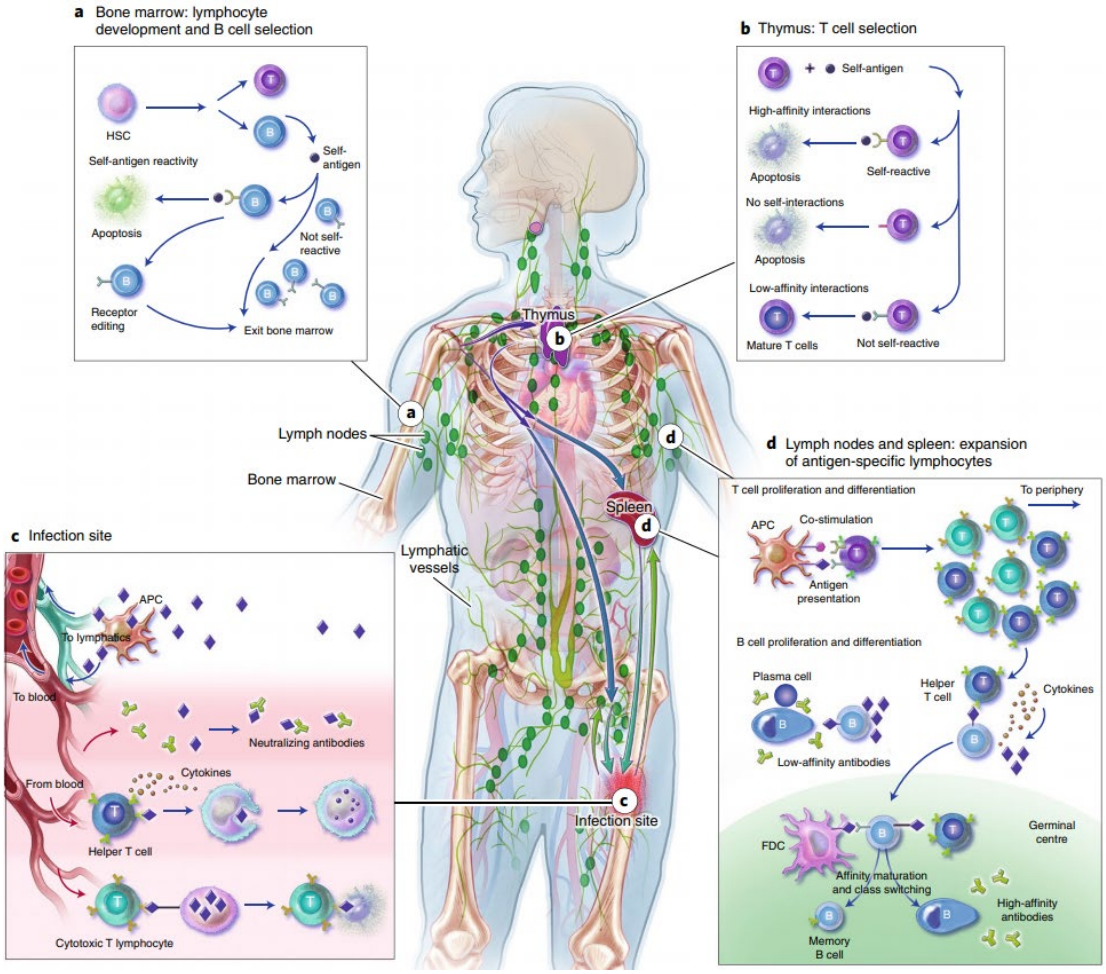

Figure 2.1. Immune tissues play distinct roles in immune cell development.
a. In bone marrow (BM), lymphocytes develop from hematopoietic stem cells (HSCs). Most B cells then travel to secondary lymphoid organs (SLOs). A small fraction of B cells that strongly bind self-antigens are deleted or undergo receptor editing. **b.** T cell precursors develop in BM and migrate to the thymus for maturation and selection. T cells that strongly bind self-antigens

or do not interact with self-molecules are deleted. Non-self-reactive precursors become mature T cells. **c.** Antigen presenting cells (APCs) search for foreign antigens in peripheral tissues. After collecting these antigens, APCs travel through lymphatics to lymph nodes (LNs). Foreign antigens in the blood move to the spleen. **d.** At the SLO, antigen-specific T and B lymphocytes become activated, then proliferate and differentiate into effector cells. APCs present antigen and co-stimulatory danger signals to naive, mature T cells, which undergo clonal expansion and differentiate into $CD4^+$ helper T cells or $CD8^+$ cytotoxic T lymphocytes. Antigen-specific B cells become activated and expand after exposure to the antigen, which the B cell presents to an activated, antigen-specific helper T cell. This T cell then secretes cytokines to activate the B cell, enabling proliferation. With T cell help, some of the proliferated cells form germinal centers, where memory B cells and high affinity antibody-secreting plasma cells arise through processes including affinity maturation and isotype switching. The effector T and B lymphocytes arising in these tissues then perform their respective protective functions at the infection site. Upon reaching this site (**c**), antibodies neutralize and tag pathogens for clearance or destruction, helper T cells stimulate phagocytosis and destruction of pathogens by macrophages and other innate immune cells, and cytotoxic T lymphocytes kill host cells presenting cognate antigen—such as those infected with viral pathogens. Credit: printed with permission from © Fairman Studios, LLC. Reproduced with permission from Springer Nature.

2.4 Immune organoids and organs-on-a-chip

2D cultures have limited ability to recapitulate the immune interactions in the body. These models over-simplify the host environment using simplified cell subsets, extracellular matrix features, fluid flows and mechanical forces. 3D microenvironments that better mimic tissue structure can be created using organoids seeded with stem cells or heterogeneous cell populations, or using microfabrication to design well-defined organs-on-a-chip[48, 49]. Both of these approaches are being extended to immune organs – LNs, thymus and BM – to create tools to elucidate immune cell interactions and the link to immune response and disease. This work has already identified matrix porosity, fluid flow, cytokine expression and stromal cell interactions as important design parameters[50-54].

2.4.1 Recapitulating organ-level immune function with organoids

Recently, Purwada et al. generated immune organoids to create GC-like structures using porous hydrogels reinforced with nanoparticles to match the stiffness of natural SLOs (**Figure 2.2a**)[6, 7]. B cells were encapsulated in these gels, along with fibroblasts transduced to express two important B cell survival and activation signals (CD40L, BAFF) (**Figure 2.2b**)[51]. This approach allowed B cells to develop phenotypic markers, such as GL7, indicative of GCs (**Figure 2.2c**). Further, the mechanical properties of the gel impacted formation of a stromal organoid network and the expression levels of the activation signals. 3D organoids – but not 2D approaches – promoted a 100-fold increase in naive B cell proliferation and differentiation to a GC phenotype (B220+ Fas+ GL7+) (**Figure 2.2d**). Antibody class switching to IgG1 and IgE isotypes also occurred in the organoids; these antibodies promoted phagocytic destruction of pathogens and provided protection in mucosal tissues, respectively (**Figure 2.2e**)[6, 7]. While class switching is one important process in GCs, these organoids have not yet integrated secretion of antigen-specific antibodies or affinity maturation; the latter generates antibodies that strongly bind their cognate antigen. As such capabilities are integrated into LN organoids, these technologies will be increasingly useful for in vitro study or diagnosis of GC pathologies—such as B cell malignancies—through seeding organoids with patient cells. Engineered SLOs might further allow for more realistic in vitro assessment of vaccine performance by determining which antigen and adjuvant combinations maximize antibody affinity. There are also opportunities to generate fundamental insight; for example, LN

organoids recently revealed the role of control pathways involved in unconstrained cell proliferation characteristic of GCs[55].

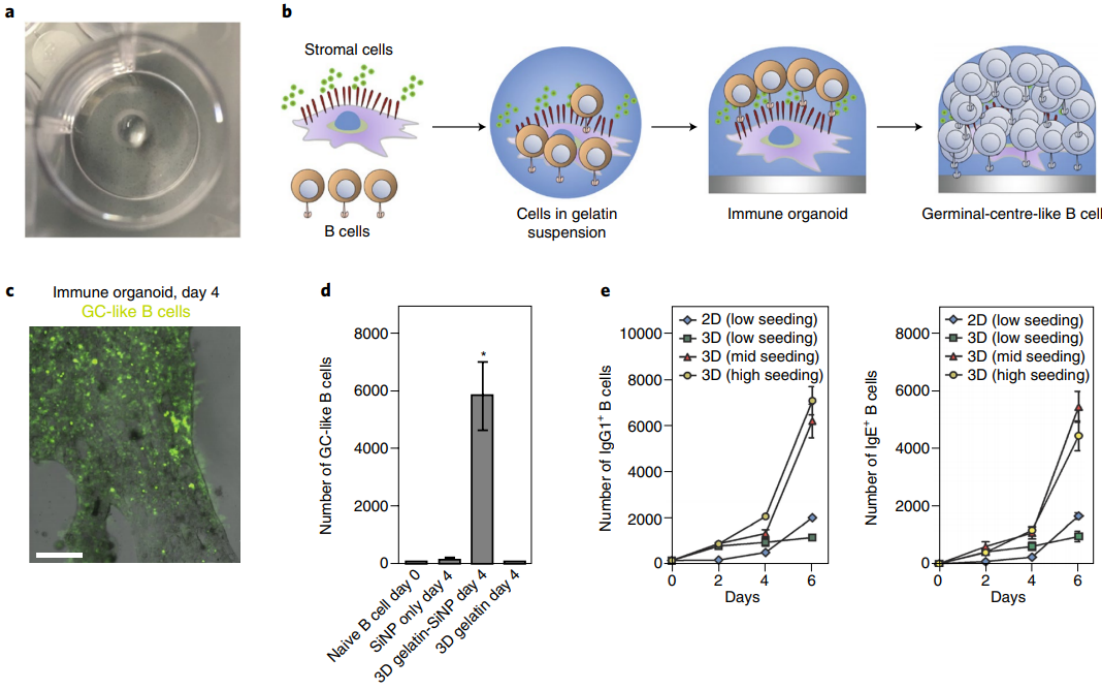

Figure 2.2 Immune organoids allow for the development of germinal-center-like B cells that undergo complex immunological processes
a. Gel-encased immune organoids in culture. **b.** Schematic of immune organoid development to create germinal center-like tissues. B cells and stromal cells are encapsulated in a gelatin suspension, and B cells interact with stromal cells causing proliferation and differentiation to a germinal center (GC) phenotype. **c.** After 4 days in culture, GC-like B cells (green) are visible in the immune organoid. **d.** Both the gelatin matrix for bioactivity and the silica nanoparticles (SiNP) for mechanical support are necessary for developing GC-like B cells. **e.** B cells cultured in 3D with mid and high seeding densities of stromal cells undergo class switching to IgG1 (left) and IgE (right) more effectively than 2D or 3D cultures at low stromal cell density. Adapted from ref. [7], Macmillan Publishers Ltd (a-c); and ref. [6], Elsevier (d,e). Figure Reproduced with permission from Springer Nature.

In addition to SLOs, thymus and BM organoids are being developed by seeding scaffolds with stem cells or other progenitors. As generative tissues, thymus and BM organoids could provide insight into immune cell development, and how these environments malfunction during diseases that cause deficient or self-reactive immune cells. Models of the thymus, where T cell selection occurs, have confirmed that 3D

structure, ligand composition, and scaffold dimensions all impact function[8-10]. Similarly, BM organoids—where many immune cells and precursors are generated—are influenced by 3D structure and mechanical properties such as scaffold stiffness and extracellular matrix (ECM) porosity[11, 12, 56]. Kotov and colleagues developed a BM model from porous 3D colloidal crystals seeded with HSCs and human BM stromal cell lines[11]. Compared with 2D cultures, 3D constructs enhanced differentiation of HSCs to B cells. These cells matured and secreted antigen-specific antibodies upon stimulation with inactivated virus. While this work did not test how strongly the antibodies bind target antigens, the studies make clear that 3D structure and a small number of defined cell populations- three in this case – can mimic some of the key processes of B cell development.

Natural BM microenvironments are enormously complex. Thus, in contrast to the approaches above using defined cell populations, other engineered BM niches are exploring scaffolds populated with heterogeneous mixtures of cell types and stromal cues. Torisawa et al. prepared a poly(dimethylsiloxane) (PDMS) device loaded with demineralized bone powder, collagen and bone-inducing factors (BMP-2, BMP-4)[12]. This device was implanted subcutaneously in mice and cultured for eight weeks to populate the BM niche before excision (**Figure 2.3a, Figure 2.3b**). After removal, the engineered BM construct was inserted in a microfluidic device (**Figure 2.3c**), allowing maintenance of B cells, T cells, and myeloid cells in proportions characteristic of natural mouse BM for at least one week (**Figure 2.3d**). This in vitro niche mimicked responses of lymphoid cells to radiation when compared to responses observed in irradiated mice (**Figure 2.3e**).

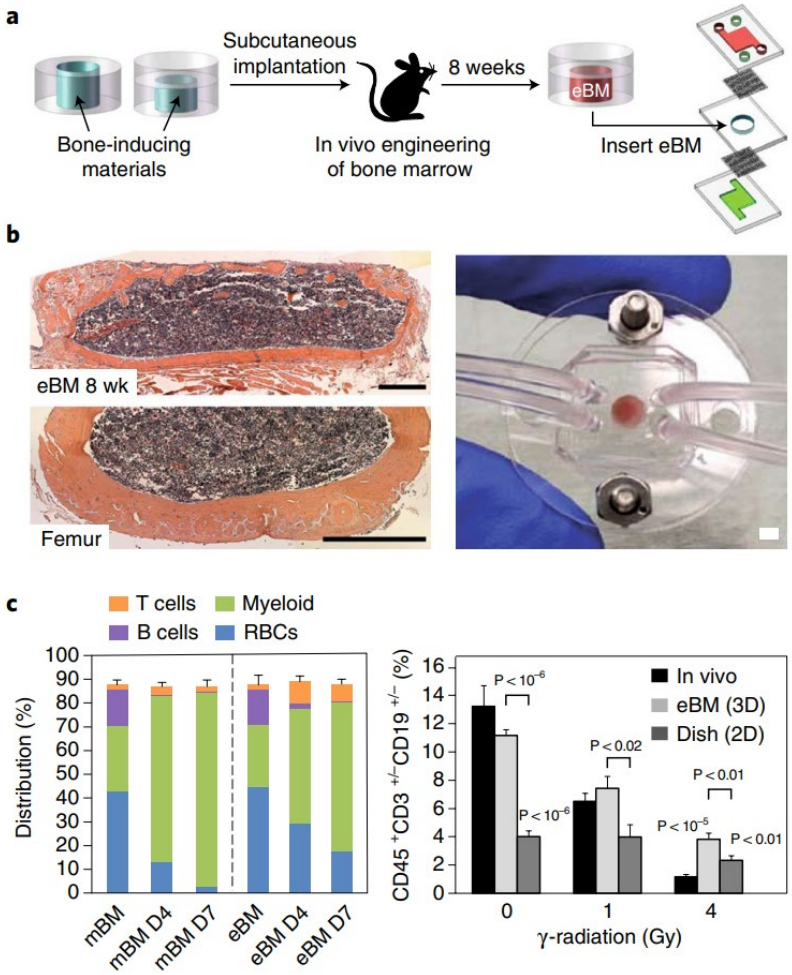

Figure 2.3 Engineered bone marrow on-a-chip replicates function of bone marrow in vivo

a. A schematic representing the process for developing the engineered bone marrow (eBM) on-a-chip. Scaffolds are loaded with bone-inducing materials and implanted subcutaneously into mice, where they are cultured in vivo for eight weeks before removal and placement into a microfluidic device. **b.** The eBM after culture in vivo has similar structure to native mouse femur. Scale bars are 500 µm. **c.** An image of the microfluidic device loaded with the eBM for study in vitro. Scale bar is 2 mm. **d.** The eBM exhibited similar blood cell distribution as the mouse femur bone marrow (mBM) at the time of excision, continuing to mimic mBM over seven days. **e.** The eBM can act as a model for radiation toxicity, typically studied in live animals, more effectively than stroma-supported culture of BM cells (Dish). Four days after exposure to radiation, a significant, dose-dependent reduction in lymphoid cells in the eBM was found, similar to the trend observed in the BM of live, irradiated mice. Adapted from ref. [12], Macmillan Publishers Ltd. Figure reproduced with permission from Springer Nature.

Functional tests—such as the radiation response just mentioned—are important in pushing engineered immune tissues forward. Most reports seek to confirm an

immune cell population of interest develops, or replicate a particular native immune process. Much less frequently are data reported that are relevant to the end-goal of diagnosis or therapy. Thus, translational applications of engineered immune tissues could directly accelerate clinical progress. For example, BM constructs could be used to screen for radiation toxicity and countermeasures in vitro as above, or to generate red blood cells for transfusions. Blood donations are limited by supply and compatibility. As one solution, synthetic blood that carries oxygen has been explored, but these carriers have limited capacity, lack cell function and could trigger host inflammatory responses[57]. Stem cells and immortalized cell lines have demonstrated promise in animals and in one human volunteer, but these cultures do not produce cells at acceptable quantities or costs[58-60]. Since 3D structure appears to improve performance of engineered BM niches, exploiting this idea might create viable options for large-scale blood production.

2.4.2 On-a-chip tools to study immune cell interactions

Beyond recreating organ- or tissue-level function in culture, new strategies are employing on-a-chip designs that harness microfabrication for precision control over the interactions of distinct immune cells or with defined extracellular signals. Considering the strong spatially governed nature of immunity (see **Figure 2.1**), immune cell migration is a key area of study for these technologies. For example, the migration of both APCs and lymphocytes are being probed through perturbations in adhesion molecule type and concentration[13], polymer scaffold composition and mechanical properties[14], and fluid flow or cytokine gradients[15, 16, 61]. Additionally, real-time quantitative analysis of APC and T cell interactions—which mimic those

occurring in SLOs—is helping to isolate the roles of T cell receptor binding affinities and valencies in controlling T cell activation[17, 18].

Hybrid devices integrating aspects from organoids and organs-on-a-chip are also being developed to study immune function. As one illustration, Ross et al. designed a strategy to place live LN slices in a perfusion chamber equipped with a microfluidic injector[19]. This approach allowed introduction of fluorescent probes and model therapeutics to distinct LN microdomains with spatial and temporal control. Such approaches could be useful in initiating, perturbing or blocking specific processes—such as GC reactions—or T cell egress from LNs during activation. However, the ability to generate functional responses to immune cues, and how well those responses mimic native LN processes have not yet been addressed.

2.5 Reprogramming existing immune tissues in animals

In this section, we highlight studies aimed at reprogramming the structure and function of existing host immune tissues. One approach exploits 3D scaffolds to recruit and prime immune cells that then migrate back to SLOs to direct the function of these tissues. Another strategy uses direct injection of micrometer-scale depots into LNs to retain modulatory immune cues in these sites and reprogram the local microenvironment. Last, we discuss efforts to expand T cells using particles that mimic the function of APC without reliance on stromal cues present in SLOs.

2.5.1 Scaffolds to recruit immune cells and direct SLO function

Traditional vaccines are designed to drain or be carried to SLOs, where APCs and lymphocytes cooperate to generate adaptive responses to antigens in the vaccines.

In contrast, biomaterial scaffolds are now being used to mimic the immunogenicity of natural infection environments by recruiting and activating APCs that subsequently return to SLOs to program the specific features of immune responses arising in these tissues[62]. One application of particular interest for these scaffolds is cancer vaccines, which contain fragments of tumors in an effort to generate potent and selective anti-tumor immune responses. Because tumors are composed of host cells, a challenge for cancer vaccination is the difficulty of generating a large number of tumor-specific T cells. These cells must also remain functional despite the local immune-suppressing tumor environment. Toward addressing these challenges, early scaffolds were implantable structures loaded with tumor lysate as an antigen, granulocyte macrophage colony-stimulating factor (GM-CSF) as a signal to recruit APCs, and CpG as a stimulatory adjuvant[20, 21]. This approach increased DC recruitment to scaffolds in mice, allowing these cells to encounter tumor lysate and become activated. The tumor antigen-presenting DCs migrated back to LNs and greatly expanded tumor-specific T cells. As a result, expanded CD4+ and CD8+ T cells infiltrated tumors at much higher levels (**Figure 2.4a**), ultimately clearing established tumors in an aggressive melanoma model.

More recently, surgical implantation has been eliminated using scaffolds that gel or self-assemble upon injection. Kim et al. used mesoporous silica rods (MSRs) to incorporate model antigens (ovalbumin; OVA), GM-CSF, and CpG (**Figure 2.4b**)[22]. The MSRs create an environment to recruit DCs by spontaneously assembling into scaffolds, enhancing both migration of tumor-primed DCs to LNs (**Figure 2.4c**) and survival in mice (**Figure 2.4d**). These effects required the scaffold component.

Additionally, MSR scaffolds generated superior antibody responses in mice compared to the vaccine adjuvant, alum[22].

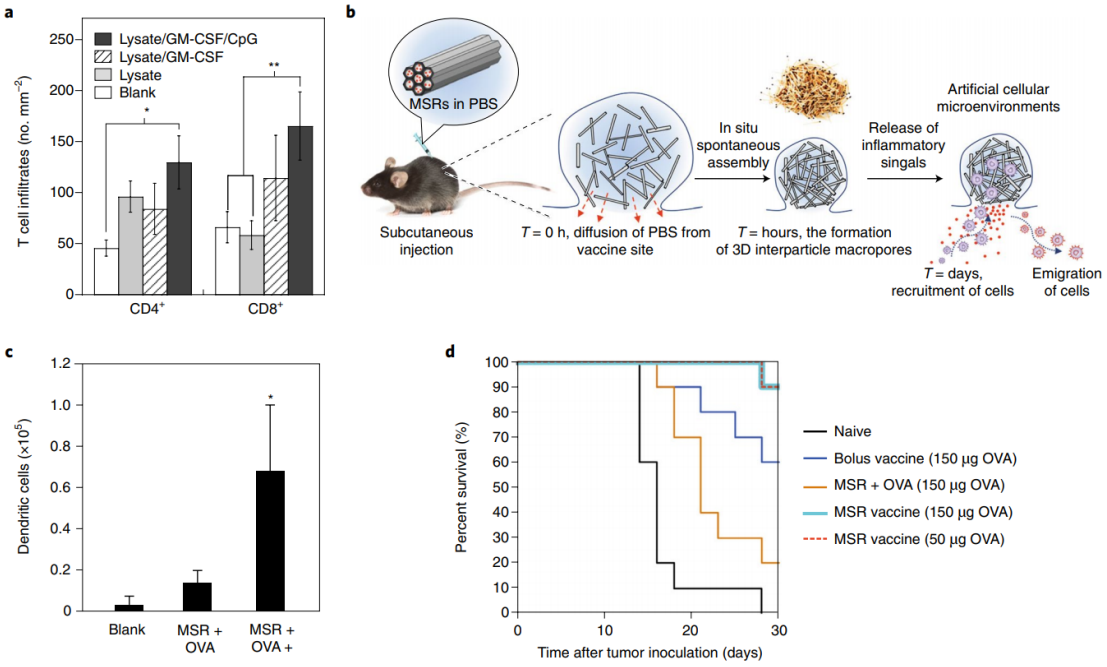

Figure 2.4 Engineered scaffolds recruit APCs to access tumor antigen and improve function after migration to LNs
a. Earlier implantable porous poly(lactide-co-glycolide) scaffolds containing tumor lysates, along with migration and inflammatory signals, recruit APCs that subsequently travel to secondary lymphoid organs. These cells expand tumor-specific CD4+ and CD8+ T cells, improving T cell infiltration into tumors. **b.** A newer injectable scaffold that self-assembles from mesoporous silica rods (MSRs) after subcutaneous injection. The scaffold releases inflammatory signals that recruit and reprogram immune cells, which then leave the scaffold environment to interact with other immune cells and promote immune response. **c.** MSR scaffolds loaded with model tumor antigen ovalbumin (OVA) and inflammatory signal granulocyte macrophage colony-stimulating factor (GM-CSF) recruit significantly more dendritic cells (DCs) than MSR scaffolds alone or MSR scaffolds loaded with OVA. **d.** The MSR scaffolds loaded with OVA, GM-CSF and an adjuvant (CpG) provide significant protection against tumors expressing OVA compared with soluble bolus vaccine with the same components, even with lower antigen dose. These results together highlight the importance of the scaffold. Adapted from ref. [20], Macmillan Publishers Ltd (a); and ref. [22], Macmillan Publishers Ltd (b – d). Figure reproduced with permission from Springer Nature.

Recruiting APCs to implanted scaffolds could be useful in several translational contexts, including infectious disease and cancer, or to promote immune tolerance by omitting stimulatory signals[23]. Controlling APC activation and antigen loading to

subsequently direct the function of T cells generated in LNs might also eliminate ex vivo manipulation during adoptive transfer cancer therapies. Adoptive therapies require isolating patient T cells, engineering the cells ex vivo, then reinfusing the cells back to the patient. Eliminating the ex vivo processing would dramatically decrease cost and complexity. However, realizing these possibilities using scaffolds will require more clinically relevant models and comparisons. Further, cancer vaccines are not administered as monotherapies but in combination with resection, checkpoint blockade or other therapies. Thus, new materials approaches should be tested against or in combination with existing clinical regimens.

Another important direction in the biomaterials field centers on non-tissue engineering strategies for vaccines and immunotherapies, such as nanoparticles that drain to SLOs to direct responses to a foreign antigen[63-67]. This goal overlaps with some of the goals of engineered immune tissues—for example, generation of a response to a foreign antigen by implanting an engineered SLO pre-primed with the antigen. Similarly, the APC-recruiting scaffolds discussed for cancer vaccines could be compared with injectable nanodiscs that have recently generated exciting results in aggressive mouse cancer models using personalized tumor antigens[68], or against new peptide–antibody conjugates exploited in models of melanoma and breast cancer[69]. Benchmarking tissue engineering approaches against nanoparticle technologies that target similar immunological goals could create frameworks for earlier assessment of parallel technologies, and identify where each approach provides distinct advantages.

2.5.2 Diffusion-limited depots to reprogram the LN environment

Another emerging strategy to control immune tissue uses degradable polymer depots injected directly to LNs to reprogram the LN microenvironment. This approach leverages microparticles too large to drain from LNs, allowing mechanical retention of depots in LNs. Local controlled release of adjuvant from these particles increases adjuvant persistence in LNs, quickly and potently expanding antigen-specific T cells in mice[24]. These responses are much higher than adjuvant-loaded nanoparticles or free adjuvant, both of which drain out of LNs more quickly. While the added complexity makes this approach less appealing for traditional prophylactic vaccination, as a tool, intra-LN depots offer opportunities to directly control the kinetics and combinations of signals in LNs to study immune cell function. For example, release of defined doses of regulatory cues in LNs during vaccination reveals the role of local concentration in polarizing antigen-specific T cells between suppressive, inflammatory and memory functions[25].

Several clinical trials have used ultrasound-guided injection of free peptides into LNs to investigate tolerance induction for allergies (NCT01982474) and type 1 diabetes (NCT01536431)[70]. Tostanoski et al. recently combined intra-LN injection with microparticle depots to combat autoimmunity by encapsulating a modulatory immune signal, rapamycin (Rapa), with a peptide self-antigen, myelin oligodendrocyte glycoprotein (MOG), that is attacked during MS[26]. A single injection of these depots into LNs of mice during a model of MS (**Figure 2.5a**) at the peak of disease permanently reversed disease-induced paralysis (**Figure 2.5b**). This reversal was MOG-specific, as OVA-loaded depots conferred no therapeutic effect (**Figure 2.5c**).

Furthermore, the composition and structure of treated LNs and distant, untreated LNs both exhibited reorganization and increased regulatory T cells (**Figure 2.5d**). In the central nervous system (CNS) – a location far from the treated node, inflammatory cell infiltration was reduced, correlating with reduced paralysis (**Figure 5e**)[26]. This work showed that reprogramming the local environment of distinct LNs can promote tolerance that is systemic and myelin-specific. Thus, understanding the parameters to induce desired structures and functions in LNs can also enable control over immune function in other tissues.

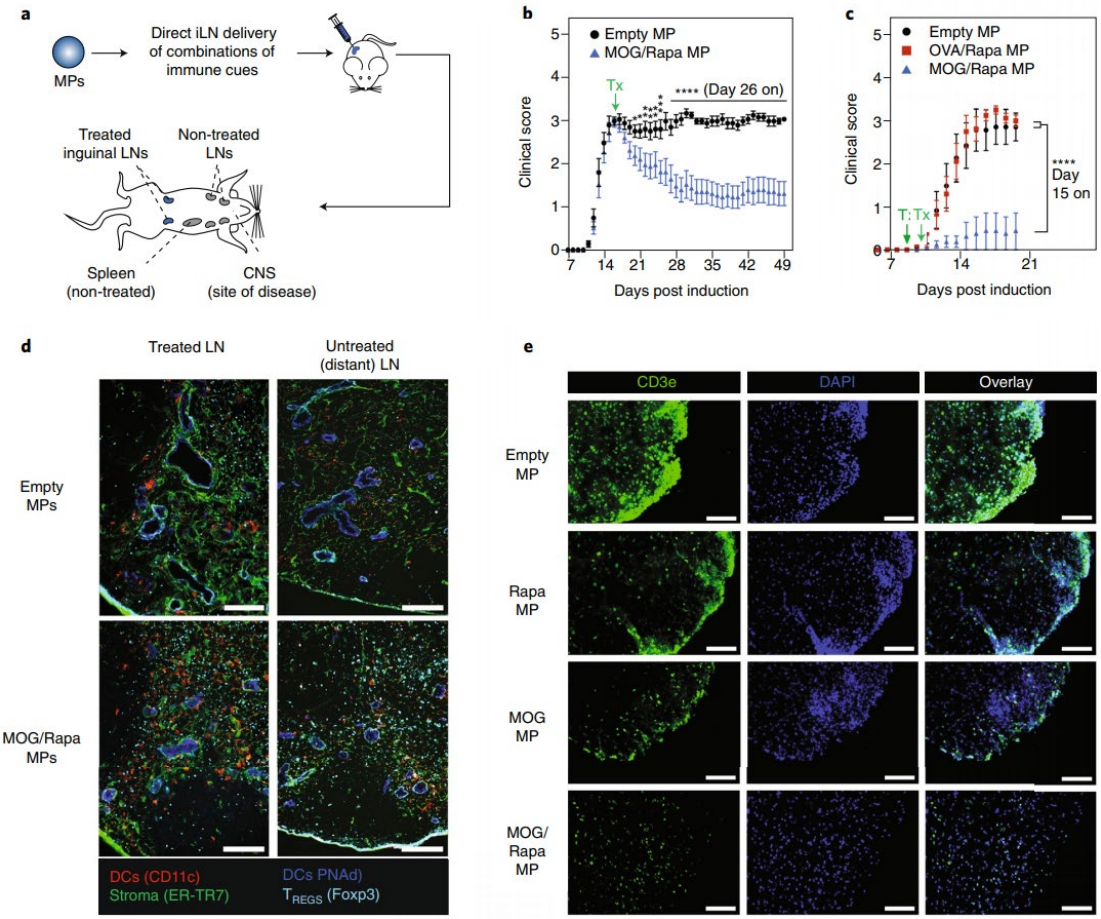

Figure 2.5 Local changes in lymph node structure from direct injection of tolerogenic microparticles into the lymph nodes of mice with autoimmune disease drives systemic changes in immune signaling

a. Schematic of treatment setup for introducing tolerogenic microparticles (MPs) into LN of mice using intra-lymph node (iLN) injection. Following local LN injection, local and systemic changes were assessed in LNs, the spleen and the central nervous system (CNS). **b.** Mice were induced with a model of multiple sclerosis and treated with tolerogenic MPs loaded with the autoimmune disease-relevant antigen, myelin oligodendrocyte glycoprotein (MOG), and a broadly acting immune regulatory signal, rapamycin (Rapa). A single treatment at peak of disease, where a higher clinical score corresponds to a greater degree of paralysis, results in a permanent reduction of disease severity. **c.** The MP treatment promoted antigen-specific tolerance. MPs loaded with Rapa and a disease irrelevant peptide, ovalbumin (OVA) provides no protection from disease. Scale bars are 100 μm. **d.** Treatment with tolerogenic MPs causes LN structural changes at the treated LN, as well as distant, untreated LN. Treatment with tolerogenic MPs promotes the formation of regulatory T cells (T_{REGS}, light blue) known to modulate autoimmune disease. Scale bars are 100 μm. **e.** Tolerogenic MP treatment significantly reduces T cell (green) infiltration into the CNS. Adapted from ref. [26], Elsevier. Figure reproduced with permission from Springer Nature.

Despite the feasibility of intra-LN administration in clinical trials, implementing this approach involves some unique considerations that may highlight its advantages. First, treatments for autoimmune disease involve non-specific suppression of excess inflammation accompanying these diseases with small molecules drugs and, more recently, monoclonal antibodies. These treatments – such as methotrexate, fingolimod, natalizumab and rituximab – provide patients with real gains, but cause off-target effects resulting from lack of selectivity. Monoclonal antibodies, for example, can target specific receptors but do not differentiate between expression of these receptors on normal and self-reactive cells. Thus, intra-LN reprogramming may be beneficial if more selective tolerance is demonstrated during direct comparisons to existing therapies. Second, while there are a number of injectable nanoparticle strategies being explored to promote tolerance[65], a distinction between these approaches and direct LN reprogramming is the distribution and dose of cargo (that is, local LN injection versus systemic injection). Therapies integrating immunosuppressive components to polarize immune cells may be safer or more

effective if concentrated in LNs. For example, control over the cells developing in a target SLO after depot injection could enable the programmed cells to subsequently migrate to sites of disease while exposing only the patient's SLO to a local immunosuppressant dose. In contrast, systemic inflammatory conditions might benefit from conventional injections that distribute immunosuppressant throughout the patient.

2.5.3 Using artificial APCs to control T cell expansion in vivo

Artificial APCs (aAPCs) aim to directly expand and control T cells. This approach involves nano- or microparticles that present co-stimulatory molecules and antigen to locally stimulate T cells in peripheral tissues without requiring priming in LNs[71]. Artificial APCs first gained attention to support adoptive transfer therapies[72]; however, ex vivo cell handling is complex and expensive, motivating use of aAPCs to directly expand T cells in vivo. Altering aAPC shape to maximize contact with T cells[27, 28] and combining aAPCs with modulatory signals[29, 30] have both been used to enhance aAPC function.

The potential to directly enhance T cell expansion in vivo using aAPCs is becoming more intriguing as the power of T cell therapy has emerged. For example, recently approved T cell gene therapies (Novartis, Kite) are on the order of US$500,000 per treatment because these therapies require expansion of patient cells ex vivo before reinfusion. Harnessing shape and molecular interactions to maximize valency and contact time could improve the efficiency of T cell expansion. aAPCs enabling this control might eventually allow T cell therapy to be carried out in patients without need for ex vivo expansion, greatly reducing treatment cost and preparation time. Another

clinically relevant example is Provenge, the first approved DC vaccine, which relies on infusion of modified DCs to provide a modest survival increase for patients with advanced prostate cancer (NCT00065442). Future approaches using aAPCs as artificial DCs that efficiently expand tumor specific T cells against target antigens—such as prostate cancer antigens—might provide new opportunities to improve these therapies. As with the other emerging ideas above, aAPCs should be tested in combination with checkpoint blockade and other common components of cancer treatment plans[30].

2.6 Designing immune tissues for implantation

Perhaps the ultimate goal of immune tissue engineering is the implantation of designed tissues that promote or restore desired immune functions. Implantable LNs or other SLOs primed for a specific response might effectively clear infections or tumors – or regulate distinct inflammatory cells to combat autoimmune disease, without the hurdle of vaccines or immunotherapies reaching an existing SLO. On another front, engineering generative lymph organs – thymus and BM might help correct immune deficiencies, improve BM transplants, relax donor–recipient matching requirements and enable more accurate humanized animal models to study immunity and disease.

2.6.1 Mimicking adaptive functions with engineered SLOs

Tissue engineered LNs and spleens are being investigated in mice using scaffolds formed from natural materials—such as decellularized LNs that retain ECM components[73]. Alternatively, more defined materials, including alginate and collagen[31], provide easily controlled mechanical and chemical properties[62]. The inclusion of stromal components needed for artificial SLO function distinguishes constructs in this

section from scaffolds for recruitment of immune cells in the previous section; the latter aim to prime APCs that return to existing SLOs.

In one approach decellularized mouse LNs were seeded with splenocytes from donor mice, then implanted into syngeneic (the same mouse strain) or allogeneic (a different strain) mice[73]. While functionality was not tested, the cells survived for at least 14 days and the implants did not induce host responses. Suematsu et al. developed LN-like organoids by loading 3D collagen sponges with a mouse thymic stromal cell line and activated primary DCs[31]. In mice, these constructs developed distinct B and T cell zones resembling those in natural SLOs (**Figure 2.6a**). These scaffolds also exhibited B cell proliferation and development of high endothelial venules, a tissue microdomain that enables immune cell entry from blood (**Figure 2.6b**). The scaffold structure was important, as neither collagen gels nor synthetic sponges recruited cells as effectively. As a functional proof of concept, DCs loaded with a model antigen were used to generate antigen-specific responses in healthy recipient mice (**Figure 2.6c**). Subsequent re-transplantation of the organoids into a second mouse lacking functional B and T cells (that is, SCID) resulted in migration of B cells to the spleen and BM of recipients. The immunocompromised hosts were then able to generate antigen-specific antibodies, indicating artificial SLOs restored at least some immune function (**Figure 2.6c**). Implantation also promoted B cell affinity maturation and, notably, memory T and B cells[32]. However, in all of these studies, donor mice required pre-injection of the model antigen before organoid implantation. A related approach eliminated the requirement of cell seeding onto the scaffolds by loading scaffolds with particles that

release chemokines and cytokines to direct cell distribution and recruitment, as well as GC formation[74].

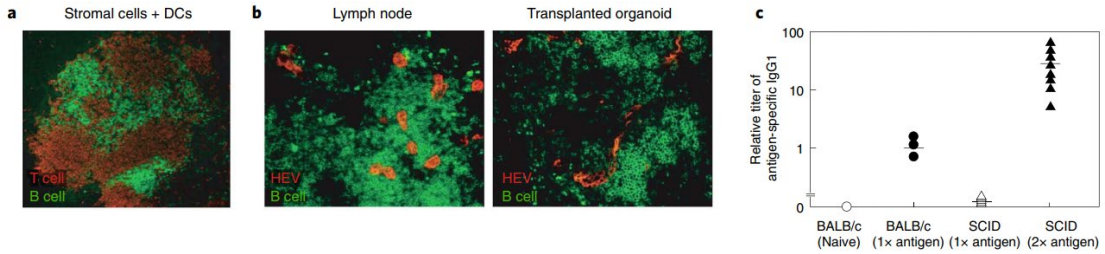

Figure 2.6 Engineering secondary lymphoid tissues can restore immune functions in vivo

a. Collagen-sponge scaffolds loaded with stromal cells and activated dendritic cells (DCs) promote T cell (red) and B cell (green) recruitment to distinct regions within the LN organoids after transplantation. **b.** Transplanted organoids promote high endothelial venule (HEV) formation (red). B cells are stained in green. **c.** Re-transplantation of organoids promotes humoral responses against an antigen, ovalbumin (OVA) in both healthy (BALB/c) and severely immunocompromised (SCID) mice. Adapted from ref. [31], Macmillan Publishers Ltd. Figure reproduced with permission from Springer Nature.

For artificial SLOs to have a direct translational impact as vaccines and immunotherapies, these strategies will ultimately need to be compared against or tested with current human options or emerging candidates. For example, as vaccines, the magnitude and duration of antibody and T cells responses induced by pre-primed implantable SLOs might be more long-lasting than conventional vaccines by establishing a local tissue niche. These comparisons could build understanding of potency and durability that lead to artificial SLOs able to protect against pathogens that are otherwise intractable using conventional vaccine technologies, such as HIV, hepatitis C and malaria. Similarly, in cancer, tumor-primed SLOs might serve as potent new cancer vaccines, but should be tested in tandem with common combination therapies (for example, checkpoint blockade or adoptive transfer), since most treatment plans are multipronged. In autoimmunity, artificial SLOs incorporating self-antigens

and regulatory signals might provide a route to promote antigen-specific tolerance that selectively controls disease. However, comparison to approved immunosuppressants and monoclonal antibodies is needed since these therapies currently provide benefits to patients but are hindered by the lack of specificity. Using the best available pre-clinical animal models is also important for meaningful comparisons in pre-clinical studies.

One recent approach in a more translational cancer model assessed alginate scaffolds containing T cell binding domains and particles loaded with stimulatory T cell signals (**Figure 2.7a**)[33]. These scaffolds were seeded with engineered tumor-specific T cells, then implanted in mice. To mimic challenging clinical settings, the scaffolds were tested in an incomplete resection model of breast cancer and in an inoperable, disseminated model of ovarian cancer. Scaffolds containing particles with proliferative T cell signals greatly expanded tumor-specific T cells compared to other aggressive adoptive cell therapies using the same cells and signals, but without scaffolds (**Figure 2.7b**). The expanded T cells migrated to tumors and caused complete regression in both cancer models (**Figure 2.7c**). Subsequently, Smith et al. used a

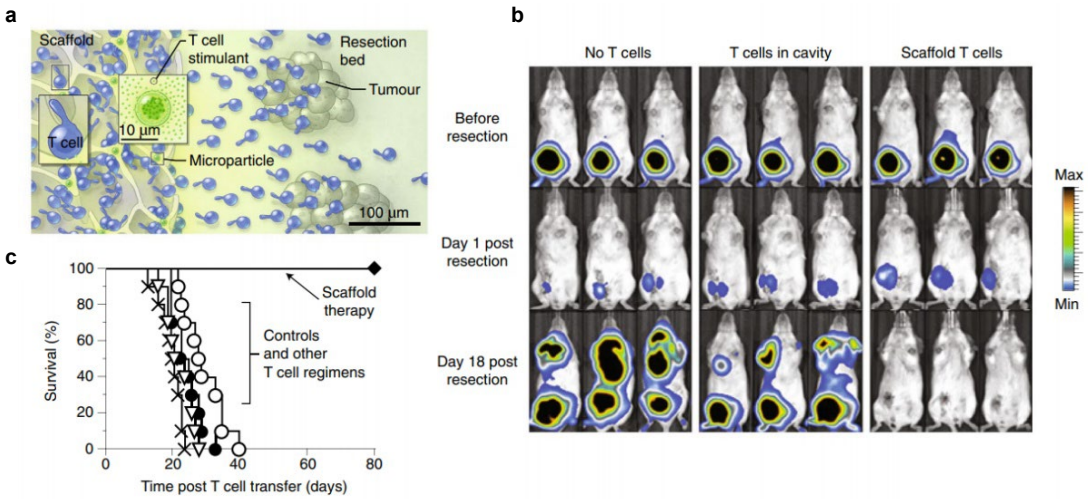

Figure 2.7 Engineering T cell activating reservoirs to promote anti-tumor efficacy

a. Biopolymer scaffolds loaded with tumor-specific T cells and stimulants inserted into tumor resection beds can target incompletely resected tumor cells. **b.** T cells delivered by the scaffold into the resection bed of an incompletely resected tumor enhance protection against tumor relapse, whereas T cells alone do not. **c.** Scaffold delivery of tumor specific T cells significantly enhances survival compared to control treatments. Adapted from ref. [33], Macmillan Publishers Ltd. Figure reproduced with permission from Springer Nature.

similar design to deliver tumor-targeting T cells displaying chimeric antigen receptors (CAR)[34]. In solid tumor models of pancreatic cancer and melanoma that are difficult to treat, scaffold-based delivery was critical to eradicate tumors and protect against relapse.

As is becoming apparent from the examples above, an important theme is the need for comparison of emerging technologies aimed at similar problems. For example, the T cell scaffolds above require ex vivo preparation and seeding in the scaffold before implantation; a parallel approach by the same lab uses injectable nanoparticles that can introduce CAR T cell genes into circulating T cells to clear leukemia in mice at levels similar to adoptive transfer therapies[75]. Direct comparisons between emerging technologies – scaffolds versus nanoparticles in this case – could help reveal settings where each is most useful. Further, artificial SLO technology has not yet leveraged a number of ubiquitous tissue engineering tools. Some of these include rigorous mechanical characterization of stress, strain and fatigue, along with techniques to control structure and signal density with high precision, such as 3D printing and lithography. These capabilities are of particular importance since the LN, spleen, thymus and BM all have spatial microdomains with distinct functions and mechanical

properties, yet none of the examples here integrate spatial control beyond simple porosity.

2.6.2 Engineered thymus to enable organ transplantation

As introduced above, the thymus is critical in T cell selection, deleting cells that strongly bind self-antigens. Thymic tissue engineering offers potential to combat autoimmune disease driven by self-reactive cells, or improve transplantation by eliminating recipient- or donor-reactive T cells without broad or permanent immunosuppression[35, 76]. Thymic epithelial cells (TECs) are important in thymic T cell recruitment and selection, as are the other stromal cell interactions, chemokines and ECM cues needed for development of mature T cells. Decellularized thymic tissue can be seeded with thymic-derived cells (including TECs) to mimic this environment, creating a simple thymic framework[76]. When implanted in athymic nude mice lacking T cells, the resulting scaffolds attract hematopoietic progenitors from BM that can produce naive $CD4^+$ and $CD8^+$ T cells.

To induce tolerance in transplanted tissue, Fan et al. combined decellularized thymic tissue scaffolds with thymic stromal cells containing TECs, fibroblasts, and BM-derived T cell progenitors (**Figure 2.8a**)[35]. Implanting these organoids in athymic nude mice generated naive T cells that could migrate to SLOs and provide functional T cell support required for B cells to generate high affinity, antigen-specific antibodies. Mice with the implants also rejected skin allografts displaying non-self-antigen, indicating functional, antigen-specific T cell response. Importantly, however, when the organoids were instead designed with a mixture of TECs from donors and recipients,

donor-derived skin grafts were accepted by the recipients, demonstrating immunologic tolerance (**Figure 2.8b**). Since the studies above used athymic mice which do not generate a host response, an important question is how this approach would translate to human transplants; mature T and B cells in the periphery would still be donor reactive. Perhaps some gains could be realized through generation of tolerized cells in the thymus, or combining such approaches with immunosuppression to limit peripheral donor-reactive cells. Engineered thymus may also have utility in treating patients with immunodeficiencies – where human thymus transplants are being investigated – to restore missing immune functions, such as the DiGeorge anomaly and severe combined immunodeficiency (SCID)[77].

2.6.3 Engineered BM to support hematopoiesis and immunity

Implantable BM scaffolds loaded with stem cells or other progenitors that differentiate into functional immune populations could help treat immune deficiencies, blood cancers or self-antigen specific lymphocytes arising during autoimmunity. However, engineered BM in this therapeutic context shares many of the translational challenges discussed for thymus with respect to mature lymphocytes present in recipients with intact immune systems. While implantable BM niches may one day be used in humans, engineered constructs may be useful in the nearer term for diagnosis and therapeutics screening in vitro or in humanized animal models. Better understanding of how material properties impact BM scaffold function could lead to constructs that support efficient engraftment with fewer patient cells for screening, or that maintain viability of cells in the niches for longer intervals. These properties would be useful for diagnostic applications where patient cells are limited or particular

phenotypes are rare. Already, scaffold stiffness and cell density have both been shown to impact differentiation of BM stromal cells encapsulated in collagen gels[78], while mimicking the modulus and porosity of native BM improves HSC homing and retention in mice[79]. One study exploring the idea of distinct spatial domains within engineered immune tissues has used scaffolds mineralized externally to recreate the function of bone, and non-mineralized internally to provide features of the hematopoietic niche that enable cell engraftment[80]. These studies might help define parameters for constructs designed to screen responses of patient cells to therapeutics in humanized mice.

In addition to material design considerations, advancing engineered BM niches to clinical utility will require human cells. One emerging strategy to generate these humanized niches involves seeding scaffolds with human stromal and progenitor cells[5, 36-38]. Holzapfel et al. generated a BM mimic using polycaprolactone scaffolds coated with calcium phosphate and bone inducing factors (rhBMP-7)[36]. Scaffolds cultured with human mesenchymal progenitor cells were then implanted into mice lacking key components of the immune system (NSG mice). After ten weeks, these constructs mimicked many mechanical, cellular and biochemical features of human BM. During similar studies, mice were irradiated ten weeks after scaffold implantation, then infused with human HSCs. The humanized BM environment preferentially recruited and maintained these HSCs, enhancing human leukocytes, T cells and progenitor cells in the construct and the host BM.

Engineered BM may be particularly useful in studying or eventually treating hematopoietic diseases and malignancies. Several reports combine bone-forming scaffolds and human mesenchymal stem cells (MSCs) to engraft leukemic cells[5, 37, 38]. In one example, NSG mice were irradiated and infused with hematopoietic progenitor cells from acute myeloid leukemia (AML) patients with distinct risks groups; alternatively, calcium phosphate scaffolds seeded with human mesenchymal stromal cells were implanted 6–8 weeks prior to injecting mice with AML cells (**Figure 2.8c**)[5]. Without scaffolds, only 43% of AML patient samples could be engrafted; scaffolds, however, allowed engraftment and development of AML from 74% of the patient samples. Of note, scaffolds supported engraftment of some risk groups that simple infusions did not. Thus, 3D structure and tunable scaffold properties might improve

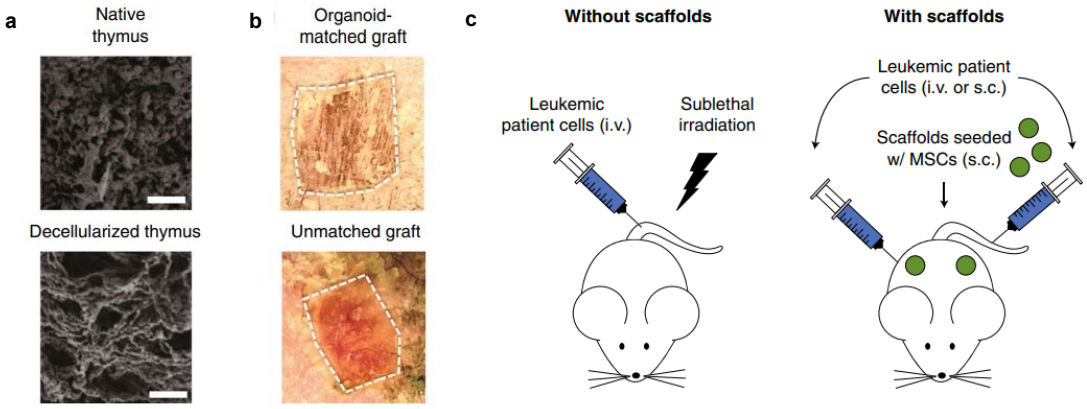

Figure 2.8 Engineering primary lymphoid tissues to reprogram immune functions in vivo

a. Decellularizing native thymic tissue preserves 3D extracellular matrix structures. Scale bars are 10 μm. **b.** Engineered thymus organoids include donor and recipient thymic epithelial cells (TECs). Donor mouse skin grafts are well-tolerated after four weeks by recipients with matched thymic organoid implants, while third party skin grafts are rejected. **c.**, Schematic depicting development of leukemic humanized bone marrow (BM) model. Mice were irradiated, then infused with hematopoietic progenitor cells from leukemia patients in distinct risk groups, or implanted with calcium phosphate scaffolds containing human mesenchymal stromal cells (MSCs) 6–8 weeks before infusion with the leukemic patient samples. Scaffolds created an artificial BM niche that enabled engrafting of some risk groups that could not be engrafted using the infusion alone. Adapted from ref. [35], Elsevier (a, b). Figure reproduced with permission from Springer Nature.

study or diagnoses through faster, more robust engraftment of cancers from patients using these animal models to accurately mimic the human setting. While cancer is a key area for these tools, recent evidence reveals that patient-derived tumor grafts implanted in immunodeficient mice quickly lose resemblance to the patient tumor during selection pressures occurring in host animals[81]. Coupling patient grafts with engineered BM scaffolds might be useful in overcoming this divergence by recreating human immune selection pressures in humanized mice displaying human tumors.

Most of the work in this section focuses on the function of an organoid itself, but the physical connection of the organoids to the lymphatic system is another area that should be pursued. For example, lymphatic endothelial cells, fibroblasts and adipose-derived stem cells have been incorporated in scaffolds comprised of fibrin or collagen I[82, 83]. When combined with lymphangiogenic factors, such as VEGF-C, or fluid flow, lymphatic endothelial cells in these constructs grow into lymphatic capillary networks in vitro[84]. Lymphatic vessels are vital for immune cell homing and surveillance, so controlling lymphangiogenesis in or around engineered immune tissues could increase antigen and immune cell recruitment to, or dissemination from, these sites.

2.7 New immunological insight informs immune engineering

In this section we highlight some recent immunological advances in fields distinct from tissue engineering that have important implications for engineering immune tissues. The ways in which this knowledge translates to design criteria for immune tissues, such as LNs, are presented in **Figure 2.9**.

2.7.1 Dynamic stromal cues in SLOs influence cell differentiation

The stroma provides distinct cues to attract and organize immune cells at different stages of response in LNs and spleen. These interactions are coordinated through the types of signals presented[85, 86], as well as the locations[87-89] and timing[90]. Stromal cells, such as fibroblastic reticular cells, blood endothelial cells and lymphatic endothelial cells, can all present antigens to T cells[91, 92]. For example, Tamburini et al. found that after a viral infection or vaccination, lymphatic endothelial cells can proliferate and capture antigens, continuing to display the antigens for weeks[93]. In designing artificial LNs or spleen, this finding could be leveraged by incorporating lymphatic endothelial cells in constructs, along with T cell homing molecules, to provide prolonged antigen exposure and development of memory T cells (**Figure 2.9a**).

Immune cells actively interact with stromal cues, such as the distinctive compositions of ECM laminin fibers secreted by stromal cells. Warren et al. discovered that during immunity and inflammation, laminin α4 decreases and laminin α5 increases, while during tolerance, laminin α4 increases and laminin α5 decreases[94]. These changes alter the interactions of DCs and T cells to help promote either pro-immune or regulatory T cell responses. Thus, tissue engineering scaffolds could integrate specific compositions of laminins, or other stromal components, to direct tolerogenic or stimulatory responses (**Figure 2.9b**).

2.7.2 Matrix mechanical properties direct immune cell function

Mechanical properties play an important role in controlling immune cell migration and function. Interestingly, new studies reveal that in natural LNs, ECM properties change over the course of immune response. In particular, fibroblastic

reticular cells, which form the collagen network that enables immune cell trafficking, work with DCs to contract fibers during resting states, then relax the network during immunostimulatory conditions to accelerate cell mobility (**Figure 2.9c**)[95]. This discovery implies a potential route to enable 'on-demand' access of immune cells to specific signals at different stages of response by coupling collagen networks of different densities with defined concentrations of antigen and adjuvant.

Beyond SLO tissues, matrix mechanical properties are important in the tumor microenvironment, where immunosuppressive conditions severely limit immunotherapies. In addition to suppressive biochemical cues, tumors confront immune cells with rigid ECM environments that create high solid stress forces not encountered in healthy tissue[96]. This feature may impact immune cell function or deter infiltration in tumors; these stresses could be mimicked to limit or direct migration of immune cells to and within immune tissue scaffolds (**Figure 2.9c**).

2.7.3 Peripheral tissues alter immune cell homing and function

Immune cells function and interact differently depending on their location within the body, making immune cell migration and homing critical for immune responses. These movements are directed partly by lymphatic endothelial cells displaying homing signals for specific sites[97]. For example, lymphatic vasculature comprises two vessel types—afferent vessels that bring antigens and leukocytes to LNs, and efferent vessels by which only lymphocytes and antigens can leave LNs. Iftakhar-E-Khuda et al. recently used gene expression to define molecular profiles differentially expressed on afferent and efferent lymphatic endothelial cells[98]. Designed

immune tissues could exploit these molecular homing signals to recruit lymphocytes or promote rapid egress of activated T cells from LN during vaccination; conversely, constructs targeting autoimmunity or transplantation could display molecules that restrict immune cell egress (**Figure 2.9d**).

Beyond promoting or suppressing inflammatory functions, immune cell interactions with peripheral tissues influence wound healing for regenerative medicine applications. Thus, much effort in tissue engineering is directed at understanding pathways involved in inflammatory responses to design scaffolds that instead drive wound healing[99, 100]. One recent study revealed colony stimulating factor-1 in macrophages as a key pathway to prevent fibrosis—which often leads to failure of implants—without interfering with other macrophage functions[101]. In another example, Guc et al. showed the importance of inducing lymphangiogenesis—lymphatic vessel generation—to promote wound healing. Controlling the release of lymphangiogenic factors promoted lymphatic capillaries that regulated the levels of leukocytes delivered to diabetic wound sites, enhancing ECM deposition and healing (**Figure 2.9e**)[102]. This work highlights another important design consideration: implantable immune tissues could include factors to promote lymphangiogenesis to enhance recruitment or dissemination of lymphocytes (**Figure 2.9e**). Whether this approach might allow for direct connection with existing lymphatic vascular or SLOs—and how important this link is—are open questions.

2.7.4 Vaccine and immunotherapy design informs tissue engineering

In tissue engineering, recent studies reveal that the choice of scaffold material itself can impact immune cell signalling[103]. This observation is in line with findings confirming many common biomaterials can directly activate the inflammasome and other innate stimulatory pathways through intrinsic material properties[104, 105]. Thus, physicochemical material properties (for example, charge, molecular weight, chemical functionality) may provide a new route to program pro-immune or regulatory responses into scaffold frameworks used in engineered immune tissues. Furthermore, several new studies have taken quantitative approaches toward developing immunological design parameters that could be harnessed for scaffolds. These include the impact of antigen display density on immune response[106, 107], and the role that specific types and ratios of stromal cells play in directing lymph node function, such as fibroblastic reticular cells[108]. For example, Singha et al. combined computational modelling, immunology and materials fabrication to show with molecular precision that changing the dose of self-peptide presented to self-reactive T cells during autoimmunity controls T cell expansion, while the phenotype of the expanding T cells is dependent on the density of the peptide complexes[107]. Recent studies have also shown density plays an important role in how an antigen is processed in APCs. Hess et al. discovered delivering the same total amount of self-peptide on particles at a low density was more effective in promoting tolerance than display at high density on fewer particles[106]. Thus, controlling the number and density of antigen on designed immune tissues—or in spatially distinct regions of these constructs—could help control the phenotypes of expanding cells (**Figure 2.9f**).

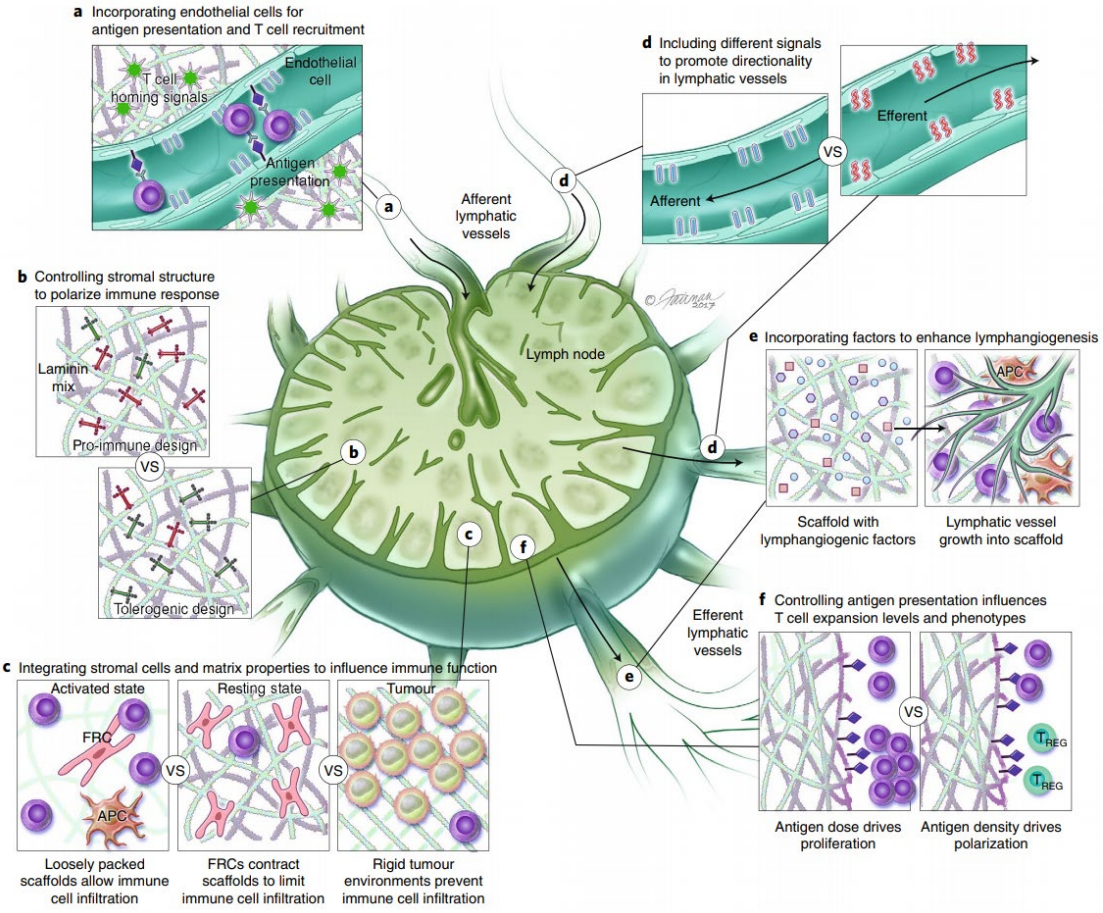

Figure 2.9 New immunological insight informs immune tissue engineering design
a. Including endothelial cells that present antigen and T cell homing signals could promote T cell activation and enhance immune responses. **b.** Controlling stromal structures can direct immune response—for example, using different relative ratios of laminins on a scaffold to polarize responses toward pro-immune or tolerogenic functions. **c.** Matrix mechanical properties influence immune cell function. Stiff, densely packed regions due to fibroblastic reticular cells (FRCs) contracting the stroma or tumor microenvironments limit immune cell infiltration and activity. Activated immune sites rely on relaxation of FRCs to enhance immune infiltration. **d.** Endothelial cells in afferent and efferent lymphatic vessels express different homing cues on their surfaces. These signals could be included in a tissue engineering design to promote a specific type of lymphatic vessel or immune cell in target locations. **e.** Delivering lymphangiogenic factors using a scaffold could promote lymph vessel growth, allowing for delivery of immune cells, which could enhance wound-healing abilities of the scaffold. **f.** Antigen-presenting scaffolds could be used to influence both the degree of immune cell proliferation and the specific phenotypes that arise, properties shown to be a function of both antigen dose and antigen display density. Credit: printed with permission from © Fairman Studios, LLC. Figure reproduced with permission from Springer Nature.

2.8 Outlook

While engineering functional, implantable immune tissues to restore or reprogram immune responses is daunting, emerging immunological discoveries are bringing this vision closer. More realistic in vitro models and on-a-chip designs continue to improve our ability to interrogate basic immunological interactions. Combining this knowledge with emerging tissue engineering technologies could enable designer immune tissues that accelerate screening of candidate vaccines and immunotherapies, and that improve the success or robustness of vaccines and therapies targeting cancer, transplantation and autoimmunity.

Chapter 3: Using Biomaterials to Promote Immune Tolerance in Autoimmunity

While Chapter 2 provided some specific examples of engineering strategies that highlight biomaterials and techniques that can be used to study and control immune function, this chapter highlights specific considerations for the development of therapies aimed for MS. In particular, this chapter discusses current clinical strategies for MS patients, and how specific features of biomaterials can be tuned and leveraged to overcome these limitations in current strategies.

3.1 The adaptive immune system allows for potent, antigen-specific responses

The immune system is comprised of two major branches – innate immunity and adaptive immunity. Innate immunity is a broadly-acting, quick response first line of defense that involves a combination of blood proteins and immune cells – phagocytic cells and natural killer cells, that can react to features typically associated with pathogens or foreign cells[109, 110]. These features can either include the presence of pathogen-associated molecular patterns (PAMPs) that are not commonly found in the body (e.g. pieces of double-stranded RNA, single-stranded DNA, cell wall components, among others), or the absence of "self" molecules of cells (e.g. loss of MHC-I during infection)[109, 111]. Thus, innate immunity allows rapid, but relatively broad and non-specific protection. However, in addition to their first-line response, another major function of the cells of the innate immune system is supporting the potent and antigen-specific functions of adaptive immunity discussed in **Chapter 2.3**[110, 112].

In particular, the work in this thesis targets the interactions between dendritic cells (innate immune cell) and T cells (adaptive immune cell). As discussed in **Chapter**

2.3, dendritic cells (DCs), survey peripheral tissues for foreign molecules, which they collect and bring back to lymph nodes to present to T and B lymphocytes to initiate an adaptive immune response[39]. The context of the antigen presentation by DCs to T cells is key in defining the type of adaptive immune response initiated in response to the antigen[113]. In particular, this thesis focuses on the induction of regulatory helper T cells to promote antigen specific tolerance, so understanding this DC:CD4+ T cell interaction is important.

3.1.1 Interactions between DCs and naïve T cells influence T cell differentiation

As shown in **Figure 3.1A**, DCs present or release several signals that are taken up by naïve T cells to polarize T cell function[39, 113, 114]. The first signal identifies the specificity of the response: the T cell must be able to recognize the antigen the DC is presenting in a major histocompatibility complex II (MHCII) molecule. This means the T cell must be specific for the antigen presented by the DC. The second signal provides stimulation to and activates the T cells. In the absence of co-stimulatory molecules on DCs, the T cells will not acquire inflammatory phenotypes. The third signal is a polarization signal – this helps determine the phenotypic fate of the T cells after their encounter with the DC. **Figure 3.1B** shows some of the phenotypic fates of these T cells after interacting with a DC that are of particular interest for this work, including inflammatory phenotypes T_H1 and T_H17, as well as regulatory phenotype T_{REG}[115]. All three of these phenotypes are important in the context of Multiple Sclerosis and tolerance. T_H1 and T_H17 T cell have both been implicated in pathogenesis in MS, and T_{REGS} are critical in the suppression of both of these inflammatory phenotypes[116, 117].

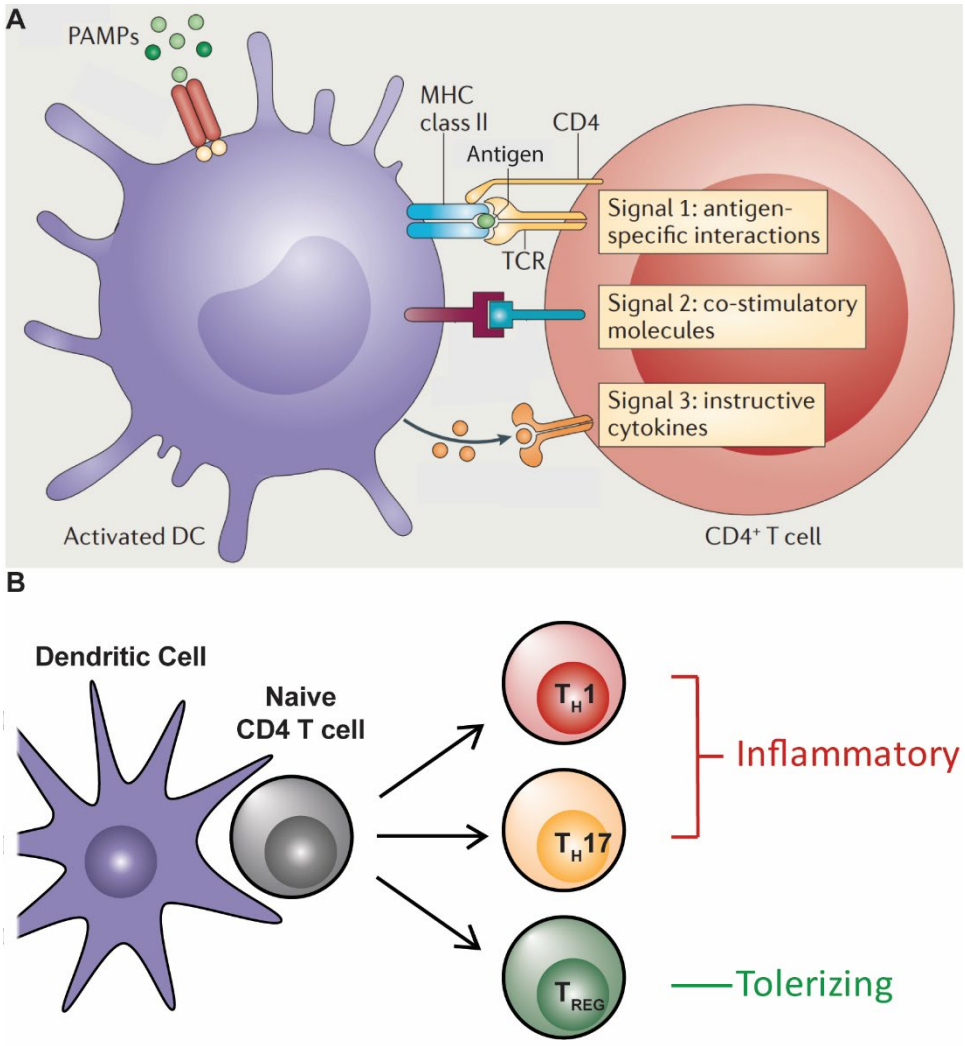

Figure 3.1 DC: T cell interactions influence T cell phenotypic fate
a. DCs present antigen to CD4+ T cells in major histocompatibility complex class II molecules (MHCII). These antigens and the MHCII molecules interact with the T Cell Receptor (TCR) to initiate and antigen specific response. Co-stimulatory molecules presented on the surface and secreted by DCs inform CD4+ T cell differentiation and instruct T cell function upon future encounters with the antigen. Adapted from Kamayashi and Laufer, *Nature Reviews Immunology*, 2014[113] with permission from Springer Nature **b.** Naïve CD4+ T cells can acquire several different phenotypes after interacting with DCs depending on the signals present. Some of these phenotypes include inflammatory T_H1 and T_H17, as well as regulatory T_{REG}.

In MS, and during other inflammatory diseases and infections, the cytokines the T cells receive from the DC are essential in determining T cell fate. DCs secrete IL-12 to upregulate T-bet in naïve T cells, polarizing them to T_H1 cells, which then secrete

IFNγ to activate other immune cells (e.g. DCs and macrophages) to upregulate expression of surface pathogen receptors and MHC expression, increase proinflammatory cytokine secretion, and increase phagocytosis[116]. T_H17 cells are induced when DCs secrete IL-6 and IL-23, causing them to activate RORγt. T_H17 cells are particularly pathogenic in MS – they secrete IL-17 among other cytokines, which enables them to recruit additional innate immune cells, activate the innate immune cells, enhance B cell antibody production, and induce the release of proinflammatory cytokines[116, 117].

In contrast to the inflammatory activity of the T_H1 and T_H17 cells, T_{REGS} exert immunosuppressive functions into their environment[116, 118]. Some T_{REGS} are derived in the thymus, and then patrol the periphery to prevent autoimmunity and control severe immune responses to pathogens[118, 119]. These cells play a role in central tolerance, which was introduced in **Chapter 2.3** and will be further discussed in **Chapter 3.1.2** below. However, these cells can also be induced in the periphery, where naïve CD4+ T cells can gain regulatory functions after interacting with DCs. DC secretion of TGF-β results in increased expression of Foxp3, which then allows the secretion of key anti-inflammatory cytokines such as IL-10 and TGF-β. These cytokines can then act on surrounding innate immune cells and reduce inflammatory functions (e.g. proinflammatory cytokine secretion, surface stimulatory molecule expression) of these cells[116].

3.1.2 Central and peripheral tolerance fail in cases of autoimmunity

In cases of MS, the adaptive, inflammatory myelin-specific response of lymphocytes is due to a failure in the regulation lymphocytes generated for adaptive immunity. The antigen-specific nature of the adaptive immune response is due to the specificity of T and B cell receptors. In order to make such a wide array of receptors that each binds a different antigen, the gene encoding these receptors is randomly rearranged by splicing and recombining the DNA during development[120, 121]. As discussed in **Chapter 2.3**, for T cells, this process occurs in the thymus before T cells are released into the periphery[122]. This recombination process would theoretically allow for ~10^{15} different possible T cell receptors[123], though in actuality, there are only ~10^{7} different T cell receptors in the body at one time[120, 122]. This, in part, is due to the T cell maturation process that occurs in the thymus. T cells undergo two selection processes in the thymus – positive and negative selection. The positive selection process ensures that T cells will be able to recognize the MHC molecules that will be presenting antigens to T cells in the body. The negative selection process removes T cells that are reactive to self-molecules – pieces of proteins that are normally found in tissues in the body[42, 43]. This process, central tolerance, typically ensures that no self-reactive immune cells enter the periphery. T cells that fail these checkpoints are either deleted, die from lack of stimulation, mutate their receptors until they pass selection, or differentiate into regulatory T cells.

However, the stromal cells in the thymus cannot present every single possible self-antigen that is present in the body. This means that some self-reactive T cells do leave the thymus and enter the body, where they are exposed to organ-specific antigens

as they circulate the periphery[124]. As a second line of defense, the immune system uses peripheral tolerance to keep these self-reactive cells unreactive[125]. One mechanism of peripheral tolerance involves inducing a state of anergy (unreactiveness) in the T cells when DCs present self-antigens without co-stimulation. Another involves presenting self-antigens from cells undergoing apoptosis. In addition, similar to the stromal cells of the thymus, stromal cells in the lymph nodes (fibroblastic reticular cells, follicular DCs, and lymphatic endothelial cells) all present self-antigens. These stromal cells expressing tissue-specific antigens can cause apoptosis (deletion) of tissue-reactive T cells. Self-reactive inflammatory T cells can also be suppressed by natural (from the thymus) or inducible (generated in the periphery) regulatory T cells[118, 119, 125].

If both of these mechanisms of tolerance fail, and self-reactive inflammatory immune cells cannot be suppressed, autoimmune disease occurs. Unfortunately, autoimmune diseases are relatively common, affecting ~3-5% of the population[126]. Some of the most prevalent autoimmune diseases include Multiple Sclerosis, Type 1 Diabetes, Rheumatoid Arthritis, Systemic Lupus Erythematosus, and Inflammatory Bowel Disease. There are more than 80 different autoimmune diseases.

3.2 MS is a debilitating disease that impacts more than 2.3 million people worldwide

In the United States alone, nearly 1 million people are living with Multiple Sclerosis[127]. MS occurs when the immune system incorrectly recognizes myelin, the matrix surrounding neurons in the central nervous system, as foreign[128]. Myelin protects the axons on nerve cells, allowing for efficient signal propagation through the nervous system. In patients with MS, both central and peripheral tolerance have failed,

leaving inflammatory myelin-specific immune cells that cause inflammation and demyelination in the CNS[129-131]. The tissue damage is debilitating, causing chronic pain, loss of muscle control, and impaired senses[128].

MS patients experience a wide range of symptoms that can severely impact quality of life. Some of the most common early symptoms include: fatigue, numbness in a part of the body, and deterioration in vision. As disease becomes more established, and nerve damage progresses, common symptoms including severe or chronic pain, difficulty walking, involuntary movements, weakness in the body, dizziness, loss of control over bladder and bowels, and cognitive and emotional changes may emerge[128]. Some less common, but severe symptoms also may occur as disease further progresses, including: problems in speech and swallowing, uncontrollable shaking, seizures, respiration problems, and hearing loss. Collectively, these symptoms severely impact the lives of patients and their loved ones.

3.2.1 MS symptom severity is influenced by stage of disease

There are four stages of MS, and patients can experience one or several throughout their lifetimes (**Figure 3.2**). The first episode of MS symptoms a patient experiences is known as Clinically Isolated Syndrome (CIS). One episode of CIS does not constitute a diagnosis of MS – patients who with CIS may or may not develop MS in the future. When a patient experiencing CIS also has lesions caused by inflammation and demyelination in the CNS that can be visualized by Magnetic Resonance Imaging (MRI), the likelihood of a future MS diagnosis increases[128]. CIS patients at risk for

developing MS can be prescribed some of the disease-modifying therapies used to treat MS, which often delays onset of MS in these patients.

After being diagnosed with MS, patients can experience one of three disease courses: Primary Progressive MS, Relapsing-Remitting MS, or later stage Secondary-Progressive MS (**Figure 3.2**)[128, 132]. New MS patients (85%) typically present with Relapsing-Remitting MS (RR-MS), in which patients experience periods of relapse – attacks on the CNS in which patients experience neurological symptoms – that last for days to weeks. These patients then either fully or partially recover, but don't experience disease progression between bouts of relapse. These incidences are shown in the blue bars in **Figure 3.2**. New patients (15%) who are diagnosed with Primary Progressive MS (PPMS), experience gradual, but worsening symptoms over time. This disease progression is seen in the blue line in **Figure 3.2**. Nearly 80% of patients with Relapsing-Remitting MS eventually progress to Secondary Progressive MS (SPMS), in which the periods of complete remission stop and disease progresses more consistently (with or without relapses). This phase, indicated by the black line in **Figure 3.2**, is associated with the progression of neurological disfunction, with more severe symptoms than the Relapsing-Remitting Phase[132]. Importantly, disease progression and damage to neurons (axonal loss) and CNS occurs at all phases of disease – evidenced by the red axonal loss and brain volume curves indicated in **Figure 3.2**.

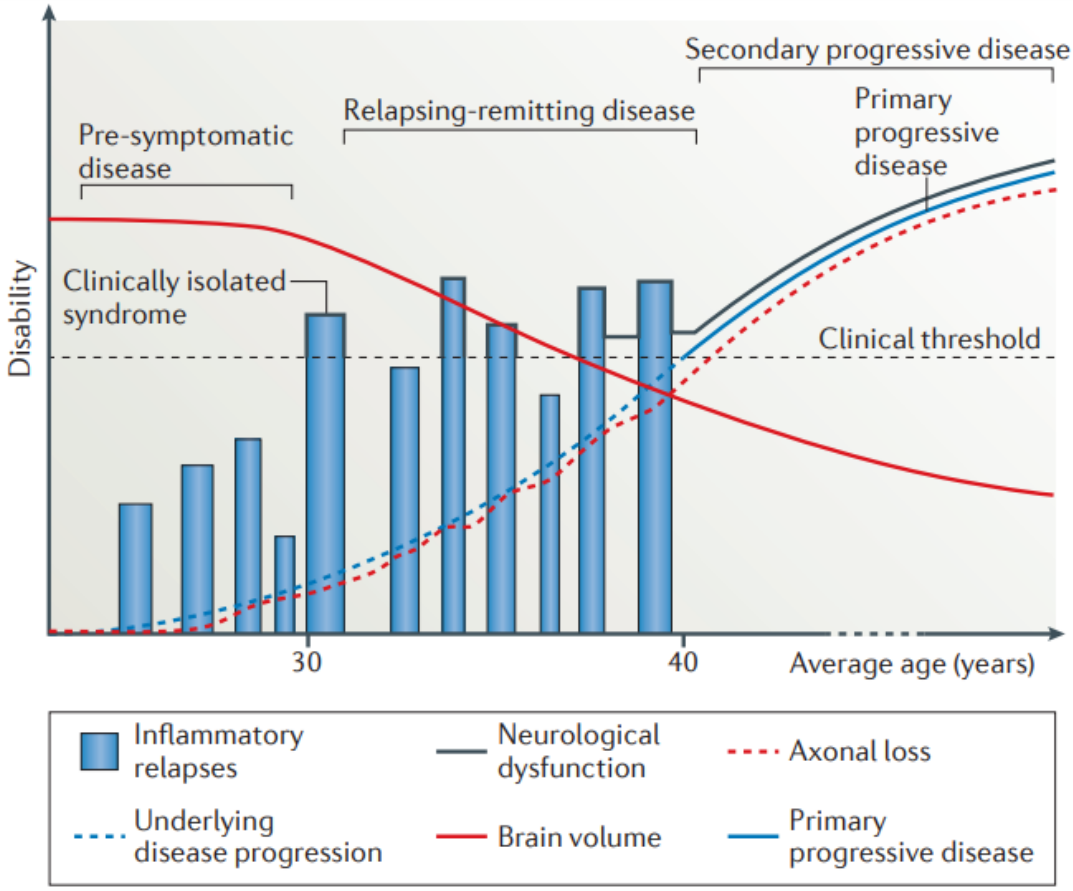

Figure 3.2 MS symptom severity changes throughout disease course.
The inflammation and attack on myelin typically begin before symptoms manifest. The first clinical appearance of symptoms – Clinically isolated syndrome – may or may not be followed by an MS diagnosis, though if inflammation is evident on MRI scans, it is likely MS will develop. Relapsing-Remitting MS is the most commonly diagnosed form of MS, in which patients experience symptom relapses followed by periods of remission. Over time, most RR-MS patients typically develop Secondary Progressive MS, in which there is continual worsening of symptoms over time with no periods of remission. Some patients may be diagnosed with Primary Progressive MS, in which there is a gradual worsening of symptoms over time. In all stages of disease, underlying inflammation is damaging nerves – evidenced by increasing axonal loss and decreased brain volume. Reproduced from Dendrou et al, *Nature Reviews Immunology*, 2015[132] with permission from Springer Nature.

3.2.2 MS is caused by myelin-specific auto-reactive immune cells

In early stage MS, disease is initiated by myelin-reactive immune cells that cause inflammation and neurodegeneration in the central nervous system[130, 133, 134].

These immune cells damage the myelin coating the neuronal axons (**Figure 3.3**), and the oligodendrocytes that produce the myelin to coat the neurons. This loss of myelin exposes neurons to the inflammation in the environment, allowing for damage to neurons, in addition to loss of efficiency in signal propagation through the nerve cells.

Several myelin-specific immune cells contribute to inflammation and neurodegeneration in the CNS[129, 132, 135-137]. Myelin-reactive $CD4^+$ T cells infiltrate the CNS and secrete inflammatory signals that damage tissues and recruit additional inflammatory cells – including inflammatory B cells, macrophages, and CD8+ T cells that propagate inflammation and degeneration in the CNS[129, 130, 133, 135, 137]. Myelin-specific $CD8^+$ T cells and antibodies work to directly promote demyelination and neural cell destruction[129, 138-140]. The inflammation in the CNS also activates tissue-resident cells – microglia and astrocytes that typically function to protect brain tissue and tightly regulate inflammation in the brain[132]. Over time, chronic inflammation in the brain from activated innate immune cells is what ultimately causes the damages to nerve cells and neurodegeneration associated with progressive disease. In addition, recent research has shown that as MS evolves, additional self-reactive immune cells specific to proteins present in neuronal bodies (e.g. β synuclein) contribute to neurodegeneration in late stage disease[141, 142].

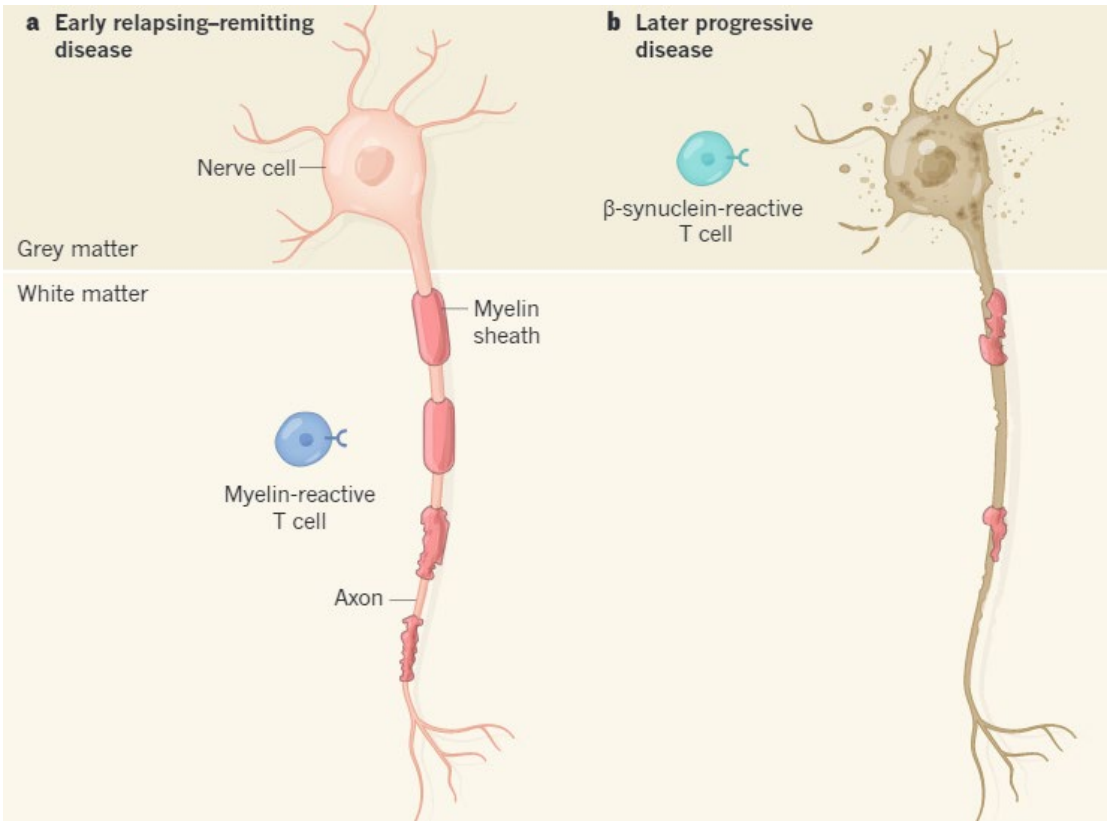

Figure 3.3 Myelin-reactive immune cells initiate inflammation in MS.
a. Myelin-reactive T cells that escape central and peripheral tolerance initiate inflammation in the CNS by activating immune cells that attack myelin in MS. Myelin typically insulates and protects axons and enables signal propagation. **b.** Late stage MS, which is associated with the greatest neurological damage, is linked to direct attacks on the neuronal bodies, causing cell death. Reproduced from Pappalardo and Halfer, *Nature*, 2019[141] with permission from Springer Nature.

3.3 Myelin-specific tolerance would enhance efficacy and selectivity of MS therapies

3.3.1 MS therapies aim to slow disease progression, not cure disease

MS is treated with non-specific therapies that block certain receptors or functions of immune cells but cannot differentiate between myelin-reactive immune cells and other lymphocytes[143-147]. These disease-modifying therapies (DMTs) work through different mechanisms of action, including: broadly suppressing inflammation and immune cell activity, depleting immune cell numbers, preventing immune cell

departure from lymph nodes, preventing immune cell adhesion, and limiting activation of specific immune cell types (e.g. B or T cells)(**Figure 3.4**)[148-150].

Over time, MS therapies have become increasingly specific as breakthrough MS research has provided new insights into disease. Some of these key therapies and their mechanism of action are outlined in **Figure 3.4**. However, even the newest monoclonal antibodies cannot differentiate between healthy and diseased cells displaying the antibody target, leaving patients susceptible to opportunistic infections. In addition, all disease modifying therapies aim to delay the progression of disease – they are non-curative, and require routine, life-long treatments to maintain disease remission[151]. Further complicating treatment, 85% of patients initially present with relapsing-remitting MS[128], in which patients experience waves of paralysis as they develop reactivity to different sections of myelin over time[152]. This epitope spreading complicates treatments, and therapies do not consistently work at all stages of disease[144-146].

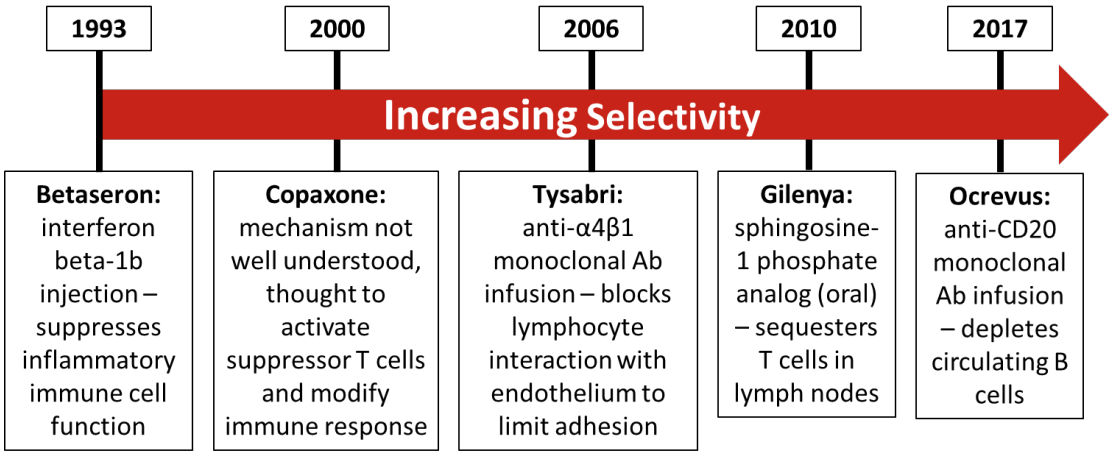

Figure 3.4 MS therapies have become increasingly selective with new insight into disease.
MS therapies have become increasingly specific for disease-causing immune cells over time. Initial therapies for MS knocked down all immune cell function, and the newest monoclonal antibodies target only cells displaying the antibody target. However, even

the newest therapies cannot differentiate between healthy immune cells displaying the target and disease-causing immune cells, which can leave patients vulnerable to some infections.

3.3.2 Generating myelin-specific regulatory T cells could enhance selectivity of MS therapies

As discussed in **Chapter 3.1.2**, peripheral tolerance relies on a couple different mechanisms to suppress self-reactive cells that escape central tolerance. In the case of MS, there is a breakdown of this peripheral tolerance, and self-reactive cells take on inflammatory phenotypes and attack the myelin in the CNS. One potential strategy for restoring this tolerance to myelin would be to generate myelin-specific regulatory cells that can restrain the activity of myelin-reactive immune cells[153, 154].

As T cells gain their function after interacting with DCs in the LN, one potential method to generate regulatory T cells would be to engineer this interaction to promote tolerogenic signaling between the DCs and developing myelin-reactive T cells. One target for promoting tolerogenic signaling in DCs and T cells is the molecular target of Rapamycin (mTOR). The mTOR pathway is a key regulator of cell metabolism, and integrates information from the environment, such as nutrients, growth factors, energy, and stress[155-158]. Inhibiting mTOR has been shown to induce TREGS that can suppress inflammatory T cell phenotypes[159, 160], and provide protection from disease in mouse models of MS[153, 154, 161].

However, rapamycin is poorly water soluble, and has a short half-life in vivo, necessitating frequent systemic injections. In addition, rapamycin non-specifically suppresses immune cell expansion. Biomaterials offer a solution to these problems, allowing for encapsulation and delivery of hydrophobic cargo such as rapamycin. As a

result, to address the limitations in selectivity in current MS therapies, this work sought to promote tolerance to myelin by controlling the release of rapamycin, which inhibits mTOR, and key disease-relevant myelin peptides from polymeric particles in LNs to influence the DC:T cell interactions and promote regulatory myelin-specific T cells to ameliorate disease at different stages of disease in mouse models of MS.

3.4 Using biomaterials to enhance specificity of immunotherapies

As discussed in **Chapter 2,** biomaterials have many advantageous properties in the context of immunotherapies. The term "biomaterials" encompasses many materials that have been used in biological applications – materials including synthetic polymers, lipids, proteins, nucleic acids, and engineered artificial cells. These materials can be processed into many forms, including liposomes, polymer nanoparticles and microparticles, self-assembled particles, polymer scaffolds, and microneedles (**Figure 3.5**)[162] with a variety of features that can help effectively deliver drugs or immune cargo

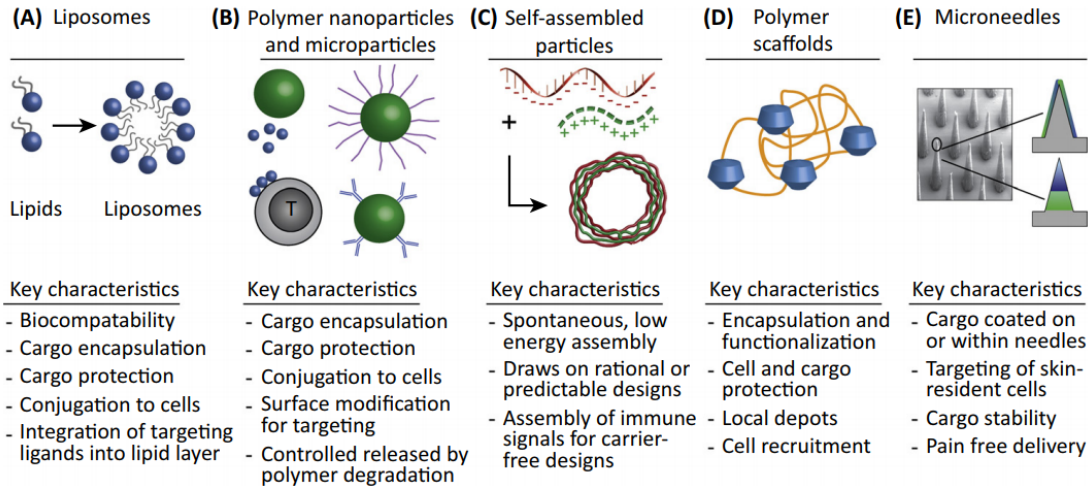

Figure 3.5 Biomaterials can be used to precisely deliver immunomodulatory cargo.
Biomaterials can be made into a variety of forms for immune signal delivery to meet the needs of an immunotherapy application. A couple of these forms include liposomes (**a**), polymer particles (**b**), self-assembled particles (**c**), polymer scaffolds (**d**), and

microneedles (**e**). Each type of material system has different advantages in immune cargo delivery. Reproduced from Bookstaver et al, *Trends in Immunology*, 2018[162] with permission from Elsevier.

to improve vaccine and immunotherapy design. Important for this work in particular, biomaterials offer improvement over soluble cargo delivery, by allowing co-delivery of cargo, targeted delivery of cargo, cargo protection, and control over rate of cargo release[162-166].

As medicine moves toward more personalized, patient-specific treatments to improve patient outcomes, biomaterials will become critical not just as delivery agents and tools to better understand immune function. As discussed in **Chapter 2**, biomaterials are incredibly tunable, with properties that can be engineered to meet many different functions[162, 167-169]. For the purposes of engineering immune responses for immunotherapies, this customizability will be essential. Polarizing a T cell toward a regulatory phenotype requires the correct combination of cell types, surface antigen display, surface signaling molecules, and soluble signal transduction, all while being in immunologically relevant locations (e.g. LNs). Biomaterials can be designed with or conjugated with targeting properties to ensure they are delivered to and remain in tissues and cells of interest[75, 170, 171]. Biomaterials can display antigens, antibodies, or other molecules on their surface to interact with cells in their environment[172-174]. Biomaterials can be loaded with specific soluble molecules to attract or deliver their contents to cells[22], and they can be designed to degrade at specific rates or under specific conditions to release their cargo in a controlled manner[175]. And the size, shape

and specific materials used for these applications can provide direct control over the strength and duration of cellular responses[28, 176-178].

3.4.1 Promoting tolerance by targeting APCs

As discussed in **Chapter 3.3**, initiating myelin-specific regulatory T cells could enable tolerance to myelin and reduce inflammatory activity in the CNS. By ensuring anti-inflammatory DC:T cell interactions, TREG phenotypes can be promoted. Importantly, biomaterials can work in several ways to passively or actively target LN or APCs (**Fig. 3.6A**) to allow for this interaction[168]. This targeting allows for control over antigen localization and processing, and for delivery of regulatory immune cues directly to APCs to generate tolerance (**Fig. 3.6B,C**). While biomaterials have been well-studied in the context of drug delivery, cancer therapy, and prophylactic vaccination, they have only recently begun being studied with the goal of developing tolerance[65, 67, 168].

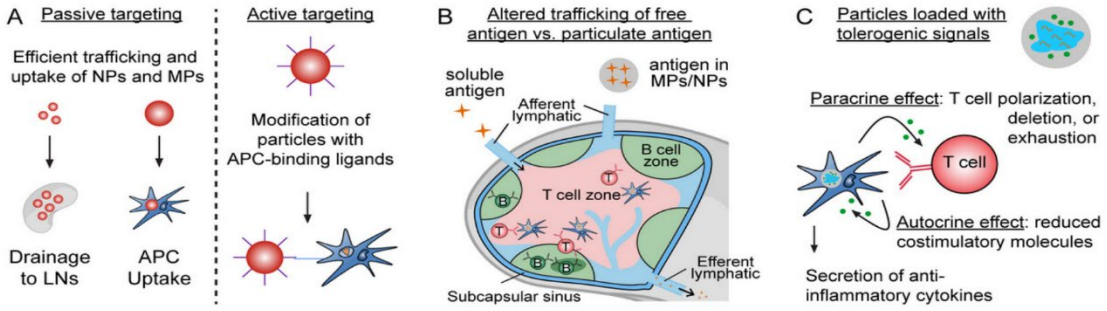

Figure 3.6 Harnessing the potential of biomaterials in targeting APCs to promote immune tolerance.
a. Biomaterials can be used to enhance both passive (draining and peripheral APC uptake) and active (APC-targeting molecules) trafficking to APCs. **b.** Including antigens in MPs/NPs using biomaterials can prolong antigen exposure to APCs and lymphocytes in LNs and reduce clearance from LN. **c.** Loading biomaterials with tolerogenic signals and targeting to APCs promotes anti-inflammatory signaling to T cells and enhances regulatory T cell phenotypes. Reproduced with permission from Tostanoski, **Gosselin**, and Jewell, *Discovery Medicine*, 2016[168].

Chapter **3.3** introduced three ways peripheral tolerance works to keep self-reactive cells from attacking self-tissues. Research is ongoing in each of these three mechanisms of promoting antigen specific tolerance: linking self-antigens to apoptotic cells, promoting T cell anergy, and inducing regulatory T cells.

Several labs have shown that linking myelin self-antigens to apoptotic cells can induce tolerance to myelin in mouse models of MS. For instance, the Miller lab has shown that pulsing splenocytes with myelin peptides, then killing them with a fixative and injecting them i.v. promotes tolerance to myelin in a mouse model of relapsing-remitting MS[179, 180]. This technique was also well-tolerated in humans in a Phase I (safety) clinical trial[181]. This idea has been built upon by other groups, who covalently linked self-antigens to red blood cells, which are relatively short-lived (~ 4 months) and cleared from circulation by splenocytes in a non-inflammatory manner. Pishesha et al. showed that linking self-antigens to blood cells prevented the onset of type 1 diabetes and reversed symptoms of paralysis in mouse models of disease[182].

However, using cells makes a treatment process more complicated, less repeatable, and as a result, more expensive, which could make biomaterials-based treatments particularly useful for this application. Several labs have used approaches that promote anergy in self-reactive T cells, by supplying T cells with antigen presentation from DCs without any co-stimulating, inflammatory factors[106]. For example, the Miller Lab has also conjugated myelin self-antigens to the surface of 500 nm polystyrene beads and degradable 500 nm PLG particles and injected them iv. Treatment promoted T cell anergy, which protected against onset of disease and reverse

paralysis in mouse models of MS[183]. They further went on to refine their PLG particle synthesis, modifying the PLG particles with poly(ethylene-co-maleic acid) as a surfactant and found they could improve myelin peptide coupling efficiency to the ~400 nm particles, which corresponded to better disease protection in a mouse model of relapsing-remitting MS[184]. Further, they saw they could encapsulate myelin in PLG nanoparticles to include self-antigen without chemically linking it, and also see protection from paralysis in vivo[185].

Other groups have taken the approach of conjugating self-antigens to scaffolds and recruiting immune cells to interact with cargo loaded in the scaffolds. For example, the Mooney lab has conjugated a peptide attacked during type 1 diabetes to alginate gels, and shown that injecting the gels without any inflammatory signals allows for the promotion of antigen-specific regulatory T cells in the pancreatic islets[23].

Several groups have even built on the idea of providing self-antigen without inflammatory signals to DCs by adding regulator molecules that promote tolerogenic interactions between DCs and T cells. This method is the basis for this thesis, and is further explained below.

3.4.2 Engineering immune tolerance with self-antigens and regulatory molecules

In addition to adding self-antigens to enhance the selectivity of therapies for autoimmunity, many groups have added tolerogenic molecules to ensure the promotion of antigen-specific regulatory T cells. For example, Yeste et al conjugated a myelin peptide (MOG) and an aryl hydrocarbon receptor ligand (ITE) that promotes T_{REGS} in vivo and in vitro to gold nanoparticles (NPs). These NPs were able to ameliorate

symptoms in a mouse model of progressive MS when administered weekly by intra-peritoneal injection[186]. In another study, Maldonado et al. encapsulated a myelin peptide and rapamycin, an immunomodulator that promotes TREGS, into degradable polymer NPs. When injected intravenously, these NPs significantly reduced disease in a mouse model of relapsing-remitting MS[187].

The Jewell lab has shown that delivering myelin peptides with GpG, a regulatory signal that works against one of the DC's innate pathogen detection molecules, promotes regulatory T cells and provides protection against a progressive model of MS. This has been shown for both micron-size immune polyelectrolyte multilayer capsules that are picked up by APCs and trafficked to LN[188] and for nano-sized polyplexes that passively drain to the LN[189].

The Jewell lab has also previously shown that a single treatment of PLGA microparticles (3-4 μm in diameter) loaded with MOG and rapamycin injected into lymph nodes of mice with a progressive model of MS promoted TREGS and permanent, systemic tolerance to myelin[26]. The work presented in this thesis builds on this idea of intra-lymph node delivery, which is presented in more detail below.

3.5 Intra-lymph node delivery of tolerogenic cargo from polymer particles offers a new therapeutic strategy for autoimmune disease

As LNs are the sites that initiate adaptive immunity, vaccine and immunotherapy strategies require trafficking of cargo to LN. To improve the delivery of cargo to LN, recently, an intra-LN (iLN) injection technique has recently been tested in clinical trials with traditional soluble antigens using ultrasound guidance, and has

shown promise for allergen therapy[190-192], cancer[193, 194], and recently, type I diabetes[70]. However, these soluble cargo are rapidly drained from- LNs, resulting in limited exposure of immune cells in LNs to cargo. To enhance cargo persistence in LN, soluble cargo can be encapsulated in microparticles that degrade slowly and are too large to drain from LN[24].

The Jewell lab has developed a direct injection technique to deliver polymer microparticles (MPs) to LNs of mice without requiring surgery (**Fig. 3.7**)[24, 26, 195, 196]. To enable LN visibility, a small volume of tracer dye is injected subcutaneously at the tail base. The dye drains to the LNs, which can then be visualized through the skin for injection. Using this technique, we recently showed that a single iLN injection of MPs containing myelin self-antigen (MOG) and rapamycin (Rapa) prior to disease onset prevents paralysis in a mouse model of progressive MS (EAE) (**Fig 3.8A**)[26]. In this model, disease scoring is as follows: 0, no paralysis; 1, tail paralysis; 2, partial hind limb paralysis; 3, total hind limb paralysis. We found that while Empty and Rapa MPs did not provide any disease protection, MPs combining MOG and Rapa showed a synergistic effect, with a significant reduction in disease related paralysis when

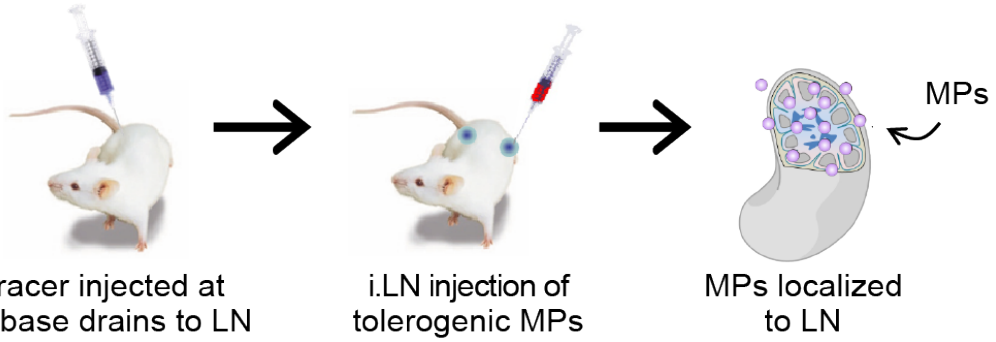

Figure 3.7 MPs can be injected iLN non surgically due to LN visualization following tracer dye injection.
Reproduced with permission from Andorko et al, *Journal of Visualized Experiments*, 2014[195].

compared to MOG MPs (**Fig. 3.8A**). Interestingly, we also saw a significant effect with MOG MPs. This effect was also antigen specific, as treatment with MPs containing an irrelevant antigen (ovalbumin, OVA) and Rapa MPs provided no protection (**Fig. 3.8B**). Importantly, iLN treatment with MOG/Rapa MPs at peak disease reversed paralysis and provided a permanent reduction in disease severity. Of note, altering the environment of a single LN by treating with MOG/Rapa MPs provided systemic, but antigen-specific tolerance. This outcome was underpinned by increased T_{REG} in treated LNs and in distant, untreated CNS-draining LNs (**Fig. 3.8C**). T cell infiltration in the CNS was also reduced (**Fig. 3.8D**).

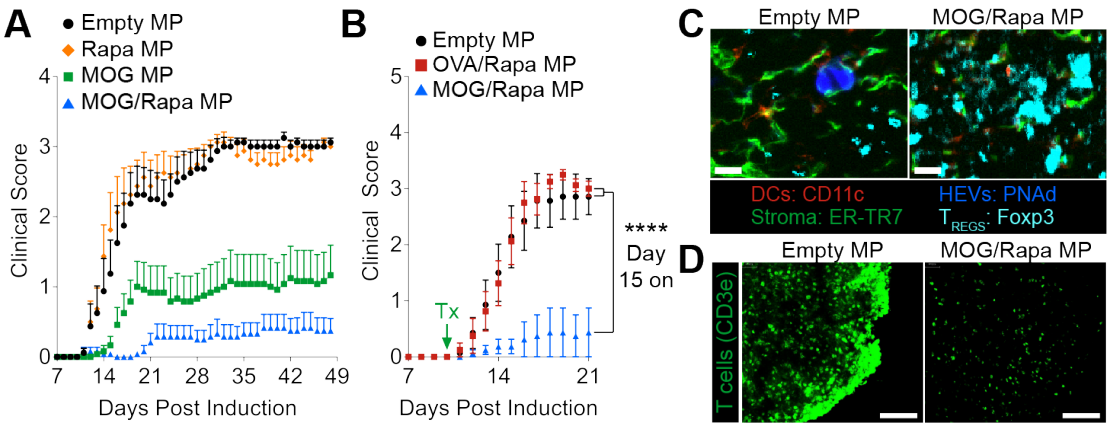

Figure 3.8 iLN treatment with MOG/Rapa depots prevents disease onset in a model of progressive MS.
a. MOG/Rapa MP treatment on day 10 provides synergistic protection compared to MOG or Rapa MPs. **b.** Treatment MPs loaded with irrelevant antigen (OVA) and Rapa do not prevent disease, suggesting tolerance is antigen-specific. **c.** Treatment with MOG/Rapa MPs results in increased TREGS in distant CNS-draining LNs (scale bar, 10 μm), and reduced T cell infiltration in CNS (scale bar, 100 μm) **d**. Adapted from Tostanoski et al, *Cell Reports,* 2016[26] with permission from Elsevier.

These results are striking, as one iLN treatment with MOG/Rapa MPs provided permanent protection against disease. However, the majority of patients present with relapsing-remitting MS, so to make this therapy relatable to most cases of human

disease, I applied this platform to a relapsing-remitting MS model (RR-EAE). Using this model, I tested this iLN delivery platform in a relapsing-remitting model of MS (RR-EAE), in which mice become reactive to different sections of myelin over time, causing relapse. This model better mimics the type of disease that impacts a much larger number of MS patients. I also investigated the epitope spreading of disease, and how disease progresses when protection is conferred to an epitope at an earlier disease stage. This is critical, and cannot be studied in a progressive model of MS. This work, presented in **Chapter 5**, showed that across both progressive and relapsing-remitting disease, one tolerogenic intra-LN treatment promoted long-lasting improvements in disease-induced paralysis. Tolerogenic MPs delivered prior to symptom onset promoted tolerance and protected against disease. Treatment at peak disease reversed paralysis and prevented relapse, while treatment during relapse limited disease progression. Strikingly, mice vaccinated against a foreign protein on the same day as intra-LN treatment generated protein-specific T cells and antibodies at similar levels to healthy vaccinated mice, while simultaneously exhibiting significantly reduced paralysis – highlighting the myelin-specific nature of this therapy.

However, clinical translation of biomaterials-based immunotherapies requires investigation into manufacturing, preservation, storage, and stability of this immunotherapy. Even well-established materials such as PLGA MPs have ongoing issues for clinical translation in therapeutic contexts. While PLGA is commonly used in humans – degradable sutures for example, the degradation hydrolysis products - lactic acid and glycolic acid, can be metabolized by cells[197, 198]. Further, any type of storage of particles in an aqueous state requires consideration of unwanted cargo

release, particle aggregation and fusion, and how effectively cargo integrity is maintained during storage[199]. As such, the stability, transport, and storage of immunotherapeutic particles formed from degradable biopolymers is an important focus area. Thus, the work presented in **Chapter 6** tested the impact of lyophilization (freeze-drying) and excipients (stabilizing molecules) on MP stability after storage. Lyophilization with low concentrations of excipients significantly improved MP stability and formulation recovery after reconstitution. Storage for 5 months at room temperature did not negatively impact cargo loading, MP size, or biofunctionality. MP formulations with excipients could deactivate inflammatory signaling and restrict myelin-specific immune cell proliferation as well as formulations without excipients.

Together, these studies motivate the development of intra-LN delivery of tolerogenic MPs as a potential MS immunotherapy for clinical translation. As a first step, in **Chapter 4**, I started with investigating the immunomodulatory cue to include in the tolerogenic MP therapy to safely and efficiently bias myelin-specific immune cells away from inflammatory phenotypes and toward regulatory phenotypes. **Chapter 4** leverages primary cell co-cultures to lay the groundwork for translational studies in later chapters. In addition, this chapter explains many of the biomaterial synthesis techniques and characterization methods used to evaluate microparticle-mediated immune cargo delivery that will be used throughout this work.

Chapter 4: Controlled Release of Second Generation mTOR Inhibitors to Restrain Inflammation in Primary Immune Cells[2]

4.1 Introduction

As introduced in **Chapter 3.2**, autoimmune disease occurs when the immune system incorrectly targets the body's own tissue. Inflammatory CD4+ T cell phenotypes, such as T_H1 and T_H17, are key drivers of this attack. Recent studies demonstrate treatment with rapamycin—a key inhibitor of the mTOR pathway—can skew T cell development, moving T cell responses away from inflammatory phenotypes and toward regulatory T cells (T_{REGS}). T_{REGS} are important in inducing and maintaining tolerance to self-antigens, creating new potential to treat autoimmune diseases more effectively and specifically. Next generation analogs of rapamycin, such as everolimus and temsirolimus, confer increased potency with reduced toxicity, but are understudied in the context of autoimmunity. Further, these drugs are still broadly-acting and require frequent treatment due to short half-lives. Thus, there is strong interest in harnessing the unique properties of biomaterials—controlled drug release and targeting, for example, to improve autoimmune therapies. Using second generation mTOR inhibitors and rapamycin, we prepared sets of degradable polymer particles from poly(lactide-co-glycolide). We then used these materials to assess physicochemical properties and the ability to control autoimmune inflammation in a primary cell co-culture model. Treatment with particle formulations resulted in significant dose-dependent decreases in dendritic cell activation, T cell proliferation,

[2] Adapted with permission from Springer Nature from: **E.A. Gosselin**, L.H. Tostanoski, and C.M. Jewell, "Controlled Release of Second Generation mTOR Inhibitors to Restrain Inflammation in Primary Immune Cells." *The AAPS Journal* 2017, 19(4): 1175-1185.

inflammatory cytokines, and frequencies of inflammatory T_H1 phenotypes. Considering the current limitations of rapamycin, and the potential of next-generation analogs, this work provides a screening platform for biomaterials and sets the stage for in vivo evaluation, where delivery kinetics, stability, and targeting could improve autoimmune therapies through biomaterial-enabled delivery.

4.2 Background

The molecular target of rapamycin (mTOR) pathway is a central pathway regulating cell growth and metabolism[200, 201]. Not surprisingly, the mTOR pathway has been studied fundamentally and exploited translationally in areas from human development to cancer, transplantation, and autoimmunity[187, 200, 202-204]. One of the central inhibitors of mTOR, rapamycin (Rapa) is approved, as a long-standing immunosuppressant to limit transplant rejection, and as a coating for coronary stents[202]. Rapa is also in clinical trials for use as a cancer therapeutic[203], and in clinical and preclinical trials as a treatment for autoimmune diseases[26, 153, 187, 205-208]. Newer generations of Rapa, "Rapalogs," have been developed to improve efficacy through increased potency, improved solubility, and altered pharmacokinetics[209]. Some of these rapalogs, including everolimus (Evero) and temsirolimus (Tems), have been approved for use as cancer therapeutics, and others are in clinical or pre-clinical trials[209-214]. In several of these cases, rapalogs work as well as or better than Rapa to reduce cell proliferation, and range in application from preventing stent failure in coronary artery disease[215], to enhancing allograft survival after transplant[216], treating nephropathy[217], and reducing prostate cancer cell proliferation[218].

One area where rapalogs have great potential, but where clinical applications lag behind the areas above, is autoimmunity. Autoimmune diseases occur when the immune system incorrectly targets the body's own tissues. In the case of multiple sclerosis (MS), myelin, which surrounds and protects nerves in the central nervous system, is attacked by immune cells, causing neurodegeneration and inflammation. A key cell population in this attack are myelin-specific $CD4^+$ T cells, whose inflammatory subsets help drive disease[129, 130]. These subsets include T_H1 and T_H17 cells, which also promote other immune responses, including $CD8^+$ cytotoxic T cells, antibody production by B cells, and complement activation; all of these cause damage to myelin[130].

For inflammatory $CD4^+$ T cells to develop, myelin-specific $CD4^+$ T cells must undergo clonal expansion after being activated by dendritic cells (DCs) or other antigen presenting cells (APCs) in the lymph node. T cells must receive two signals – antigen presentation and co-stimulation[219]. This co-stimulatory signal is partially regulated by the mTOR pathway, which integrates immune and microenvironmental cues to determine the fate of the T cell [158, 220]. These signals, which include cytokines, growth factors, energy, nutrients, and oxygen, must be considered, as rapid T cell expansion and effector functions require significant metabolic activity. mTOR helps direct T cells to become either activated, effector cells (T_H1 and T_H17) or regulatory cells (T_{REGS})[158, 219, 220]. Without mTOR activity to promote expansion, $CD4^+$ T cells differentiate toward a higher frequency of T_{REGS}, which are important in maintaining tolerance and moderating autoimmune disease[221-224].

Despite the potential of targeting mTOR, Rapa and many rapalogs are poorly water soluble, require frequent administration for efficacy, and are broadly immunosuppressive. For example, in mice with experimental autoimmune encephalomyelitis (EAE), a model of MS, intraperitoneal treatment with Rapa is required at least every 3 days to reduce disease symptoms. When Esposito et al. stopped treatment, the mice became paralyzed and exhibited no improvement compared with untreated mice with EAE[153, 205]. In addition, oral gavage treatments using Evero for treatment of experimental autoimmune neuritis and uveoretinitis also involved daily administration[225, 226]. Thus, great interest has developed in combining mTOR inhibitors or other small molecule immunomodulators with biomaterials to deliver these tolerogenic signals with improved targeting, release kinetics, and stability. These advances could enhance both the selectivity and effectiveness of new therapies by altering disease progression, either by delaying disease onset or reducing severity of symptoms[105, 168, 183, 184, 227, 228]. Further, coupling rapalogs with delivery of self-antigen also appears to create new potential for long-term, curative therapies for MS or other antigen-specific autoimmune diseases[26, 187].

Biomaterial carriers offer several advantages over soluble treatments, including cargo protection, controlled release of cargo, encapsulation and release of multiple immune signals, and targeting to specific immune cells or tissues[105, 168]. Recently, biomaterial carriers have been used to generate tolerance to self-antigens in the context of autoimmunity[26, 66, 168, 183, 186, 187, 189, 207, 227, 229]. For instance, the Miller Lab has shown that altering how self-antigen is presented to the immune system can reduce or reverse paralysis during relapsing-remitting EAE[183]. This was accomplished by linking myelin

peptide self-antigen to polymer particles and administering the particles intravenously. The Quintana Lab developed gold nanoparticles that could encapsulate both myelin antigens and 2-(1′H-indole-3′-carbonyl)-thiazole-4-carboxylic acid methyl ester (ITE), a tolerogenic small molecule. These nanoparticles induced T_{REG} generation after treatment, which resulted in lower disease severity in mice induced with EAE[186]. A large focus has also been placed on combining Rapa with self-antigens to modulate an immune response specific to the antigen[26, 187]. Maldonado et al. have shown that by treating mice systemically with Poly(D,L-lactide-co-glycolide) (PLGA) nanoparticles incorporating Rapa and an antigen, a tolerogenic response can be initiated—T_{REGS} can be generated, and the inflammatory immune response can be modulated[187]. Our lab has shown that local delivery of microparticles co-loaded with Rapa and myelin self-antigen can reprogram the local microenvironment of this tissue. The impact of this alteration is tolerance that is systemic and myelin-specific, resulting in reversal of disease symptoms[26, 195]. However, to date, little work exists using biomaterials to delivery rapalogs for the treatment of autoimmune disease.

Since delivery of rapalogs with biomaterials has great potential, but is understudied, we used PLGA particles to encapsulate either Rapa or one of two important second-generation Rapa analogs, Evero and Tems. Using these formulations, we studied the ability of rapalog-loaded microparticles (MPs) to restrain inflammatory responses in a myelin-driven co-culture model of autoimmune inflammation. We show that each drug loads at similar levels in the particles, yields similarly sized particles, and releases drugs at similar rates. Further, all three particle types reduce DC activation, proliferation of myelin-reactive transgenic T cells, and secretion of inflammatory

cytokines. These reductions occur in a dose-dependent manner and polarize T cell differentiation, decreasing the frequency of inflammatory T_H1 phenotypes. This work supports future pre-clinical and clinical development aimed at evaluating key differences in efficacy of rapalogs formulated in biomaterials in the context of autoimmunity and tolerance.

4.3 Materials and Methods

4.3.1 MP Synthesis

MPs were generated using a water/oil/ water emulsion as previously described[24, 26]. The inner aqueous phase was made using 500 μL of water, while the oil phase was made of 80 mg of PLGA (Durect) in 5 mL of dicholoromethane. The different drugs, Rapa, Evero, and Tems (LC Laboratories) were loaded at 2 mg into the oil phase before mixing. The water and solvent mixture was sonicated for 30 s at 12 W. The emulsion was then homogenized with 40 mL of 2% w/v polyvinyl alcohol (Sigma) for 3 min at 16,000 RPM. The particles were then placed on a stir plate for 16 h to allow solvent evaporation, after which they were poured through 40-μm cell strainers into 50 mL conical tubes, and centrifuged for 5 min at 5000 g and 4°C. The particles were then washed three times in 1 mL of water, centrifuging between washes to collect the particles. The particles were then resuspended in water. MPs used for comparisons between free drug and drug-loaded MPs were generated using 8-mg drug input.

4.3.2 MP Characterization.

MPs were characterized for size, zeta potential, yield, loading, and release. Size of MPs was determined using laser diffraction (Horiba LA-950), and zeta potential was

measured using a Malvern Zetasizer Nano ZS90. MP morphology and size distribution were evaluated by scanning electron microscopy (SEM) using a Hitachi SU70 SEM. To determine the yield, known volumes of the MP suspensions were dried under air, and the mass of the dried MPs was used to calculate yield. Loading was measured using UV/Vis spectrophotometry after dissolving dried MPs in dimethyl sulfoxide and comparing absorbance measurements to a standard curve to determine drug concentration. Encapsulation efficiency was determined by normalizing measured loading to drug input. Kinetic release from particles was measured at sink conditions. MPs were placed in a volume equal to 125% of the solubility limit for the drug loaded in the MPs, mixed well, and incubated at 37°C. At each time point, the MPs were centrifuged for 5 min at 500×g and 4°C, and a 1 mL aliquot of the supernatant was taken to measure drug released using UV/Vis spectrophotometry as when measuring the loading. The aliquot was then returned to the MPs and mixed well.

4.3.3 DC Activation

All animal care and use was conducted in full compliance with local, national, ethical, and regulatory principles and local licensing regulations, per the Association for Assessment and Accreditation of Laboratory Animal Care (AAALAC) expectations for animal care and use/ethics. To evaluate DC activation, DCs were removed from spleens of female C57BL/6J mice (The Jackson Laboratory) with positive selection for CD11c using a magnetic isolation kit according to manufacturer's instructions (Miltenyi). DCs were plated at 100 K cells per well into a 96 well plate, and cultured with RPMI1640 media (Lonza), supplemented with 10% fetal bovine serum (Corning), 2 mM L-glutamine (Gibco), 55 μM βmercaptoethanol (Sigma-Aldrich) 1 X Non-

Essential Amino Acids (Fisher Scientific), 10 mM HEPES (Fisher Scientific), and 1 X Pen/Strep (Gibco). Media and media stimulated with lipopolysaccharide (LPS) (Invitrogen) at 1 μg/mL wells were used as controls for low and high activation levels, respectively. All samples were treated with LPS to induce activation and then treated with drug-loaded MPs in an effort to reduce activation levels. The wells at the highest dose were treated with 50 μg of particles, with serial 10× dilutions. The cells were incubated for 16 h, after which they were stained for activation. This staining first involved blocking the cells using Fc block (BD Biosciences), then staining with anti-CD40, anti-I-A/I-E, anti-CD86, antiCD80 (BD Biosciences), and resuspending in 4′,6-Diamidino-2- Phenylindole, Dihydrochloride (DAPI). The cells were then run through flow cytometry using a Canto II (BD Biosciences) to evaluate levels of activation and viability, as measured by percent of parent and mean fluorescence intensity (MFI). In comparisons between free drug and rapalog-loaded MPs, the wells at the highest dose were treated with 250 μg of particles and drug matched, with serial 5× dilutions. All flow cytometry data analysis was completed using Flowjo software (Tree Star).

4.3.4 Transgenic T Cell Proliferation

To measure T cell proliferation specific to the self-antigen myelin oligodendrocyte glycoprotein (MOG) peptide (MEVGWYRSPFSRVVHLYRNGK, Genscript), a DC/T cell co-culture was used. DCs were collected and plated as in DC activation and cultured for 16 h. $CD4^+$ T cells were collected from the spleens of transgenic "2D2" mice, C57BL/6-Tg(Tcra2D2,Tcrb2D2)1Kuch/J (The Jackson Laboratory), in which all T cells are specific for MOG, with negative selection using a magnetic isolation kit according the manufacturer's instructions (STEMCELL

Technologies). T cells were stained with carboxyfluorescein succinimidyl ester (CSFE) for a fluorescence dilution assay and were plated at a 3:1 T cell to DC ratio, with 300 K cells added to each well. In addition to the media and media + LPS controls that were included in the DC activation, media +MOG and media + MOG + LPS controls were included, allowing for low and high proliferation controls. All samples were treated with LPS and MOG to induce activation and antigen presentation and then treated with drug-loadedMPs to reduce proliferation. Samples were cultured for an additional 72 h and then blocked and stained with anti-CD4 (BD Biosciences) and DAPI. The cells were then run through flow cytometry to evaluate levels of proliferation and viability. In comparisons between free drug and rapalog-loaded MPs, the wells at the highest dose were treated with 250 μg of particles and drug matched, with serial 5× dilutions.

4.3.5 Cytokine Secretion

Enzyme-linked Immunsorbent Assays (ELISAs) were completed following manufacturer's instructions (BD Biosciences) to determine IL-17 and IFN-γ cytokine secretion. Media was collected from co-culture samples and evaluated at 10× dilutions for IFN-γ and 2× dilutions for IL-17.

4.3.6 T Cell Phenotypes

To measure T cell phenotype, a DC/T cell co-culture was used as in the T cell proliferation assay. DCs were collected as in DC activation and plated at 100 K cells per well in a 96 well plate and cultured for 16 h. $CD4^+$ T cells were collected as in the T cell proliferation and plated at a 3:1 T cell to DC ratio, with 300 K cells added to each well. Media, media + LPS, media + MOG, and media + MOG + LPS controls were included. All samples were treated with LPS and MOG to induce activation and

antigen presentation and then treated with drug-loaded MPs. Samples were cultured for an additional 72 h. Following the incubation, cells were blocked and stained for CD4 and CD25 (BD Biosciences), then fixed and permeabilized, and stained for T-bet (BD Biosciences). The cells were then run through flow cytometry to evaluate levels of markers for phenotype.

4.3.7 Statistics

Statistical tests were performed using GraphPad Prism software. Analysis of Variance (ANOVA) was used to compare three or more groups, and t tests were used to make comparisons between two groups. All error bars in figures represent SEM and p values ≤ 0.05 were indicated significant. For each experiment, at each concentration of MPs, comparisons were made to a positive control treatment, and included all control treatments, empty MP treatments, and drug-loaded MP treatments. Six comparisons were run per figure (one at each dilution).

4.4 Results

4.4.1 MPs Allow Tunable Loading and Controlled Release of Rapalogs

MPs were first formulated with each drug, which have similar structures but variations at one carbon position in the lactone ring (**Figure 4.1**). For each MP formulation, the particle yield, diameter, zeta potential, drug loading, and drug encapsulation efficiency were measured as summarized in **Table 4.1**. Each particle type exhibited similar yields, ranging from 66.9% ± 0.8% (Tems) to 69.5% ± 0.3% (Rapa). Drug loading levels were also similar, with Evero and Tems loading at 15.2 ± 0.1 and

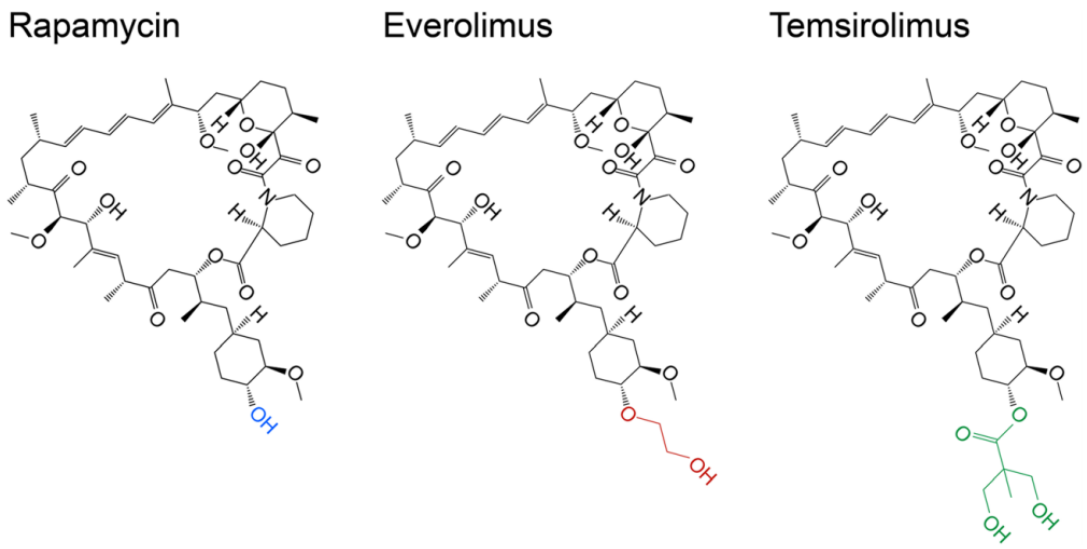

Figure 4.1 Structures of rapamycin and the rapalogs everolimus and temsirolimus
Figure reproduced with permission from Springer Nature.

15.3 ± 0.1 μg drug/mg particles and Rapa at 19.3 ± 0.1 μg drug/mg particles, respectively. Encapsulation efficiencies varied between 34.3% ± 1.4% for Tems and 52.8% ± 0.5% for Rapa. Zeta potentials for the four formulations were similar, ranging from −26.10 ± 0.68 mV to −26.47 ± 1.33 mV across the drug cargos. The particle diameters ranged from 2.34 ± 0.04 μm (Tems) to 3.83 ± 0.02 μm (Empty). The size

Table 4.1 Rapalog-Loaded Microparticle Characterization

	Polymer Core		Drug Loading	
	% Yield	Diameter (μm)	μg drug/ mg polymer	Encapsulation Efficiency (%)
Empty MPs	67.7 ± 1.1	3.83 ± 0.02	N/A	N/A
Rapa MPs	69.5 ± 0.3	2.86 ± 0.02	19.3 ± 0.1	52.8 ± 0.5
Evero MPs	67.7 ± 0.3	3.59 ± 0.07	15.2 ± 0.1	40.4 ± 0.4
Tems MPs	66.9 ± 0.8	2.34 ± 0.04	15.3 ± 0.1	34.3 ± 1.4

N/A indicates that there was no drug loading in these particles

distributions are shown in **Figure 4.2a**, and the expected spherical morphologies are evident in the images of **Figure 4.2b**. Kinetic drug release studies at sink conditions revealed similar release profiles across the drug formulations (**Figure 4.2c**).

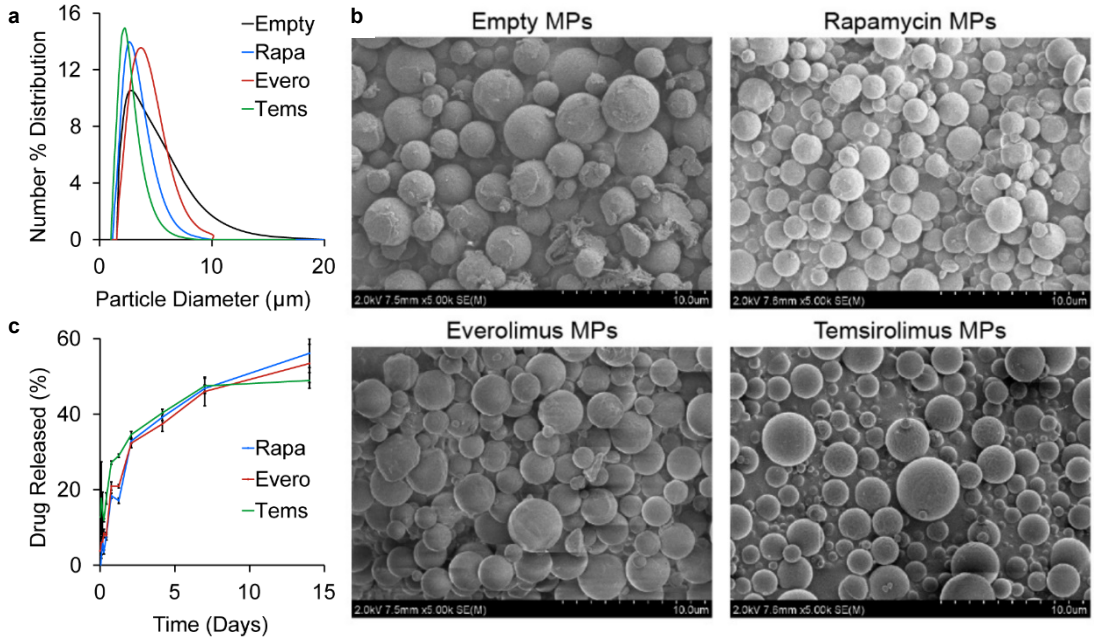

Figure 4.2 Rapalog MPs have similar characteristics when compared to Rapa MPs
a. Representative size distributions show that Rapa-loaded MPs are similar in size to Evero- and Tems-loaded MPs. **B.** Representative size distributions show that Rapa-loaded MPs are similar in size to Evero- and Tems-loaded MPs. **c.** Similar release profiles for drugs from PLGA MPs are shown over two weeks in sink conditions. Figure reproduced with permission from Springer Nature.

4.4.2 Drug-Loaded MPs Reduce Expression of Key Markers of DC Activation

To test the impact of rapalog-loaded MPs on DC function, we first cultured DCs with LPS, a strong inflammatory signal, and treated with MPs at a range of dilution factors (DF) for 16 h. Cells were then stained and analyzed by flow cytometry. First, we assessed the viability of the cells after treatment, which revealed only minor variations (**Figure 4.3a**). While there were some significant differences in viability due to the high level of consistency across measurements, the magnitude of the differences

was small, indicating treatment with MPs did not cause any important differences in viability. As expected, media samples were low compared to other samples due to the lack of stimulation. DC activation was studied by assessing the expression levels of key activation markers, including CD80, CD86, CD40, along with I-A/I-E as an indicator of antigen presentation complexes. In the case of all activation markers, media controls showed very little activation, while LPS controls indicated the expected high levels of activation. MP-treated samples were also treated with LPS, allowing reductions in activation levels to be measured. At the highest concentration, 1×, all drug-loaded MPs significantly reduced CD80 expression compared with LPS-treated samples ($p < 0.0001$ ****). At the 10× dilution, Evero ($p < 0.0001$****) and Tems ($p < 0.01$**), the rapalogs caused significantly lower CD80 expression (**Figure 4.3b**). Significant decreases were also observed at the 100× dilution for Evero ($p < 0.001$***) and Tems ($p < 0.01$**). For CD86, at the highest concentration (1×), all drug-loaded MPs significantly reduced expression compared with samples treated with LPS alone with Rapa $p < 0.01$**, and Evero and Tems $p < 0.0001$**** (**Figure 4.3c**). At the 10× dilution for Evero ($p < 0.001$***) and Tems ($p < 0.05$*), and at the 100× dilution for Evero ($p < 0.01$**), the drug-loaded MPs also caused significantly lower CD86 expression. With the case of CD40 activation, at the highest concentration (1×), all drug-loaded MPs drove significantly lower CD40 expression compared with the LPS-treated samples (Rapa $p < 0.001$***, Evero, and Tems $p < 0.0001$****) (**Figure 4.3d**). Differences in CD40 activation were also significant at the 105 dilution for all drugs ($p < 0.001$***). For all drugs, significant differences in IA/I-E MFI between LPS-treated control and MP-treated samples were only observed for the 1× dilution ($p < 0.01$**)

(**Figure 4.3e**). In a subset of studies, we compared the toxicity to DCs of rapalogs delivered in either MP form or a matched dose of free drug (**Figure 4.4**). These studies revealed drug-loaded MPs were significantly less toxic compared to free rapalogs.

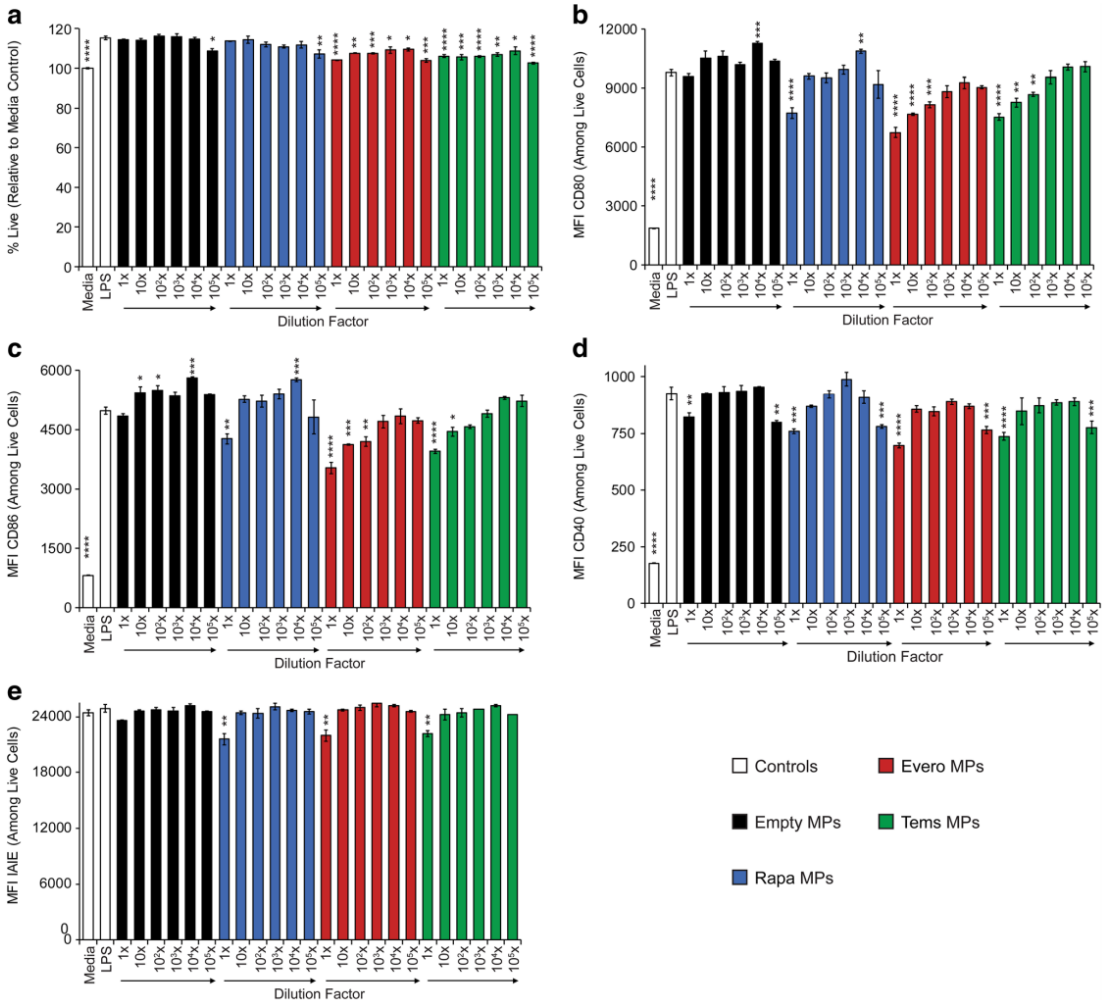

Figure 4.3 Rapalog MP treatment reduces DC activation in a primary immune cell culture after stimulation

a. Treatment with all MPs over a range of concentrations does not affect cell viability compared to media control. At the highest concentrations of drug-loaded MP treatments, Evero and Tems MPs reduce DC activation similarly to Rapa MPs when compared to an LPS-stimulated control. Activation was quantified by assessing levels of **b** CD80, **c** CD86, **d** CD40, and **e** I-A/I-E for antigen presentation. DCs from wild-type mice were collected and left untreated, treated with LPS, or treated with an equivalent dose of LPS and indicated dilutions of MPs. Samples were cultured for 16 h before analysis. MP-treated samples were compared to LPS - treated controls using ANOVA at each dilution (* indicates $p \leq 0.05$, ** $p \leq 0.01$, *** $p \leq 0.001$, **** $p \leq 0.0001$). The legend applies to all panels in the figure. Figure reproduced with permission from Springer Nature.

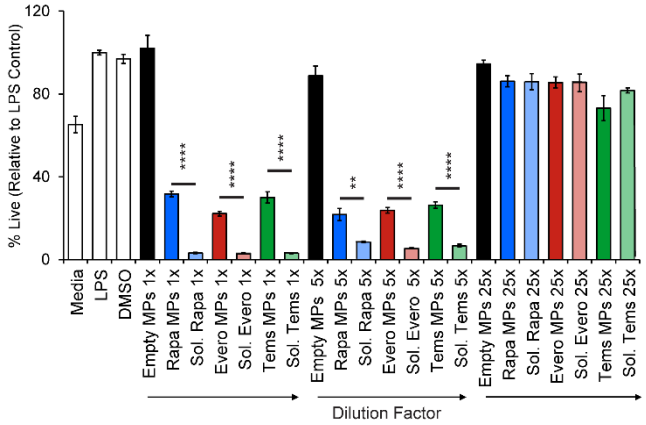

Figure 4.4 Rapalog MPs exhibit lower toxicity compared to free rapalog treatment. DC treatment with rapalogs shows lower toxicity for rapalog-loaded MPs than free drug treated samples with matched drug dose over a range of concentrations. MP-treated samples were compared to free drug treated samples using t-tests at each dilution (** indicates $p \leq 0.01$, **** $p \leq 0.0001$). Figure reproduced with permission from Springer Nature.

4.4.3 Rapalog MPs Restrain CD4+ T Cell Proliferation in a Transgenic Co-Culture Model

Next, we tested the hypothesis that the reduced DC activation seen in **Figure 4.3** would correlate to reduced T cell effector activity and inflammatory function. For these studies, $CD4^+$ T cells were isolated from "2D2" mice, a strain where all T cells have T cell receptors that are reactive to MOG. Thus, if these cells encounter MOG in the presence of co-stimulation from activated DCs, they proliferate into inflammatory effector T cells. The isolated T cells were fluorescently labeled with CSFE dye then co-cultured for 72 h with DCs that had been treated with LPS, MOG, and rapalog MPs. Compared to the media only sample, treatments had little impact on cell viability (**Figure 4.5a**). As above, while some significant differences in viability were observed, these were due to the consistency of the data. CFSE MFI was evaluated for each of the samples, with lower MFIs corresponding to higher proliferation as the dye is diluted during successive rounds of cell division. At 1, 10, and 100× dilutions, samples treated with Rapa, Evero, and Tems MPs had significantly higher MFIs ($p < 0.0001$****) than

the MOG + LPS-treated samples, with no significant difference between the Empty MP-treated samples and the MOG + LPS-treated samples (**Figure 4.5b**). In addition, the MFIs for the 1000× dilutions were also significantly higher than the MOG + LPS-treated samples (Rapa p< 0.001***, Evero and Tems p< 0.01**). The percentage of cells proliferated beyond generation 0 was also assessed. For the 1, 10, 100, and 1000× dilutions, the drug-loaded MPs all significantly restrained proliferation compared to the MOG + LPS-treated samples (p< 0.0001****)(**Figure 4.5c**). Only the Rapa MP-treated samples at the 104×dilution showed significantly restrained proliferation compared to the MOG + LPS-treated samples (p< 0.01**).We also tested the ability of rapalogs to restrain T cell proliferation by directly comparing matched doses of rapalogs in either MP form or free form (**Figure 4.6**). These studies revealed MPs restrained proliferation significantly more compared to equivalent dose of free drug.

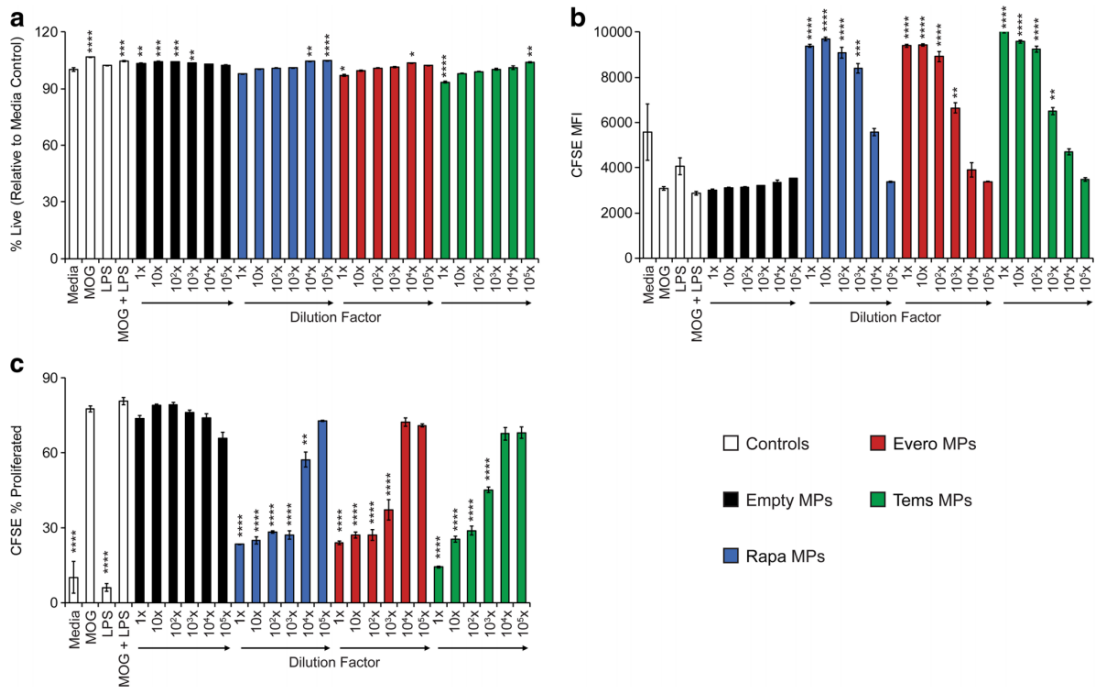

Figure 4.5 Rapalog MPs restrain T cell proliferation in a primary immune cell co-culture after stimulation with antigen and adjuvant.

a. Treatment with all MPs over a range of concentrations does not affect cell viability compared to media control. At the highest concentrations of drug-loaded MP treatments, Evero and Tems MPs restrain MOG-specific CD4+ T cell proliferation similarly to Rapa MPs after stimulation with LPS and MOG, as can be quantified by **b,** mean fluorescence intensity (MFI) and **c,** proliferation past generation 0. MOG-specific CD4+ T cells were collected from spleens of transgenic "2D2" mice, labeled using a proliferation dye, CFSE, and cultured for 72 h with DCs from wild-type mice that had been left untreated, treated with MOG and/or LPS, or treated with equivalent doses of MOG and LPS and indicated dilutions of MPs for 16 h. After co-culture, cells were analyzed for proliferation based on dilution of the dye. MP-treated samples were compared to MOG and LPS - treated controls using ANOVA at each dilution (* indicates $p \leq 0.05$, ** $p \leq 0.01$, *** $p \leq 0.001$, **** $p \leq 0.0001$). The legend applies to all panels in the figure. Figure reproduced with permission from Springer Nature.

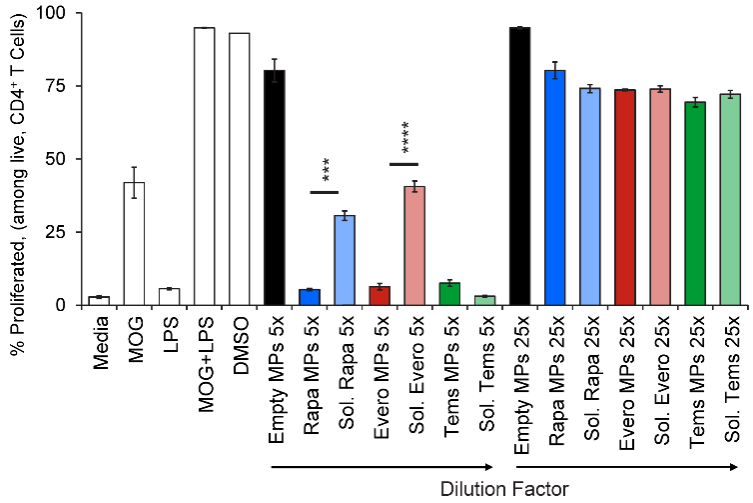

Figure 4.6 Rapalog MPs exhibit enhanced anti-inflammatory properties compared to free rapalog treatment
In a primary immune cell coculture after stimulation with an antigen and adjuvant, treatment with rapalog-loaded MP samples restrain inflammatory proliferation past G0 more than free drug treated samples at the same dose. MP-treated samples were compared to free drug treated samples using t-tests at each dilution (*** indicates $p \leq 0.001$, **** $p \leq 0.0001$). Figure reproduced with permission from Springer Nature.

4.4.4 Drug-Loaded MPs Reduce Inflammatory Cytokine Secretion in a Transgenic Co-Culture Model

Supernatants from the T cell proliferation study were next analyzed for secretion of inflammatory cytokines IFN-γ (T_H1 response) and IL-17 (T_H17 response) as a measure of changes in T cell function. IL-17 secretion was significantly reduced by all drug-loaded MPs at the 1× (Rapa $p < 0.05$*, Evero, and Tems $p < 0.01$**), 10×

($p < 0.01$**) and 100× ($p < 0.01$**) dilutions and reduced at the 1000× dilution ($p < 0.05$*) by Rapa-loaded MPs (**Figure 4.7a**) IFN-γ secretion was also significantly reduced for the samples treated with all drug loaded MPs at the 1, 10, 100, and 1000× dilutions ($p < 0.0001$****) (**Figure 4.7b**), and was significantly reduced at the 10^4 × dilution by Rapa-loaded MPs.

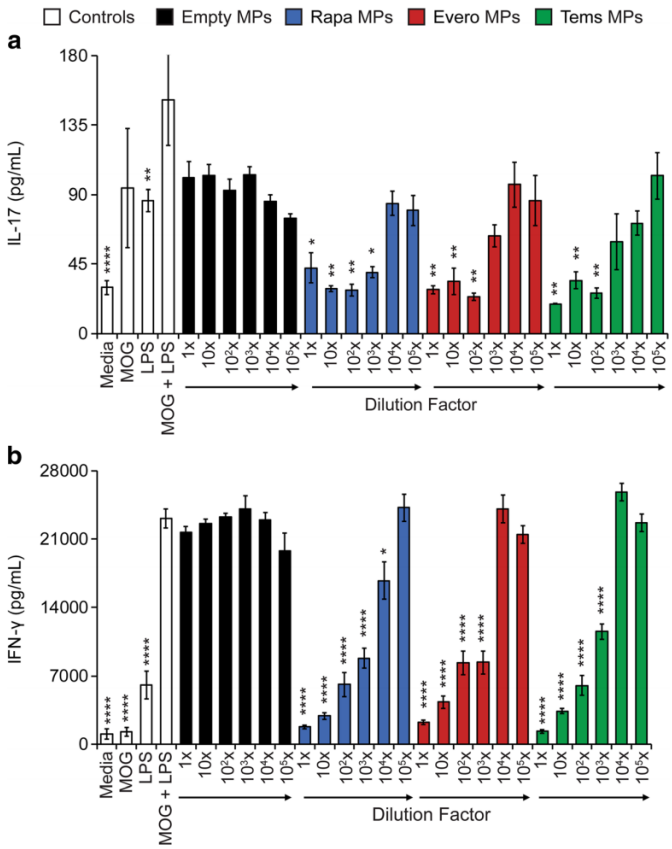

Figure 4.7 Rapalog MP treatment decreases inflammatory cytokine secretion in co-culture after stimulation

a, IL-17 and **b,** IFN-γ levels were analyzed to study T_H17 and a T_H1 CD4+ T cell responses, respectively. ELISAs were used to analyzed media samples collected from "2D2" co-cultures, with supernatants collected after 72 h of co-culture. MP-treated samples were compared to MOG-and LPS-treated controls using ANOVA at each dilution (* indicates $p \leq 0.05$, ** $p \leq 0.01$, **** $p \leq 0.0001$). The legend applies to all panels in the figure. Figure reproduced with permission from Springer Nature.

4.4.5 Drug-Loaded MPs Reduce Inflammatory T_H1 Phenotypes in a Transgenic Co-Culture Model

Next, we directly assessed phenotypic changes in the T_H1 phenotype using the T-bet transcription factor. Transgenic T cells were co-cultured with DCs for 72 h in a similar manner to the studies above, then antibody staining was used to quantify T-bet MFI and frequency among CD4+ T cells in each sample; higher MFIs and percentages correspond to higher expression of T-bet, and correspondingly, TH1 cells. At 1 and 10× dilutions, samples treated with drug-loaded MPs exhibited significantly decreased T-bet MFI (all samples at 1× dilutions $p < 0.0001$****; Evero at 10× dilution $p < 0.0001$****; and Rapa and Tems at 10× dilutions $p < 0.01$**), while Empty MP-treated samples showed a significant increase in T-bet MFI ($p < 0.0001$***) at all dilutions compared to MOG + LPS controls (**Figure 4.8a**). This result indicates that at higher drug concentrations, rapalogs are able to restrain inflammatory T_H1 cell levels more effectively. These data also show PLGA MPs generate an immune response, as Empty MP treatments elicited an inflammatory response stronger than the LPS-stimulated controls. At lower concentrations of drug loaded MPs, (10^3 ×–10^5 × dilutions), T-bet MFI was significantly increased compared to MOG + LPS-treated controls. Similar trends were measured when analyzing the percentage of T-bet+ cells among CD4+ T cells, with Empty MP treatments significantly increasing inflammatory T_H1 cells ($p < 0.0001$****), drug-loaded MPs at higher concentrations (1×, 10× dilutions) significantly restraining the inflammatory T_H1 phenotype, and MPs at lower concentrations (10^3 ×–10^5 ×dilutions) unable to restrain this population (**Figure 4.8b**).

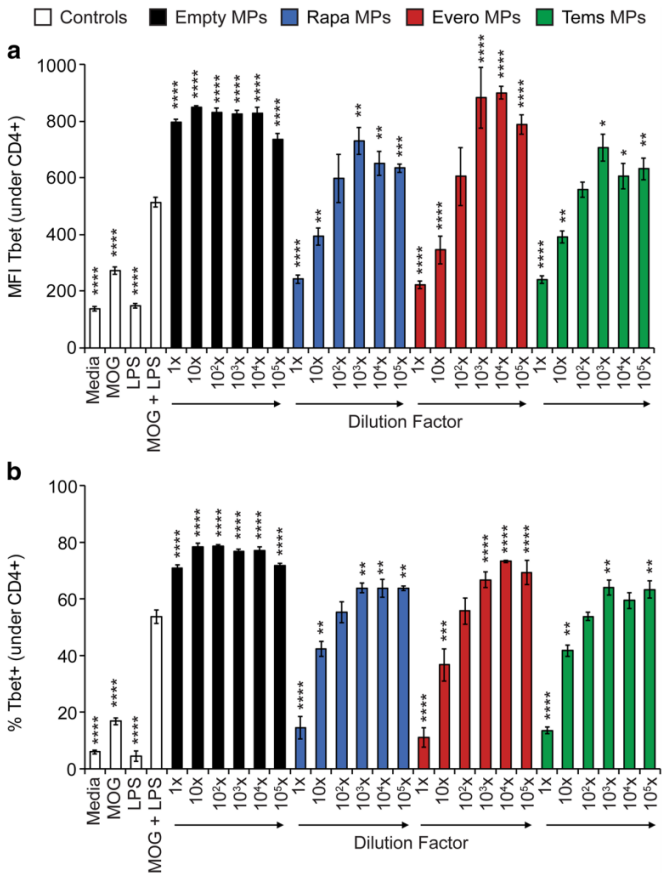

Figure 4.8 Rapalog MPs limit inflammatory T cell phenotypes in co-culture after stimulation.
MOG-specific CD4+ T cells were co-cultured for 72 h with wild-type DCs that had been left untreated, treated with MOG and/or LPS, or treated with equivalent doses of MOG and LPS and indicated dilutions of MPs for 16 h. After co-culture, T cells were analyzed by flow cytometry for transcription factor T-bet to directly evaluate T_H1 phenotypes. T-bet expression was quantified by **a,** mean fluorescence intensity (MFI) and **b**, percentage of T-bet+ cells. MP-treated samples were compared to MOG-and LPS-treated controls using ANOVA at each dilution (* indicates $p \leq 0.05$, ** $p \leq 0.01$, *** $p \leq 0.001$, **** $p \leq 0.0001$). The legend applies to all panels in the figure. Figure reproduced with permission from Springer Nature.

4.5 Discussion

As discussed in the introduction, mTOR plays a key role in regulating immune function. Inhibiting this pathway with Rapa can alter the development of T cells and promote T_{REGS}[153, 230-232]. This in turn has been shown to reduce severity of paralysis and disease symptoms in EAE when administered daily or every other day by

intraperitoneal injection[153, 205]. Interest in rapalogs, including Evero and Tems, as well as Rapa, has also been important in progressing therapies into pre-clinical and clinical studies for diseases which require altering cell proliferation, such as in the cases of cancer, transplant rejection, and autoimmune disorders[153, 187, 203, 205, 209-214]. In particular for our work, several new studies are investigating rapalogs for the treatment of autoimmune disease[225, 226]. Han et al. have shown that in mice with experimental autoimmune neuritis, daily administration of Evero by oral gavage reduces the severity of paralysis and inflammatory cytokines compared to control-untreated mice[225]. Administration of Evero by daily oral gavage has also been studied for the treatment of experimental autoimmune uveoretinitis. Evero treatment results in decreased intraocular inflammatory cytokines, increased T_{REGS}, and reduced severity of uveitis compared to mice given a sham control[226].

These newer generations of Rapa analogs have been designed for a variety of purposes: to enhance drug efficacy, potency, or solubility[209]. However, despite their widespread use, few studies have sought to differentiate their efficacy, particularly in the field of autoimmune therapy. The value of such screening information for immunomodulatory drugs has recently been reported[233]. In this study, we laid the foundation for differentiating the effects of the biomaterial formulations of the rapalogs Evero and Tems—and for extension to other next generation rapalogs, compared with the traditional mTOR inhibitor, Rapa. As a next step, these rapalogs could be evaluated in pre-clinical models of autoimmune diseases. In vivo testing could allow for the assessment of any differences in efficacy between rapalogs, where cell uptake and controlled release can largely influence disease progression.

We used a rapid, systematic approach to investigate the impact on inflammation of the second generation mTOR inhibitors delivered in biomaterials. These were tested in a self-antigen driven, ex vivo model of autoimmunity. Using this platform, we observed dose-dependent drops in DC activation, particularly when evaluated by CD80 and CD86. We also saw corresponding drops in T cell proliferation, measured by CFSE dilution, and in the inflammatory cytokines IFN-γ and IL-17. During autoimmune diseases such as MS, T_H1 and T_H17 cells are some of the key drivers of disease, with IFN-γ and IL-17 as key indicators of their inflammatory functions. Thus, the decreases we measured suggest that rapalog-loaded particles altered T cell phenotype. To directly test this idea, we also evaluated the T-bet transcription factor, a hallmark of the T_H1 phenotype. For the more concentrated drug-loaded MP treatments, it was clear that the effects of the drug attenuated T_H1 levels in a dose-dependent manner.

Interestingly, Empty MP treatments had a stimulatory effect on T-bet levels compared to the MOG + LPS-treated controls. This suggests that the PLGA MP carrier also had some level of intrinsic immunogenicity, possibly driven by non-specific activation of pathways (e.g., inflammasomes) that detect particulates or other debris that resemble pathogens. These findings support those of other groups, which have shown biomaterial carriers can elicit pro-immune responses or inflammation, even without the addition of adjuvants or other inflammatory cues[234-237]. Given that the goal of autoimmune therapy is suppression of excess or incorrect inflammation, an important aspect to consider is the dose and release rate of immunosuppressant that can overcome any carrier effects. For example, in MPs with low doses of drug, it was clear that the drug effects did not overcome this intrinsic effect, whereas the higher drug

loading levels reduced T_H1 levels to baseline (i.e., unstimulated). While the studies above focused on reducing inflammation, an important cell population to study in the future, are T_{REGS}. Animal data and recent human studies reveal these cells have the capacity to directly reduce or inactivate self-reactive, inflammatory T cells[221-223].

This work represents a generalizable approach to study biomaterial-enabled delivery of rapalogs in the context of autoimmunity. We showed incorporation of each drug into common, approved biomaterials and found rapalogs performed similarly to Rapa in a primary immune co-culture system; all maintained the ability to restrain inflammatory T cell phenotypes in the context of autoimmunity. However, while this system allowed us a clear, consistent way for comparisons, there are key differences between ex vivo testing and animal or human settings that all ultimately require testing in vivo. For example, in vivo, differences in drug efficacies and disease progression often arise from differences in cell uptake, biodistribution, or controlled release. Given the fluid motion resulting from blood and lymph circulation in vivo, maintaining therapeutic drug levels is a challenge not experienced in static, ex vivo culture. In addition, it is important to monitor off-target effects of drug treatments, particularly because many autoimmune diseases have specific tissue targets (i.e., the central nervous system during MS), whereas other organs may function normally. Thus, while this study sets the stage for evaluating biomaterials loaded with rapalogs or other drugs by allowing consistent comparisons, pre-clinical disease models of autoimmunity should be used in parallel with the most promising candidates.

4.6 Conclusion

The mTOR pathway is an important regulator of cell growth and metabolism and has been studied for its ability to influence cell proliferation in the context of cancer, transplantation, and autoimmunity. In the case of autoimmune diseases, inhibiting mTOR has been shown to alter the development of T cells, reducing effector cells and promoting TREGS. Rapa is already being translated as a human-relevant autoimmune treatment, so we tested this important class of immunomodulators ex vivo using biomaterials. Ultimately, screening rapalogs in cells and pre-clinical models could identify better drugs to pair with self-antigens. These combinations could lead to safer, more selective, and more durable treatments for patients with autoimmune diseases. In particular, such advances would be a vast improvement over the life-long treatments with broadly-acting immunosuppressive therapies that patients currently face.

Chapter 5: Intra-Lymph Node Delivery of Tolerogenic Microparticles Promotes Immune Tolerance, Reverses Paralysis, and Prevents Relapse in a Model of Multiple Sclerosis

5.1 Introduction

As discussed in **Chapter 3.3**, current therapies for MS and other autoimmune diseases aim to limit disease symptoms and progression without treating the cause. These therapies lack of specificity, and cannot differentiate between healthy and myelin-reactive inflammatory immune cells. To overcome these limitations, this dissertation investigated biodegradable polymeric microparticles (MPs) co-loaded with myelin peptides and rapamycin, an immunomodulatory signal, as an a myelin-specific immunotherapy. Directly injecting these tolerogenic MPs into key immune tissues (e.g. lymph nodes, LNs), induces myelin-specific regulatory immune cells that selectively control myelin-specific inflammation. This work aimed to advance pre-clinical studies and motivate clinical research by investigating the systemic impact of intra-LN tolerogenic MPs in two mouse models of MS – progressive MS (EAE, experimental autoimmune encephalomyelitis), and relapsing-remitting (RR) MS (RR-EAE). In particular, this work showed that even at different stages of disease, one tolerogenic intra-LN treatment promoted recovery from paralysis and prevented relapse. In addition, this work showed that tolerogenic intra-LN treatments did not prevent mice from mounting healthy, antigen-specific immune responses to foreign antigens in a vaccine challenge. The work presented in this chapter, in combination with the work presented in **Chapter 6** motivate development of intra-LN delivery of tolerogenic MPs as a candidate immunotherapy for human MS.

5.2 Background

As discussed in **Chapter 3.2**, multiple sclerosis (MS) occurs when immune cells aberrantly attack myelin, the matrix insulating neurons[128-130]. New MS patients (85%) typically present with Relapsing-Remitting MS (RR-MS), in which patients experience periods of relapse – attacks on the CNS in which patients experience neurological symptoms – that last for days to weeks. These patients then either fully or partially recover, but don't experience disease progression between bouts of relapse. Nearly 80% of patients with Relapsing-Remitting MS eventually progress to Secondary Progressive MS (SPMS), in which the periods of complete remission stop and disease progresses more consistently (with or without relapses). Existing treatments are non-curative, and therefore require frequent and continued dosing throughout the lifetime of the patient to maintain disease remission. As most MS patients are diagnosed between 20-50 years of age, these repeated therapy requirements can result in up to $4 million in lifetime costs for care per patient[238]. In addition, current therapies are non-specific, and cannot differentiate between healthy and dysfunctional myelin-reactive immune cells, which can leave patients vulnerable to infection[148-150].

To overcome these limitations, this dissertation sought to promote myelin-specific tolerance to selectively control disease. As mentioned in **Chapter 2.3**, lymph nodes (LNs) are sites where T cells expand against antigens (e.g. myelin) in response to immune cues[39, 45]. Thus, one approach to promote tolerance is to alter the LN environment to polarize T cells away from inflammatory phenotypes and toward regulatory phenotypes (T_{REGS}). To enable this therapeutic potential, signaling in key

immune tissues (e.g. lymph nodes, LNs) must be controlled during immune cell development. Providing disease-relevant immune cues – myelin peptides and rapamycin, an immunomodulatory signal – to LNs promotes the expansion of myelin-specific regulatory T cells[26, 187]. To improve the delivery of cargo to LN, intra-LN (iLN) injections have been used under ultrasound guidance in clinical trials with soluble antigens for allergen therapy[190-192], cancer[193, 194], and recently, type I diabetes[70]. However, soluble signals rapidly drain from the LN, which makes control over the LN environment transient. To enhance signal retention in LN, biomaterial-based delivery systems can be used to provide control over co-delivery of cargo, cargo protection, and controlled release of cargo, allowing for long-term exposure to the cargo loaded into the biomaterial[24, 26, 105, 162, 168].

The Jewell Lab has developed a direct injection technique to deliver polymer microparticles (MPs) to LNs of mice without requiring surgery[195]. Tostanoski et al have previously shown that loading myelin peptides and rapamycin – an immunomodulatory cue – into biodegradable polymeric microparticles (MPs) that are directly injected into LN ensures that both immune cues remain in LN over time and can reprogram the local LN microenvironment[26]. These micron-scale depots were designed to be too large to drain from LN. Instead, they slowly degrade and release tolerogenic cargo that condition the LN for tolerance. A single iLN treatment with tolerogenic MPs in mice with a progressive model of MS promoted T_{REGS} and permanent, systemic tolerance to myelin; treatment permanently stopped and reversed disease paralysis.

To build on this work, this dissertation aimed to advance pre-clinical studies and motivate clinical research by investigating the systemic impact of intra-LN tolerogenic MPs in two mouse models of MS – progressive MS (EAE, experimental autoimmune encephalomyelitis), and relapsing-remitting (RR) MS (RR-EAE). This work showed that even at different stages of disease, one tolerogenic intra-LN treatment promoted recovery from paralysis and prevented relapse. Tolerogenic MPs delivered prior to symptom onset promoted tolerance and protected against disease onset. Treatment at peak disease reversed paralysis and prevented relapse, while treatment during relapse limited disease progression. Importantly, even when vaccinated against a foreign protein (OVA) on the same day as intra-LN treatment, mice generated OVA-specific T cells and antibodies at similar levels to healthy vaccinated mice.

5.3 Materials and Methods

5.3.1 Materials and Reagents

Myelin peptides proteolipid protein ($PLP_{139-151}$), $PLP_{178-191}$, and myelin oligodendrocyte glycoprotein (MOG_{35-55}) were purchased from GensScript at >98% purity. Ovalbumin peptide $OVA_{323–339}$ was also synthesized by GenScript at >98% purity. Rapamycin was purchased from LC Laboratories. Poly(lactide-co-galactide) (PLGA) was purchased from Durect, and poly(vinyl alcohol) (PVA) was purchased from Sigma and Alfa Aesar.

5.3.2 MP Synthesis

Microparticles (MPs) were synthesized by double emulsion and solvent evaporation as previously described[195]. Briefly, an inner aqueous phase of 500 µL was prepared with either water, 1 mg $OVA_{323-339}$, 0.75 mg $PLP_{139-151}$, 0.5 mg $PLP_{178-191}$, or 1 mg MOG_{35-55} in 500 µL water. Peptide input was chosen to allow similar loading levels of peptides with slightly different charges or hydrophobicities. The oil phase consisted of 80 mg of PLGA dissolved in 5 mL dichloromethane; for rapamycin (Rapa) loaded MPs, 2 mg of Rapa was loaded into the organic phase prior to synthesis. The inner aqueous and organic phases were sonicated for 30 s at 12 W to form a water/oil emulsion. The primary emulsion was then homogenized with an outer aqueous phase of 40 mL 2% w/v PVA for 3 min at 16,000 rpm. MPs were stirred at 350 rpm for 16 h to allow for solvent evaporation, then poured through a 40µm cell strainer and collected using centrifugation (5 min at 5000 g, 4°C). The supernatants were removed, the MPs were washed three times in 1 mL water with collection by centrifugation after each wash. The particles were then resuspended in water.

5.3.3 MP Characterization

MPs were characterized for size and loading prior to use in animal studies. Particle size was measured using an LA-950 laser diffraction size analyzer (Horiba Instruments). To measure the loading of Rapa and peptide in MPs, a known volume of MPs was air-dried to remove water from the sample. Dried MPs were dissolved in dimethyl sulfoxide. Rapa loading was measured by UV/Vis spectrophotometry, and peptide loading was measured using a Micro Bicinchoninic Acid (mBCA) Protein

Assay kit (ThermoFisher Scientific Pierce) according to manufacturer's instructions. Standard curves of known concentrations of Rapa and peptide were used to calculate loading, reported as the mass of cargo per mass of dried MP formulation. Cargo loading and sizing measurements were made on at least 3 different batches of each MP.

5.3.4 Mouse MS Model Induction and Monitoring

RR-EAE was induced in 9 week old female SJL/J mice (The Jackson Laboratory) according to manufacturer's instructions (Hooke Laboratories). Briefly, mice were given four subcutaneous injections of an emulsion containing Complete Freund's Adjuvant (CFA) and [Ser^{140}]-$PLP_{139-151}$. EAE was induced in 10 week-old female C57BL/6J mice (The Jackson Laboratory) according to the manufacturer's instructions (Hooke Laboratories). Briefly, mice were given two subcutaneous injections of an emulsion of CFA and MOG_{35-55}. Two and 24 hours later, mice were injected intraperitoneally with pertussis toxin to open the blood-brain barrier. All RR-EAE studies started with n=14 to n=16 mice per group, due to variability associated with the model. EAE studies started with n = 8 per group. Starting on day 7 post-induction (or earlier), mice were monitored daily for weight loss and severity of paralysis (clinical score), where a score of 0 indicates no paralysis, 1 indicates tail paralysis, 2 indicates partial hind limb paralysis, 3 indicates total hind limb paralysis, and 4 indicates partial front limb paralysis. Disease incidence was defined as the first day a mouse exhibited a clinical score >0; paralysis incidence was defined as the first day a mouse exhibited a clinical score >2; relapse incidence was defined as the first day a mouse exhibited a clinical score >2 during their second wave of disease.

All animal studies were fully compliant with local, state, and federal guidelines per the Association for Assessment and Accreditation of Laboratory Animal Care (AAALAC) expectations for animal care and use/ethics. All studies were approved by and carried out under the supervision of the University of Maryland Institutional Animal Care and Use Committee (IACUC). Mice were carefully monitored for weight and clinical score, and were euthanized according to established humane endpoints.

5.3.5 Intra-Lymph Node Tolerogenic MP Injections

Tolerogenic MP treatments were delivered directly to LN using a non-surgical, iLN injection technique as previously described by the Jewell Lab[24, 26, 195, 196]. Briefly, at least one day prior to iLN injection, the mice were shaved above the injection site and remaining fur was removed using a mild depilatory cream. One day prior to iLN injection, a tracer dye (Evans blue, Alfa Aesar) was injected subcutaneously at each side of the tail base. On the day of treatment, each mouse received two injections – one into each inguinal LN – containing 1 mg of indicated MP formulation in 10 μL.

For iLN treatments prior to disease onset, mice were induced with disease and randomized into treatment groups following induction. For iLN treatments following disease onset, mice were assigned to groups to ensure consistent clinical scores between groups on the day of injection.

5.3.6 Ovalbumin Vaccination Studies

At timepoints indicated in the results and figures below, to test the specificity of the tolerogenic MP treatment, mice were vaccinated with a foreign protein,

ovalbumin to test healthy immunity. On vaccination days, mice were given a subcutaneous injection at the scruff of 200 μg ovalbumin (Worthington Biochemical Corporation) with 50 μg CpG (Integrated DNA Technologies) to act as an adjuvant. If the mice received a boost, the same dose and injection scheme was used to boost the mice three weeks later.

5.3.7 Tissue Processing and Immune Cell Collection

At the indicated time points, immune tissues were collected from mice induced with EAE or RR-EAE. Treated inguinal LNs, as well as distant axillary and brachial LN, CNS draining cervical LNs, spleen, or spinal cords were collected and manually dissociated through a 40 μm cell strainer. Cells were collected by centrifugation (5 min, 800xg, 4°C). LN cells were washed with PBS without lysis. Spleen cells were resuspended in Ack lysis buffer (Invitrogen) to remove red blood cells and then washed with PBS. Cells were collected from spinal cord using a gradient to remove debris (Debris Removal Kit, Miltenyi), and then treated with Ack lysis buffer to remove red blood cells. Cells were then counted using counting beads according to the manufacturer's instructions (BD biosciences), and either analyzed by flow cytometry or plated for ex vivo restimulation assays.

5.3.8 Flow Cytometry Studies

To analyze tissues for cell populations of interest, cells were stained and analyzed by flow cytometry. Following incubation times listed in the figures and results, cells were prepared for analysis by flow cytometry. Antibodies for flow cytometry, including CD16/CD32, APC CD8a (clone 53), APC CD45 (clone 30-F11),

and APC-Cy7 CD4 (clone RM4-5), were purchased from BD Biosciences. FITC counting beads were purchased from BD Biosciences. SIINFEKL tetramer (iTAg Tetramer/PE - H-2 Kb OVA) was purchased from MBL International. 4′,6-Diamidino-2- Phenylindole,Dihydrochloride (DAPI) was purchased from Sigma Aldrich. All analyses were completed performed on a FACS Celesta or FACS Canto II (BD Biosciences) and data analysis was conducted using FlowJo version 10.6 (BD Biosciences, Tree Star).

Cells were first blocked with anti-CD16/CD32. For vaccination studies, cells were stained for SIINFEKL-specific receptors using the tetramer stain. Cells were then stained for surface markers CD4, CD8,or CD45 depending on the study. Lastly, cells were stained with DAPI for viability, and immediately analyzed.

5.3.9 Ex Vivo Restimulation Assays

To characterize immune cell responses to antigen exposure, 1 million cells were plated from each tissue sample and cultured with 25 µg/mL disease-relevant myelin peptides (MOG_{35-55}, $PLP_{139-151}$, or $PLP_{178-191}$), disease irrelevant peptide ($OVA_{323-339}$), or vaccine related whole ovalbumin. After 72 hours in culture, supernatants were collected for analysis by ELISA. ELISA All ELISAs were performed according to the manufacturer's instructions for IL-17 (R&D Systems), GM-CSF (R&D Systems), and IFN-g (BD Biosciences) detection. Supernatants were collected from cell culture samples and analyzed at 4-10x dilutions.

5.4 Results

5.4.1 $PLP_{139-151}$/Rapa tolerogenic MPs can reverse disease and prevent paralysis in RR-EAE

We previously had shown that MOG_{35-55}/Rapa tolerogenic MPs could durably reverse disease in a progressive model of MS, which is induced with an emulsion of MOG_{35-55} and Complete Freund's Adjuvant (CFA). To test if this immune tolerance could be promoted in a model of relapsing-remitting MS, which is more relevant for human disease, we synthesized MPs loaded with $PLP_{139-151}$ and rapa using a water/oil/water double-emulsion synthesis technique (**Fig. 5.1A**). This double emulsion synthesis allowed us to load our water soluble cargo ($PLP_{139-151}$) into the inner aqueous phase, our water-insoluble cargo (rapa) into the oil phase. This was then mixed with an outer aqueous phase containing a stabilizing molecule (PVA). This high energy mixing resulted in MPs that could be injected into the LN. To inject the LN of mice, the fur was first removed from above the injection site with clippers and a mild depilatory cream (e.g. Nair), and a tracer dye was injected subcutaneously at the tail base (**Fig. 5.1B**). This tracer dye then drains to the LN, so the LN are visible through the skin, and can be injected with tolerogenic MPs. The size of the MPs prevents them from draining from the LN, ensuring that most of the cargo remains in the LN and interacts with APCs and T cells (**Fig. 5.1B**, right) to condition the LN for myelin-specific tolerance.

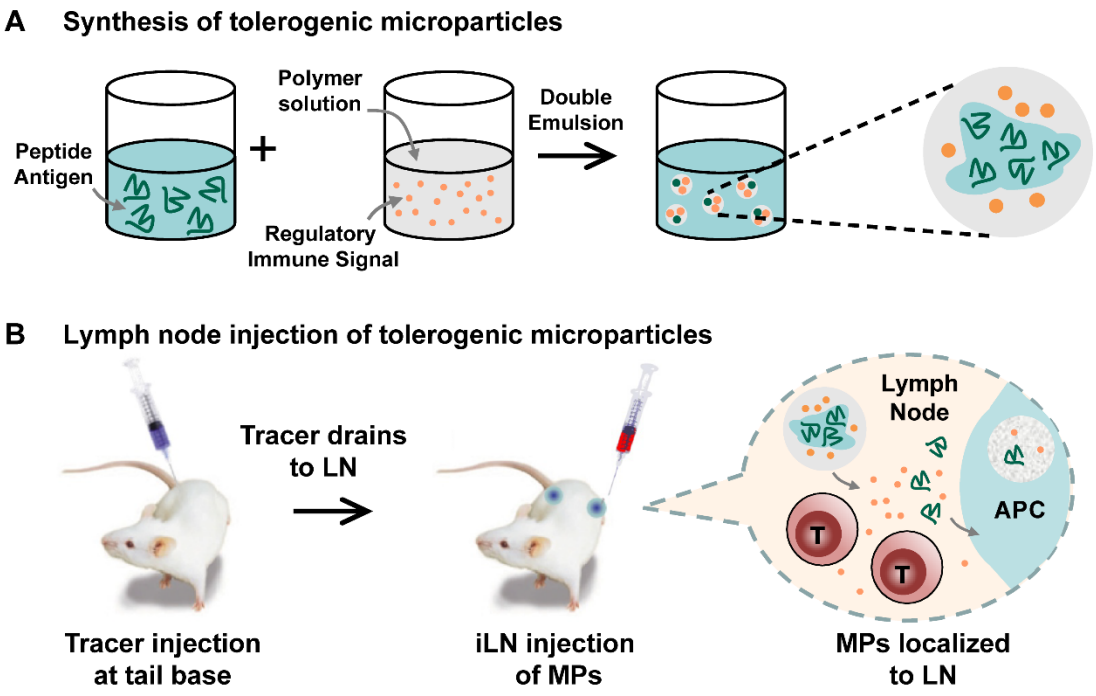

Figure 5.1 Tolerogenic MP Synthesis and Lymph Node Injection
(A) Tolerogenic MPs are synthesized using a w/o/w emulsion in which peptide antigens are loaded into the inner aqueous phase, and rapa (regulatory immune signal) is loaded into the polymer-containing oil solution. These are mixed at high energy with an outer aqueous phase containing a stabilizer, resulting in micron-scale microparticles, which can be injected into the LN. (B) Non-surgical LN injections in mice use a tracer dye that, when injected subcutaneously at the tail base, drains to the inguinal LN. Inguinal LN can then be visualized through the skin and injected. Tolerogenic MP size ensures the MPs stay in the LN and continuously release cargo to APCs and T cells to condition the LN microenvironment for myelin-specific tolerance. Adapted with permission from Andorko et al, *Journal of Visualized Experiments*, 2014[195].

To test if tolerance to myelin could be induced in the relapsing-remitting mouse model of MS, mice were induced with RR-EAE on Day 0, and treated iLN on Day 13, after symptom onset – an early intervention. Mice treated on Day 13 were either given PBS, Empty MPs, or $PLP_{139-151}$/Rapa MPs. Mice were weighed and disease severity (clinical score) was assessed daily starting 7 days after induction. Increasing disease severity is indicated by an increase in clinical score; a score of 0 indicates no paralysis,

1 indicates tail paralysis, 2 indicates partial hind limb paralysis, 3 indicates total hind limb paralysis, and 4 indicates partial front limb paralysis. Compared to mice treated with PBS, mice treated with Empty MPs showed no change in mean clinical score after treating on D13 (**Fig 5.2A**). However, mice treated with PLP_{139}/Rapa MPs showed significantly reduced disease starting on day 22; this effect remained throughout the duration of the study. This significantly reduced disease was not due to differences in the induction between groups, as there were no differences in the percentage of mice that reached their first symptoms of paralysis before treatment (score 2.5+) (**Fig. 5.2B**), mean clinical score (**Fig. 5.2A**), or relative weight (**Fig. 5.2C**) between mice given tolerogenic MPs and control mice given PBS on day 13. This reduction in clinical score was also followed by a significant increase in relative weight of mice given PLP_{139}/Rapa MPs iLN. PLP_{139}/Rapa MPs also protected mice against relapse, which is evident in the clinical score difference starting on day 22 (**Fig. 5.1A**), as well as the significantly decreased incidence of severe paralysis (clinical score 2.5+) after the first wave of disease (**Fig. 5.1D**). This reduced score was also clear in the mean cumulative score curve, in which the score from that day is added to the scores from all previous days. Beginning on Day 28, the cumulative score curve for PLP_{139}/Rapa treated mice begins to significantly diverge from cumulative scores for the Empty MP and PBS-treated mice. This study suggested that the tolerogenic iLN therapy could be applied to different models of MS, and launched the investigation into how treatment composition and treatment timepoint influence disease progression and protection from future relapses in disease.

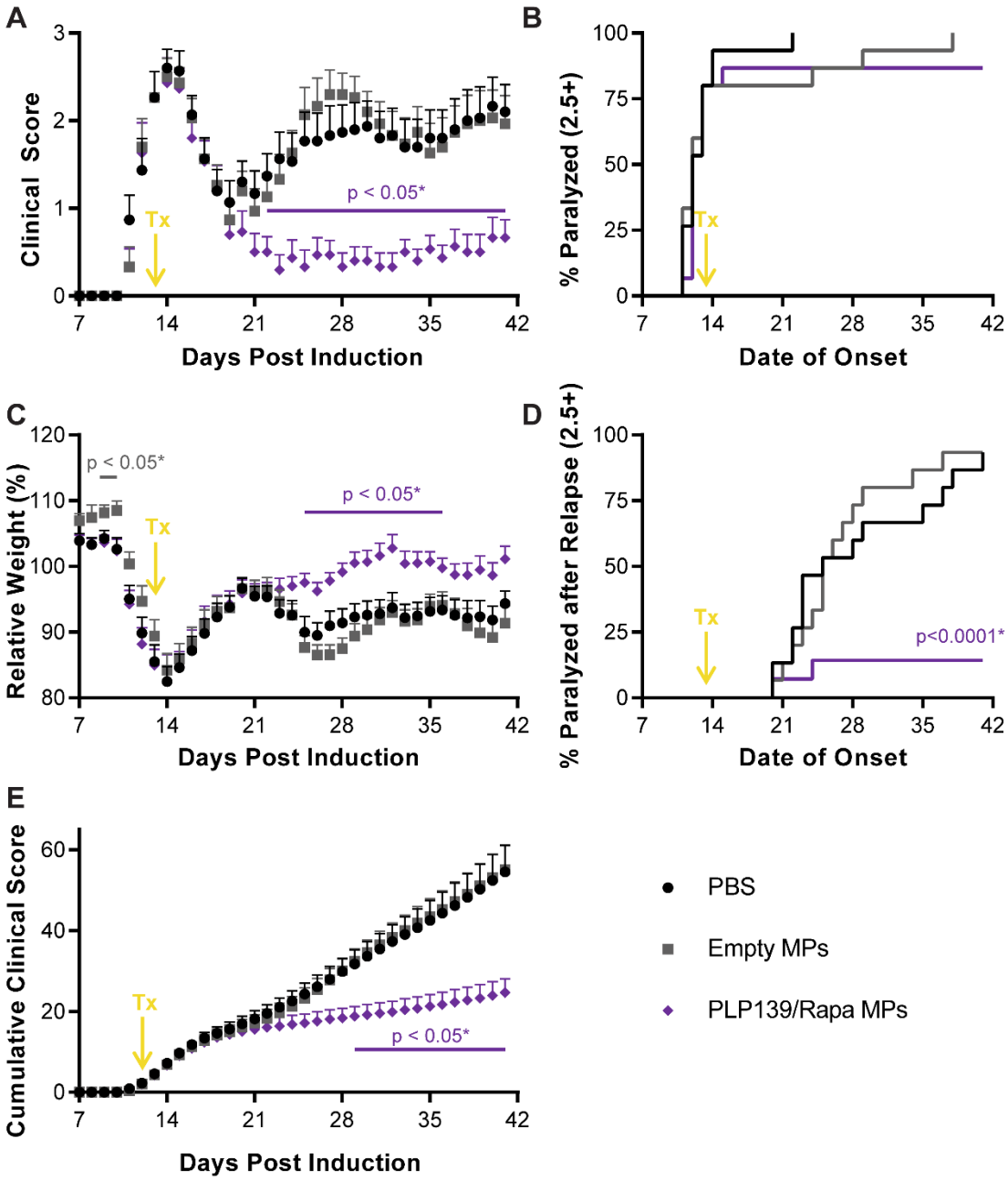

Figure 5.2 Treatment with tolerogenic MPs reverses disease and prevents relapse in a model relapsing-remitting MS.

Mice were induced with RR-EAE on Day 0, and treated iLN with either PBS, Empty MPs, or PLP_{139}/Rapa MPs on Day 13. (A) Mean clinical score for PLP_{139}/Rapa MPs is significantly reduced compared to PBS treated control mice starting on Day 22. (B) Paralysis incidence is not significantly different between groups prior to iLN treatment. (C) Mice treated with PLP_{139}/Rapa have significantly increased relative weights compared to PBS treated mice. (D) PLP_{139}/Rapa treated mice have significantly reduced relapse paralysis compared to PBS treated mice. (E) Mice treated with PLP_{139}/Rapa MPs iLN show significantly reduced clinical scores compared to PBS treated mice. Relative weights were analyzed using a one way analysis of variance

(ANOVA) by day with a correction for multiple comparisons to PBS treated mice using Dunnett's Method. Clinical score and Cumulative score were analyzed using a non-parametric rank test with a correction for multiple comparisons to PBS treated mice using the Steel Method. Percent Paralyzed and % Paralyzed after Relapse were analyzed using a long-rank test with a Bonferroni correction for multiple comparisons to PBS. N = 15 mice per group. The legend in the bottom right applies to all panels in the figure. Average + SEM is shown for relative weight and clinical score plots. Error bars are shown in one direction for simplicity.

5.4.2 MPs can be loaded with peptides and rapa at similar levels and remain similar in size

To test the importance of treatment composition on the efficacy of the iLN treatment, MPs were synthesized using different combinations of peptides with or without rapa. MPs were synthesized using two different PLP peptides for use in the RR-EAE model – $PLP_{139-151}$ and $PLP_{178-191}$. Disease is induced with $PLP_{139-151}$, but over the course of disease, there is epitope spreading to $PLP_{178-191}$. This epitope spreading happens when other myelin peptides get presented in inflammatory contexts to lymphocytes because of the inflammation around the entire myelin protein in the CNS. As such, we wanted to test both PLP epitopes to see how treatments regimens may change over different stages of disease. To test if tolerance generated in response to iLN treatment is antigen-specific, MPs were also synthesized using a disease-irrelevant peptide ($OVA_{323-339}$) and rapa to study the antigen-specificity of tolerance that protects against disease. MOG_{35-55} MPs were used in the final studies in EAE to further assess antigen-specificity of treatment, in which mice were vaccinated on the same day as the iLN treatments.

In total, 8 MP formulations were used for this dissertation: Empty MPs, Rapa MPs, OVA_{323}/Rapa MPs, PLP_{139} MPs, PLP_{139}/Rapa MPs, PLP_{178} MPs, PLP_{178}/Rapa

MPs, and MOG_{35} MPs (**Table 5.1**). MPs sizing was assessed using laser diffraction. All MPs showed similar sizes, suitable for iLN studies. The 2-4 μm range of MPs is too large to easily drain from LN, but small enough to be taken up by APCs[239]. **Table 5.1** shows that MPs were synthesized to contain similar levels of peptides and rapa. This was achieved through optimization of input mass of peptide, as the different peptides have different charges and hydrophobicities that enable different encapsulation efficiencies. Only the MOG_{35-55}/Rapa MPs showed a substantially higher loading, but they were only used in the final EAE studies for vaccination, and not compared to any of the other groups.

Table 5.1 Tolerogenic Microparticle Characterization

MPs Formulation	Size (μm)	Peptide Loading (μg/mg MP)	Rapa Loading (μg/mg MP)
Empty MPs	2.78 ± 0.22	N/A	N/A
Rapa MPs	2.65 ± 0.14	N/A	19.4 ± 1.8
OVA_{323}/Rapa MPs	2.79 ± 0.01	3.77 ± 1.14	20.4 ± 2.9
PLP_{139} MPs	3.10 ± 1.15	4.87 ± 0.46	N/A
PLP_{139}/Rapa MPs	2.88 ± 0.69	4.36 ± 0.62	20.4 ± 1.1
PLP_{178} MPs	3.61 ± 0.68	5.59 ± 0.78	N/A
PLP_{178}/Rapa MPs	3.23 ± 0.95	4.98 ± 1.01	19.4 ± 2.0
MOG_{35}/Rapa MPs	3.16 ± 0.53	7.97 ± 1.08	20.0 ± 0.8

*N/A indicates that there was no peptide or rapamycin loading in these particles

5.4.3 Tolerogenic MPs prevent disease when administered prior to disease onset

To better understand the importance of treatment composition on the induction of myelin-specific tolerance that can protect from disease, MPs loaded with the combinations of myelin peptides (with or without rapa) listed in **Table 5.1** were administered prior to disease onset, but after disease induction. Mice were induced with disease on Day 0, and then treated iLN with MPs on Day 7. Importantly, only PLP_{139}/Rapa MPs showed a significantly reduced disease severity for the duration of the study (with the exception of the recovery period) (**Fig. 5.3A**). Mice treated with PLP_{139} MPs, PLP_{178}/Rapa MPs, and Rapa MPs also showed reduced disease severity compared to during the first wave of disease, though effect was not sustained throughout the duration of the study. These reductions in clinical score corresponded to a significant delay in the onset of paralysis (score 2.5+) (**Fig. 5.3B**) for Rapa MPs, PLP_{178}/Rapa MPs, PLP_{139} MPs, and PLP_{139}/MPs. From this paralysis incidence curve, its is clear that Rapa MPs lost their protective effect over time, followed by PLP_{178}/Rapa MPs. Importantly, PLP_{178} MPs offered no protection from the first wave of disease, clear in both the clinical score curve and the % paralysis+ curve. Similar to the clinical score curve trends, Rapa MPs, PLP_{178}/Rapa MPs, PLP_{139}, PLP_{139}/Rapa MPs exhibited significantly higher relative weights compared to PBS treated mice, though this effect was lost for Rapa MPs over time. Only PLP_{139} and PLP_{139}/Rapa MPs showed a significant reduction in the percentage of mice that were paralyzed during relapse compared to PBS treated mice (**Fig. 5.3D**). Interestingly, though the difference was not significant, mice that were treated iLN with PLP_{178} experienced exacerbated disease, with a higher percentage of mice paralyzed in earlier relapses. This was also clear in

the clinical score curve. These trends, with Rapa MPs, PLP_{178}/Rapa MPs, PLP_{139} MPs, and PLP_{139}/Rapa MPs showing less severe disease, are also clear in the cumulative clinical score curve (**Fig. 5.3E**). As with clinical score and % paralyzed, Rapa MPs lost their protective effect over time.

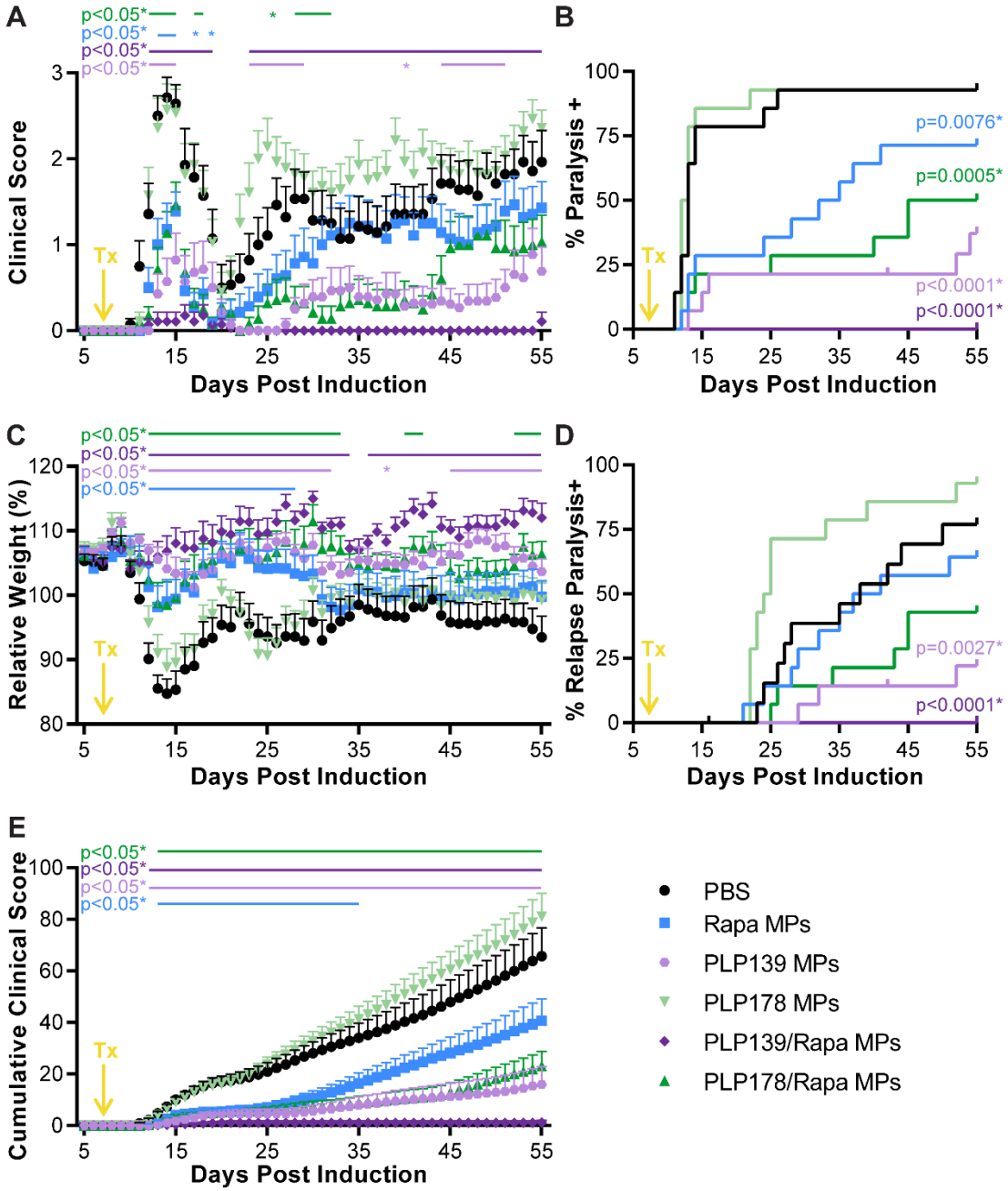

Figure 5.3 Tolerogenic MPs prevent disease onset when administered prior to disease onset.

(A) Mice were induced with RR-EAE on Day 0, and treated iLN with either PBS, Rapa MPs, $PLP1_{39}$ MPs, PLP_{178} MPs, PLP_{139}/Rapa MPs or PLP_{178}/Rapa MPs on Day 7. (A) Mean clinical score for PLP_{139}/Rapa MPs is significantly reduced compared to PBS treated control mice for the duration of the study, with the exception of the recovery period. Rapa, PLP_{139}, and PLP_{178}/Rapa MPs also showed reduced clinical score, though this effect was lost over time for Rapa and PLP_{178}/Rapa MPs. (B) Mice treated with Rapa MPs, PLP_{139}, PLP_{139}/Rapa, and PLP_{178}/Rapa MPs have significantly delayed or reduced paralysis onset. (C) Mice treated with Rapa MPs, PLP_{139}, PLP_{139}/Rapa, and PLP_{178}/Rapa MPs have significantly increased relative weights compared to mice treated with PBS. (D) Only mice treated with PLP_{139} and PLP_{139}/Rapa MPs showed reduced or delayed paralysis onset compared to mice treated with PBS. (E) Similar trends were seen for cumulative clinical score – with mice treated with Rapa MPs losing protection from disease over time. Relative weights were analyzed using a one way analysis of variance (ANOVA) by day with a correction for multiple comparisons to PBS treated mice using Dunnett's Method. Clinical score and Cumulative score were analyzed using a non-parametric rank test with a correction for multiple comparisons to PBS treated mice using the Steel Method. Percent Paralyzed and % Paralyzed after Relapse were analyzed using a long-rank test with a Bonferroni correction for multiple comparisons to PBS. N = 14 mice per group. The legend in the bottom right applies to all panels in the figure. Average + SEM is shown for relative weight and clinical score plots. Error bars are shown in one direction for simplicity.

This study was repeated, with an additional OVA_{323}/Rapa control. This OVA_{323}/Rapa control was added to show the specificity of the myelin-specific therapy. Since this set of MPs does not generate myelin-specific tolerance, if PLP_{139}/Rapa MPs or PLP_{178}/Rapa MP formulations do not reduce disease compared to OVA_{323}/Rapa, then efficacy seen in **Fig. 5.3** would be due only to the presence of Rapa with an antigen in the MPs. Excitingly, this study showed that PLP_{139}/Rapa MPs and PLP_{139} MPs significantly reduced clinical score for the duration of the study, except for the recovery period (**Fig. 5.4A**). The same trends were seen in % paralysis (**Fig. 5.4B**), relative weight (**Fig. 5.4C**), % paralyzed during relapse (**Fig. 5.4D**), cumulative score (**Fig. 5.4E**) – with Rapa MPs, PLP_{178}/Rapa MP, as well as OVA_{323}/Rapa MPs showing a temporary reduction in disease severity, which is lost over the duration of the study.

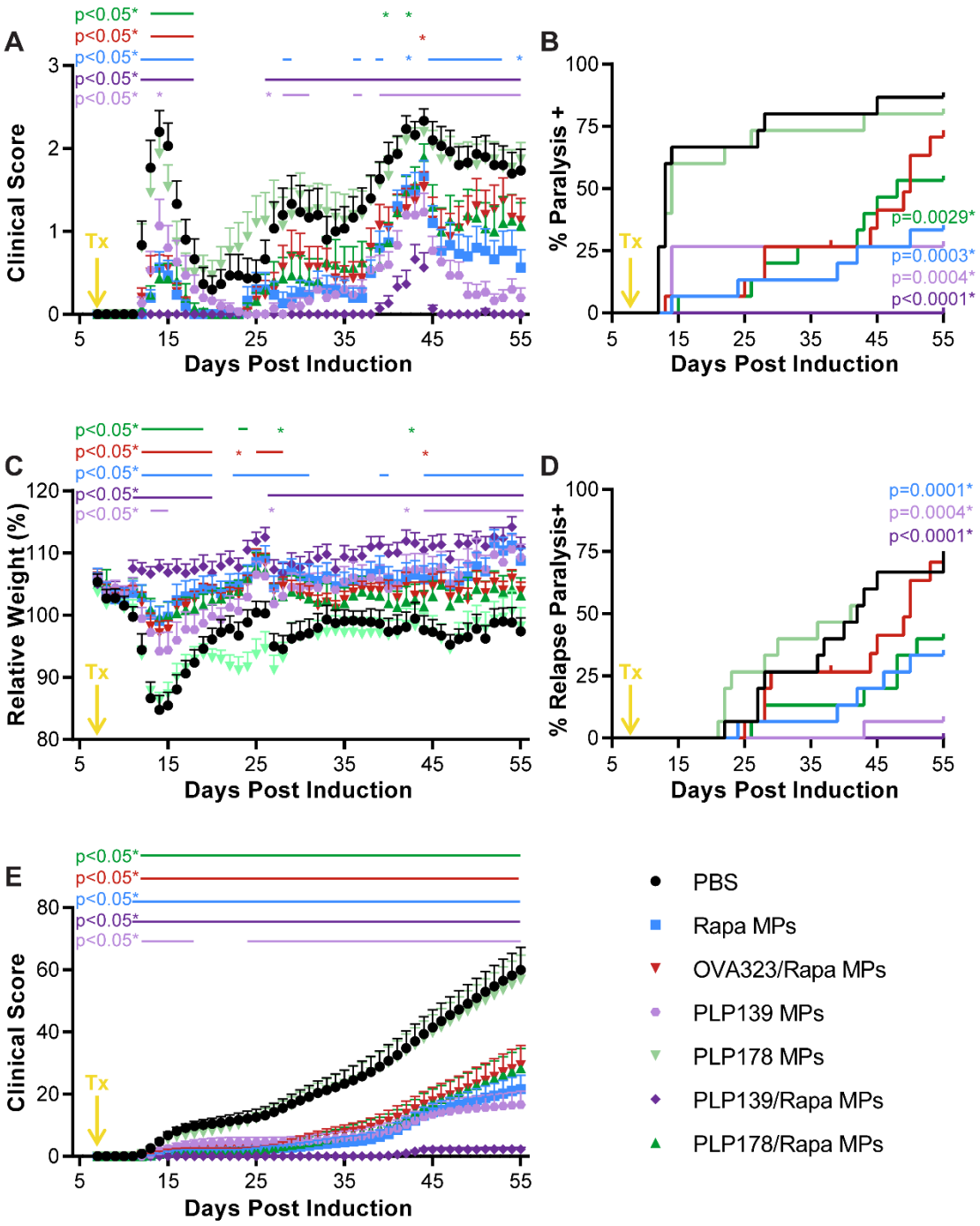

Figure 5.4 D7 treatment with tolerogenic MPs iLN delays disease onset and reduces severity.

Mice were induced with RR-EAE on Day 0, and treated iLN with either PBS, Rapa MPs, OVA_{323}/Rapa MPs, PLP_{139} MPs, PLP_{178} MPs, PLP_{139}/Rapa MPs or PLP_{178}/Rapa MPs on Day 7. Similar for the study in Figure 5.3, (A) Mean clinical score for PLP_{139}/Rapa MPs is significantly reduced compared to PBS treated control mice starting for the duration of the study, with the exception of the recovery period. Rapa, PLP_{139}, and PLP_{178}/Rapa MPs, as well as OVA_{323}/Rapa MPs also showed reduced

clinical score, though this effect was lost over time for Rapa, OVA_{323}/Rapa MPs and PLP_{178}/Rapa MPs. (B) Mice treated with Rapa MPs, PLP_{139}, PLP_{139}/Rapa, and PLP_{178}/Rapa MPs have significantly delayed or reduced paralysis onset. (C) Mice treated with Rapa MPs, OVA_{323}/Rapa, PLP_{139}, PLP_{139}/Rapa, and PLP_{178}/Rapa MPs have significantly increased relative weights compared to mice treated with PBS. (D) Mice treated with PLP_{139} and PLP_{139}/Rapa MPs, as well as Rapa MPs showed reduced or delayed paralysis onset during relapse compared to mice treated with PBS. (E) All treatment groups saw reduced cumulative clinical scores compared to mice treated with PBS. Relative weights were analyzed using a one way analysis of variance (ANOVA) by day with a correction for multiple comparisons to PBS treated mice using Dunnett's Method. Clinical score and Cumulative score were analyzed using a non-parametric rank test with a correction for multiple comparisons to PBS treated mice using the Steel Method. Percent Paralyzed and % Paralyzed after Relapse were analyzed using a long-rank test with a Bonferroni correction for multiple comparisons to PBS. N= 15 mice per group. The legend in the bottom right applies to all panels in the figure. Average + SEM is shown for relative weight and clinical score plots. Error bars are shown in one direction for simplicity.

Adding the OVA_{323}/Rapa MPs control showed that the temporary disease protection seen using PLP_{178}/Rapa MPs was due only to the addition of the Rapa in the MPs, but it did not ensure long-term myelin specific immune tolerance that provided durable protection. This is important, as a major goal for this study was to improve on human MS therapies by promoting myelin-specific tolerance.

To assess the durability of myelin-specific tolerance following treatment, mice were treated iLN with PLP_{139}/Rapa MPs 28 days before induction. Excitingly, even with induction occurring 28 days following iLN treatment, PLP_{139}/Rapa MPs caused significantly reduced clinical scores compared to PBS treated mice throughout the duration of the study (with the exception of the recovery period) (**Fig. 5.5A**).This reduction in score meant the PLP_{139}/Rapa caused a significant reduction in paralysis incidence (**Fig. 5.5B**). This also correlated with a significant increase in relative weight

(**Fig. 5.5C**), a significant reduction in mice experiencing paralysis during relapse (**Fig. 5.5D**), and a significant reduction in cumulative score throughout the duration of this study (**Fig. 5.5E**). These results suggests that the tolerance induced to myelin is long-

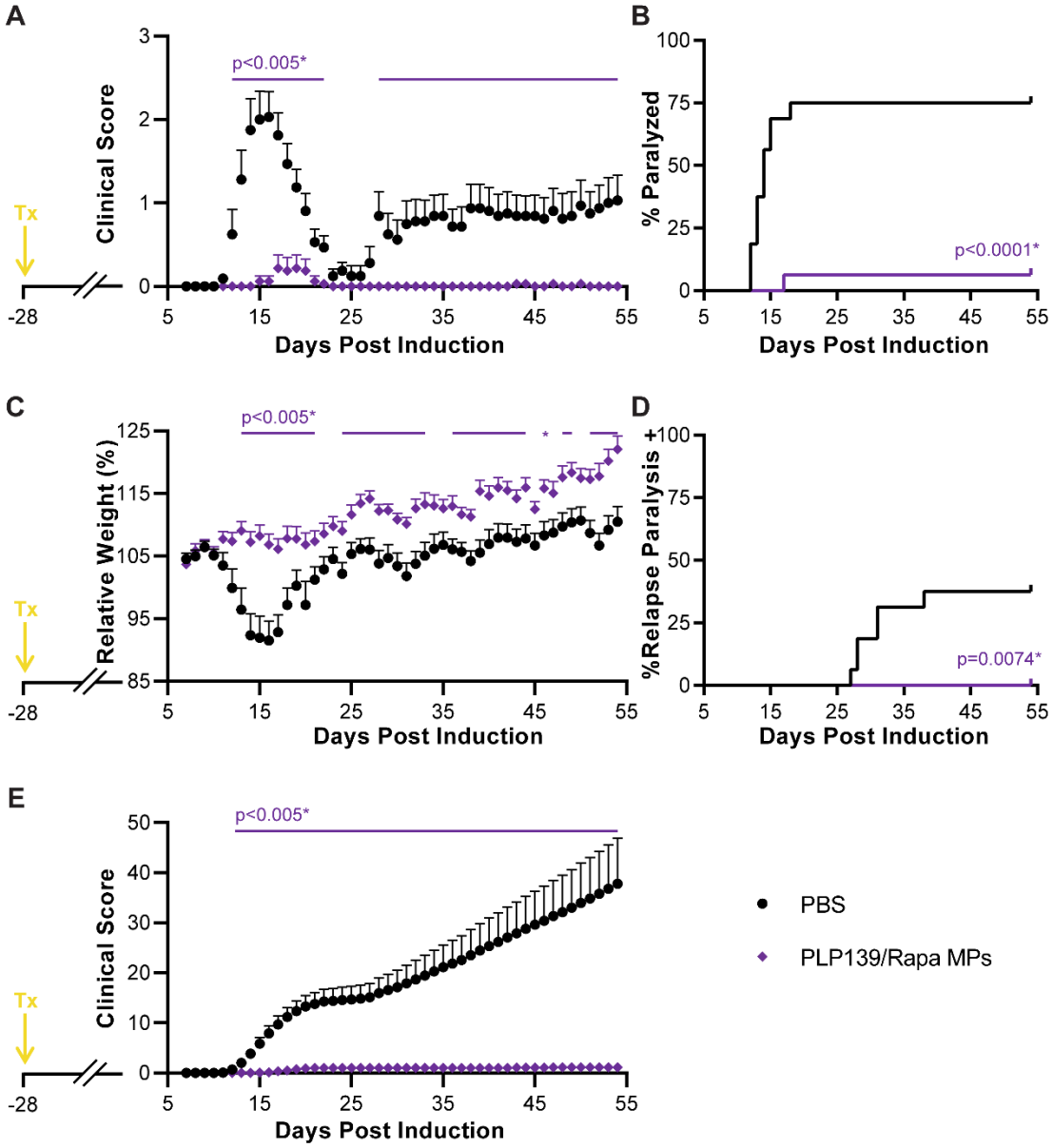

Figure 5.5 Tolerogenic iLN treatment 28 days before induction protects against disease onset.

Mice were injected iLN with either PBS or PLP_{139}/Rapa MPs, and induced with RR-EAE 28 days later. (A) Mean clinical score for PLP_{139}/Rapa MPs is significantly reduced compared to PBS treated control mice for the duration of the study, with the exception of the recovery period. (B) Mice treated with PLP_{139}/Rapa have significantly

reduced paralysis onset. (C) Mice treated with PLP_{139}/Rapa MPs have significantly increased relative weights compared to mice treated with PBS. (D) Mice treated with PLP_{139}/Rapa MPs showed reduced paralysis onset during relapse compared to mice treated with PBS. (E) PLP_{139}/Rapa MP treatment groups saw reduced clinical scores compared to mice treated with PBS. Relative weights were analyzed using t tests by day. Clinical score and Cumulative score were analyzed using a Wilcoxon rank test. Percent Paralyzed and % Paralyzed after Relapse were analyzed using a long-rank test. N = 16 mice per group. The legend in the bottom right applies to all panels in the figure. Average + SEM is shown for relative weight and clinical score plots. Error bars are shown in one direction for simplicity.

lasting, and could enable fewer treatments throughout the lifetime of the patient. It is possible that this prolonged tolerance (in the absence of ongoing MS), is due to myelin-specific memory cells, though future studies analyzing cellular phenotypes would be required to verify this hypothesis.

5.4.4 Tolerogenic MP treatment at peak diseases reverses paralysis and prevents relapse in mice with RR-EAE

While the studies listed in **Chapter 5.4.3**, gave insight into the fact that PLP_{139} was required to promote tolerance to myelin, and that Rapa acted synergistically to prevent disease, treatments were administered before disease onset. Since patients don't know they have MS until after their first event, we also tested late stage treatments – 14 days after induction (peak disease) and 30 days after induction (relapse). These regimens simulate more clinically relevant settings, as patients are would not seek treatment for MS until they begin experiencing symptoms. Importantly, only PLP_{139}/Rapa MPs showed a significantly reduced disease severity after treatment (**Fig. 5.6A**). Mice treated with Rapa MPs, PLP_{139} MPs, PLP_{178} MPs, and PLP_{178}/Rapa MPs did not see reductions in disease severity or protect against relapse, unlike the effects

seen for PLP_{139} MPs in the studies with treatment at Day 7. This reduction in clinical score was not due to differences in paralysis incidence at the time of treatment (**Fig. 5.6B**). Similar to the clinical score curve trends, PLP_{139}/Rapa MPs exhibited significantly higher relative weights compared to PBS treated mice (**Fig. 5.6C**). Rapa MPs and PLP_{178}/Rapa MPs also showed significantly higher relative weights compared to PBS treated mice at different points throughout the study. Only PLP_{139}/Rapa MPs showed a significant reduction in the percentage of mice that were paralyzed during relapse compared to PBS treated mice (**Fig. 5.6D**). In addition, only PLP_{139}/Rapa MPs showing less severe cumulative disease scores (**Fig. 5.3E**). These results suggest that the timing of treatment (i.e. the level of inflammation) plays a role in the signals required to induce myelin-specific tolerance.

To further evaluate how effective tolerogenic PLP_{139}/Rapa iLN treatment is at later disease timepoints, mice were treated 30 days after induction, during relapse. Mice were treated with either PBS, Rapa MPs, PLP_{139}/Rapa MPs on day 30, during peak relapse. This timepoint is incredibly challenging to treat due to the established chronic disease that develops later in RR-EAE disease course. Mice treated with PLP_{139}/Rapa showed a reduced clinical score compared to PBS treated mice, though these differences were not significant until Day 44 (**Fig. 5.7A**). Relative weights for mice treated with PLP_{139}/Rapa MPs and PLP_{178}/Rapa MPs began increasing toward the end of the study (**Fig. 5.7B**), and cumulative clinical scores for PLP_{139}/Rapa and PLP_{178}/Rapa MP-treated mice began diverging from PBS and Rapa MP-treated mice around Day 35, though the results were not significant (**Fig.5.7C**). It is possible that with a longer study, differences in clinical scores would have become significant.

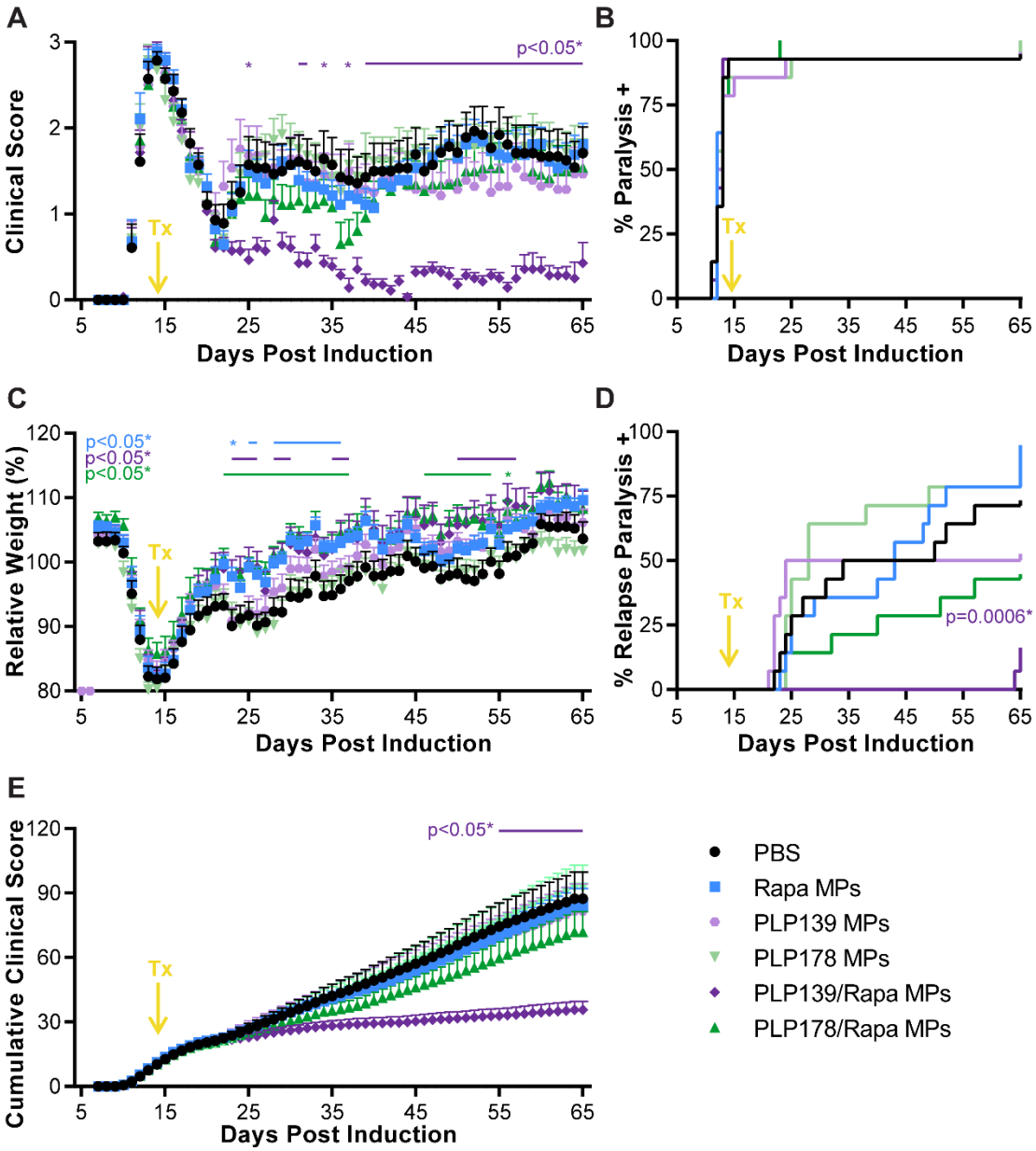

Figure 5.6 iLN treatment with PLP$_{139}$/Rapa MPs reverses disease and prevents relapse.

Mice were induced with RR-EAE on Day 0, and treated iLN with PBS, Rapa MPs, PLP$_{139}$ MPs, PLP$_{178}$ MPs, PLP$_{139}$/Rapa MPs or PLP$_{178}$/Rapa MPs on Day 14. (A) Only mean clinical score for PLP$_{139}$/Rapa MPs is significantly reduced compared to PBS treated control mice at any point during the study. Rapa, PLP$_{139}$, PLP$_{178}$, and PLP$_{178}$/Rapa MPs did not offer protection from relapse. (B) There were no differences in paralysis incidence between groups on the day of treatment. (C) Mice treated with Rapa MPs, PLP$_{139}$/Rapa, and PLP$_{178}$/Rapa MPs had significantly increased relative weights compared to mice treated with PBS at some point during the study. (D) Only mice treated with PLP$_{139}$/Rapa MPs showed reduced relapse paralysis incidence relapse compared to mice treated with PBS. (E) Only PLP$_{139}$/Rapa MP-treated mice saw reduced cumulative clinical scores compared to mice treated with PBS. Relative

weights were analyzed using a one way analysis of variance (ANOVA) by day with a correction for multiple comparisons to PBS treated mice using Dunnett's Method. Clinical score and Cumulative score were analyzed using a non-parametric rank test and corrected for multiple comparisons to PBS treated mice using the Steel Method. Percent Paralyzed and % Paralyzed after Relapse were analyzed using a long-rank test with a Bonferroni correction for multiple comparisons to PBS. N = 14 mice per group. The legend applies to all panels. Average + SEM is shown for relative weight and clinical score plots. Error bars are shown in one direction for simplicity.

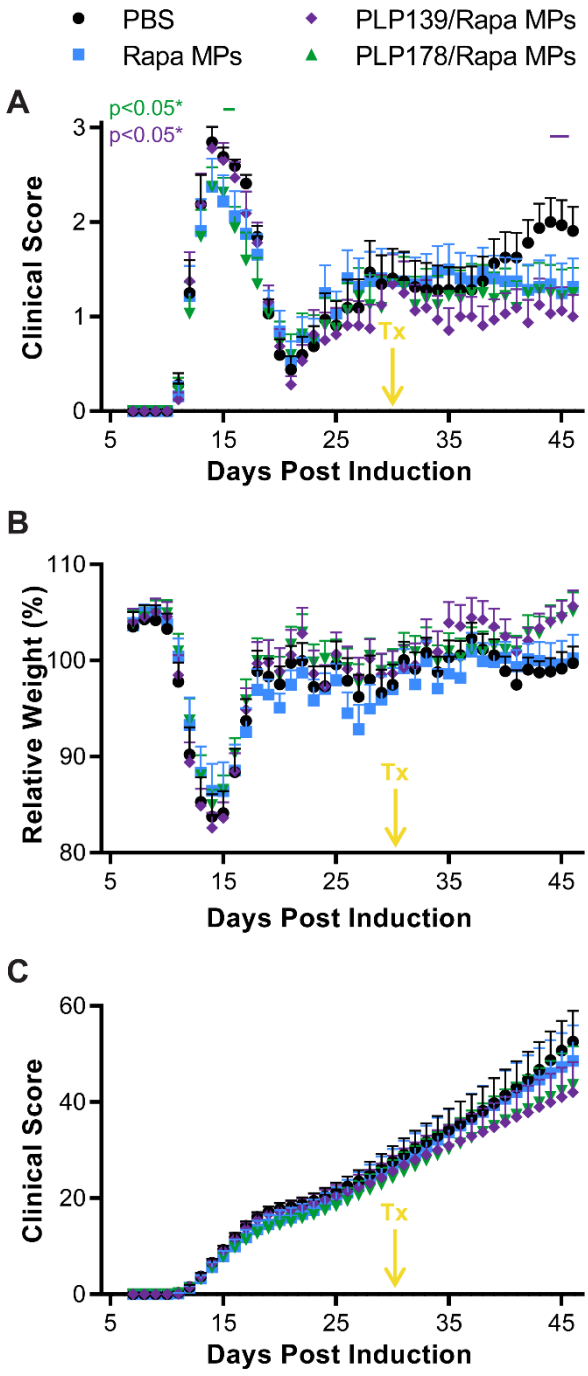

Figure 5.7 Treatment with PLP_{139}/Rapa MPs prevents disease worsening.
Mice were treated iLN 30 days after induction. Mice were treated with either PBS, Rapa MPs, PLP_{139}/Rapa MPs, or PLP_{178}/Rapa MPs. (A) Mice treated with PLP_{139}/Rapa MPs showed reduced clinical score compared to PBS treated mice, with significant differences starting Day 44. (B) Relative weights for mice treated with PLP_{139}/Rapa MPs and PLP_{178}/Rapa MPs began increasing toward the end of the study. (C) Cumulative clinical scores for PLP_{139}/Rapa and PLP_{178}/Rapa MP-treated mice began diverging from PBS and Rapa MP-treated mice around Day 35, though the results were not significant. Relative weights were analyzed using a one way analysis of variance (ANOVA) by day with a correction for multiple comparisons to PBS treated mice using Dunnett's Method. Clinical score and Cumulative score were analyzed using a non-parametric rank test with a correction for multiple comparisons to PBS treated mice using the Steel Method. Percent Paralyzed and % Paralyzed after Relapse were analyzed using a long-rank test with a Bonferroni correction for multiple comparisons to PBS. N = 16 mice per group. The legend at the top applies to all panels in the figure. Average + SEM is shown for relative weight and clinical score plots. Error bars are shown in one direction for simplicity.

Unfortunately, many of the mice in the PBS treated group needed to be censored after the last timepoint on the graph (Day 46), for non-study related reasons (i.e. not because they met their humane endpoints). However, it is clear from this study that mice treated with PLP_{139}/Rapa MPs do not get progressively worse after treatment, as PBS-treated mice do.

5.4.5 Tolerogenic MP treatment reduces immune cell infiltration into CNS.

To assess the impact of iLN therapy on the distant sites in the CNS – where disease occurs, the tissues from the mice treated 28 days before induction (**Fig. 5.5**), were collected 54 days after induction for analysis by flow cytometry. Inguinal LN and spinal cord tissues were collected. Counting beads were added to samples according to manufacturer's instructions to provide a count of cells present in each tissue. As shown

in **Fig. 5.8**, PLP139/Rapa MP treatment did not significantly impact the total number of cells present in the treated inguinal LNs (**Fig. 5.8A**) or in the spinal cord (**Fig. 5.8B**).

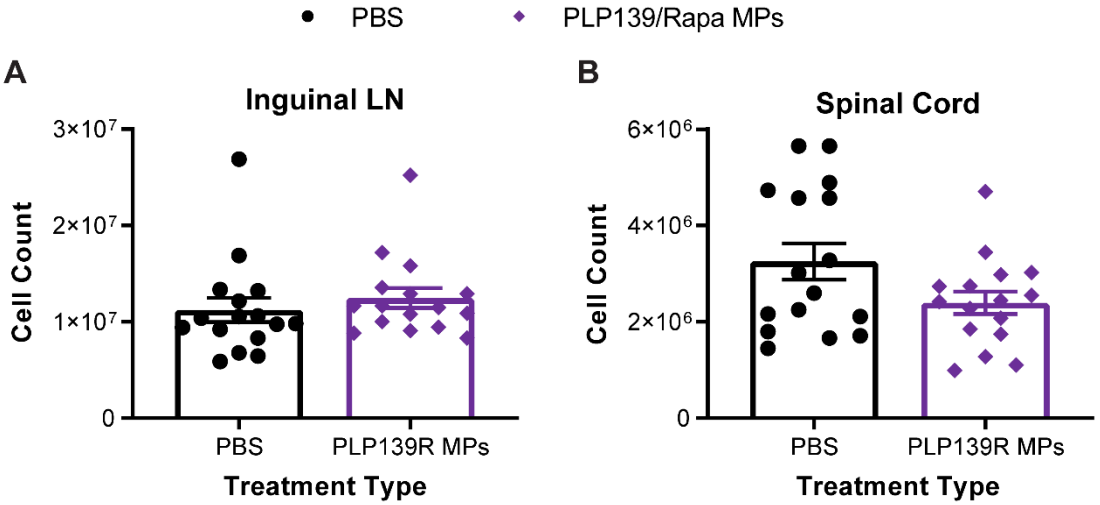

Figure 5.8 Tolerogenic MP iLN therapy does not impact cell counts in inguinal LN or spinal cord.
Mice were treated iLN 28 days before induction with RR-EAE on Day 0. Inguinal LNs and spinal cord were collected for flow analysis on Day 54. Tolerogenic MP treatment does not significantly impact cell count in the inguinal LN (A) or spinal cord (B). Counts were analyzed using a t test. The legend at the top applies to both panels in the figure. N = 16 mice per group. Average ± SEM is shown.

However, upon analysis for immune cell infiltration into the spinal cord, it became clear that there were differences (even after 54 days) in immune cell presence in the spinal cords between mice treated with PLP_{139}/Rapa MPs and mice treated with PBS. **Figure 5.9A** shows the gating scheme for analysis. A cell gate (of singlets) was drawn on the forward/side scatter plot. Live (DAPI negative) cells were selected, and then immune cells were identified using a CD45hi signal. CD4+ T cells were identified from Live cells with a CD45hi/CD4+ signal. PLP_{139}/Rapa iLN treatment significantly reduced immune cell infiltration, both by count (**Fig. 5.9B**), and by % of live cells (**Fig. 5.9C**). This reduction in immune cell infiltration also corresponded to a reduction in

CD4+ T cells in the spinal cords by both count (**Fig. 5.9D**), and by % of live cells (**Fig. 5.9E**).

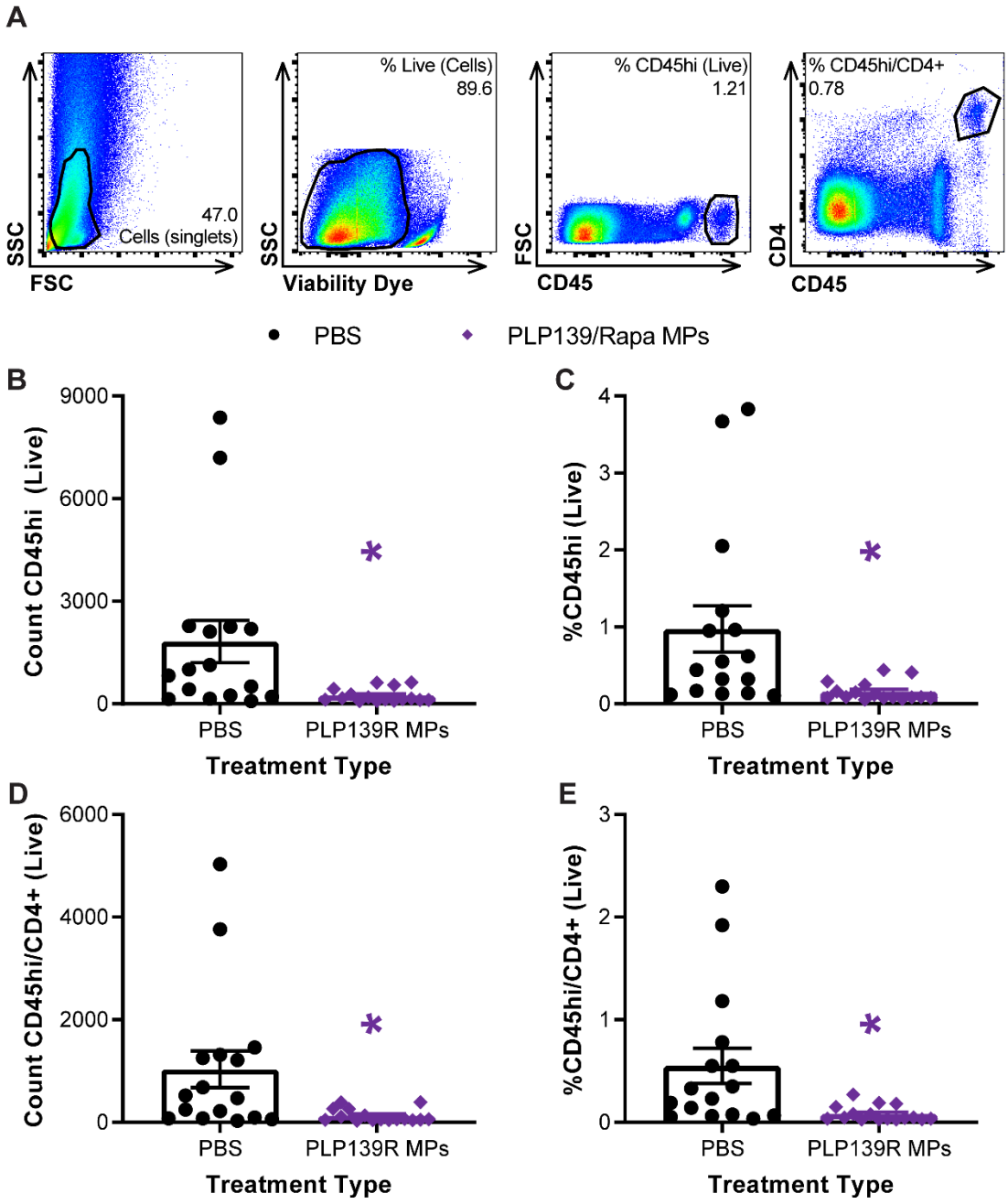

Figure 5.9 Tolerogenic iLN treatment with PLP_{139}/Rapa MP 28 days before induction causes reduced immune cell infiltration in CNS even 54 days after induction.

Mice were treated iLN 28 days before induction with RR-EAE on Day 0. Spinal cords were collected for flow analysis on Day 54. (A) Gating scheme for immune cell infiltration analysis. A cell gate (of singlets) was drawn on the forward/side scatter plot.

Live (DAPI negative) cells were selected, and then immune cells were identified using a CD45hi signal. CD4+ T cells were identified from Live cells with a CD45hi/CD4+ signal. (B) PLP_{139}/Rapa iLN treatment significantly reduced immune cell infiltration, both by count, and by % of live cells (C). (D) PLP_{139}/Rapa iLN treatment significantly reduced CD4+ T cell infiltration, both by count, and by % of live cells (E). Counts were analyzed using a t test. N = 16 mice per group. The legend above panels B and C at the top applies to panels B-D. Average ± SEM is shown.

These results, in combination with the results previously collected by our lab that show reduced T cell infiltration in mice with EAE treated iLN with MOG_{35}/Rapa MPs, motivate additional investigation into the impact of iLN therapy on the distant site of disease. Some ongoing and future work in this area is described in **Chapter 7.2 and Chapter 7.3**. These sections highlight studies that look into immune cell infiltration and myelin degeneration by immunohistochemistry, and look into the presence of inflammatory lesions in the CNS by magnetic resonance imaging.

5.4.6 Tolerogenic MP treatment does not impair healthy immunity

As discussed in **Chapter 3.3**, one major limitation of current MS therapies is the lack of specificity in treatments – current MS therapies cannot distinguish between healthy, normal lymphocytes and dysfunctional myelin-specific inflammatory cells, so they knock down immune function broadly. To assess the ability of tolerogenic MPs to induce myelin-specific tolerance without impacting healthy immunity.

In the second study presented where mice were treated 7 days after induction (**Figure 5.4**), after monitoring disease course as a result of iLN treatment, mice were vaccinated against a foreign protein, ovalbumin (OVA). **Figure 5.10A** shows the study schematic, in which mice were induced on day 0, treated on day 7, monitored until day

63. Mice were then vaccinated with OVA and adjuvant CpG to initiate an inflammatory immune response to OVA. Three weeks later, mice were boosted with another vaccine dose. Weekly blood doses were collected starting on day 63 (day 0 post vaccination). In addition to the iLN treated groups (PBS, Rapa MPs, PLP_{139} MPs, PLP_{178} MPs, PLP_{139}/Rapa MPs, and PLP_{178}/Rapa MPs), two additional groups were added to the vaccination study: age-matched naïve and age-match vaccinated mice (no RR-EAE). Serum was collected from the weekly blood draws, and anti-OVA IgG titers were assessed by ELISA. Excitingly, all groups given the vaccine were able to mount anti-OVA antibody levels statistically identical to or higher than healthy vaccinated mice that did not receive iLN therapy.

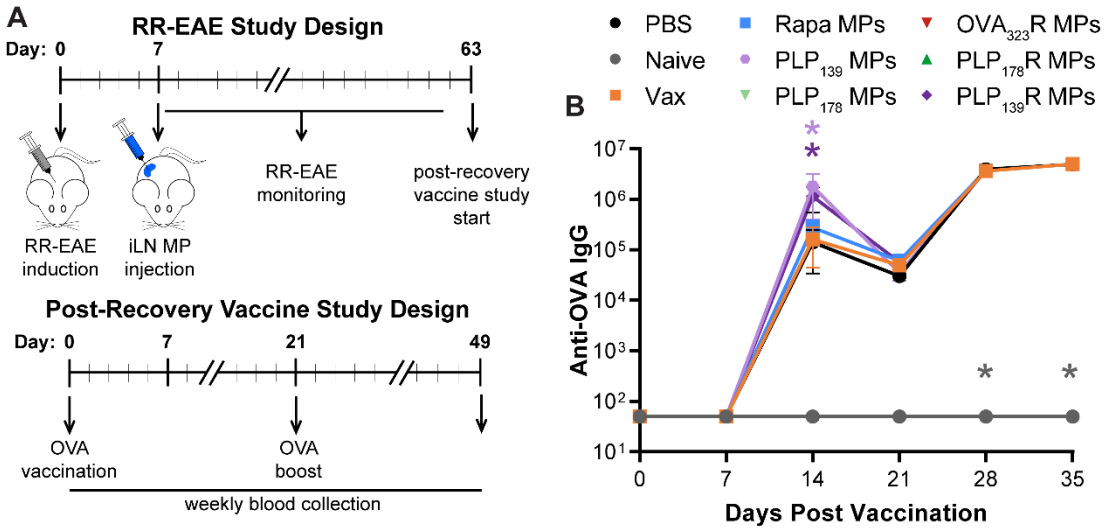

Figure 5.10 Mice treated iLN with tolerogenic MPs mount antibody responses to foreign protein at similar levels to healthy mice.
(A) Study schematic for RR-EAE study and post-recovery vaccine design.e Mice were induced on day 0, treated on day 7, and monitored until day 63. Mice were then vaccinated with OVA and adjuvant CpG, and boosted three weeks later. Weekly blood doses were collected starting on day 63 (day 0 post vaccination). Two groups were added to the study at the beginning of the post-recovery vaccine study: age-matched naïve and age-match vaccinated mice (no RR-EAE). (B) All groups given the vaccine were able to mount anti-OVA antibody levels similar to healthy vaccinated mice. Antibody titers were analyzed using a one way analysis of variance (ANOVA) by day

with a correction for multiple comparisons to healthy vaccinated mice using Dunnett's Method. N = 8 mice per group at start of study. Average ± SEM is shown.

As the previous vaccination study was started 56 days after the iLN therapy, a more rigorous study was designed to test the relative localization of immunotherapy and vaccination in tissues, to assess how intra-LN therapy impacted healthy immunity. This study was designed so that mice were treated iLN and vaccinated against OVA on the same day at peak disease. In addition, antibodies are only one aspect of an immune response, so this study as also designed to evaluate OVA-specific CD8+ T cell presence in blood after vaccination. This study was done in an EAE model so that OVA-specific CD8+ T cells could be reliably assessed. **Figure 5.11A** shows the study design. Mice were induced with EAE on Day 0, and weekly blood collections began on Day 8 post induction. On Day 15, mice were both vaccinated against OVA with CpG as an adjuvant at the scruff and treated iLN with MOG_{35}/Rapa tolerogenic MPs. Three weeks later, (Day 36), mice were boosted with OVA and CpG. Tissues were collected for restimulation with OVA and MOG_{35-55} on Day 58.

White blood cells were collected weekly during blood draws for analysis of OVA-specific CD8+ T cells. Cells were gated on singlets, then live cells, then CD8+ cells. OVA-specific CD8+ T cells were identified using a tetramer stain that presents OVA in the context of MHC-I so that OVA-specific T cells can bind the OVA and therefore be stained by the tetramer. Excitingly, all mice given the vaccine, including mice treated with the MOG_{35}/Rapa tolerogenic MPs, were able to make CD8+ T cells specific for OVA at similar levels to healthy vaccinated mice (**Fig. 5.11B**). Similar to the study presented in Fig. 5.10, all mice given the vaccine, including the tolerogenic

MPs, were able to mount anti-OVA antibody responses similar to healthy vaccinated mice (**Fig. 5.11C**). On day 58, LN tissues were isolated and restimulated ex vivo for 72 hours with OVA to assess T cell function by inflammatory cytokine signaling. Supernatants were collected at the end of the culture and inflammatory cytokine secretion was assessed by ELISA. Three sets of LN were collected – an axillary/brachial LN pool (vaccine draining LNs), the cervical LN (geographically close to vaccination site, additional draining LNs), and the treated inguinal LN (distant from vaccine site). Excitingly, cells collected from the axillary/brachial pool (**Fig. 5.11D, left**), and cervical LN pool (**Fig. 5.11D, middle**) of mice vaccinated with OVA/GpG and given tolerogenic MP treatments were able to produce inflammatory IFNg at similar levels to healthy vaccinated mice in response to OVA restimulation. Very little IFNg secretion was seen in any of the inguinal LN samples that were distant from the site of vaccination (**Fig. 5.11D, right**).

In addition to ensuring that mice were able to mount an immune response even during iLN therapy, it was important to ensure that iLN therapy still worked even given an inflammatory vaccine. Mice were monitored daily for clinical score. Excitingly, the tolerogenic treatment worked just as well in mice given the vaccine as it did in mice that only received the tolerogenic iLN treatment (**Fig. 5.12A**). Both groups were significantly different from mice given PBS treatments iLN. This also corresponded to significantly increased relative weights compared to PBS treated mice (**Fig. 5.12B**), and significantly decreased cumulative scores compared to PBS treated mice **(Fig. 5.12C**).

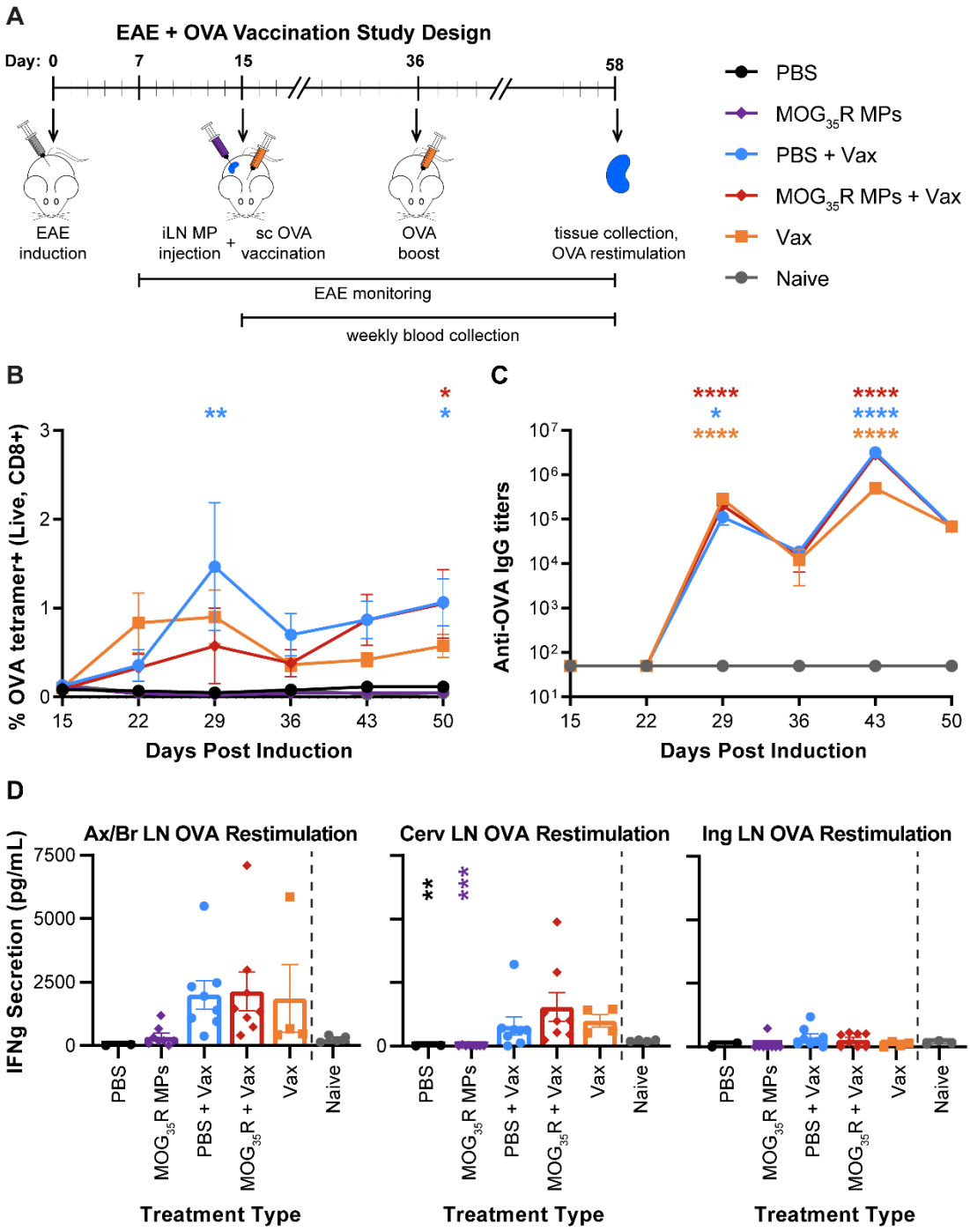

Figure 5.11 Mice given tolerogenic iLN treatment and vaccinated against OVA on the same day mount similar immune responses to healthy vaccinated mice.
(A) Study schematic. Mice were induced with EAE on day 0. On day 15, mice were given both an iLN tolerogenic treatment and vaccinated with OVA/CpG at the same time. Weekly blood draws were used to collect white blood cells and serum. On day 58, immune tissues were collected from mice and restimulated for 72 hours using OVA to assess inflammatory T cell activity. Supernatants from cultures were collected and

assessed for inflammatory cytokine secretion. (B) Tolerogenic MP treatment does not prevent mice from producing OVA-specific CD8+ T cells at similar levels to healthy, vaccinated mice. (C) Mice given tolerogenic iLN treatment are able to mount similar anti-OVA antibody responses. (D) Cells from mice treated iLN with tolerogenic MPs are able to produce IFNg at similar levels to healthy, vaccinated mice in vaccine-draining axillary/brachial LN (left) and cervical LN (center). Very little IFNg is seen in response to OVA at the distant, non-draining, iLN treated inguinal LN (right). Tetramer, antibody titers, and IFNg secretion were analyzed using a one way analysis of variance (ANOVA) by day with a correction for multiple comparisons to naive mice using Dunnett's Method. N = 8 mice per group at start of study for PBS, PBS + Vax, $MOG_{35}R$ MPs, $MOG_{35}R$ MPs + Vax groups. N = 4 for Naïve and Vax groups. Average ± SEM is shown.

On Day 58, the same day as the OVA restimulations, cells from the LN of mice were also restimulated with MOG_{35-55} to assess if there were changes in inflammatory cytokine secretion as a result of the vaccination. Cells from LN were cultured for 72 hours with MOG_{35-55}, and supernatants were collected at the end of the culture and analyzed for cytokine secretion by ELISA. Excitingly, cells from the axillary/brachial LN of mice treated the iLN tolerogenic therapy, regardless of the vaccination, showed decreased IFNg (**Fig. 5.13A**) and GM-CSF (**Fig. 5.13B**) secretion. This was also true for CNS draining cervical LN (IFNg, **Fig, 5.13C**, and GM-CSF, **Fig. 5.14D**), and for iLN therapy treated inguinal LN (IFNg, **Fig, 5.13E**, and GM-CSF, **Fig. 5.14F**).

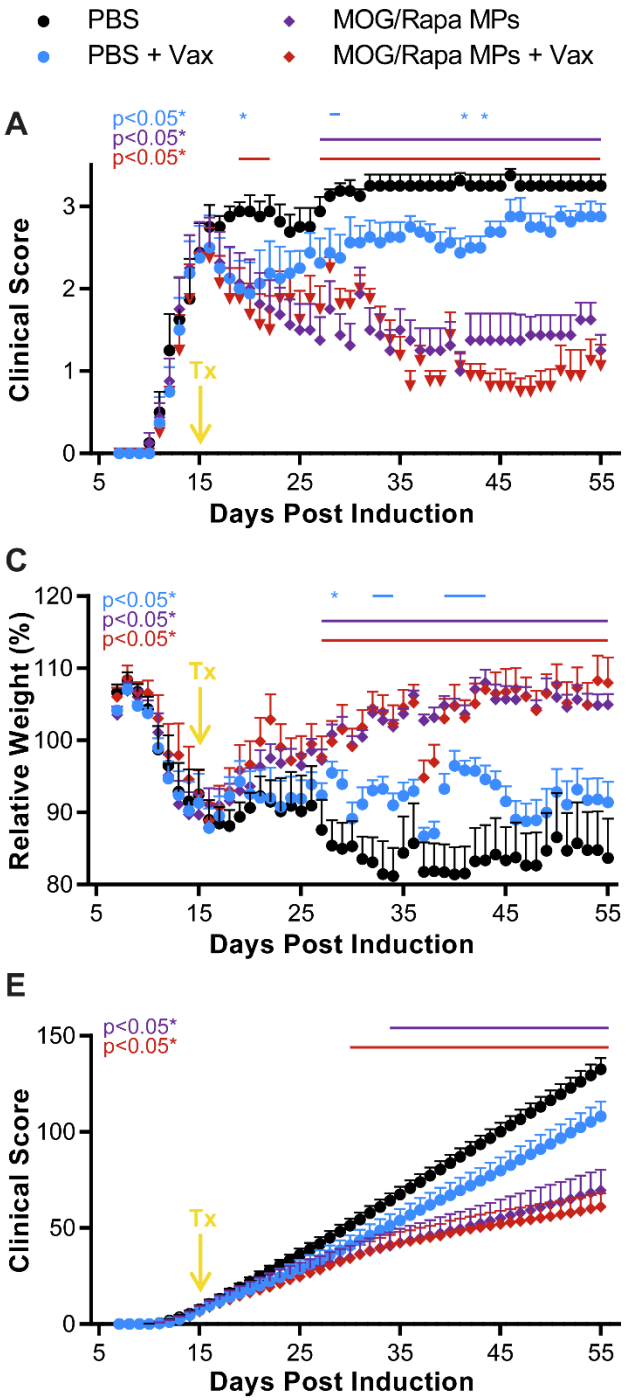

Figure 5.12 Vaccination does not interfere with tolerogenic iLN treatment efficacy.

Mice were induced on day 0, and treated iLN with tolerogenic MPs on day 15. On the same day, mice were vaccinated against OVA at the scruff. Mice were boosted with the same vaccine regimen on day 36. (A) Mice treated with MOG_{35-55}/Rapa MPs, regardless of vaccination, showed significantly reduced clinical scores compared to PBS treated mice. Tolerogenic MP treatment, with or without vaccination, allowed for significantly increased relative weights (B) and significantly reduced cumulative scores

(C) compared to PBS treated mice. Relative weights were analyzed using a one way analysis of variance (ANOVA) by day with a correction for multiple comparisons to PBS treated mice using Dunnett's Method. Clinical score and Cumulative score were analyzed using a non-parametric rank test with a correction for multiple comparisons to PBS treated mice using the Steel Method. Percent Paralyzed and % Paralyzed after Relapse were analyzed using a long-rank test with a Bonferroni correction for multiple comparisons to PBS. The legend at the top applies to all panels in the figure. Average + SEM is shown for relative weight and clinical score plots. Error bars are shown in one direction for simplicity.

Excitingly, these results combined suggest that tolerogenic iLN treatment does not impair a mouse's ability to mount normal immune responses, similar to healthy mice. This study showed that in the same mouse, at the same time, the tolerogenic MPs could induce tolerance to myelin while the vaccine stimulated an inflammatory response to OVA. This is important, as a major limitation of current MS therapies is the lack of specificity of treatment, and therefore the inability to differentiate between healthy immune cells and dysfunctional, myelin-reactive inflammatory cells, leaving patients vulnerable to infections.

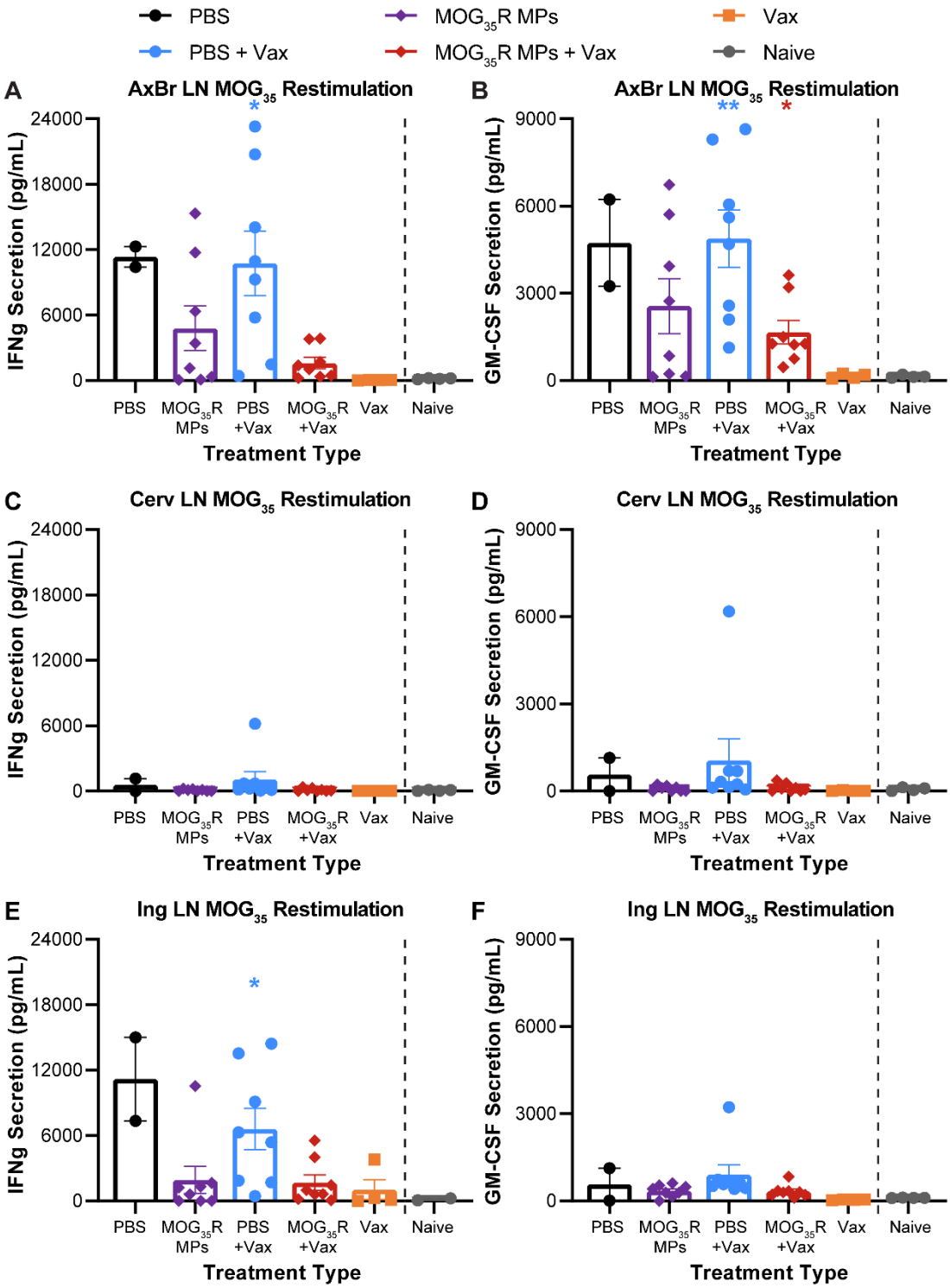

Figure 5.13 Treatment with tolerogenic MPs reduces inflammatory cytokine response to myelin, regardless of vaccination against OVA.

Mice were induced on day 0, and treated iLN with tolerogenic MPs on day 15. On the same day, mice were vaccinated against OVA at the scruff. Mice were boosted with the same vaccine regimen on day 36, then cells were collected from inguinal LN on day 58 and restimulated with MOG_{35}. Cells from the axillary/brachial LN of mice

treated the iLN tolerogenic therapy, regardless of the vaccination, showed decreased IFNg (A) and GM-CSF (B) secretion following re-stimulation with MOG_{35}. This was also true for CNS draining cervical LN IFNg (C) and GM-CSF (D) secretion, as well as iLN therapy treated inguinal LN IFNg, (E), and GM-CSF (F) secretion. IFNg and GM-CSF secretion were analyzed using a one way analysis of variance (ANOVA) with a correction for multiple comparisons to naive mice using Dunnett's Method. N = 8 mice per group PBS + Vax, MOG_{35}R MPs, MOG_{35}R MPs + Vax groups. N = 4 for Naïve and Vax groups. N = 2 for PBS group, as mice were censored for non-study related reasons. Average ± SEM is shown.

5.5 Discussion

As discussed in **Chapter 3.3**, therapies that enable myelin-specific tolerance could provide both more selective and more effective therapies for MS. Tolerogenic MP treatment provide an opportunity to reprogram the LN microenvironment to condition myelin-specific T cells for tolerance. This work aimed to advance pre-clinical studies and motivate clinical research by investigating the systemic impact of intra-LN tolerogenic MPs in two mouse models of MS – progressive MS (EAE, experimental autoimmune encephalomyelitis), and relapsing-remitting (RR) MS (RR-EAE). Importantly, this dissertation tested the impact of treatment with different combinations of immune cues at different time, and found that only the set of MPs loaded with rapamycin and the peptide that matched the main inflammatory antigen ($PLP_{139-151}$) was able to significantly reduce disease severity at different timepoints.

This was an important finding for the iLN platform. Prior to disease onset in RR-EAE, treating with MPs loaded with $PLP_{139-151}$ alone does significantly reduce the incidence of paralysis during the first wave of disease (**Fig. 5.3B** and **Fig. 5.4B)**, and does reduce the incidence of paralysis during relapse (**Fig. 5.3D** and **Fig. 5.4D**), suggesting that there is the promotion of tolerance following these treatments. This is

in line with previous work in the Jewell lab that shows treatment with MOG_{35-55} MPs prior to disease onset significantly reduces disease severity compared to Empty MP treated mice[26]. These findings are supported by several studies that have shown that delivering myelin alone, in the absence of inflammatory (or regulatory) signaling, promotes tolerance to myelin[106, 183, 184]. However, in the case of iLN therapy, once disease is established (e.g. treatment at peak disease), treatment with $PLP_{139-151}$ alone is not enough to promote tolerance (**Fig. 5.6**). Given that inflammation is already present in the CNS around $PLP_{139-151}$ peptides, and given that myelin peptides are trafficked from the CNS to peripheral LN in human MS patients and in animal MS models[240, 241], it is possible that after disease has been established, $PLP_{139-151}$ is presented to myelin-specific T cells in an inflammatory context, eliminating the tolerogenic impact of the iLN therapy. These studies motivate the use of the combined therapy – with rapa and the myelin peptide of interest for the mouse model.

The fact that the PLP_{178} MP therapy did not work at any treatment timepoint, and the PLP_{178}/Rapa MP efficacy seemed to be due mostly to the inclusion of Rapa in the MPs suggests the importance of selecting appropriate antigens for the iLN tolerogenic therapy. While PLP_{178} is a myelin epitope, and while it is responsible for some of the inflammation associated with the relapse period in RR-EAE[242, 243], treatment with this epitope alone was not enough to overcome inflammation to $PLP_{139-151}$. This is important knowledge for this study, as mouse models do not completely recreate the epitope spreading present in human disease. Within weeks of a patient's first event, epitope spreading occurs – in which patients become reactive to other sections of myelin, not just the one they were originally reactive to – as inflammation

in the CNS and damage to myelin enables inflammatory signaling around other sections of myelin. This epitope spreading can occur both intra-molecularly (i.e. one PLP epitope to another), or even intermolecularly (e.g. PLP to MBP), and varies from patient-to-patient. As such, recent clinical trials that aim to promote myelin tolerance by conjugating myelin epitopes to tolerogenic DCs or autologous PBMCs typically use seven different myelin epitopes (MBP_{13-32}, MBP_{83-99}, $MBP_{111-129}$, $MBP_{146-170}$, MOG_{1-20}, MOG_{35-55}, and $PLP_{139-154}$)[181, 244-246]. In addition, recent research has shown that as MS evolves, additional self-reactive immune cells specific to proteins present in neuronal bodies (e.g. β synuclein) contribute to neurodegeneration in late stage disease[141, 142]. Importantly, the modular nature of the iLN therapy synthesis process allows for the incorporation of multiple myelin epitopes into a tolerogenic iLN therapy treatment, either by incorporating them all into the same MPs with rapamycin or by mixing known ratios of individual peptide-loaded MPs. However, this study does highlight the importance of identifying appropriate antigens for iLN therapy.

Further, the day 30 treatment study (**Fig. 5.7**) showed that while late stage (relapse, chronic disease stage in RR-EAE) treatment did not reverse paralysis in 15 days, it did prevent worsening of symptoms. It is possible that if the study had been further elongated, changes in clinical score may have been clear. However, it is important to note that goal of currently available MS therapies is delaying disease progression, so these results align closely with the clinical goal. This also brings up an important limitation of MS therapies: they do not promote remyelination. Without remyelination of their nerve cells, it is unlikely patients will experience improvements in symptoms. Myelin is deposited around nerve cells by oligodendrocytes in the CNS.

As myelin-reactive immune cells attack myelin and induce inflammation in the CNS, they also activate tissue-resident cells – microglia and astrocytes, causing chronic inflammation in the brain[132]. Over time, this chronic inflammation causes damage to nerve cells and oligodendrocytes, which in turn limits the deposition of new myelin to repair damaged myelin sheaths. If the iLN therapy enables regulatory T cells that can resolve the inflammation in the CNS, and damaged myelin can be removed, it is possible that oligodendrocyte precursor cells present in the brain could differentiate into mature oligodendrocytes that could deposit new myelin in damaged areas[247, 248]. Several clinical trials are ongoing for therapies that are specifically aimed at remyeliniating nerve cells[248] (NCT03993171, NCT03536559, NCT03222973, NCT02398461[247]), so it is also possible iLN therapy could work in combination with a promising remyelinating therapy for best results. To better assess the impact of iLN therapy on the state of myelination in the CNS, we will be looking into myelination in the CNS following iLN therapy by immunohistochemistry and MRI. These ongoing and future work areas are described in **Chapter 7.2 and Chapter 7.3**.

Lastly, the results collected in the vaccination study (**Chapter 5.4.6**) suggest that the tolerogenic iLN treatment does not impair a mouse's ability to mount antibody and T cell responses to vaccines at similar levels to healthy mice. This study showed that in the same mouse, at the same time, the tolerogenic MPs could induce tolerance to myelin while the vaccine stimulated an inflammatory response to OVA. This is important, as a major limitation of current MS therapies is the lack of specificity of treatment, and therefore the inability to differentiate between healthy immune cells and

dysfunctional, myelin-reactive inflammatory cells, leaving patients vulnerable to infections.

5.6 Conclusion

Current therapies for MS lack specificity, and limit functions of both dysfunctional myelin-reactive inflammatory cells and healthy immune cells. Intra-LN treatment with biodegradable polymeric microparticles (MPs) co-loaded with myelin peptides and rapamycin, promotes myelin-specific regulatory immune cell function to control myelin-specific inflammation in mouse models of MS. The work in this dissertation was done to advance pre-clinical knowledge and motivate clinical research by investigating the systemic impact of intra-LN tolerogenic MPs in mouse models of relapsing-remitting MS and progressive MS. The results in this is chapter show that even at different stages of disease, one tolerogenic intra-LN treatment promoted recovery from paralysis and prevented relapse. In addition, these results showed that tolerogenic intra-LN treatments did not prevent mice from mounting healthy immune responses to vaccination. The work in this chapter, in combination with the work in **Chapter 6** motivate investigation into intra-LN delivery of tolerogenic MPs as a potential MS immunotherapy candidate for clinical translation.

Chapter 6: Enhancing the Stability of Polymer Microparticles for Autoimmune Therapy[3]

6.1 Introduction

While the low dosage requirements of the studies presented in **Chapters 4 and 5** allowed for on-demand preparation, clinical translation requires investigation into manufacturing, preservation, storage, and stability of this immunotherapy. Here, we test the stabilizing effects of excipients and lyophilization on polymeric PLGA microparticles (MPs) loaded with a peptide antigen and a small molecule immunomodulator. We synthesized and lyophilized particles with three different excipients: mannitol, trehalose, and sucrose, and then characterized and evaluated each formulation in vitro. Adding excipients either during the synthesis process or prior to lyophilization promoted MPs stability, evident in smaller changes in MP size distribution over time, lyo-cake quality, and MPs reconstitution efficiency. In vitro treatment of immune cells revealed that MPs lyophilized with excipients maintained the biofunctionality of their cargo as well as MPs lyophilized without excipients. The characterization revealed that adding low concentrations of excipients was best suited for this application. Knowledge of methods that can control the effects of excipients and lyophilization of PLGA MPs will advance the development for carriers of biologics and small molecules in immunotherapy.

[3] Adapted From: **E.A. Gosselin***, M. Noshin*, S.K. Black, and C.M. Jewell, "Enhancing the Stability of Polymer Microparticles for Autoimmune Therapy." Submitted to: *Frontiers in Bioengineering and Biotechnology.*
*E.A. Gosselin and M. Noshin contributed equally to this work.

6.2 Background

Polymeric particles and scaffolds have been widely researched as carriers for biologics and small molecules to improve delivery of cargo to cell and tissue targets[197, 249-251]. One important emerging area applies these carriers to immunotherapies by delivering peptides recognized by the immune system (antigens) and immune cues to modulate immune response[65, 105, 168, 252, 253]. This development is motivated by the unique benefits of polymeric and other designed carriers in the context of immunotherapy, including co-delivery of immune signals, controlled release, prolonged cargo exposure, cargo protection, and preferential delivery to target immune cells[168, 252]. While incorporating biomaterial carriers into these exciting new therapies adds potential, these components also add complexity for manufacturing and regulatory characterization. This is an important area to address at an early stage to support more efficient translation of new immunotherapies.

We and others have recently explored biomaterials to correct the excess inflammation and defects that occur in autoimmune disease using the control that polymer carriers provide[67, 168, 254, 255]. MS occurs when the body's immune system incorrectly attacks myelin, the matrix that surrounds neurons in the central nervous system. This attack is driven by myelin-specific immune cells, resulting in inflammation, neurodegeneration, and demyelination in the central nervous system (CNS)[129-131]. MS is treated with disease-modifying therapies that have improved patient quality of life, but that are non-curative and non-specific. Even the newest monoclonal antibodies do not differentiate between normal cells and dysfunctional myelin-reactive immune cells or lymphocytes; this can leave patients susceptible to

infection[146]. Therefore, an important goal for next generation therapies is the induction of antigen-specific tolerance – correcting defects that occur in autoimmune disease without impacting normal immune responses. For example, using a simple, easily scalable degradable polymer (poly(lactide-co-glyolide), PLGA), we developed microparticle depots that promote regulatory immune function and reverse disease in preclinical models of multiple sclerosis (MS). These depots recondition the local environment of lymph nodes – tissues that coordinate immune function – by co-delivering myelin self-peptide (MOG) and an immunomodulatory cue, rapamycin (Rapa). This shifts the response to myelin away from inflammation and toward tolerance in a selective fashion[26].

While these and other pre-clinical studies often afford the ability to make and begin testing immunotherapies on demand, translating candidates therapies requires additional considerations to chemistry and manufacturing controls (CMCs), stability, and characterization after storage. These are all crucial aspects for regulatory approval, but receive little attention in the drug delivery field relative to the number of pre-clinical therapeutic studies. Even well-established materials such as PLGA MPs have ongoing issues for clinical translation in therapeutic contexts. While PLGA is commonly used in humans – degradable sutures for example, the degradation hydrolysis products - lactic acid and glycolic acid, can be metabolized by cells[197, 198]. Further, any type of storage of particles in an aqueous state requires consideration of unwanted cargo release, particle aggregation and fusion, and how effectively cargo integrity is maintained during storage[199]. Thus, the stability, transport, and storage of

immunotherapeutic particles formed from degradable biopolymers is an important focus area.

As the pharmaceutical industry has long shown, freeze-drying (lyophilization) – a controlled dehydration process – is a common route to support particle storage that stabilizes particles and reduces degradation and aggregation. Lyophilization dehydrates particle suspensions via three steps: (1) freezing, (2) water removal by sublimation, and (3) desorption of unfrozen water by vacuum[199]. However, polymer particles are complex, and their structure is susceptible to damage from the stresses of freeze-drying[199, 256], as well as the risks to the sensitive cargos that incorporated in these cargos as part of many immunotherapies. To limit this stress, cryoprotectants and lyoprotectants, including sugars such as mannitol, sucrose, and trehalose, can be added to alter the glass transition temperature of polymers and allow for a higher freezing rate[256-259]. These changes to the lyophilization process hinder ice crystal formation and limit mechanical stresses on particles, which results in better resuspension of the particles[260-263]. The resulting glassy matrix also immobilizes MPs to protect from aggregation and degradation[199, 262]. Further, in the context of immunotherapies aimed at autoimmunity, these issues are crucial since the immune system amplifies responses; this means the homogeneity and stability of therapies that rely on particle delivery have an equally important role in determine efficacy and safety.

Although PLGA particles have been extensively characterized, there are new knowledge gaps to address for immunotherapies and autoimmune therapies to ensure CMC considerations (e.g., lyophilization, long-term storage) do not impact integrity

and cargo immune function during translation. To study the role of sugars as cryoprotectant in the freeze-drying of PLGA MP depots co-loaded with the candidate autoimmune therapeutic components mentioned above, we prepared samples of MPs loaded with MOG and Rapa, along with cryoprotectants. These cryoprotectants included mannitol, sucrose, or trehalose that were either encapsulated in the MP depots during particle synthesis, or incorporated externally by resuspending in an aqueous solution with the cyroprotectant. The therapeutic MPs were then lyophilized and characterized to assess the long-term particle stability and cargo functionality following lyophilization and storage at room temperature. In this study, we show that low concentrations of encapsulated and externally incorporated excipients enhance the stability of MPs after 5 months in storage at room temperature. MPs loaded with low concentrations of excipients were resuspended more effectively than MPs without excipients, and also showed a smaller increase in size after storage than MPs with no excipients. In addition, loading excipients into MPs did not impact cargo biofunctionality – all MPs loaded with Rapa caused a decrease in immune cell activation, while all MPs loaded with MOG caused proliferation of MOG-specific T cells.

6.3 Materials and Methods

6.3.1 Materials

50:50 Poly(lactide-co-glycolide) (PLGA) [inherent viscosity range: 0.55-0.75 dL/g] was purchased from Durect Corporation (Birmingham, AL USA). High molecular weight poly(vinyl alcohol) (PVA) was purchased from Alfa Aesar

(Tewksbury, MA USA). Dichloromethane, mannitol, sucrose, and trehalose were purchased from Sigma Aldrich (St. Louis, MO, USA). Dimethyl sulfoxide was purchased from ThermoFisher Scientific (Waltham, MA, USA). Myelin oligodendrocyte glycoprotein peptide (MOG_{35-55}, MEVGWYRSPFSRVVHLYRNGK) was synthesized by Genscript (Piscataway, NJ, USA) with ≥98% purity, and Rapamycin was obtained from LC Laboratories (Woburn, MA, USA).

6.3.2 Preparation of Microparticles

6.3.2.1 Synthesis of MPs

Microparticles (MPs) were synthesized by double emulsion and solvent evaporation as previously described[26]. Briefly, an inner aqueous phase of 500 µL was prepared with either water or 1 mg MOG_{35-55} in 500 µL water. For MPs with encapsulated excipients, mannitol, sucrose, or trehalose was loaded in the inner aqueous phase at 1%/5%/ 10% w/v. An organic phase of 80 mg of PLGA dissolved in 5 mL dichloromethane; for Rapamycin (Rapa) loaded MPs, 2 mg of Rapa was loaded into the organic phase prior to synthesis. The inner aqueous and organic phases were sonicated for 30 s at 12 W to form a water/oil emulsion. The primary emulsion was then homogenized with an outer aqueous phase of 40 mL 2% w/v PVA for 3 min at 16,000 rpm. MPs were stirred at 350 rpm for 16 h to allow for solvent evaporation, then poured through a 40µm cell strainer and collected using centrifugation (5 min at 5000 g, 4°C). The supernatants were removed, the MPs were washed three times in 1 mL water with collection by centrifugation after each wash. The particles were then

resuspended in 1 mL of water. For MPs with externally incorporated excipients, the MPs were resuspended in 1 mL of 1%/5%/10% w/v of mannitol, sucrose, or trehalose. Each MP formulation was prepared once and separated into vials for lyophilization.

6.3.2.2 Lyophilization of MPs

MPs prepared with or without the cryoprotectants (mannitol, sucrose, or trehalose) incorporated either externally or by encapsulation at different concentrations (1%, 5%, 10%) were placed into glass vials and flash frozen on dry ice. Frozen samples were loaded into a FreeZone 6 L Console -84C Freeze Dryer (Labconco, Kansas City, MO, USA) and lyophilized over 48 h. Samples were removed from the freeze dryer, capped and sealed air-tight, and allowed at least 24 h to acclimate to room temperature and pressure before samples were characterized. Lyophilized samples were stored at room temperature.

6.3.3 Characterization of Microparticles

6.3.3.1 Stability and Reconstitution Studies

Lyophilized MPs were stored at room temperature for 5 months post lyophilization. MPs were then reconstituted in 200 μL of water and vortexed for 10 seconds. To assess ease of reconstitution, supernatants were extracted, and remaining MPs were air dried. The mass of remaining MPs was measured. Measurements were performed once. Percent reconstituted MPs was calculated using the following equation:

$$\textbf{Reconstitution Efficiency}\ (\%) = \frac{\textbf{Initial Mass MPs} - \textbf{Remaining Mass MPs}}{\textbf{Initial Mass MPs}} \times \mathbf{100}$$

6.3.3.2 MPs Loading Analysis

To measure the loading of Rapa and MOG_{35-55} in MPs, a known volume of MPs was either air-dried or lyophilized to remove water from the sample. Dried MPs were dissolved in dimethyl sulfoxide. Rapa loading was measured by UV/Vis spectrophotometry, and MOG_{35-55} loading was measured using a Micro Bicinchoninic Acid (mBCA) Protein Assay kit (ThermoFisher Scientific Pierce, Waltham, MA USA) according to manufacturer's instructions. Standard curves of known concentrations were used to calculate loading, reported as the mass of cargo per mass of dried MP formulation. Loading analysis was performed twice for consistency. Encapsulation efficiency was calculated by normalizing loading to drug input during MP synthesis:

$$\textbf{Loading Efficiency}\ (\%) = \frac{\textbf{Drug entrapped in MPs}}{\textbf{Total drug added initially}} \times \mathbf{100}$$

6.3.3.3 MPs Size and Polydispersity Index

Particle size and polydispersity index (PDI) were measured using an LA-950 laser diffraction size analyzer (Horiba Instruments, Irvine, CA, USA). Size was measured twice to ensure consistency. Polydispersity index was assessed using the following equation:

$$\textbf{PDI} = \left(\frac{\textbf{standard deviation}}{\textbf{mean diameter}}\right)^{\mathbf{2}}$$

6.3.4 In vitro Cargo Functionality Cellular Assays

6.3.4.1 Cell Culture

Primary dendritic cells were isolated from spleens of female C57BL/6J mice (The Jackson Laboratory, Bar Harbor, ME, USA, IMSR Cat# JAX:000664, RRID:IMSR_JAX:000664) female mice. DCs were isolated by positive selection for CD11c using a magnetic isolation kit according to manufacturer's instructions (Miltenyi Biotech, Bergisch Gladbach, Germany). Primary $CD4^+$ MOG_{35-55} specific T cells were isolated from the spleens of transgenic "2D2" mice (C57BL/6-Tg(Tcra2D2,Tcrb2D2)1Kuch/J), (The Jackson Laboratory, IMSR Cat# JAX:006912, RRID:IMSR_JAX:006912). MOG_{35-55} specific T cells were isolated using a magnetic $CD4^+$ T cell negative selection kit according to manufacturer's instructions (STEMCELL Technologies, Vancouver, BC, Canada).

All cells were cultured with DC 2.4 Media, comprised of RPMI1640 media + L-glutamine (ThermoFisher Scientific, Gibco), supplemented with 10% fetal bovine serum (Sigma Aldrich), 1X Pen/Strep, 2 mM L-glutamine (ThermoFisher Scientific, Gibco), 1 X Non-Essential Amino Acids and 10 mM HEPES (ThermoFisher Scientific, Hyclone GE Healthcare Life Sciences), and 55 μM β-mercaptoethanol (Sigma Aldrich), and incubated at 37°C.

All animal studies were fully compliant with local, state, and federal guidelines per the Association for Assessment and Accreditation of Laboratory Animal Care (AAALAC) expectations for animal care and use/ethics. All studies were approved and

carried out under the supervision of the University of Maryland Institutional Animal Care and Use Committee (IACUC).

6.3.4.2 Flow Cytometry Studies

Following incubation times listed below, cells were prepared for analysis by flow cytometry. All antibodies were purchased from BD Biosciences (Franklin Lakes, NJ, USA). All analyses were completed performed on a FACS Celesta (BD Biosciences) and data analysis was conducted using FlowJo (BD Biosciences Tree Star, FlowJo, RRID:SCR_008520) version 10.6).

6.3.4.3 In Vitro DC Activation Studies

Lyophilized MPs were stored at room temperature for 5 months. Fresh MPs for comparison were prepared without sugars the night before uptake studies. Primary DCs were seeded into a 96 well plate at 10^5 cells per well and cultured with DC2.4 media. DCs were activated with lipopolysaccharide (Sigma Aldrich) at 0.25 μg/mL, and then treated with 5-21 μg of MPs formulation, dose-matched to provide 91 ng Rapa per well. Empty MPs were used as controls for Rapa-loaded MPs to assess differences due to MPs formulation. Cells and MPs were cultured for 18 hours. DCs were then stained for activation. Cells were first blocked with anti-CD16/CD32, then stained for CD11c, CD40 (BD Biosciences Cat# 553791, RRID:AB_395055), CD80 (BD Biosciences Cat# 560016, RRID:AB_1645212), CD86 (BD Biosciences Cat# 560582, RRID:AB_1727518), and viability using DAPI. Functionality of Rapa was assessed by a change in expression of DC activation markers. All flow cytometry data analysis was completed using Flowjo software (Tree Star). All samples were compared to Rapa MPs

lyophilized with no excipient using Welch's ANOVA with a Dunnett's test for multiple comparisons. DC activation studies were performed twice, in triplicate, to ensure consistency.

6.3.4.4 In Vitro T Cell Proliferation Studies

Lyophilized MPs were stored at room temperature for 5 months. Fresh MPs for comparison were prepared without sugars the night before uptake studies. Similar to DC activation studies, primary DCs were seeded into a 96 well plate at 10^5 cells per well and cultured with DC2.4 media. DCs were activated with lipopolysaccharide at 0.25 μg/well, and then treated with 5-10 μg of MPs, dose-matched to provide 68 ng of MOG_{35-55} per well. DCs and MPs were cultured for 24 hours, after which MOG_{35-55} specific $CD4^+$ T cells were added to the wells at $3x10^5$ cells per well. To assess T cell proliferation, prior to addition to the wells, T cells were labeled with Cell Proliferation Dye eFluor 450 (ThermoFisher Scientific eBioscience). A media only and a soluble MOG_{35-55} + LPS well served as controls for low and high T cell proliferation, respectively. Cells were cultured for 72 h more and then stained for proliferation. Cells were first stained for viability using Fixable Viability Stain 510 (BD Biosciences), then blocked with anti-CD16/CD32, and stained for CD4 BD Biosciences Cat# 552051, RRID:AB_394331). Functionality of MOG_{35-55} was evident by proliferation of MOG_{35-55} specific T cells treated with MPs loaded with MOG_{35-55}. Rapa functionality was evident by a decrease in proliferation of T cells treated with MPs co-loaded with Rapa. All flow cytometry data analysis was completed using Flowjo software (Tree Star). The Proliferation Index of the sample was calculated using Flowjo Proliferation software analysis, and is calculated using the following equation:

$$\textbf{\textit{Proliferation Index}} = \frac{\textbf{\textit{Total Number of Cell Divisions}}}{\textbf{\textit{Total Number of Dividing Cells}}}$$

All samples were compared to MOG MPs lyophilized with no excipient using Welch's ANOVA with a Dunnett's test for multiple comparisons. T cell proliferation studies were performed twice, in triplicate, to ensure consistency.

6.3.4.5 Cytokine Secretion

Inflammatory cytokine secretion was quantified by ELISA according to manufacturer's instructions (IFN-γ and IL-6, BD Biosciences; IL-17, biotechne, R&D Systems). Media samples were collected from DC activation and T cell proliferation studies and analyzed for inflammatory cytokine concentrations. T cell supernatants were run at 10x dilutions for IFN-γ and 5x dilutions for IL-17. DC supernatants were run at 4x dilutions for IL-6. All IL-6 samples were compared to Rapa MPs lyophilized with no excipient using Welch's ANOVA with a Dunnett's test for multiple comparisons. IL-17 and IFN-γ samples were compared to MOG MPs lyophilized with no excipient using Welch's ANOVA with a Dunnett's test for multiple comparisons. Cytokine secretion studies were performed in triplicates to ensure consistency.

6.4 Results

6.4.1 Characterization of Microparticles

6.4.1.1 Incorporating Excipients Prior to Lyophilization Allows for Better Lyo Cake Formation and Resuspension

In order to prolong MP stability, MPs were lyophilized with or without excipients that were loaded either into the MPs in the inner aqueous phase during

synthesis (encapsulated, top left, **Fig. 6.1**), or added after the final washing steps (externally incorporated, top right, **Fig. 6.1**). Three excipients were selected based on previous research on protein stabilization in PLGA particles – mannitol, sucrose, and trehalose [259-262]. These were added to MP batches at 1%, 5%, and 10% w/v during synthesis or after washing (**Table 6.1**), then samples were lyophilized and stored (**Fig. 6.1**, bottom).

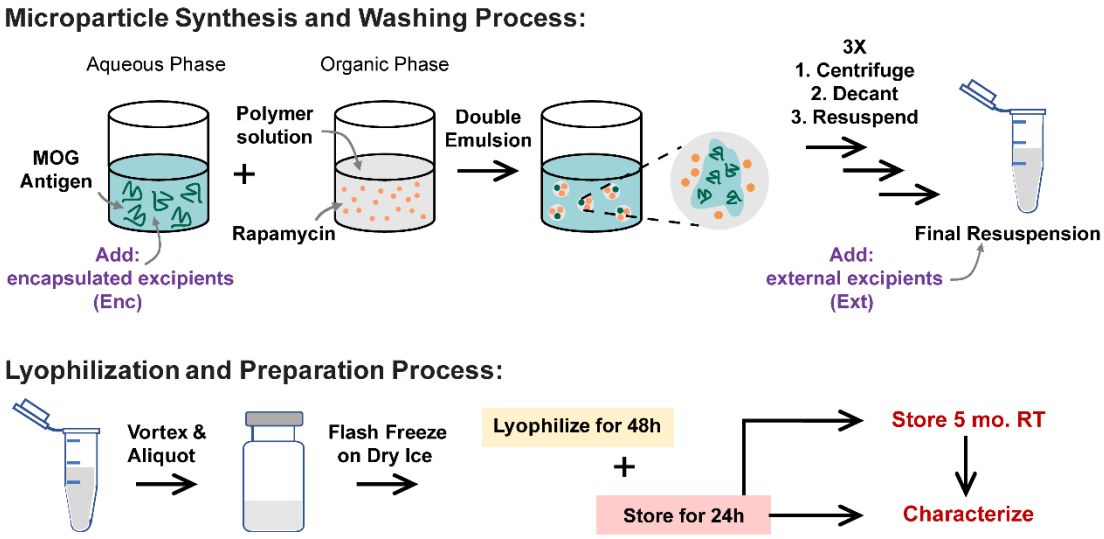

Figure 6.1 MPs synthesis and lyophilization process
MPs are synthesized using a double emulsion synthesis with an inner aqueous phase, organic phase, and outer aqueous phase mixed using sonication (first emulsion) and homogenization (second emulsion). The inner aqueous phase is loaded with water soluble cargo including MOG peptide and any excipients that were to be encapsulated in the MPs (Enc). The organic phase contains the PLGA polymer and the water-insoluble cargo including Rapamycin. The outer aqueous phase contains 2% polyvinyl alcohol as a stabilizer. These MPs are washed and resuspended three times, after which any excipients that were to be externally incorporated are added (Ext). These MPs are mixed well and aliquoted into lyo vials, then flash frozen on dry ice. The frozen vials were lyophilized for 48 hours, and then the lyophilized vials were allowed 24 hours to acclimate to room temperature (RT) and atmospheric pressure before MPs were characterized for loading and sizing. MPs were stored for 5 months, then characterized and used in in vitro biofunctionality and reconstitution assays.

To assess the quality of the cakes formed by MPs remaining after lyophilization, the lyo cakes were visually inspected for indicators of crystallization and malformed appearance. High quality lyo cakes are smooth with even color and do not contain crevices or pockets from ice crystal formation. This assay revealed that MPs lyophilized and stored without excipients form fragile lyo cakes that crumble apart (**Fig. 6.2A**). MPs with encapsulated excipients form less dense lyo cakes that are less brittle than MPs without excipients. MPs with externally incorporated excipients form less fragile lyo cakes than MPs without excipients; however, at higher concentrations of excipients, the lyo cakes become more glassy. To assess the ease of reconstitution of the MPs, lyo cakes were resuspended in water and vortexed for 10 seconds. The

Table 6.1 MOG/Rapa MPs Formulation Information and Abbreviations

MPs Formulation	Cargo Included	Excipient Included	Excipient Inclusion Method	Concentration of Excipient
MR 0	MOG/Rapa	None	N/A	0%
MR Man Enc 1	MOG/Rapa	Mannitol	Encapsulated	1%
MR Man Enc 5	MOG/Rapa	Mannitol	Encapsulated	5%
MR Man Enc 10	MOG/Rapa	Mannitol	Encapsulated	10%
MR Man Ext 1	MOG/Rapa	Mannitol	External	1%
MR Man Ext 5	MOG/Rapa	Mannitol	External	5%
MR Man Ext 10	MOG/Rapa	Mannitol	External	10%
MR Suc Enc 1	MOG/Rapa	Sucrose	Encapsulated	1%
MR Suc Enc 5	MOG/Rapa	Sucrose	Encapsulated	5%
MR Suc Enc 10	MOG/Rapa	Sucrose	Encapsulated	10%
MR Suc Ext 1	MOG/Rapa	Sucrose	External	1%
MR Suc Ext 5	MOG/Rapa	Sucrose	External	5%
MR Suc Ext 10	MOG/Rapa	Sucrose	External	10%
MR Tre Enc 1	MOG/Rapa	Trehalose	Encapsulated	1%
MR Tre Enc 5	MOG/Rapa	Trehalose	Encapsulated	5%
MR Tre Enc 10	MOG/Rapa	Trehalose	Encapsulated	10%
MR Tre Ext 1	MOG/Rapa	Trehalose	External	1%
MR Tre Ext 5	MOG/Rapa	Trehalose	External	5%
MR Tre Ext 10	MOG/Rapa	Trehalose	External	10%

MR = MOG_{35-55}/Rapa, Man = Mannitol, Suc = Sucrose, Tre = Trehalose, Enc = Encapsulated, Ext = Externally Incorporated, 0/1/5/10 = Concentration of excipient (w/v) in solution during addition step

resuspended portion was removed, and the remaining formulation mass was determined. MPs with any excipient at any concentration were more completely resuspended after vortexing that MPs lyophilized without excipients (**Fig. 6.3**). This allowed for greater recovery of MPs formulations with excipients than MPs without excipients (**Fig. 6.2B, Table 6.2**).

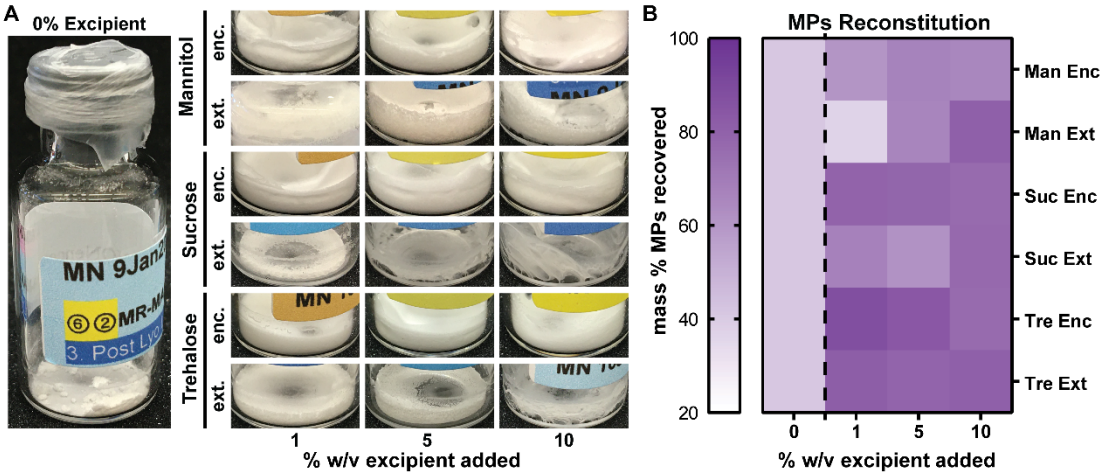

Figure 6.2 MPs lyophilized with excipients form better lyo cakes and are more easily reconstituted.
(A) MPs lyophilized and stored without excipients form fragile lyo cakes that crumble apart. MPs with encapsulated excipients form less dense lyo cakes that are less easily broken than MPs without excipients. MPs with externally incorporated excipients form more resilient lyo cakes than MPs without excipients; however, at higher concentrations of excipients, the lyo cakes become more glassy. Images shown are representative of three samples. **(B)** MPs lyophilized with excipients are more completely resuspended after vortexing for 10 seconds. This assay was performed once.

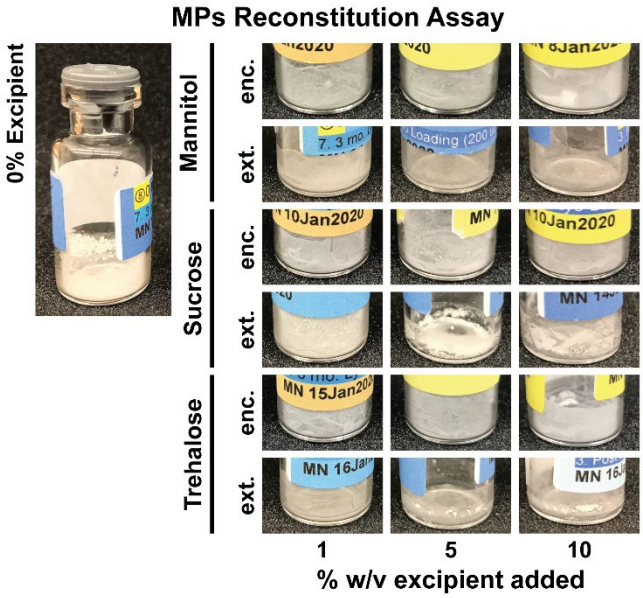

Figure 6.3 MPs lyophilized with excipients are more completely reconstituted. MPs lyophilized with excipients are more completely resuspended after vortexing for 10 seconds. MPs lyophilized without excipients have more MPs formulation remaining in the vials following the reconstitution assay. This assay was performed once.

Table 6.2 MPs Reconstitution Assay

MPs Formulation	% Resuspended After 10s vortex
MR 0%	41.3
MR Man Enc 1	60.6
MR Man Enc 5	67.4
MR Man Enc 10	65.5
MR Man Ext 1	37.2
MR Man Ext 5	66.7
MR Man Ext 10	80.6
MR Suc Enc 1	79.4
MR Suc Enc 5	78.6
MR Suc Enc 10	76.3
MR Suc Ext 1	68.1
MR Suc Ext 5	61.4
MR Suc Ext 10	77.2
MR Tre Enc 1	88.3
MR Tre Enc 5	84.0
MR Tre Enc 10	76.4
MR Tre Ext 1	81.8
MR Tre Ext 5	79.3
MR Tre Ext 10	80.9

6.4.1.2 MPs Loading Efficiency is Influenced by Excipient Encapsulation Levels

To evaluate the impact of adding excipients to the MP formulations during synthesis on immune cargo loading, loading on excipient-loaded MPs was assessed using UV/Vis spectrophotometry and mBCA and compared to MPs lyophilized without excipients. Rapa loading, in μg/mg formulation, did not substantially change for MPs lyophilized with encapsulated excipients; however, rapa loading did decrease with increasing concentrations of externally incorporated excipients (**Fig. 6.4A**, left, **Table 6.3**). However, this decrease is likely due to the increased formulation mass from the sugars, as the Rapa Loading Efficiency remained consistent across MPs lyophilized with different concentrations encapsulated or externally incorporated excipients (**Fig. 6.4A,** right, **Table 6.3).** Unlike rapa loading, MOG loading, in μg/mg formulation, was impacted by increasing excipient concentrations for both encapsulated and externally incorporated excipients (**Fig, 6.4B,** left, **Table 6.3**). It is likely this decrease at high concentrations of excipients is due to the displacement of MOG by the excipients, as increasing concentrations for both methods of excipient inclusion result in a decrease in MOG Loading Efficiency (**Fig. 6.4B**, right, **Table 6.3**).

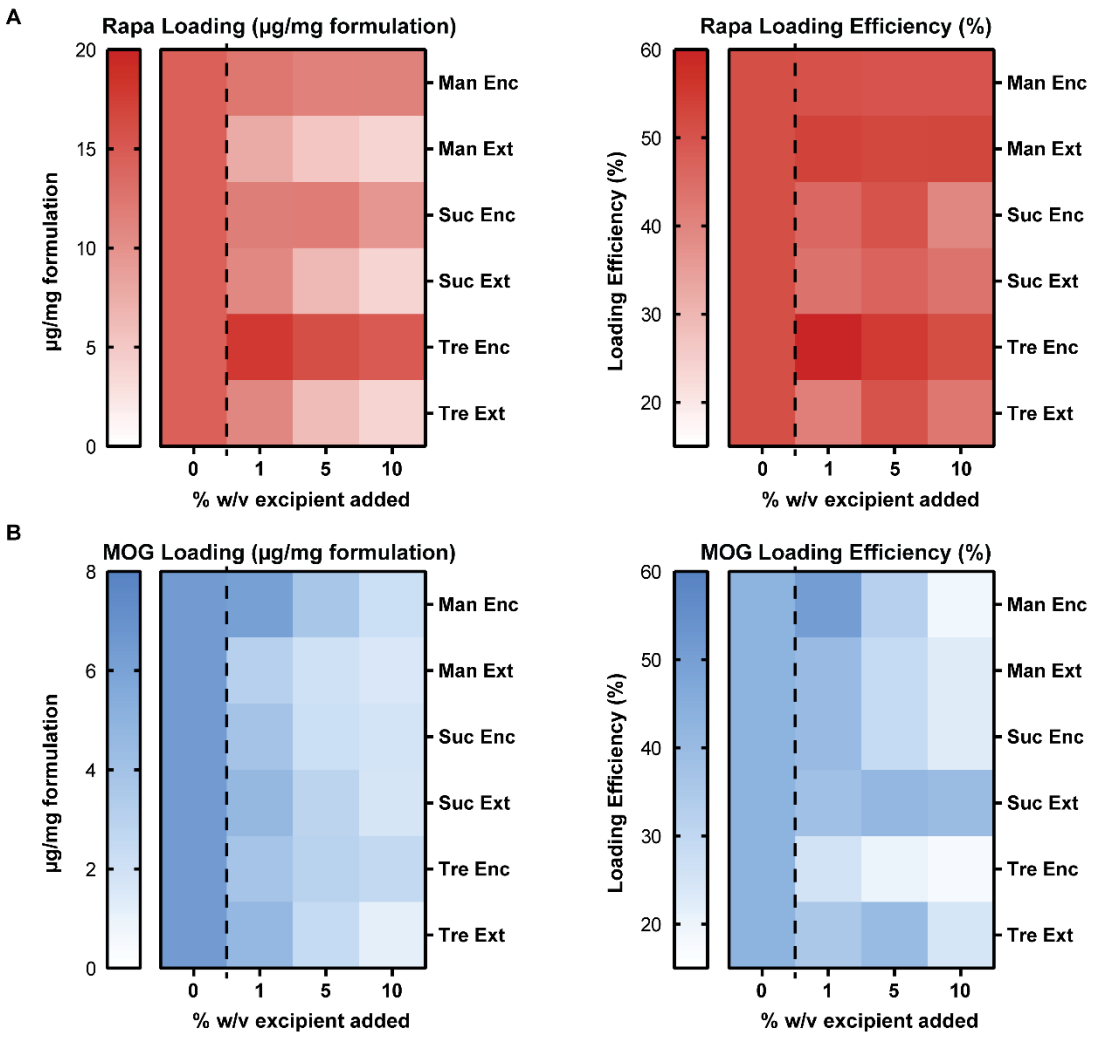

Figure 6.4 Loading efficiency of aqueous cargo decreases with increasing concentration of encapsulated excipients.

(A) Rapamycin loading per mg of formulation decreases as the mass of formulation increases due to externally incorporated (Ext) excipient addition. However, this does not correspond to a change in Rapamycin loading efficiency. **(B)** MOG loading per mg of formulation decreases as the concentration (percent weight/volume, % w/v) of excipients increases in the formulation. This does not correspond to a change in MOG loading efficiency for externally incorporated (Ext) excipients; however, increasing encapsulated (Enc) excipient concentration does decrease loading efficiency of MOG. Loading analyses were performed twice for consistency.

Table 6.3 MPs Rapa and MOG_{35-55} Loading

MPs Formulation	Rapa Loading (µg Rapa/ mg formulation)	Rapa Loading Efficiency (%)	MOG_{35-55} Loading (µg MOG_{35-55}/ mg formulation)	MOG_{35-55} Loading Efficiency (%)
MR 0	14.5	51.0	6.41	43.5
MR Man Enc 1	12.3	50.6	6.16	50.6
MR Man Enc 5	11.5	50.0	3.75	32.5
MR Man Enc 10	11.4	49.9	2.15	18.8
MR Man Ext 1	11.7	53.5	3.10	40.2
MR Man Ext 5	11.9	52.6	2.06	28.9
MR Man Ext 10	9.6	52.7	1.62	22.8
MR Suc Enc 1	11.7	46.0	3.91	40.2
MR Suc Enc 5	11.9	50.0	2.14	28.9
MR Suc Enc 10	9.6	39.7	1.87	22.8
MR Suc Ext 1	10.8	43.9	4.70	38.2
MR Suc Ext 5	6.4	46.7	2.88	41.8
MR Suc Ext 10	3.9	43.6	1.78	39.9
MR Tre Enc 1	17.9	59.9	3.83	25.7
MR Tre Enc 5	16.2	54.9	2.96	20.2
MR Tre Enc 10	15.0	51.5	2.61	17.9
MR Tre Ext 1	11.0	41.1	4.72	35.3
MR Tre Ext 5	6.1	50.1	2.47	40.4
MR Tre Ext 10	3.9	42.7	1.13	24.8

6.4.1.3 Encapsulating Excipients Increases MPs Size

To assess the stability of MPs formed with excipients, MP diameter increases were assessed as a measure of MP instability and aggregation. MPs were sized before lyophilization **(Fig. 6.5A,** left**)**, after lyophilization **(Fig. 6.6A,** left **& Fig. 6.5A,** right**)**, and after 5 months in storage **(Fig. 6.6A,** right)(**Table 6.4**). In most cases, encapsulating excipients within the MPs resulted in increased diameter of MPs (**Fig. 6.6A, Fig. 6.5A, Table 6.4**). Lyophilization did not greatly impact MP sizes for MPs lyophilized with or without excipients, which is clear in both mean diameter size (**Fig. 6.5A, Table 6.4**), and size distributions (**Fig. 6.5B**). However, after storage in sealed lyo vials for 5 months, all MPs, stored with or without excipients showed an increase in MP size, evident in both mean diameter (**Fig. 6.6A, Table 6.4**), and size distributions (**Fig. 6.6C**)**.** However, in many cases – in particular for the Man Enc, Man Ext, Suc Enc, and

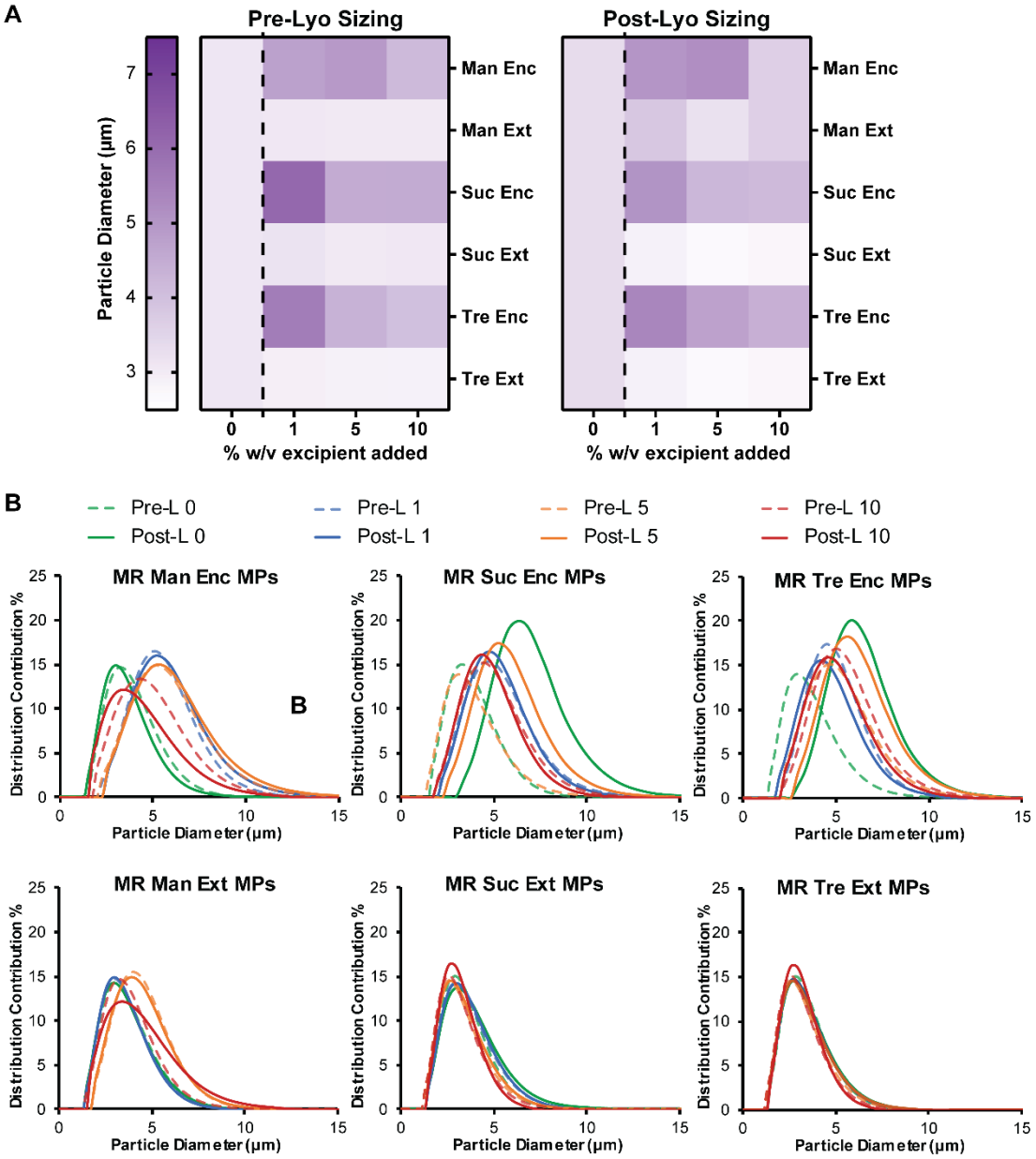

Figure 6.5 Encapsulated excipients increase MP size, and lyophilization does not change MP size.

(A) MPs were sized prior to lyophilization and immediately following lyophilization (as in main text). Encapsulating excipients (Enc) results in increased MPs size, both immediately after synthesis and after lyophilization. **(B)** Individual size curves for MOG/Rapa MPs prepared using different excipient conditions. MPs with encapsulated excipients are typically larger than MPs prepared with externally incorporated excipients. Sizing analyses were performed twice for consistency.

Tre Enc, incorporating an excipient prior to lyophilization resulted in a smaller increase in diameter – both in the % increase in size (**Fig. 6.6B**), and absolute change in diameter (**Fig. 6.7A**) and the. In addition, incorporating excipients protected from an increase in PDI of the MPs over the 5 month storage period (**Fig 6.7B, Table 6.4**).

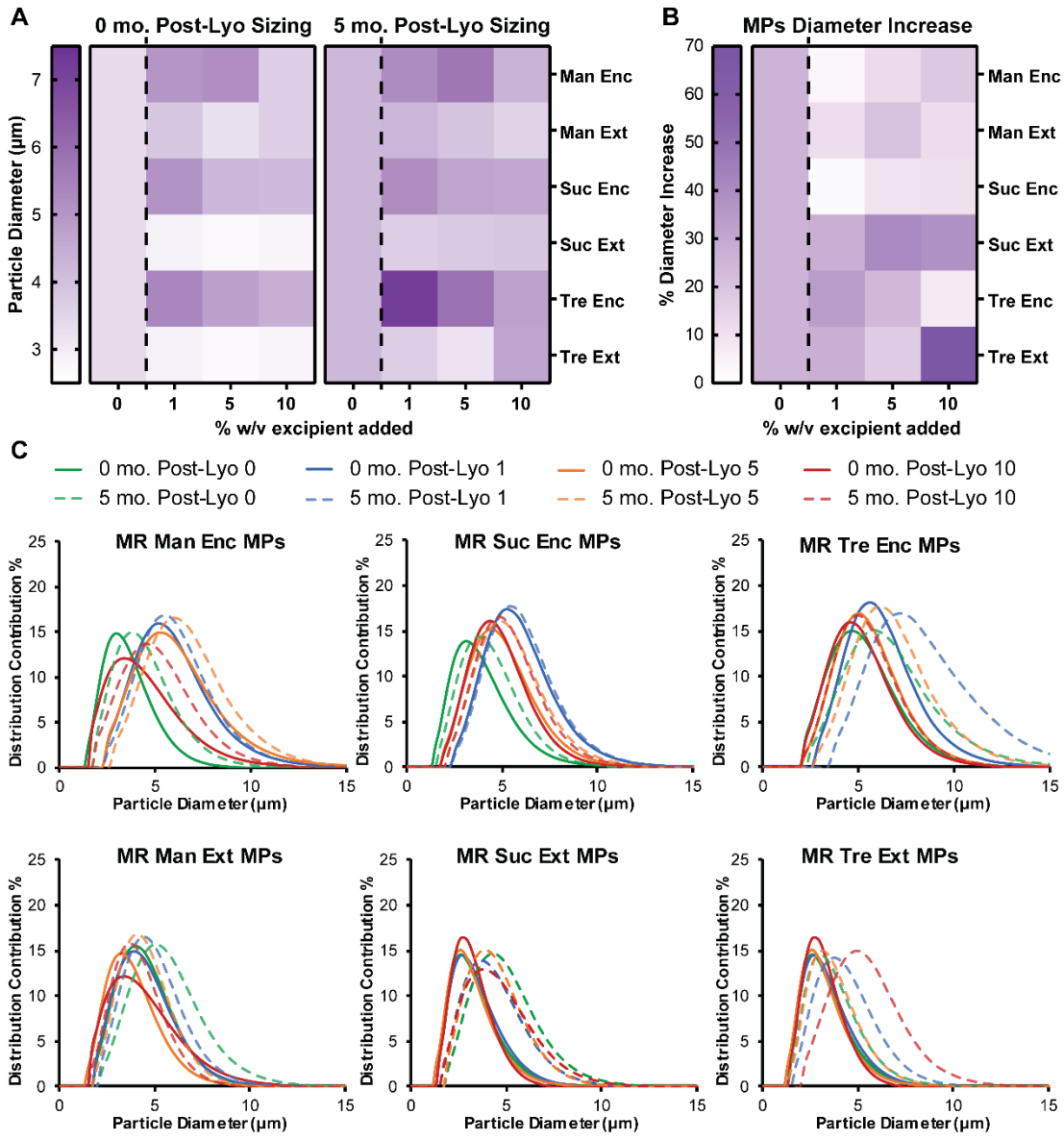

Figure 6.6 Encapsulated excipients increase MP size, and adding excipients protects against aggregation.

(A) MPs were sized immediately following lyophilization, and again after storage at room temperature for 5 months. Encapsulating excipients (Enc) results in increased MPs size, both immediately after lyophilization and after 5 months in storage. All MPs formulations showed increased MPs size after 5 months of storage; however, this

increase in size was typically lower for MPs that were lyophilized and stored with excipients **(B)**. **(C)** Individual size curves for MOG/Rapa MPs stored at different excipient conditions. MPs with encapsulated excipients are typically larger than MPs stored with externally incorporated excipients. Sizing analyses were performed twice for consistency.

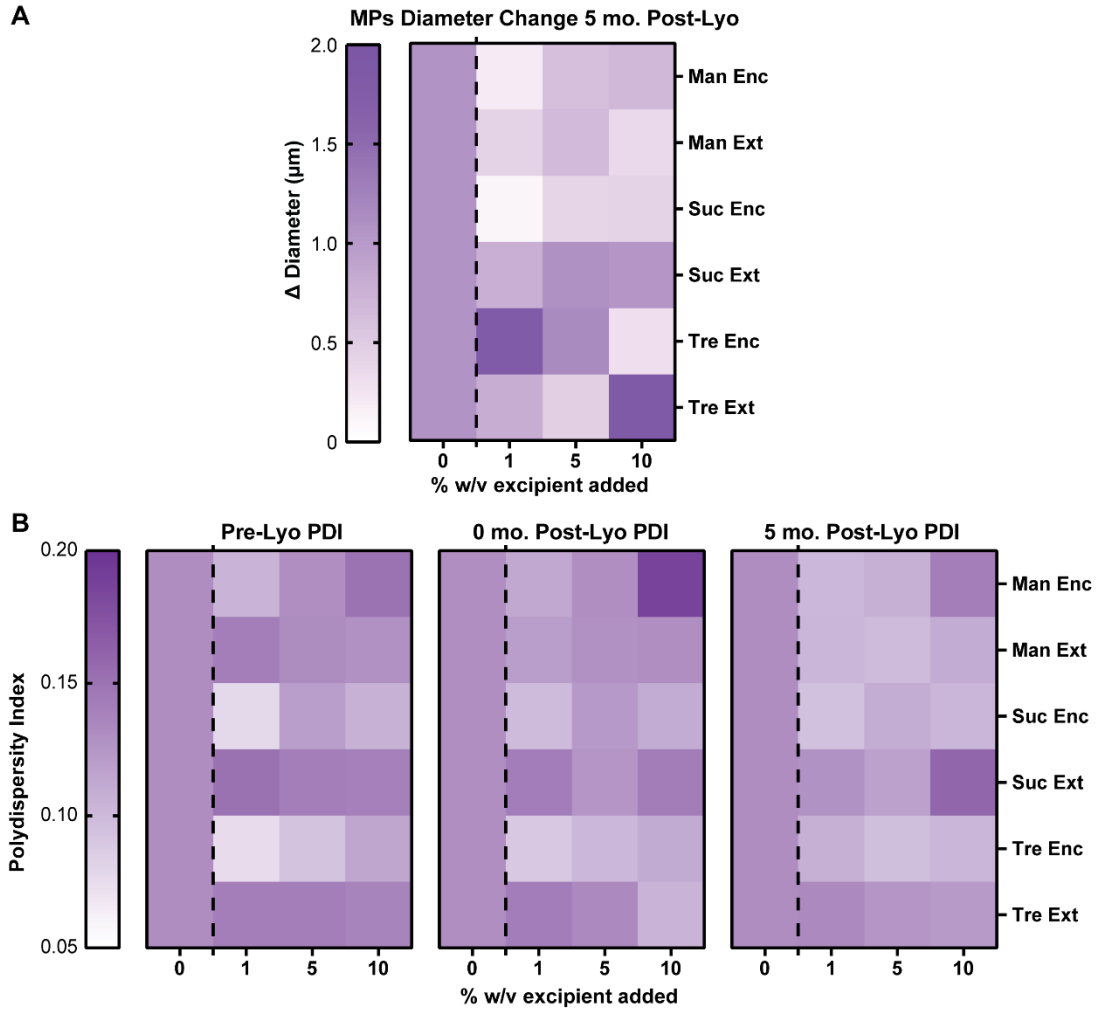

Figure 6.7 Adding excipients protects against aggregation following long-term storage.

(A) MPs were sized immediately following lyophilization, and again after storage at room temperature for 5 months. All MPs formulations showed increased MPs size after 5 months of storage; however, this increase in diameter was typically lower for MPs that were lyophilized and stored with excipients. **(B)** Immediately following synthesis, MPs formulations exhibit varied polydispersity indices (PDIs), with higher PDIs indicating less uniform MP sizes. Following lyophilization, some of these differences are less clear. After 5 months, MPs lyophilized and stored with excipients showed lower polydispersity indices (PDIs), indicating a greater uniformity in MP sizes. Sizing analyses were performed twice for consistency.

Table 6.4 MPs Sizing and Polydispersity Index Pre-Lyo, Post-Lyo, and 5 months Post-Lyo

MPs Formulation	Pre-Lyo		Post-Lyo		5 mo. Post-Lyo	
	Diameter (µm)	PDI	Diameter (µm)	PDI	Diameter (µm)	PDI
MR 0%	3.122	0.131	3.358	0.130	4.199	0.131
MR Man Enc 1	4.771	0.104	5.020	0.113	5.221	0.102
MR Man Enc 5	4.930	0.130	5.156	0.130	5.774	0.107
MR Man Enc 10	4.166	0.151	3.627	0.186	4.312	0.142
MR Man Ext 1	3.085	0.142	3.828	0.120	4.262	0.103
MR Man Ext 5	3.074	0.132	3.235	0.129	3.905	0.099
MR Man Ext 10	3.050	0.129	3.183	0.130	3.554	0.110
MR Suc Enc 1	6.119	0.077	5.079	0.099	5.195	0.095
MR Suc Enc 5	4.526	0.120	4.243	0.123	4.657	0.109
MR Suc Enc 10	4.533	0.106	4.152	0.110	4.585	0.103
MR Suc Ext 1	3.191	0.152	2.889	0.143	3.679	0.128
MR Suc Ext 5	3.070	0.142	2.697	0.126	3.788	0.118
MR Suc Ext 10	3.101	0.141	2.764	0.144	3.817	0.160
MR Tre Enc 1	5.617	0.076	5.384	0.089	7.209	0.107
MR Tre Enc 5	4.329	0.093	4.759	0.102	5.911	0.096
MR Tre Enc 10	4.024	0.114	4.415	0.111	4.734	0.103
MR Tre Ext 1	2.934	0.142	2.889	0.143	3.695	0.134
MR Tre Ext 5	2.907	0.142	2.697	0.134	3.171	0.126
MR Tre Ext 10	2.900	0.138	2.764	0.104	4.643	0.122

6.4.2 In Vitro Cargo Functionality Cellular Assays

6.4.2.1 Rapa-loaded MPs with or without Excipients Reduce Activation Marker Expression on Dendritic Cells

To confirm the potency of immune cargo is retained after lyophilization with excipients, changes in DC activation were assessed following treatments with Rapa-loaded MPs. After isolation, DCs were treated with LPS, which induces an inflammatory response in DCs, and either Empty (X) MPs or Rapa-loaded (R) MPs. For these candidate therapies, the Rapa cargo plays a role in reducing the activation of DCs, an important step to restrain the downstream destructive effects of self-reactive T cells. Levels of activation were quantified by Median Fluorescence Intensity (MFI) of DC co-stimulatory signals CD80 and CD86. **Figure 6.8A** shows the gating scheme

with representative samples (negative control, positive control, an Empty MP sample, and a Rapa-loaded MP sample). CD11c DCs were selected for viability (**Fig. 6.8A,** top), then assessed for activation using the intensity of the CD80 (**Fig. 6.8A**, middle) and CD86 (**Fig. 6.8A,** bottom). Samples that were activated with LPS showed increased DC viability compared to unstimulated (black) controls (**Fig. 6.8A,** top). Samples that were treated with lyophilized Empty MPs (gray) stimulated DCs beyond the activation of LPS alone (orange), while samples treated with lyophilized Rapa samples (red) reduced activation below the activation of LPS treated samples (**Fig. 6.8A,** middle and bottom).

In assessing viability, we found that MPs lyophilized with any of the 3 excipients—Mannitol, Sucrose, or Trehalose—in either Enc or Ext form did not negatively impact cell viability **(Fig. 6.8B, Fig. 6.9A).** Treatment with Rapa MPs reduced DC activation compared to Empty MPs, clear in reductions in MFI of CD80 (**Fig. 6.8C, Fig. 6.9B**), and CD86 (**Fig. 6.8D, Fig. 6.9C**). Most Empty MPs lyophilized with or without excipients had significantly more activation than Rapa MPs lyophilized without excipient. All Rapa-loaded MP formulations lyophilized with excipients reduced DC activation at similar levels to MPs lyophilized without excipients. There were no apparent differences in rapa functionality between rapa loaded MPs with excipients encapsulated or externally incorporated.

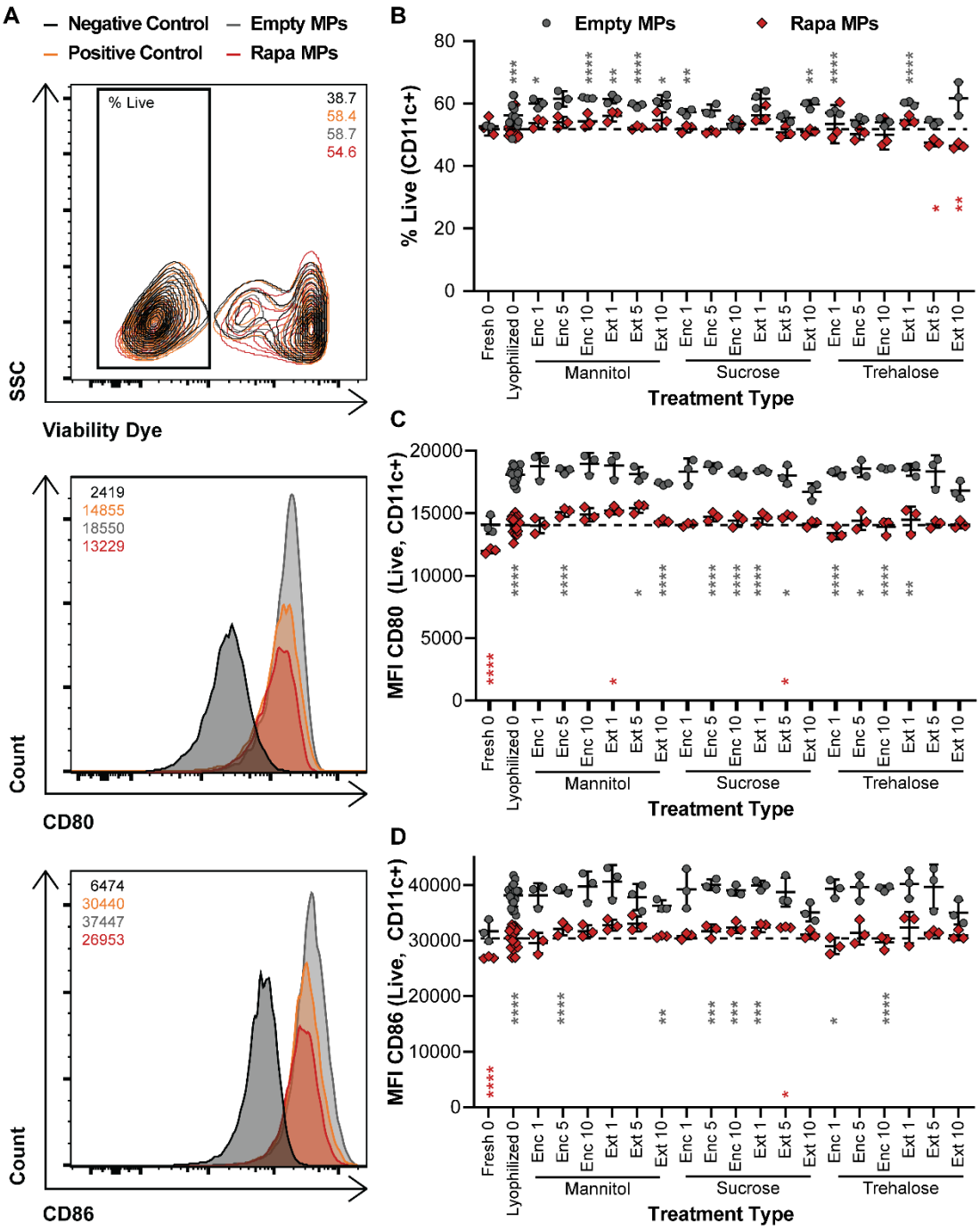

Figure 6.8 Rapa MPs with or without excipients reduce dendritic cell activation after stimulation.

Primary DCs were collected and cultured for 18h with LPS and Empty or Rapa-loaded MPs to observe changes in activation of DCs and ensure Rapa biofunctionality after lyophilization and storage. **(A)** Flow cytometry gating scheme for DC Activation analysis. Singlet CD11c+ dendritic cells were analyzed for viability. The numbers in the top right of the contour plot indicate viability for the corresponding representative plot. Live cells were then evaluated for intensity of staining for co-stimulation signals

CD80 and CD86. The numbers in the top left corner of the histograms indicate the median fluorescent intensity (MFI) for the corresponding representative plot. **(B)** Compared to DCs treated with Rapa MPs lyophilized without excipient, many cells treated with Empty MPs exhibited significantly increased viability. Compared to DCs cultured with Rapa MPs lyophilized with no excipient, lyophilized Empty MPs with or without excipients showed increased activation by both CD80 **(C)** and CD86 **(D)**. Rapa MPs stored with excipients showed no differences compared to Rapa MPs without excipients. However, Rapa MPs prepared fresh and not lyophilized did show significantly reduced activation compared to Rapa MPs lyophilized and stored for 5 months. All samples were compared to Rapa MPs lyophilized with no excipient using Welch's ANOVA with a Dunnett's test for multiple comparisons. (* indicates $p \leq 0.05$, ** $p \leq 0.01$, *** $p \leq 0.001$, **** $p \leq 0.0001$). DC activation studies were performed twice, in triplicate, to ensure consistency. Average ± SD is shown. The legend in panel A applies to all gating schemes in panel A. The legend above panel B applies to panels B-D.

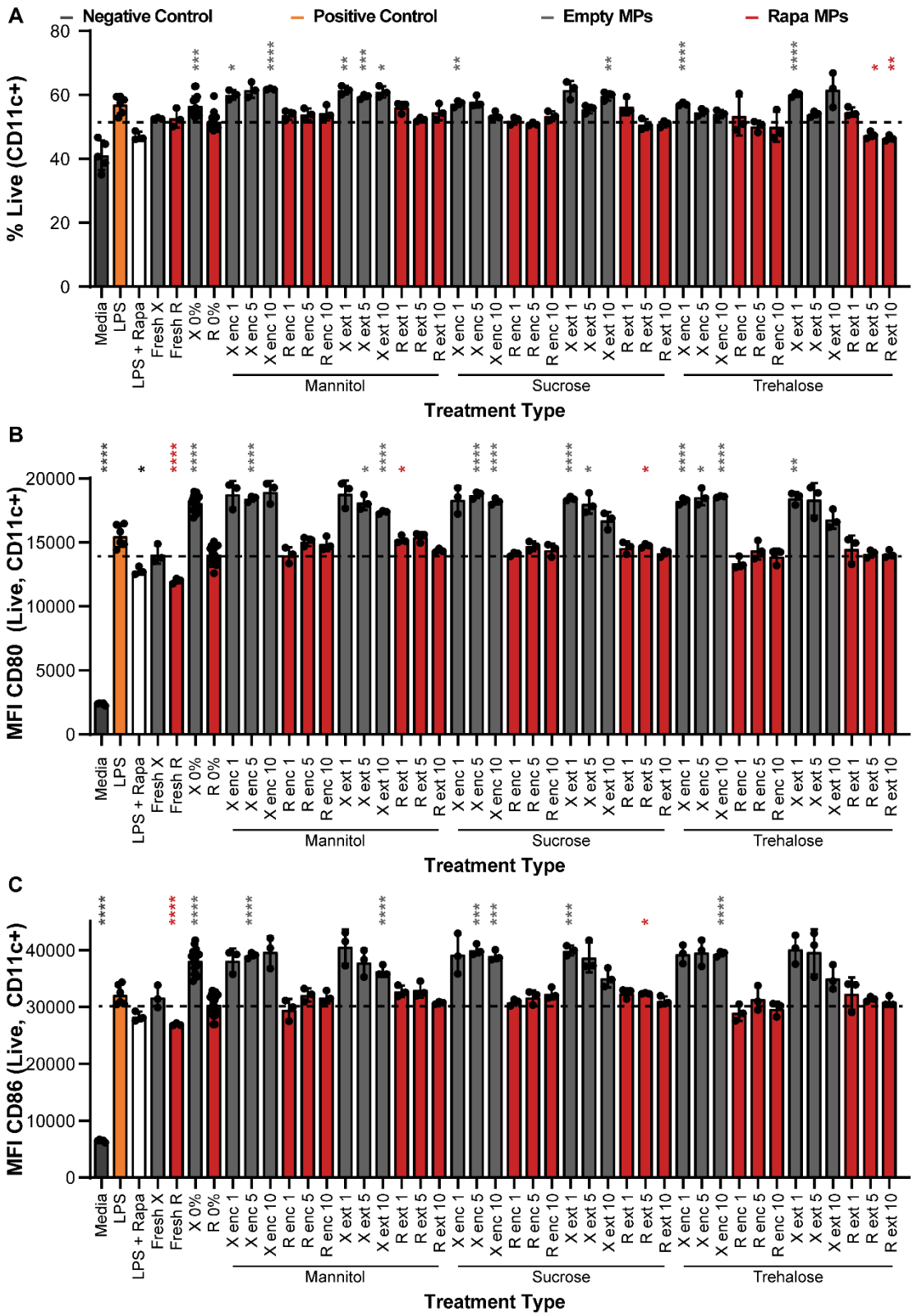

Figure 6.9 Rapa MPs with or without excipients reduce dendritic cell activation after stimulation.

Primary DCs were collected and cultured for 18h with LPS and Empty or Rapa-loaded MPs to observe changes in activation of DCs and ensure Rapa biofunctionality after lyophilization and storage. This data with MPs treatments is shown in **Figure 6.8**; there are additional controls included here for assay validation. **(A)** Compared to DCs treated with Rapa MPs lyophilized without excipient, many cells treated with Empty MPs exhibited significantly increased viability. Viability was not significantly different for DCs that were not activated with LPS (negative control) or that were only treated with LPS (positive control). Compared to DCs cultured with Rapa MPs lyophilized with no excipient, lyophilized Empty MPs with or without excipients showed increased activation by both CD80 **(C)** and CD86 **(D)**. Rapa MPs stored with excipients showed no differences compared to Rapa MPs without excipients. However, Rapa MPs prepared fresh and not lyophilized did show significantly reduced activation compared to Rapa MPs lyophilized and stored for 5 months. Cells that were not stimulated with LPs were significantly less activated. All samples were compared to Rapa MPs lyophilized with no excipient using Welch's ANOVA with a Dunnett's test for multiple comparisons. (* indicates $p \leq 0.05$, ** $p \leq 0.01$, *** $p \leq 0.001$, **** $p \leq 0.0001$). DC activation studies were performed twice, in triplicate, to ensure consistency. Average ± SD is shown. The legend in panel A applies to all gating schemes in panel A. The legend above panel A applies to all panels.

6.4.2.2 MPs Containing MOG with or without Excipients Expand MOG-specific T Cells

We next determined if lyophilization and storage impacts the ability of MPs to limit proliferation of antigen-specific T cells. MPs loaded with MOG or MOG/Rapa and stored with or without excipients were cultured with DCs and fluorescently-labeled T cells isolated from transgenic mice in which the T cells exhibit receptors specific for MOG. Thus, when these cells encounter MOG displayed by DCs with co-stimulatory signals, they proliferate and secrete inflammatory cues. Proliferation was assessed by quantifying the intensity of dye in the T cells at the end of culture, where a decrease in staining signal corresponds to an increase in proliferation (as a result of dye dilution during cell division). Proliferation was evaluated in three ways: Median Fluorescence Intensity, % of cells that proliferated (cells past initially stained generation, G0), and

Proliferation Index of dividing cells. **Figure 6.10A** shows the gating scheme with representative samples (negative control, positive control, a MOG MP sample, and a MOG/Rapa MP sample). CD4+ T cells (**Fig. 6.10A,** top) were selected for viability (**Fig. 6.10A,** middle), then assessed for proliferation using the intensity of the proliferation dye (eFluor450) (**Fig. 6.10A,** bottom). Samples that were stimulated with MOG – either soluble (teal) or via MOG-loaded MPs (blue) – showed increased T cell viability (**Fig. 6.10A,** middle) and proliferation (**Fig. 6.10A,** bottom) compared to unstimulated (black) or MOG/Rapa loaded MPs (purple).

Importantly, the MOG MPs lyophilized with any excipients showed either no statistical differences in MFI (**Fig. 6.10B, Fig. 6.11A**), % proliferated past G0 **(Fig. 6.10C, Fig. 6.11B**), and proliferation index (**Fig. 6.10D, Fig. 6.11C**) or increased proliferation compared to MOG MPs lyophilized without excipient. There were no differences between MOG MPs lyophilized without excipients and fresh MOG MPs that had not been lyophilized. In addition, adding Rapa to any of these MPs lyophilized with or without excipients resulted in significantly reduced proliferation compared to MOG MPs lyophilized without excipient. Combined, these results showed that both the MOG and Rapa loaded into these MPs retained biofunctionality after lyophilization and 5 months in storage.

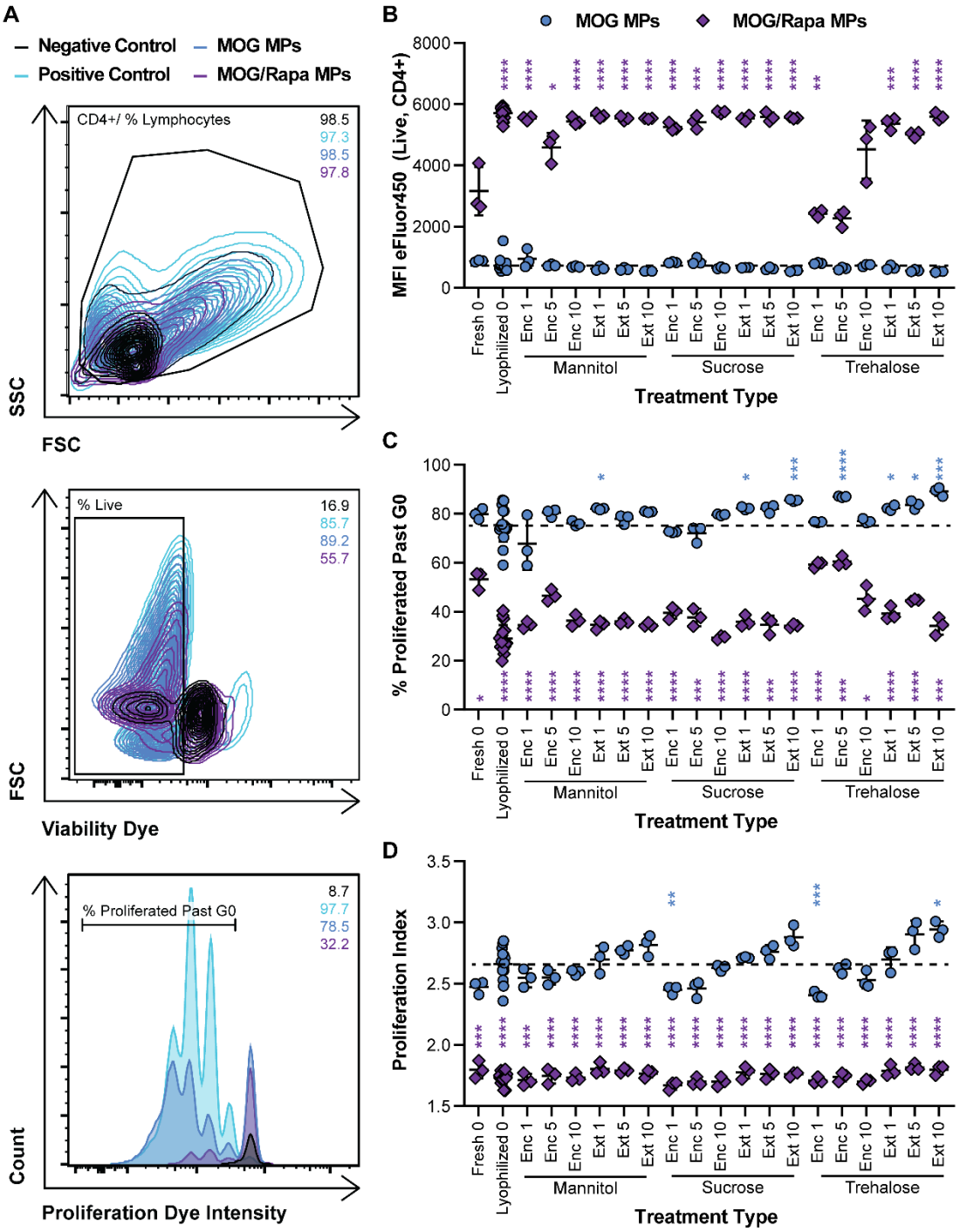

Figure 6.10 MPs containing MOG and lyophilized with or without excipients expand MOG-specific T cells.

Primary DCs were collected and cultured for 24h with LPS and MOG or MOG/Rapa MPs. After 24h, fluorescently-labeled MOG-specific transgenic T cells were added to wells and cultured for 72h to observe differences in proliferation of MOG-specific T cells and ensure MOG and Rapa biofunctionality after lyophilization and storage. **(A)** Flow cytometry gating scheme for T cell proliferation analysis. Singlet CD4+ T cells were studied for proliferation. The numbers in the top right of the contour plot indicate

percentage of lymphocytes in the CD4+ population. Lymphocytes were then analyzed for viability. The numbers in the top right of the contour plot indicate viability for the corresponding representative plot. Live cells were then evaluated for intensity of proliferation dye, where a decrease in dye intensity corresponds to an increase in cell proliferation. The numbers in the top right corner of the histograms indicate the percentage of cells that proliferated. **(B)** Compared to treatments of MOG MPs lyophilized without excipient, cells cultured with MOG MPs with excipients showed no differences in Median Fluorescent Intensity of the proliferation dye. Fresh MOG MPs also showed no difference in MFI compared to MOG MPs lyophilized without excipient. MPs that also contained Rapa showed a significantly higher MFI, indicating reduced proliferation. **(C)** Co-cultures treated with MOG MPs containing excipients proliferated similarly to MOG MPs without excipients. MOG/Rapa MP treatments significantly reduced proliferation compared to MOG MPs lyophilized without excipient. **(D)** Proliferation Index is a measure of average number of divisions undergone by dividing T cells. Compared to MOG MPs lyophilized without excipients, MOG MPs lyophilized with excipients showed similar levels of proliferation. MOG/Rapa MPs with or without excipients showed significantly lower proliferation. All samples were compared to MOG MPs lyophilized with no excipient using Welch's ANOVA with a Dunnett's test for multiple comparisons. (* indicates $p \leq 0.05$, ** $p \leq 0.01$, *** $p \leq 0.001$, **** $p \leq 0.0001$). T cell proliferation studies were performed twice, in triplicate, to ensure consistency. Average ± SD is shown. The legend in panel A applies to all gating schemes in panel A. The legend in above panel B applies to panels B-D.

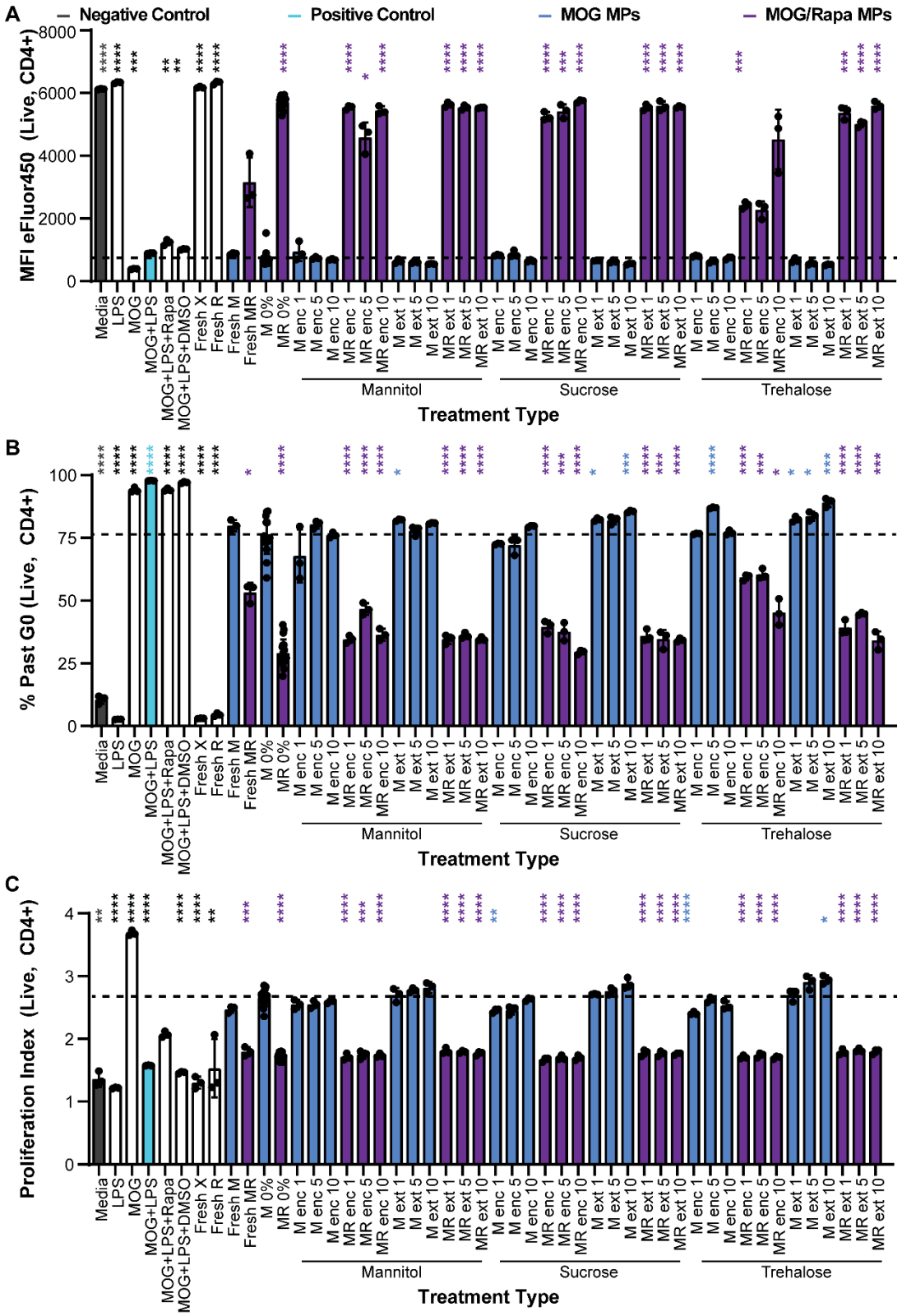

Figure 6.11 MPs containing MOG and lyophilized with or without excipients expand MOG-specific T cells.

Primary DCs were collected and cultured for 24h with LPS and MOG or MOG/Rapa MPs. After 24h, fluorescently-labeled MOG-specific transgenic T cells were added to wells and cultured for 72h to observe differences in proliferation of MOG-specific T cells and ensure MOG and Rapa biofunctionality after lyophilization and storage. Live CD4+ T cells were then evaluated for intensity of proliferation dye, where a decrease in dye intensity corresponds to an increase in cell proliferation. This data with MPs treatments is shown in **Figure 6.10**; there are additional controls included here for assay validation. **(A)** Compared to treatments of MOG MPs lyophilized without excipient, cells cultured with MOG MPs with excipients showed no differences in Median Fluorescent Intensity of the proliferation dye. Fresh MOG MPs also showed no difference in MFI compared to MOG MPs lyophilized without excipient. MPs that also contained Rapa showed a significantly higher MFI, indicating reduced proliferation. MFI was not significantly different for co-cultures that were treated with LPS and also given soluble MOG (positive control), but MFI for cells that were not given MOG or LPS (negative control), or were treated with LPS and MPS that did not contain MOG, was significantly increased (negative control). **(C)** Co-cultures treated with MOG MPs containing excipients proliferated similarly to MOG MPs without excipients. MOG/Rapa MP treatments significantly reduced proliferation compared to MOG MPs lyophilized without excipient. Cells treated with MOG + LPS (positive control) showed significantly more proliferation, while cells that were not treated with MOG showed significantly reduced proliferation. **(D)** Proliferation Index is a measure of average number of divisions undergone by dividing T cells. Compared to MOG MPs lyophilized without excipients, MOG MPs lyophilized with excipients showed similar levels of proliferation. MOG/Rapa MPs with or without excipients showed significantly lower proliferation. Cells treated with MOG + LPS (positive control), as well as cells that were not treated with MOG showed significantly reduced proliferation indices. All samples were compared to MOG MPs lyophilized with no excipient using Welch's ANOVA with a Dunnett's test for multiple comparisons. (* indicates $p \leq 0.05$, ** $p \leq 0.01$, *** $p \leq 0.001$, **** $p \leq 0.0001$). T cell proliferation studies were performed twice, in triplicate, to ensure consistency. Average ± SD is shown. The legend in panel A applies to all panels.

6.4.2.3 MPs Containing MOG/Rapa with or without Excipients can reduce IL-6, IL-17, and IFN- γ inflammatory cytokine secretion

To confirm the maintenance of immunomodulatory impact of MPs after lyophilization and storage, supernatants collected from the DC and T cell proliferation biofunctionality studies were analysed for cytokine secretion using ELISA. Detection of inflammatory cytokines—IL-6, IL-17 and IFN- γ—were used as a measure of

changes in immune cell activation. IL-6 secretion by DCs promotes inflammatory differentiation of naïve $CD4^+$ T cells. Secretion of IFN- γ is indicative of a T_H1 inflammatory response and IL-17 measures a T_H17 inflammatory response. In line with the DC activation and T cell proliferation studies, lyophilized MPs containing Rapa decreased secretion of all three inflammatory cytokines. Treatment with Rapa MPs reduced DC IL-6 secretion compared to Empty MPs lyophilized with or without excipient (**Fig. 6.12A)**. Rapa-loaded MP formulations lyophilized with excipients reduced DC activation at similar levels to Rapa MPs lyophilized without excipients. Treatment with all MOG MPs lyophilized with or without excipient induced IL-17 (**Fig. 6.12B**) and IFN-γ (**Fig. 6.12C**) secretion by T cells. This secretion was beyond that of Fresh MOG MPs – similar to the activating effect seen by Empty MPs in the DC activation study. All treatment with MOG/Rapa loaded MPs lyophilized with or without excipient significantly reduced IL-17 and IFN-γ secretion compared to MOG MPs lyophilized without excipient.

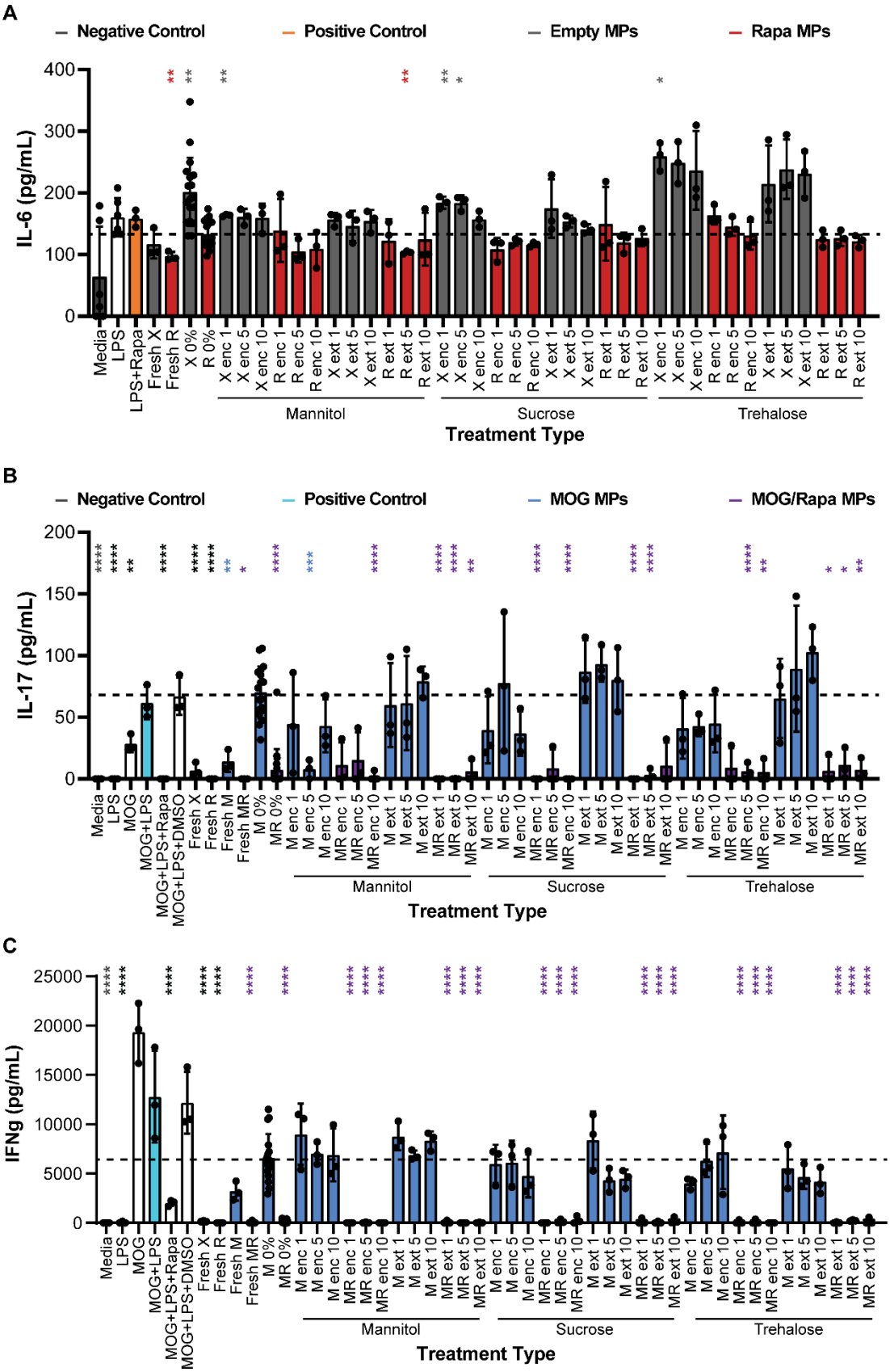
A
Negative Control
Positive Control
Empty MPs
Rapa MPs
IL-6 (pg/mL)
400
300
200
100
0
Media
LPS
LPS+Rapa
Fresh X
Fresh R
X 0%
R 0%
X enc 1
X enc 5
X enc 10
R enc 1
R enc 5
R enc 10
X ext 1
X ext 5
X ext 10
R ext 1
R ext 5
R ext 10
Mannitol
Sucrose
Trehalose
Treatment Type
B
Negative Control
Positive Control
MOG MPs
MOG/Rapa MPs
IL-17 (pg/mL)
200
150
100
50
0
Media
LPS
MOG
MOG+LPS
MOG+LPS+Rapa
MOG+LPS+DMSO
Fresh X
Fresh R
Fresh M
Fresh MR
M 0%
MR 0%
M enc 1
M enc 5
M enc 10
MR enc 1
MR enc 5
MR enc 10
M ext 1
M ext 5
M ext 10
MR ext 1
MR ext 5
MR ext 10
Mannitol
Sucrose
Trehalose
Treatment Type
C
IFNg (pg/mL)
25000
20000
15000
10000
5000
0
Media
LPS
MOG
MOG+LPS
MOG+LPS+Rapa
MOG+LPS+DMSO
Fresh X
Fresh R
Fresh M
Fresh MR
M 0%
MR 0%
M enc 1
M enc 5
M enc 10
MR enc 1
MR enc 5
MR enc 10
M ext 1
M ext 5
M ext 10
MR ext 1
MR ext 5
MR ext 10
Mannitol
Sucrose
Trehalose
Treatment Type

Figure 6.12 Rapa-loaded MPs with or without excipients restrain inflammatory activity of cells in vitro.
(A) Primary DCs treated with Rapa-loaded MPs show decreased inflammatory IL-6 secretion, though these values were often not significant when compared to Rapa MPs lyophilized without excipients. Changes in IL-6 cytokine secretion were not significant with respect to media (negative) or LPS-treated (positive) controls. IL-17 **(B)** and IFN-γ **(C)** secretion levels for co-cultures treated with MOG/Rapa MPs with or without excipients were significantly lower than those of co-cultures treated with MOG MP lyophilized without excipients. Cells treated with MOG MPs with excipients typically did not show significantly different levels of inflammatory cytokine secretion compared to MOG MPs lyophilized without excipient. Cells treated with MOG + LPS (positive control) showed similar levels of IL-17 and IFN-γ secretion, while cells that were not treated with MOG showed significantly reduced inflammatory cytokine secretion. All samples in panel A were compared to Rapa MPs lyophilized with no excipient using Welch's ANOVA with a Dunnett's test for multiple comparisons. All samples in panels B and C were compared to MOG MPs lyophilized with no excipient using Welch's ANOVA with a Dunnett's test for multiple comparisons. (* indicates $p \leq 0.05$, ** $p \leq 0.01$, *** $p \leq 0.001$, **** $p \leq 0.0001$). Cytokine secretion studies were performed in triplicate, to ensure consistency. Average ± SD is shown The legend above panel B applies to panels B and C.

6.5 Discussion

As immunotherapies become more personalized and patient-specific to improve patient outcomes, biomaterials are becoming increasingly important as delivery agents[65, 105, 168, 252, 253]. Biomaterials provide incredible flexibility in stabilizing and delivering immunotherapy cargo, as they highly tunable, with properties that can be engineered to meet many different functions[162, 167-169]. Importantly, they can provide features that traditional immune modulators don't have – including co-delivery of immune signals, controlled release of immune cues, and prolonged immune cargo exposure and protection[168, 252]. However, long-term storage of biomaterials-based immunotherapies has different considerations than long-term storage of other biologics used in immunotherapies (e.g. monoclonal antibodies), due to those specific functions, which adds complexity for manufacturing and regulatory characterization. As

preclinical studies often allow for the production of immunotherapies on-demand, relatively few pre-clinical studies have been focused on improving storage and stability of biomaterials-based immunotherapies. However, in order to translate these immunotherapies to the clinic, more research is required in these areas.

For our studies, we used a well-established material – PLGA MPs – to deliver our immunotherapy cargo – a myelin peptide and immunomodulatory signal rapamycin. PLGA is commonly used in applications for humans, as it degrades by hydrolysis, and its degradation products can be processed by cells[197, 198]. However, it is this same hydrolysis degradation process that complicates storage of immunotherapies based on PLGA MPs, as aqueous storage of PLGA MPs can lead to undesirable cargo release, particle aggregation and fusion, and degradation of cargo integrity[199]. Thus, we turned to lyophilization – a common method used in the pharmaceutical industry to control dehydration of samples – to enhance stability of PLGA MPs during storage. As the MP structure can be damaged from the stress of lyophilization due to ice crystal formation[199, 256], we tested several lyoprotectants to protect against ice crystal formation and immobilize MPs to limit aggregation. We tested several features – both in characterizing the MPs and assessing their biofunctionality using *in vitro* cellular assays – to compare MPs lyophilized and stored for 5 months without excipients to both MPs lyophilized and stored for 5 months with excipients and to MPs made on-demand, fresh immediately before use.

Throughout our testing, there were a few trends that were clear. First, lyophilizing MPs with excipients – both encapsulated and external – resulted in better

lyo cake formation that the brittle, broken cakes that resulted from lyophilizing without excipient. This was important, as damaged lyophilized formulations can possess an unfavorable appearance with component crystallization and higher residual water content[264]. In particular, all samples that were lyophilized with excipients encapsulated showed the smoothest appearances, with fewest visible pores in the bulk sample. At the 5% and 10% sugar contents for externally incorporated trehalose and sucrose, the cakes took on a more glassy appearance, indicating that this sample preparation process might not be ideal for this application. Better lyo cake formation with lower concentrations of externally incorporated excipients is not unique to PLGA MPs. Protein preservation efforts in immunotherapy have concluded that lowering concentrations of Trehalose excipient reduces formation of the glassy matrix and leads to more concentration of proteins during freezing[265]. The observations in appearance are also further supported by the ease of reconstituting the MPs with excipients. With the exception of the 1% encapsulated mannitol formulation, all MPs with excipients showed more complete reconstitution after a 10 second vortex. This is critical – in an environment where immunotherapies are carefully titrated and tested prior to approval, it is essential that patients get the entire dose.

Since dosing is such an important consideration, effective co-loading of immune cargo is another feature of PLGA MPs that must be supported by the preparation process. MOG and Rapa can both be loaded into PLGA MPs without excipients relatively efficiently (43.5% and 51.0% respectively). Importantly, while the Rapa loading efficiency was not impacted by the addition of excipients, the MOG loading efficiency decreased with increasing excipient concentrations for both

encapsulated and externally incorporated MPs. With the encapsulated excipients, this effect can possibly be attributed to MOG sharing the inner aqueous core of the MPs with either mannitol, sucrose, or trehalose. It is possible that adding more excipient displaces the volume of MOG that could be encapsulated during assembly. Even so, lower MOG loading with Ext samples cannot be explained by this competition for space in the aqueous core. Instead, excipients may induce conformational changes in the proteins which may impact loading. In polymer-based drug carrier systems, studies have speculated that excipients like sucrose may induce conformation changes in protein cargo[266]. Increasing hydrophobicity of a protein could increase its partitioning over the organic phase and reduce its concentration and therefore loading within the inner aqueous core[266].This suggests that lower excipient inclusion levels (1%) might be the best for this application. This aligns well with the results from the lyo cake formation and reconstitution assay.

Our lab has previously used these MPs to deliver MOG and Rapa to lymph nodes to reprogram autoimmune responses to myelin[26]. We directly inject MPs into lymph nodes[195], and rely on the size of the PLGA MPs (2-5μm) to prevent drainage from lymph nodes and uptake by non-phagocytic cells (i.e. APCs will take up MPs, but other cells will not)[26, 196, 239, 267, 268]. However, APC uptake is much less efficient once MPs reach sizes >5 μm[268]. After synthesis and lyophilization, MOG/Rapa MPs without excipients are on average 3.4 μm in diameter, with all of the MPs with externally incorporated excipients in the same range (2.7-3.8 μm). Adding encapsulated excipients to the aqueous phase of PLGA MPs increases the mean diameter of the batch to sizes after lyophilization to about 4.5 μm (3.6-5.4 μm). However, after storage for 5

months, the MOG/Rapa PLGA MPs without excipients had a greater increase in size compared to the MPs stored with excipients. In particular, the MPs prepared with mannitol (both enc and ext), as well as the sucrose and trehalose enc (with the exception of 1% tre enc) MPs best maintained their size after storage.

In order to maintain the benefits of a biomaterial-based immunotherapy, the excipients added to enhance storage must enable biofunctionality of immune cargo and not interrupt with drug-target interaction. From the *in vitro* DC activation cargo functionality assays, it is clear that all empty MPs that have been lyophilized and stored for 5 months enhance DC activation. This was also seen in increased inflammatory IL-6 cytokines secreted from these DCs. This is likely due to some degradation of the polymer – PLGA is known to have some intrinsic immunogenicity as it degrades[104, 235, 236]. However, in all cases, adding rapamycin to these particles, with or without excipients, decreases the expression of DC activation markers, showing that the rapamycin maintains its immunosuppressive activity during storage with or without excipients. The *in* vitro MOG-specific T-cell co-culture showed that lyophilized MOG MPs with or without excipients can successfully stimulate T-cell proliferation up to levels comparable to Fresh MOG MPs, showing the MOG in the MPs maintains biofunctionality. In addition, adding Rapa to these MPs significantly restrains this proliferation compared to lyophilized MOG MPs without excipients. In fact, MOG/Rapa MPs lyophilized with or without excipients prevent proliferation better than or similar to fresh MOG/Rapa MPs. These trends are also seen in the inflammatory IL-17 and IFN- γ, suggesting the intrinsic immunogenicity of the slightly degrading PLGA is not enough to impair the biofunctionality of the loaded immune cargo.

Effects of excipients on cellular viability and function can greatly impact the success of a vaccine carrying out proper function[269]. The excipients assisted in exerting the aims of the immune cues without any detrimental effects on cell viability. However, our test list of lyoprotectants is not exhaustive. Classes of molecules other than sugars have been studied as excipients for lyophilization. Arginine and Glutamate have largely been of interest in immunotherapy design due to beneficial function that the amino acids have as excipients[269, 270]. Primarily, amino acids are natural constituents of cells and are not a threat to cellular viability. Studies of amino acids have shown increased protein stability with vaccine development[270].

We did no optimization of the lyophilization process but controlling these parameters can further optimize preservation of PLGA MPs. One important parameter is controlling the shelf temperature[264]. Controlling the chamber pressure can provide further fine tuning with an aim of ice sublimating as rapidly as possible so as not to cause any physical changes in the solid phase of the product. Other strategies such as post-freeze heat treatment, ultrasound ice fog, vacuum-induced surface freezing, and release of the pressurized/depressurized chamber are all gaining better understanding in preservation of biologics and their carriers[264]. Cryopreservation is a simple and available technique that has shown to extend the effects of drug carriers[199, 261, 264]. Implementing these strategies would benefit rescaling of MP stabilization. The results obtained from our studies and further exploration that is evident in the field of vaccine design presents promise in development of a preservation method for biomaterial-based immunotherapies.

6.6 Conclusion

Enhancing stability of biomaterials-based immunotherapies will enable translation of these immunotherapies beyond pre-clinical studies. In this study, we incorporated the addition of excipients to the lyophilization process of PLGA MPs loaded with peptide antigens and small molecule immunomodulators to enhance the stability of cargo-loaded MPs. This study demonstrated that excipients aided in maintaining the stability and potency of cargo loaded into MPs after storage for 5 months at room temperature. The presence of the excipients reduced stresses that are exerted on the MPs during the lyophilization process and protects biologics and small molecule cargo to induce an immune response *in vitro*. In this study, both the concentration of excipient and mode of incorporation (encapsulated or external) can be controlled during particle synthesis and lyophilization to best optimize storage conditions. This modular testing of excipients for improving the stability of biomaterials-based immunotherapies can be used for many different immunotherapy approaches.

Chapter 7: Outlook and Future Work

7.1 Outlook

This work in this dissertation was designed to advance the understanding of a potential myelin-specific treatment for MS. This treatment leverages advantages of biomaterials – co-loading of cargo, cargo protection, and controlled release of cargo – to ensure controlled release of myelin peptides and rapamycin after a direct injection of MPs into the LN. This thesis added to the working knowledge of that therapy to further pre-clinical studies and motivate clinical research.

First, this work investigated the systemic impact of intra-LN tolerogenic MPs in multiple models of MS. This work showed that even at different stages of disease, one tolerogenic intra-LN treatment promoted recovery from paralysis and prevented relapse. Tolerogenic MPs delivered prior to symptom onset promoted tolerance and protected against disease onset. Treatment at peak disease reversed paralysis and prevented relapse, while treatment during relapse limited disease progression. This is important, as it is very unlikely a patient would visit a doctor before experiencing symptoms. Further, the fact that only a single treatment was needed for durable protection (more than 60 days – a significant fraction of a mouse's lifespan), and that this therapy would be administered by a healthcare professional could increase patient compliance, and result in better outcomes for MS patients. Patients exhibit greater compliance during infrequent, scheduled visits at hospitals with visit reminders and greater accountability compared to long-term use of at-home prescriptions, such as pills and subcutaneous injections. In fact, doctors that we have interviewed during our NIH

C3i Concept-to-Clinic Program have said that patients who get regularly scheduled infusion treatments for MS at the hospital typically have the best patient compliance for this reason. However, infusions can take ~ 6 hours, between the paperwork, the actual infusion, and the required observation time. In general, ultrasound visits take ~ 1 hour between the paperwork and the actual ultrasound, and an injection with small volumes (e.g. vaccines) are typically very quick (~ a minute). Even if you add an observation time of 1 hour similar to infusions, that is still 1/3 of the time required for an infusion visit, which would be easier on patients. In additions, infusions happen with a regular frequency – it is possible that the myelin-specific tolerance induced by iLN therapy would allow for fewer treatments.

In addition, we found that mice that had recovered from disease following intra-LN treatment could mount healthy immune responses to vaccination. In particular, even when vaccinated against a foreign protein on the same day as intra-LN treatment, mice generated protein-specific T cells and antibodies at similar levels to healthy vaccinated mice. This is critical for a myelin-specific therapy, as one of the limitations of current disease-modifying therapies is that they cannot distinguish between dysfunctional inflammatory myelin-specific cells and normal lymphocytes. These results showed that the normal function of lymphocytes was not impacted, meaning patients would not be more vulnerable to infection due to this therapy.

This dissertation also focused on enhancing the stability of the tolerogenic MPs used in this intra-LN therapy using Chemistry, Manufacturing, and Controls (CMC) considerations. While the low dosage requirements of the pre-clinical allowed for on-

demand preparation, clinical translation of this immunotherapy requires investigation into its manufacturing, preservation, storage, and stability. Thus, this dissertation also tested the stabilizing effects of lyophilization (freeze-drying) and excipients (stabilizing molecules) to enable storage of MPs. Significant improvements in MP stability and formulation recovery after reconstitution were seen in MPs lyophilized with low concentrations of excipients. Storage for 5 months at room temperature did not negatively impact cargo loading, MP size, or therapeutic efficacy – MP formulations with excipients could deactivate inflammatory signaling and restrict myelin-specific immune cell proliferation as well as formulations without excipients. Importantly, ensuring stability and extending shelf-life of these treatments could also reduce the cost of treatment for patients, as on-demand therapies can often be cost-prohibitive for patients.

Together, these studies motivate investigation into intra-LN delivery of tolerogenic MPs as a potential MS immunotherapy candidate for clinical translation. However, there are several ongoing and future studies in the Jewell lab I am leading that will progress our pre-clinical work to improve our understanding of the intra-LN therapy. In particular, these studies focus on better understanding the changes in inflammation and myelination in the CNS as a result of intra-LN therapy; we will be evaluating these changes using immunohistochemistry and magnetic resonance imaging. In addition, we are working with a collaborator with expertise in non-human primate (NHP) studies to run initial studies to evaluate the safety profile of intra-LN therapy.

7.2 Ongoing and Future Studies – Immunohistochemistry in the Central Nervous System

The studies completed in **Chapter 5.4,** as well as previous work completed in the Jewell lab[26], indicate that the intra-LN treatment impact the number of inflammatory cells present in the spinal cord after inducing the mouse models of MS. **Figure 7.1A**, which highlights previous work done in the Jewell lab, shows that treating prior to disease onset (day 10) with tolerogenic MPs (MOG_{35-55}/Rapa MPs), reduces the number of cells (blue, DAPI, nuclei), and T cells (green) in the spinal cord at peak disease (day 15). This was supported by the results described in **Chapter 5.4**, in which mice treated iLN with $PLP_{139-151}$/Rapa MPs showed fewer immune cells (CD45+, **Fig. 7.1B**, left) and fewer CD4+ T cells (**Fig. 7.1B**, left) compared to mice given PBS control treatments. These studies motivate additional research into how iLN therapy impacts immune infiltration, demyelination, and neurodegeneration in the CNS.

Toward this goal, with the help of Jewell lab member Dr. Robert Oakes, I have put together an immunostaining panel to evaluate degeneration of myelin basic protein (MBP), along axons of neuronal cells (neurofilament heavy chain in axons, NF200 and neuronal bodies (NeuN). A sample of this panel is included in **Fig. 7.2**, which includes a healthy mouse spinal cord with staining for DAPI (blue, nuclei), myelin (MBP, green), and neuron axons (NF200, red). In addition, this panel includes stains for T cells (CD3), as well as CNS support cells including microglia (Iba-1) and astrocytes (GFAP). Initial studies are underway.

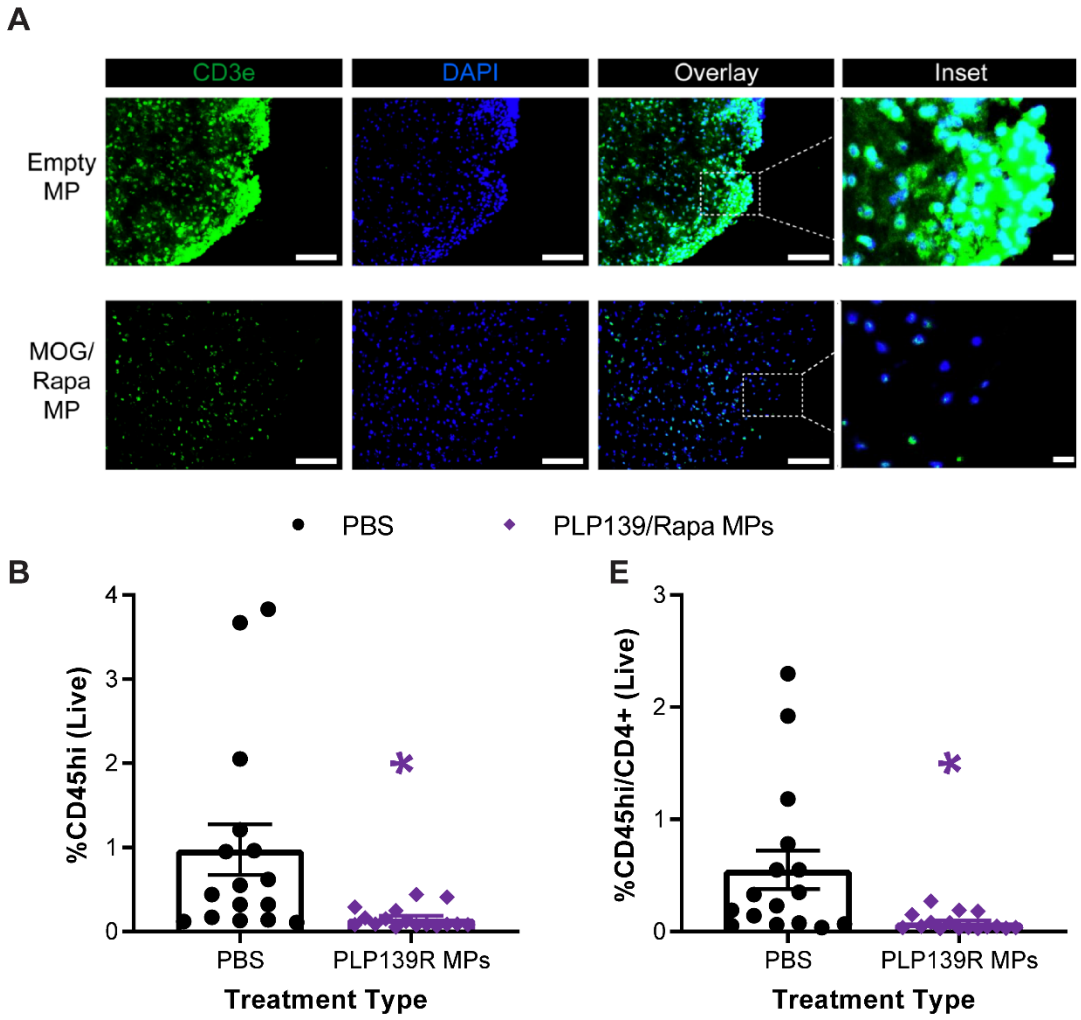

Figure 7.1 Tolerogenic iLN therapy reduces the number of T cells present in the spinal cord in mouse models of MS.

(A) Mice were induced with EAE, then treated iLN with the indicated MP formulations (n = 4) on day 10; spinal cords were collected on day 15 for immunochemistry. Spinal cords were sectioned and stained with CD3 (T cells, green), and DAPI (nuclei, blue). Scale bar, 100 mm. An inset of the overlay channel is shown in the far right column. Scale bar, 10 mm. Mice treated iLN with MOG_{35-55}/Rapa MPs have fewer cells, and fewer T cells, in spinal cord sections. Adapted from Tostanoski et al, *Cell Reports*, 2016[26] with permission from Elsevier. (B) Mice were treated iLN 28 days before inducing with RR-EAE. Spinal Cords were collected 54 days after induction and analyzed by flow cytometry for CD45hi (immune cells) and CD4+ (helper T Cells) cells. Mice treated with tolerogenic $PLP_{139-151}$/Rapa MPs had less immune cell infiltration into the spinal cord after 54 days with disease.

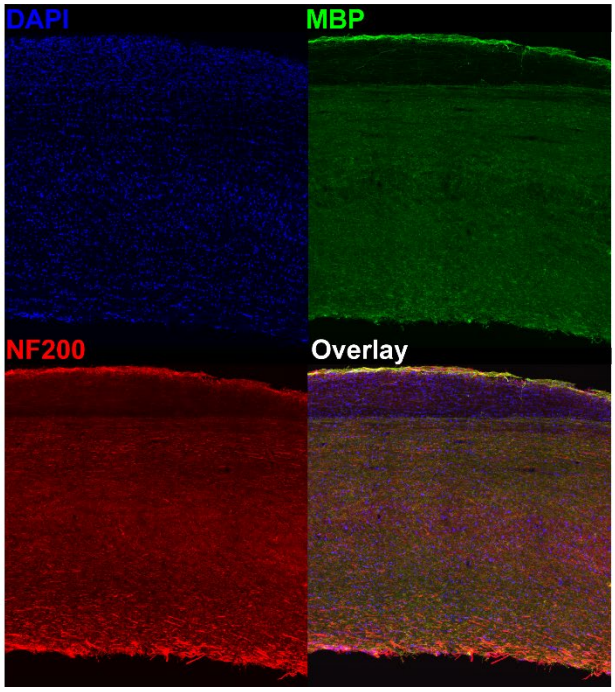

Figure 7.2 Immunostaining of healthy mouse spinal cord.
Healthy mice were perfused with PBS to remove red blood cells and fixed using 4% paraformaldehyde to stiffen the tissue. Spinal cords were removed, then sectioned and stained for nuclei (DAPI, blue), myelin (MBP, green), and axons (NF200, red).

7.3 Ongoing and Future Studies – Magnetic Resonance Imaging in the CNS

One of the most common ways MS is identified in human patients is using magnetic resonance imaging (MRI) to detect inflammatory lesions in the CNS. **Figure 7.3** shows an example of an MRI in a patient with Relapsing-Remitting MS[271]. Active inflammatory lesions can be seen in both the baseline and the image taken of the same patient 2 years later as bright white spots, with demyelinated regions indicated by a darker gray area. Here, the arrow shows a region where demyelination is evident two years after the baseline due to the active inflammation seen on the baseline image.

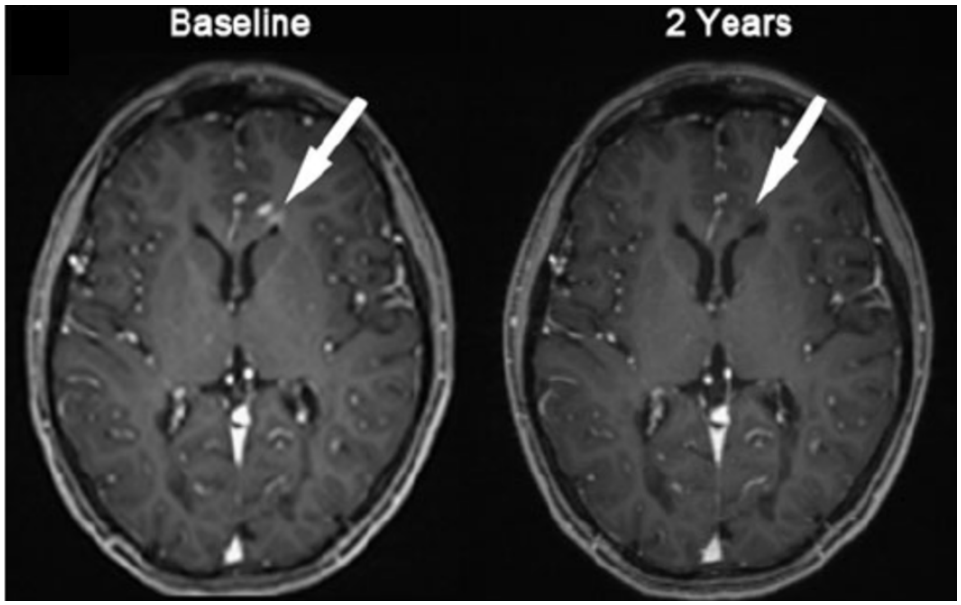

Figure 7.3 MRI imaging in a patient with Relapsing-Remitting MS.
The brain of a patient with Relapsing-Remitting MS was imaged by MRI, and again two years later. Active inflammatory lesions can be seen as bright white spots. De-myelinated areas are darker gray. The arrow indicates an active lesion in the baseline image that caused the demyelination seen in the image 2 years later. Republished from Sicotte, *Neurotherapeutics,* 2011[271] with permission from Springer Nature.

MRI and functional MRI (in which images are taken over time in response to a stimuli) have previously been used to assess brain lesions caused by EAE or RR-EAE in rodent models[272-274]. In an effort to support clinical research into tolerogenic MP delivered iLN, we plan to directly assess brain structure and function using MRI before, during, and after iLN therapy. This will be done in collaboration with my committee member Dr. Bromberg at the University of Maryland School of Medicine, with the MRI imaging done by the staff at the Center for Translational Research in Imaging (CTRIM) at the UM SoM. Initial studies begin this fall.

7.4 Ongoing and Future Studies – Evaluating the Safety and Toxicity of Tolerogenic iLN Therapy in Non-Human Primates.

To evaluate the safety profile of the tolerogenic iLN therapy, we partnered with Dr. Agnes Azimzadeh and Dr. Richard Pierson at Harvard. With their expertise in NHP studies, we designed a series of studies to evaluate the impact of iLN therapy on NHP blood counts and blood chemistry.

The primary purposes of these studies is to evaluate the safety of iLN tolerogenic MP treatment. There is limited interest by regulatory bodies in efficacy in NHP models. As such, we treated the NHP iLN with tolerogenic MPs, and then gave boosts with antigen alone to simulate an inflammatory setting. **Figure 7.4** shows the relative weights of the NHP that underwent this regimen. NHPs were given one of three treatments: tolerogenic MPs (Rapa/Ag MPs), Rapa MPs, or antigen boosts alone (Control). Tolerogenic iLN treatments had no impact on relative weight compared to control NHPs.

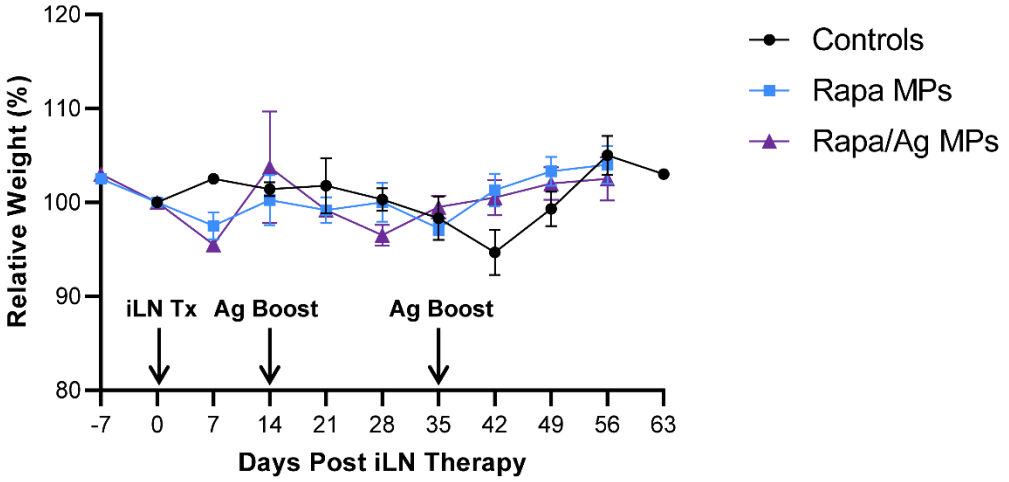

Figure 7.4 Relative Weights of Non-Human Primates Following iLN therapy. NHPs were given one of three treatments: tolerogenic MPs (Rapa/Ag MPs), Rapa MPs, or antigen boosts alone (Control), and weights were taken weekly. Tolerogenic iLN treatments had no impact on relative weight compared to control NHPs. N= 6 per group. Average ± SEM shown.

During this study, we also collected information on blood counts and blood chemistry. Blood count information included: white blood cell (WBC) counts, neutrophil counts, lymphocyte counts, hematocrit counts, and platelet counts. Blood chemistry information included: blood urea nitrogen and creatinine to assess kidney function; aspartate aminotransferase, alanine aminotransferase, and alkaline phosphatase to assess liver function; and amylase to assess pancreas function. Analysis for these parameters is ongoing, but suggests that iLN therapy was well tolerated by NHPs. These studies contributed greatly to the overall goal of improving pre-clinical knowledge for motivating clinical research into this therapy.

Chapter 8: Contributions

8.1 Research Publication Contributions

The work I completed to date during my PhD has resulted in four published manuscripts – one first author original research article, one first author review, one second-author original research article, and one second author review. I also have two first author original research articles in progress, with one recently submitted, and one with ongoing studies to complete.

In my first author research article, presented in **Chapter 4**, I outlined a series of experiments that could be used to screen potential immunotherapies before testing in animals or clinical trials to eliminate ineffective immunotherapy candidates before pre-clinical testing begins. I screened three PLGA MP based immunotherapies – PLGA MPs loaded with mTOR inhibitors: rapamycin, everolimus, and temsirolimus, and saw that all three were able to downregulate DC activation and T cell inflammatory activity. Considering the solubility and half-life limitations of rapamycin, and the potential of next-generation analogs, this work provided a screening platform for biomaterials-based immunotherapies, and set the stage for in vivo evaluation, where delivery kinetics, stability, and targeting could improve autoimmune therapies through biomaterial-enabled delivery.

My first author review article, presented in **Chapter 2**, gave an overview and insight into designing natural and synthetic immune tissues to enable new, better immunotherapies in the fields of cancer, autoimmunity, and infectious disease. Engineered immune tissues could serve as in vitro tools to more accurately study

human immune function and disease, while immune tissues engineered for implantation as next-generation vaccines or immunotherapies could enable direct, on-demand control over the generation and regulation of immune function.

Two additional first author papers are in progress, with one submitted and one in preparation. The work for these papers were introduced in **Chapter 5** (in preparation), and **Chapter 6** (submitted). Both papers worked toward the goal of advancing pre-clinical studies and motivating clinical research into the use of degradable, polymeric MPs loaded with tolerogenic signals that can be directly deposited into LN for promoting myelin-specific tolerance in MS. In **Chapter 5**, I outlined a series of studies completed to better understand the systemic impact of intra-LN tolerogenic MPs in different models of MS. In particular, this chapter showed that even at different stages of disease, one tolerogenic intra-LN treatment promoted recovery from paralysis and prevented relapse. In addition, this work showed that tolerogenic intra-LN treatments did not prevent mice from mounting healthy immune responses to vaccination. This, in combination with the future studies into the impact on the CNS outlined in **Chapter 7**, will be published as a first-author manuscript. In **Chapter 6,** I outlined the work I did with Jewell Lab undergraduate researcher Maeesha Noshin to enhance the stability of the tolerogenic MPs used for intra-LN immunotherapy using Chemistry, Manufacturing, and Controls (CMC) considerations. This work showed that low concentrations of excipients added before lyophilization enhanced MP and cargo stability over long-term storage at room temperature.

For my contributing author research publications, my contributions to this article included study design, running a drug-loaded biomaterial kinetic release study independently, statistical analysis, and contributions to writing the paper.

8.2 Research Collaborations

Beyond collaborations in the Jewell lab, during my PhD, I've had the opportunity to work with two external groups in support of the work presented in **Chapters 5** and **7**. First, our lab works closely with the Bromberg lab at the University of Maryland School of Medicine. Dr. Bromberg and his teams are experts in histology, and his lab taught me how to remove spinal cords from mice for CNS histology. I used that technique to collect cells from spinal cords in **Chapter 5** to investigate T cell infiltration. In addition, I wrote an animal protocol with Dr. Bromberg's lab to enable the MRI studies discussed in **Chapter 7** to visualize inflammatory lesions in mice with EAE. These studies leverage the imaging capabilities of the Center for Translational Imaging at the University of Maryland School of Medicine. These studies would not be possible without this collaboration.

To evaluate the safety profile of the tolerogenic iLN therapy, we partnered with Dr. Agnes Azimzadeh and Dr. Richard Pierson at Harvard. As discussed in **Chapter 7**, with their expertise in NHP studies, we were able to show iLN treatment with Rapa-loaded PLGA MPs is safe, and did not abnormalities in NHP blood counts or blood chemistry using a panel that assesses toxicities in kidney, liver, and pancreas function. These studies contributed greatly to the overall goal of improving pre-clinical knowledge for motivating clinical research into this therapy.

8.3 Research Conference Presentations

I have presented my research at six national and international conferences focused on biomaterials and immunology, including World Biomaterials Congress, two annual meetings of the Biomedical Engineering Society, one national meeting of the American Chemical Society, a virtual annual meeting of the Controlled Release Society, and a Keystone Symposia on Emerging Cellular Therapies. For these conferences, I have been awarded a number of travel awards, including a BMES Career Development Travel Award, as well as UMD Graduate School travel awards including the Jacob K. Goldhaber Travel Award and the International Conference Student Support Award.

8.4 Research Funding Support and Awards

Throughout my time at UMD, I have been received a by a number of fellowships and awards that have enabled my research. The last two years of my PhD have been supported by a National Institutes of Health F31 National Research Service Award from the National Institute of Allergy and Infectious Disease (AI143204).

At UMD, I have been a 2017 UMD Graduate School Summer Research Fellow (2 per department per year), a 2018 UMD Graduate School All-S.T.A.R. fellow (2 from the Clark School per year) and a 2018 UMD Outstanding Graduate Assistant (Top 2% of Graduate Assistants at UMD). I was selected as a University of Maryland Clark School Future Faculty Program Fellow. I was awarded the 2019 Fischell Department of Bioengineering Outstanding Graduate Student Research Award.

8.5 Service and Mentoring

Throughout my PhD, I have taken many opportunities to become involved in service and mentoring both on campus and in the community. I have participated in many activities to enhance STEM exposure. Through the NSF-funded Program to Enhance Participation in Research, I have mentored four high school students. Over a year, I help my mentees identify a research topic, find and read scientific literature, and prepare a research poster to present at a symposium at UMD. I also organized and ran 3 field trips for students from that same high school to come to the Jewell lab and gain hands-on lab experience in vaccine and biomaterial synthesis. This enabled immersive research experiences for the ~270 students who visited the lab during these visits.

In lab, I have mentored two undergraduate students – one for a summer, and one for two years. In both cases, I designed their projects, tangentially related to mine, to help them gain key research skills – experimental techniques, scientific reading, and communication. Both students presented their research at Annual Meetings of the Biomedical Engineering Society. Maeesha Noshin, the student I mentored for two years, was awarded a UMD ASPIRE fellowship for her work in the lab. In addition, Maeesha earned co-first authorship on the work on MP stability that was presented in **Chapter 6.**

Outside of research, I served as a teaching assistant for two undergraduate courses. For these courses, I wrote answer keys, graded homework and exams, and lead discussions each week. For these discussions, I prepared and presented material and practice problems to students, and moderated career discussions. As a Clark School Future Faculty Fellow, I also had the chance to co-teach an undergraduate course with

Dr. Jewell. For this course, I designed and taught 8 lectures, and designed homework and exam questions, and graded exams. I also served on the Bioengineering Graduate Student Society for 3 years – as a Class Representative, the Vice President of Academic Affairs, and then President. In these roles, I acted as a liaison between the department and the graduate students, and planned events designed to enrich the graduate student experience – focused on professional development, academic experience, volunteering, and social activities. I also planned two Student Choice Seminar events, in which I hosted two distinguished professors who gave guest lectures attended by bioengineering graduate students and professors.

Appendix: List of Publications and Intellectual Property

Published First Author:

1. **Emily A. Gosselin**, Haleigh B. Eppler, Jonathan S. Bromberg, and Christopher M. Jewell. Designing natural and synthetic immune tissues. *Nature Materials* **2018**, 17: 484-498. (cover article)
   *Featured in *Nature* Outlook on Vaccines, 2019

2. **Emily A. Gosselin**, Lisa H. Tostanoski, and Christopher M. Jewell. Controlled release of second generation mTOR inhibitors to restrain inflammation in primary immune cells. *The AAPS Journal* **2017**, 19: 1175-1180.

Published Contributing Author:

3. Joshua M. Gammon, **Emily A. Gosselin**, Lisa H. Tostanoski, Yu-Cheih Chiu, Xiangbin Zeng, Qin Zeng, and Christopher M. Jewell. Low-dose controlled release of mTOR inhibitors maintains T cell plasticity and promotes central memory T cells. *Journal of Controlled Release* **2017**, 2017: 151-161.

4. Lisa H. Tostanoski, **Emily A. Gosselin**, and Christopher M. Jewell. Targeting and control of antigen presenting cells with biomaterials to promote tolerance and combat autoimmune disease. *Discovery Medicine* **2016**, 21: 403-410.

In Progress:

5. **Emily A. Gosselin*,** Maeeha Noshin*, Sheneil K. Black, and Christopher M. Jewell. Enhancing the Stability of Polymer Microparticles for Autoimmune Therapy. *Frontiers in Bioengineering and Biotechnology*. Submitted, invited article.
   * indicates equal contributions
6. **Emily A. Gosselin**, ….., and Christopher M. Jewell. Intra-Lymph Node Delivery of Tolerogenic Microparticles Promotes Immune Tolerance, Reverses Paralysis, and Prevents Relapse in a Model of Multiple Sclerosis. In preparation.

Intellectual Property Filing:

1. "Microneedle-mediated delivery of tolerogenic immunotherapeutics." Christopher M. Jewell, Lisa H. Tostanoski, **Emily A. Gosselin**. U.S. Patent Application No. 16/492,731; Filed September 10, 2019.

References

1. Lesokhin, A.M., Callahan, M.K., Postow, M.A. & Wolchok, J.D. On being less tolerant: Enhanced cancer immunosurveillance enabled by targeting checkpoints and agonists of T cell activation. *Science Translational Medicine* **7**, 12 (2015).
2. Chen, D.S. & Mellman, I. Elements of cancer immunity and the cancer-immune set point. *Nature* **541**, 321-330 (2017).
3. DeFrancesco, L. CAR-T's forge ahead, despite Juno deaths. *Nature Biotechnology* **35**, 6-7 (2017).
4. Cadavid, D. et al. Safety and efficacy of opicinumab in acute optic neuritis (RENEW): a randomised, placebo-controlled, phase 2 trial. *Lancet Neurology* **16**, 189-199 (2017).
5. Antonelli, A. et al. Establishing human leukemia xenograft mouse models by implanting human bone marrow-like scaffold-based niches. *Blood* **128**, 2949-2959 (2016).
6. Purwada, A. et al. Ex vivo engineered immune organoids for controlled germinal center reactions. *Biomaterials* **63**, 24-34 (2015).
7. Purwada, A. & Singh, A. Immuno-engineered organoids for regulating the kinetics of B-cell development and antibody production. *Nature Protocols* **12**, 15 (2017).
8. Poznansky, M.C. et al. Efficient generation of human T cells from a tissue-engineered thymic organoid. *Nature Biotechnology* **18**, 729-734 (2000).
9. Lee, J. & Kotov, N.A. Notch Ligand Presenting Acellular 3D Microenvironments for ex vivo Human Hematopoietic Stem-Cell Culture made by Layer-By-Layer Assembly. *Small* **5**, 1008-1013 (2009).
10. Pinto, S. et al. An Organotypic Coculture Model Supporting Proliferation and Differentiation of Medullary Thymic Epithelial Cells and Promiscuous Gene Expression. *Journal of Immunology* **190**, 1085-1093 (2013).
11. Nichols, J.E. et al. In vitro analog of human bone marrow from 3D scaffolds with biomimetic inverted colloidal crystal geometry. *Biomaterials* **30**, 1071-1079 (2009).
12. Torisawa, Y.S. et al. Bone marrow-on-a-chip replicates hematopoietic niche physiology in vitro. *Nature Methods* **11**, 663-+ (2014).
13. Kim, S.K., Moon, W.K., Park, J.Y. & Jung, H. Inflammatory mimetic microfluidic chip by immobilization of cell adhesion molecules for T cell adhesion. *Analyst* **137**, 4062-4068 (2012).
14. Stachowiak, A.N. & Irvine, D.J. Inverse opal hydrogel-collagen composite scaffolds as a supportive microenvironment for immune cell migration. *Journal of Biomedical Materials Research Part A* **85A**, 815-828 (2008).
15. Gopalakrishnan, N. et al. Infection and immunity on a chip: a compartmentalised microfluidic platform to monitor immune cell behaviour in real time. *Lab on a Chip* **15**, 1481-1487 (2015).
16. Jones, C.N. et al. Microfluidic chambers for monitoring leukocyte trafficking and humanized nano-proresolving medicines interactions. *Proceedings of the*

National Academy of Sciences of the United States of America **109**, 20560-20565 (2012).
17. Dura, B. et al. Profiling lymphocyte interactions at the single-cell level by microfluidic cell pairing. *Nature Communications* **6**, 13 (2015).
18. Rosa, P.M., Gopalakrishnan, N., Ibrahim, H., Haug, M. & Halaas, O. The intercell dynamics of T cells and dendritic cells in a lymph node-on-a-chip flow device. *Lab on a Chip* **16**, 3728-3740 (2016).
19. Ross, A.E., Belanger, M.C., Woodroof, J.F. & Pompano, R.R. Spatially resolved microfluidic stimulation of lymphoid tissue ex vivo. *Analyst* **142**, 649-659 (2017).
20. Ali, O.A., Huebsch, N., Cao, L., Dranoff, G. & Mooney, D.J. Infection-mimicking materials to program dendritic cells in situ. *Nature Materials* **8**, 151-158 (2009).
21. Ali, O.A., Emerich, D., Dranoff, G. & Mooney, D.J. In Situ Regulation of DC Subsets and T Cells Mediates Tumor Regression in Mice. *Science Translational Medicine* **1**, 10 (2009).
22. Kim, J. et al. Injectable, spontaneously assembling, inorganic scaffolds modulate immune cells in vivo and increase vaccine efficacy. *Nature Biotechnology* **33**, 64-U241 (2015).
23. Verbeke, C.S. et al. Multicomponent Injectable Hydrogels for Antigen-Specific Tolerogenic Immune Modulation. *Advanced Healthcare Materials* **6**, 15 (2017).
24. Jewell, C.M., Lopez, S.C.B. & Irvine, D.J. In situ engineering of the lymph node microenvironment via intranodal injection of adjuvant-releasing polymer particles. *Proceedings of the National Academy of Sciences of the United States of America* **108**, 15745-15750 (2011).
25. Gammon, J.M. et al. Low-dose controlled release of mTOR inhibitors maintains T cell plasticity and promotes central memory T cells. *Journal of Controlled Release* (2017).
26. Tostanoski, L.H. et al. Reprogramming the Local Lymph Node Microenvironment Promotes Tolerance that Is Systemic and Antigen Specific. *Cell Reports* **16**, 2940-2952 (2016).
27. Sunshine, J.C., Perica, K., Schneck, J.P. & Green, J.J. Particle shape dependence of CD8+T cell activation by artificial antigen presenting cells. *Biomaterials* **35**, 269-277 (2014).
28. Meyer, R.A. et al. Biodegradable Nanoellipsoidal Artificial Antigen Presenting Cells for Antigen Specific T-Cell Activation. *Small* **11**, 1519-1525 (2015).
29. Bruns, H. et al. CD47 Enhances In Vivo Functionality of Artificial Antigen-Presenting Cells. *Clinical Cancer Research* **21**, 2075-2083 (2015).
30. Kosmides, A.K. et al. Biomimetic biodegradable artificial antigen presenting with PD-1 blockade to treat melanoma cells synergize. *Biomaterials* **118**, 16-26 (2017).
31. Suematsu, S. & Watanabe, T. Generation of a synthetic lymphoid tissue-like organoid in mice. *Nature Biotechnology* **22**, 1539-1545 (2004).

32. Okamoto, N., Chihara, R., Shimizu, C., Nishimoto, S. & Watanabe, T. Artificial lymph nodes induce potent secondary immune responses in naive and immunodeficient mice. *Journal of Clinical Investigation* **117**, 997-1007 (2007).
33. Stephan, S.B. et al. Biopolymer implants enhance the efficacy of adoptive T-cell therapy. *Nature Biotechnology* **33**, 97-U277 (2015).
34. Smith, T.T. et al. Biopolymers codelivering engineered T cells and STING agonists can eliminate heterogeneous tumors. *Journal of Clinical Investigation* **127**, 2176-2191 (2017).
35. Fan, Y. et al. Bioengineering Thymus Organoids to Restore Thymic Function and Induce Donor-Specific Immune Tolerance to Allografts. *Molecular Therapy* **23**, 1262-1277 (2015).
36. Holzapfel, B.M. et al. Tissue engineered humanized bone supports human hematopoiesis in vivo. *Biomaterials* **61**, 103-114 (2015).
37. Reinisch, A. et al. A humanized bone marrow ossicle xenotransplantation model enables improved engraftment of healthy and leukemic human hematopoietic cells. *Nature Medicine* **22**, 812-821 (2016).
38. Abarrategi, A. et al. Versatile humanized niche model enables study of normal and malignant human hematopoiesis. *Journal of Clinical Investigation* **127**, 543-548 (2017).
39. Kapsenberg, M.L. Dendritic-cell control of pathogen-driven T-cell polarization. *Nature Reviews Immunology* **3**, 984-993 (2003).
40. Loder, F. et al. B cell development in the spleen takes place in discrete steps and is determined by the quality of B cell receptor-derived signals. *Journal of Experimental Medicine* **190**, 75-89 (1999).
41. Nemazee, D. Mechanisms of central tolerance for B cells. *Nature Reviews Immunology* **17**, 281-294 (2017).
42. Hogquist, K.A., Baldwin, T.A. & Jameson, S.C. Central tolerance: Learning self-control in the thymus. *Nature Reviews Immunology* **5**, 772-782 (2005).
43. Takahama, Y. Journey through the thymus: stromal guides for T-cell development and selection. *Nature Reviews Immunology* **6**, 127-135 (2006).
44. Mebius, R.E. & Kraal, G. Structure and function of the spleen. *Nature Reviews Immunology* **5**, 606-616 (2005).
45. Butcher, E.C. & Picker, L.J. Lymphocyte homing and homeostasis. *Science* **272**, 60-66 (1996).
46. Nutt, S.L., Hodgkin, P.D., Tarlinton, D.M. & Corcoran, L.M. The generation of antibody-secreting plasma cells. *Nature Reviews Immunology* **15**, 160-171 (2015).
47. Crotty, S. in Annual Review of Immunology, Vol 29, Vol. 29. (eds. W.E. Paul, D.R. Littman & W.M. Yokoyama) 621-663 (Annual Reviews, Palo Alto; 2011).
48. Bhatia, S.N. & Ingber, D.E. Microfluidic organs-on-chips. *Nature Biotechnology* **32**, 760-772 (2014).
49. Takebe, T., Zhang, B.Y. & Radisic, M. Synergistic Engineering: Organoids Meet Organs-on-a-Chip. *Cell Stem Cell* **21**, 297-300 (2017).

50. Sardi, M., Lubitz, A. & Giese, C. Modeling Human Immunity In Vitro: Improving Artificial Lymph Node Physiology by Stromal Cells. *Applied In Vitro Toxicology* **2**, 143-150 (2016).
51. Nojima, T. et al. In-vitro derived germinal centre B cells differentially generate memory B or plasma cells in vivo. *Nature Communications* **2**, 11 (2011).
52. Kuzin, I. et al. Long-Term Immunologically Competent Human Peripheral Lymphoid Tissue Cultures in a 3D Bioreactor. *Biotechnology and Bioengineering* **108**, 1430-1440 (2011).
53. Tomei, A.A., Siegert, S., Britschgi, M.R., Luther, S.A. & Swartz, M.A. Fluid Flow Regulates Stromal Cell Organization and CCL21 Expression in a Tissue-Engineered Lymph Node Microenvironment. *Journal of Immunology* **183**, 4273-4283 (2009).
54. Singh, A. Biomaterials innovation for next generation ex vivo immune tissue engineering. *Biomaterials* **130**, 104-110 (2017).
55. Beguelin, W. et al. EZH2 enables germinal centre formation through epigenetic silencing of CDKN1A and an Rb-E2F1 feedback loop. *Nature Communications* **8**, 16 (2017).
56. Cook, M.M. et al. Micromarrows-Three-Dimensional Coculture of Hematopoietic Stem Cells and Mesenchymal Stromal Cells. *Tissue Engineering Part C-Methods* **18**, 319-328 (2012).
57. Tao, Z.M. & Ghoroghchian, P.P. Microparticle, nanoparticle, and stem cell-based oxygen carriers as advanced blood substitutes. *Trends in Biotechnology* **32**, 466-473 (2014).
58. Giarratana, M.C. et al. Proof of principle for transfusion of in vitro-generated red blood cells. *Blood* **118**, 5071-5079 (2011).
59. Thon, J.N. et al. Platelet bioreactor-on-a-chip. *Blood* **124**, 1857-1867 (2014).
60. Trakarnsanga, K. et al. An immortalized adult human erythroid line facilitates sustainable and scalable generation of functional red cells. *Nature Communications* **8**, 7 (2017).
61. Haessler, U., Pisano, M., Wu, M.M. & Swartz, M.A. Dendritic cell chemotaxis in 3D under defined chemokine gradients reveals differential response to ligands CCL21 and CCL19. *Proceedings of the National Academy of Sciences of the United States of America* **108**, 5614-5619 (2011).
62. Hori, Y., Winans, A.M., Huang, C.C., Horrigan, E.M. & Irvine, D.J. Injectable dendritic cell-carrying alginate gels for immunization and immunotherapy. *Biomaterials* **29**, 3671-3682 (2008).
63. Irvine, D.J., Swartz, M.A. & Szeto, G.L. Engineering synthetic vaccines using cues from natural immunity. *Nature Materials* **12**, 978-990 (2013).
64. Cheung, A.S. & Mooney, D.J. Engineered materials for cancer immunotherapy. *Nano Today* **10**, 511-531 (2015).
65. Northrup, L., Christopher, M.A., Sullivan, B.P. & Berldand, C. Combining antigen and immunomodulators: Emerging trends in antigen-specific immunotherapy for autoimmunity. *Advanced Drug Delivery Reviews* **98**, 86-98 (2016).

66. Tostanoski, L.H. & Jewell, C.M. Engineering self-assembled materials to study and direct immune function. *Advanced Drug Delivery Reviews* (2017).
67. Pearson, R.M., Casey, L.M., Hughes, K.R., Miller, S.D. & Shea, L.D. In vivo reprogramming of immune cells: Technologies for induction of antigen-specific tolerance. *Advanced Drug Delivery Reviews* (2017).
68. Kuai, R., Ochyl, L.J., Bahjat, K.S., Schwendeman, A. & Moon, J.J. Designer vaccine nanodiscs for personalized cancer immunotherapy. *Nature Materials* **16**, 489-+ (2017).
69. Ishihara, J. et al. Matrix-binding checkpoint immunotherapies enhance antitumor efficacy and reduce adverse events. *Science Translational Medicine* **9**, 14 (2017).
70. Ludvigsson, J., Wahlberg, J. & Casas, R. Intralymphatic Injection of Autoantigen in Type 1 Diabetes. *New England Journal of Medicine* **376**, 697-699 (2017).
71. Ugel, S. et al. In vivo Administration of Artificial Antigen-Presenting Cells Activates Low-Avidity T Cells for Treatment of Cancer. *Cancer Research* **69**, 9376-9384 (2009).
72. Perica, K. et al. Enrichment and Expansion with Nanoscale Artificial Antigen Presenting Cells for Adoptive Immunotherapy. *Acs Nano* **9**, 6861-6871 (2015).
73. Cuzzone, D.A., Albano, N.J., Aschen, S.Z., Ghanta, S. & Mehrara, B.J. Decellularized Lymph Nodes as Scaffolds for Tissue Engineered Lymph Nodes. *Lymphatic Research and Biology* **13**, 186-194 (2015).
74. Kobayashi, Y. & Watanabe, T. Gel-Trapped Lymphorganogenic chemokines Trigger Artificial Tertiary Lymphoid Organs and Mount Adaptive Immune Reseponses In Vivo. *Frontiers in Immunology* **7**, 10 (2016).
75. Smith, T.T. et al. In situ programming of leukaemia-specific T cells using synthetic DNA nanocarriers. *Nature Nanotechnology* **12**, 813-+ (2017).
76. Hun, M. et al. Native thymic extracellular matrix improves in vivo thymic organoid T cell output, and drives in vitro thymic epithelial cell differentiation. *Biomaterials* **118**, 1-15 (2017).
77. Markert, M.L., Devlin, B.H. & McCarthy, E.A. Thymus transplantation. *Clinical Immunology* **135**, 236-246 (2010).
78. Mao, A.S. et al. Deterministic encapsulation of single cells in thin tunable microgels for niche modelling and therapeutic delivery. *Nature Materials* **16**, 236-243 (2017).
79. Lee, J. et al. Implantable microenvironments to attract hematopoietic stem/cancer cells. *Proceedings of the National Academy of Sciences of the United States of America* **109**, 19638-19643 (2012).
80. Shih, Y.-R. et al. In vivo engineering of bone tissues with hematopoietic functions and mixed chimerism. *Proceedings of the National Academy of Sciences* **114**, 5419-5424 (2017).
81. Ben-David, U. et al. Patient-derived xenografts undergo mouse-specific tumor evolution. *Nature Genetics* **49**, 1567-+ (2017).

82. Schaupper, M., Jeltsch, M., Rohringer, S., Redl, H. & Holnthoner, W. Lymphatic Vessels in Regenerative Medicine and Tissue Engineering. *Tissue Engineering Part B-Reviews* **22**, 395-407 (2016).
83. Randolph, G.J., Ivanov, S., Zinselmeyer, B.H. & Scallan, J.P. in Annual Review of Immunology, Vol 35, Vol. 35. (eds. D.R. Littman & W.M. Yokoyama) 31-52 (Annual Reviews, Palo Alto; 2017).
84. Gibot, L. et al. Tissue-engineered 3D human lymphatic microvascular network for in vitro studies of lymphangiogenesis. *Nature Protocols* **12**, 1077-1088 (2017).
85. Groom, J.R. et al. CXCR3 Chemokine Receptor-Ligand Interactions in the Lymph Node Optimize CD4(+) T Helper 1 Cell Differentiation. *Immunity* **37**, 1091-1103 (2012).
86. Malhotra, D. et al. Transcriptional profiling of steady-state and inflamed lymph node stroma reveals potential hematopoietic-stromal cross-talk pathways and suggests an active role for stroma during ongoing immune responses. *Journal of Immunology* **188**, 1 (2012).
87. Song, J. et al. Extracellular matrix of secondary lymphoid organs impacts on B-cell fate and survival. *Proceedings of the National Academy of Sciences of the United States of America* **110**, E2915-E2924 (2013).
88. Cohen, J.N. et al. Tolerogenic Properties of Lymphatic Endothelial Cells Are Controlled by the Lymph Node Microenvironment. *Plos One* **9**, 13 (2014).
89. Kastenmuller, W. et al. Peripheral Prepositioning and Local CXCL9 Chemokine-Mediated Guidance Orchestrate Rapid Memory CD8(+) T Cell Responses in the Lymph Node. *Immunity* **38**, 502-513 (2013).
90. Burrell, B.E. & Bromberg, J.S. Fates of CD4+T Cells in a Tolerant Environment Depend on Timing and Place of Antigen Exposure. *American Journal of Transplantation* **12**, 576-589 (2012).
91. Dubrot, J. et al. Lymph node stromal cells acquire peptide-MHCII complexes from dendritic cells and induce antigen-specific CD4(+) T cell tolerance. *Journal of Experimental Medicine* **211**, 1153-1166 (2014).
92. Hirosue, S. et al. Steady-State Antigen Scavenging, Cross-Presentation, and CD8(+) T Cell Priming: A New Role for Lymphatic Endothelial Cells. *Journal of Immunology* **192**, 5002-5011 (2014).
93. Tamburini, B.A., Burchill, M.A. & Kedl, R.M. Antigen capture and archiving by lymphatic endothelial cells following vaccination or viral infection. *Nature Communications* **5**, 13 (2014).
94. Warren, K.J., Iwami, D., Harris, D.G., Bromberg, J.S. & Burrell, B.E. Laminins affect T cell trafficking and allograft fate. *Journal of Clinical Investigation* **124**, 2204-2218 (2014).
95. Astarita, J.L. et al. The CLEC-2-podoplanin axis controls the contractility of fibroblastic reticular cells and lymph node microarchitecture. *Nature Immunology* **16**, 75-+ (2015).
96. Nia, H.T. et al. Solid stress and elastic energy as measures of tumour mechanopathology. *Nature Biomedical Engineering* **1**, 0004 (2016).

97. Nolan, D.J. et al. Molecular Signatures of Tissue-Specific Microvascular Endothelial Cell Heterogeneity in Organ Maintenance and Regeneration. *Developmental Cell* **26**, 204-219 (2013).
98. Iftakhar-E-Khuda, I. et al. Gene-expression profiling of different arms of lymphatic vasculature identifies candidates for manipulation of cell traffic. *Proceedings of the National Academy of Sciences of the United States of America* **113**, 10643-10648 (2016).
99. Lee, T.T. et al. Light-triggered in vivo activation of adhesive peptides regulates cell adhesion, inflammation and vascularization of biomaterials. *Nature Materials* **14**, 352-360 (2015).
100. Sadtler, K. et al. Developing a pro-regenerative biomaterial scaffold microenvironment requires T helper 2 cells. *Science* **352**, 366-370 (2016).
101. Doloff, J.C. et al. Colony stimulating factor-1 receptor is a central component of the foreign body response to biomaterial implants in rodents and non-human primates. *Nature Materials* **16**, 671-+ (2017).
102. Guc, E. et al. Local induction of lymphangiogenesis with engineered fibrin-binding VEGF-C promotes wound healing by increasing immune cell trafficking and matrix remodeling. *Biomaterials* **131**, 160-175 (2017).
103. Wang, H.M. et al. Enzyme-Catalyzed Formation of Supramolecular Hydrogels as Promising Vaccine Adjuvants. *Advanced Functional Materials* **26**, 1822-1829 (2016).
104. Sharp, F.A. et al. Uptake of particulate vaccine adjuvants by dendritic cells activates the NALP3 inflammasome. *Proceedings of the National Academy of Sciences of the United States of America* **106**, 870-875 (2009).
105. Andorko, J.I., Hess, K.L. & Jewell, C.M. Harnessing biomaterials to engineer the lymph node microenvironment for immunity or tolerance. *AAPS J* **17**, 323-338 (2015).
106. Hess, K.L. et al. Engineering Immunological Tolerance Using Quantum Dots to Tune the Density of Self-Antigen Display. *Advanced Functional Materials* **27**, 11 (2017).
107. Singha, S. et al. Peptide-MHC-based nanomedicines for autoimmunity function as T-cell receptor microclustering devices. *Nat Nanotechnol* (2017).
108. Novkovic, M. et al. Topological Small-World Organization of the Fibroblastic Reticular Cell Network Determines Lymph Node Functionality. *Plos Biology* **14**, 20 (2016).
109. Romo, M.R., Perez-Martinez, D. & Ferrer, C.C. Innate immunity in vertebrates: an overview. *Immunology* **148**, 125-139 (2016).
110. Vivier, E. et al. Innate Lymphoid Cells: 10 Years On. *Cell* **174**, 1054-1066 (2018).
111. Mogensen, T.H. Pathogen Recognition and Inflammatory Signaling in Innate Immune Defenses. *Clinical Microbiology Reviews* **22**, 240-+ (2009).
112. Liew, P.X. & Kubes, P. THE NEUTROPHIL'S ROLE DURING HEALTH AND DISEASE. *Physiological Reviews* **99**, 1223-1248 (2019).
113. Kambayashi, T. & Laufer, T.M. Atypical MHC class II-expressing antigen-presenting cells: can anything replace a dendritic cell? *Nature Reviews Immunology* **14**, 719-730 (2014).

114. Collin, M. & Bigley, V. Human dendritic cell subsets: an update. *Immunology* **154**, 3-20 (2018).
115. O'Shea, J.J. & Paul, W.E. Mechanisms Underlying Lineage Commitment and Plasticity of Helper CD4(+) T Cells. *Science* **327**, 1098-1102 (2010).
116. Raphael, I., Nalawade, S., Eagar, T.N. & Forsthuber, T.G. T cell subsets and their signature cytokines in autoimmune and inflammatory diseases. *Cytokine* **74**, 5-17 (2015).
117. Dardalhon, V., Korn, T., Kuchroo, V.K. & Anderson, A.C. Role of Th1 and Th17 cells in organ-specific autoimmunity. *Journal of Autoimmunity* **31**, 252-256 (2008).
118. Miyara, M. & Sakaguchi, S. Natural regulatory T cells: mechanisms of suppression. *Trends in Molecular Medicine* **13**, 108-116 (2007).
119. Lourenco, E.V. & La Cava, A. Natural regulatory T cells in autoimmunity. *Autoimmunity* **44**, 33-42 (2011).
120. Qi, Q. et al. Diversity and clonal selection in the human T-cell repertoire. *Proceedings of the National Academy of Sciences of the United States of America* **111**, 13139-13144 (2014).
121. Jung, D. & Alt, F.W. Unraveling V(D)J recombination: Insights into gene regulation. *Cell* **116**, 299-311 (2004).
122. Nikolich-Zugich, J., Slifka, M.K. & Messaoudi, I. The many important facets of T-cell repertoire diversity. *Nature Reviews Immunology* **4**, 123-132 (2004).
123. Zarnitsyna, V.I., Evavold, B.D., Schoettle, L.N., Blattman, J.N. & Antia, R. Estimating the diversity, completeness, and cross-reactivity of the T cell repertoire. *Frontiers in Immunology* **4**, 11 (2013).
124. Kontos, S., Grimm, A.J. & Hubbell, J.A. Engineering antigen-specific immunological tolerance. *Current Opinion in Immunology* **35**, 80-88 (2015).
125. Xing, Y. & Hogquist, K.A. T-Cell Tolerance: Central and Peripheral. *Cold Spring Harbor Perspectives in Biology* **4**, 15 (2012).
126. Wang, L.F., Wang, F.S. & Gershwin, M.E. Human autoimmune diseases: a comprehensive update. *Journal of Internal Medicine* **278**, 369-395 (2015).
127. Wallin, M.T. et al. The prevalence of MS in the United States A population-based estimate using health claims data. *Neurology* **92**, E1029-E1040 (2019).
128. Society, N.M.S. (ed. N.M.S. Society) 1-15 (2015).
129. Comabella, M. & Khoury, S.J. Immunopathogenesis of multiple sclerosis. *Clinical Immunology* **142**, 2-8 (2012).
130. Sospedra, M. & Martin, R. Immunology of multiple sclerosis. *Annual Review of Immunology* **23**, 683-747 (2005).
131. Bitsch, A., Schuchardt, J., Bunkowski, S., Kuhlmann, T. & Bruck, W. Acute axonal injury in multiple sclerosis - Correlation with demyelination and inflammation. *Brain* **123**, 1174-1183 (2000).
132. Dendrou, C.A., Fugger, L. & Friese, M.A. Immunopathology of multiple sclerosis. *Nature Reviews Immunology* **15**, 545-558 (2015).
133. Ontaneda, D., Hyland, M. & Cohen, J.A. in Annual Review of Medicine, Vol 63, Vol. 63. (eds. C.T. Caskey, C.P. Austin & J.A. Hoxie) 389-404 (Annual Reviews, Palo Alto; 2012).

134. Schiess, N. & Calabresi, P.A. Multiple Sclerosis. *Semin Neurol* **36**, 350-356 (2016).
135. McFarland, H.F. & Martin, R. Multiple sclerosis: a complicated picture of autoimmunity. *Nature Immunology* **8**, 913-919 (2007).
136. Frischer, J.M. et al. The relation between inflammation and neurodegeneration in multiple sclerosis brains. *Brain* **132**, 1175-1189 (2009).
137. Trapp, B.D. & Nave, K.A. in Annual Review of Neuroscience, Vol. 31 247-269 (Annual Reviews, Palo Alto; 2008).
138. Huseby, E.S. et al. A pathogenic role for myelin-specific CD8(+) T cells in a model for multiple sclerosis. *Journal of Experimental Medicine* **194**, 669-676 (2001).
139. Medana, I., Martinic, M.A., Wekerle, H. & Neumann, H. Transection of major histocompatibility complex class I-induced neurites by cytotoxic T lymphocytes. *American Journal of Pathology* **159**, 809-815 (2001).
140. O'Connor, K.C. et al. Antibodies from inflamed central nervous system tissue recognize myelin oligodendrocyte glycoprotein. *Journal of Immunology* **175**, 1974-1982 (2005).
141. Pappalardo, J.L. & Hafler, D.A. Multiple sclerosis enters a grey area. *Nature* **566**, 465-466 (2019).
142. Lodygin, D. et al. beta-Synuclein-reactive T cells induce autoimmune CNS grey matter degeneration. *Nature* **566**, 503-+ (2019).
143. Rosenblum, M.D., Gratz, I.K., Paw, J.S. & Abbas, A.K. Treating Human Autoimmunity: Current Practice and Future Prospects. *Science Translational Medicine* **4**, 10 (2012).
144. Stankiewicz, J.M., Kolb, H., Karni, A. & Weiner, H.L. Role of Immunosuppressive Therapy for the Treatment of Multiple Sclerosis. *Neurotherapeutics* **10**, 77-88 (2013).
145. Piehl, F. A changing treatment landscape for multiple sclerosis: challenges and opportunities. *Journal of Internal Medicine* **275**, 364-381 (2014).
146. Cross, A.H. & Naismith, R.T. Established and novel disease-modifying treatments in multiple sclerosis. *Journal of Internal Medicine* **275**, 350-363 (2014).
147. Polman, C.H. et al. A randomized, placebo-controlled trial of natalizumab for relapsing multiple sclerosis. *New England Journal of Medicine* **354**, 899-910 (2006).
148. Tintore, M., Vidal-Jordana, A. & Sastre-Garriga, J. Treatment of multiple sclerosis - success from bench to bedside. *Nature Reviews Neurology* **15**, 53-58 (2019).
149. Society, N.M.S. 1-34 (National Multiple Sclerosis Society, 2020).
150. Society, N.M.S. (2019).
151. O'Connor, P.W. et al. Disease activity return during natalizumab treatment interruption in patients with multiple sclerosis. *Neurology* **76**, 1858-1865 (2011).
152. Quintana, F.J. et al. Epitope spreading as an early pathogenic event in pediatric multiple sclerosis. *Neurology* **83**, 2219-2226 (2014).

153. Esposito, M. et al. Rapamycin inhibits relapsing experimental autoimmune encephalomyelitis by both effector and regulatory T cells modulation. *Journal of Neuroimmunology* **220**, 52-63 (2010).
154. Webster, K.E. et al. In vivo expansion of T reg cells with IL-2-mAb complexes: induction of resistance to EAE and long-term acceptance of islet allografts without immunosuppression. *Journal of Experimental Medicine* **206**, 751-760 (2009).
155. Stallone, G. et al. mTOR inhibitors effects on regulatory T cells and on dendritic cells. *Journal of Translational Medicine* **14**, 9 (2016).
156. Bi, Y.J., Liu, G.W. & Yang, R.F. mTOR Regulates T-Cell Differentiation and Activation in Immunity and Autoimmunity. *Critical Reviews in Eukaryotic Gene Expression* **21**, 313-322 (2011).
157. Liu, Y., Zhang, D.T. & Liu, X.G. mTOR Signaling in T Cell Immunity and Autoimmunity. *International Reviews of Immunology* **34**, 50-66 (2015).
158. Powell, J.D. & Delgoffe, G.M. The Mammalian Target of Rapamycin: Linking T Cell Differentiation, Function, and Metabolism. *Immunity* **33**, 301-311 (2010).
159. Zoncu, R., Efeyan, A. & Sabatini, D.M. mTOR: from growth signal integration to cancer, diabetes and ageing. *Nature Reviews Molecular Cell Biology* **12**, 21-35 (2011).
160. Strauss, L. et al. Selective survival of naturally occurring human CD4(+)CD25(+)Foxp3(+) regulatory T cells cultured with rapamycin. *Journal of Immunology* **178**, 320-329 (2007).
161. Delgoffe, G.M. et al. The kinase mTOR regulates the differentiation of helper T cells through the selective activation of signaling by mTORC1 and mTORC2. *Nature Immunology* **12**, 295-U117 (2011).
162. Bookstaver, M.L., Tsai, S.J., Bromberg, J.S. & Jewell, C.M. Improving Vaccine and Immunotherapy Design Using Biomaterials. *Trends in Immunology* **39**, 135-150 (2018).
163. Gu, L. & Mooney, D.J. Biomaterials and emerging anticancer therapeutics: engineering the microenvironment. *Nature Reviews Cancer* **16**, 56-66 (2016).
164. Reddy, S.T., Swartz, M.A. & Hubbell, J.A. Targeting dendritic cells with biomaterials: developing the next generation of vaccines. *Trends in Immunology* **27**, 573-579 (2006).
165. Andorko, J., Hess, K. & Jewell, C. Harnessing Biomaterials to Engineer the Lymph Node Microenvironment for Immunity or Tolerance. *Aaps Journal* **17**, 323-338 (2015).
166. Mora-Solano, C. & Collier, J.H. Engaging adaptive immunity with biomaterials. *Journal of Materials Chemistry B* **2**, 2409-2421 (2014).
167. Gammon, J.M., Dold, N.M. & Jewell, C.M. Improving the clinical impact of biomaterials in cancer immunotherapy. *Oncotarget* **7**, 15421-15443 (2016).
168. Tostanoski, L.H., Gosselin, E.A. & Jewell, C.M. Engineering Tolerance Using Biomaterials to Target and Control Antigen Presenting Cells. *Discovery Medicine* **21**, 403-410 (2016).

169. Fang, R.N.H. & Zhang, L.F. in Annual Review of Chemical and Biomolecular Engineering, Vol 7, Vol. 7. (ed. J.M. Prausnitz) 305-326 (Annual Reviews, Palo Alto; 2016).
170. Kim, S.Y. et al. Immune Complexes Mimicking Synthetic Vaccine Nanoparticles for Enhanced Migration and Cross-Presentation of Dendritic Cells. *Advanced Functional Materials* **26**, 8072-8082 (2016).
171. Yuan, H.F. et al. Multivalent bi-specific nanobioconjugate engager for targeted cancer immunotherapy. *Nature Nanotechnology* **12**, 763-+ (2017).
172. Hudalla, G.A. et al. Gradated assembly of multiple proteins into supramolecular nanomaterials. *Nature Materials* **13**, 829-836 (2014).
173. Gause, K.T. et al. Codelivery of NOD2 and TLR9 Ligands via Nanoengineered Protein Antigen Particles for Improving and Tuning Immune Responses. *Advanced Functional Materials* **26**, 7526-7536 (2016).
174. Kim, J. & Mooney, D.J. In vivo modulation of dendritic cells by engineered materials: Towards new cancer vaccines. *Nano Today* **6**, 466-477 (2011).
175. Dhakal, S. et al. Biodegradable nanoparticle delivery of inactivated swine influenza virus vaccine provides heterologous cell-mediated immune response in pigs. *Journal of Controlled Release* **247**, 194-205 (2017).
176. Wibroe, P.P. et al. Bypassing adverse injection reactions to nanoparticles through shape modification and attachment to erythrocytes. *Nature Nanotechnology* **12**, 589-+ (2017).
177. Kumar, S., Anselmo, A.C., Banerjee, A., Zakrewsky, M. & Mitragotri, S. Shape and size-dependent immune response to antigen-carrying nanoparticles. *Journal of Controlled Release* **220**, 141-148 (2015).
178. Lynn, G.M. et al. In vivo characterization of the physicochemical properties of polymer-linked TLR agonists that enhance vaccine immunogenicity. *Nature Biotechnology* **33**, 1201-+ (2015).
179. Turley, D.M. & Miller, S.D. Peripheral tolerance induction using ethylenecarbodiimide-fixed APCs uses both direct and indirect mechanisms of antigen presentation for prevention of experimental autoimmune encephalomyelitis. *Journal of Immunology* **178**, 2212-2220 (2007).
180. Getts, D.R. et al. Tolerance Induced by Apoptotic Antigen-Coupled Leukocytes Is Induced by PD-L1(+) and IL-10-Producing Splenic Macrophages and Maintained by T Regulatory Cells. *Journal of Immunology* **187**, 2405-2417 (2011).
181. Lutterotti, A. et al. Antigen-Specific Tolerance by Autologous Myelin Peptide–Coupled Cells: A Phase 1 Trial in Multiple Sclerosis. *Science Translational Medicine* **5**, 188ra175 (2013).
182. Pishesha, N. et al. Engineered erythrocytes covalently linked to antigenic peptides can protect against autoimmune disease. *Proceedings of the National Academy of Sciences of the United States of America* **114**, 3157-3162 (2017).
183. Getts, D.R. et al. Microparticles bearing encephalitogenic peptides induce T-cell tolerance and ameliorate experimental autoimmune encephalomyelitis. *Nature Biotechnology* **30**, 1217-+ (2012).

184. Hunter, Z. et al. A Biodegradable Nanoparticle Platform for the Induction of Antigen-Specific Immune Tolerance for Treatment of Autoimmune Disease. *Acs Nano* **8**, 2148-2160 (2014).
185. McCarthy, D.P. et al. An antigen-encapsulating nanoparticle platform for T(H)1/17 immune tolerance therapy. *Nanomedicine-Nanotechnology Biology and Medicine* **13**, 191-200 (2017).
186. Yeste, A., Nadeau, M., Burns, E.J., Weiner, H.L. & Quintana, F.J. Nanoparticle-mediated codelivery of myelin antigen and a tolerogenic small molecule suppresses experimental autoimmune encephalomyelitis. *Proceedings of the National Academy of Sciences of the United States of America* **109**, 11270-11275 (2012).
187. Maldonado, R.A. et al. Polymeric synthetic nanoparticles for the induction of antigen-specific immunological tolerance. *Proceedings of the National Academy of Sciences of the United States of America* **112**, E156-E165 (2015).
188. Tostanoski, L.H. et al. Design of Polyelectrolyte Multilayers to Promote Immunological Tolerance. *ACS Nano* (2016).
189. Hess, K.L., Andorko, J.I., Tostanoski, L.H. & Jewell, C.M. Polyplexes assembled from self-peptides and regulatory nucleic acids blunt toll-like receptor signaling to combat autoimmunity. *Biomaterials* **118**, 51-62 (2017).
190. Senti, G. et al. Intralymphatic immunotherapy for cat allergy induces tolerance after only 3 injections. *Journal of Allergy and Clinical Immunology* **129**, 1290-1296 (2012).
191. Senti, G., Johansen, P. & Kundig, T.M. Intralymphatic immunotherapy. *Current Opinion in Allergy and Clinical Immunology* **9**, 537-543 (2009).
192. Senti, G. et al. Intralymphatic allergen administration renders specific immunotherapy faster and safer: A randomized controlled trial. *Proceedings of the National Academy of Sciences of the United States of America* **105**, 17908-17912 (2008).
193. Adamina, M. et al. Intranodal Immunization With a Vaccinia Virus Encoding Multiple Antigenic Epitopes and Costimulatory Molecules in Metastatic Melanoma. *Molecular Therapy* **18**, 651-659 (2010).
194. Ribas, A. et al. Intra-Lymph Node Prime-Boost Vaccination against Melan A and Tyrosinase for the Treatment of Metastatic Melanoma: Results of a Phase 1 Clinical Trial. *Clinical Cancer Research* **17**, 2987-2996 (2011).
195. Andorko, J.I., Tostanoski, L.H., Solano, E., Mukhamedova, M. & Jewell, C.M. Intra-lymph Node Injection of Biodegradable Polymer Particles. *Jove-Journal of Visualized Experiments*, 6 (2014).
196. Andorko, J.I., Gammon, J.M., Tostanoski, L.H., Zeng, Q. & Jewell, C.M. Targeted Programming of the Lymph Node Environment Causes Evolution of Local and Systemic Immunity. *Cellular and Molecular Bioengineering* **9**, 418-432 (2016).
197. Danhier, F. et al. PLGA-based nanoparticles: An overview of biomedical applications. *Journal of Controlled Release* **161**, 505-522 (2012).
198. Mohammadi-Samani, S. & Taghipour, B. PLGA micro and nanoparticles in delivery of peptides and proteins; problems and approaches. *Pharmaceutical Development and Technology* **20**, 385-393 (2015).

199. Fonte, P., Reis, S. & Sarmento, B. Facts and evidences on the lyophilization of polymeric nanoparticles for drug delivery. *J Control Release* **225**, 75-86 (2016).
200. Pollizzi, K.N. & Powell, J.D. Regulation of T cells by mTOR: the known knowns and the known unknowns. *Trends in Immunology* **36**, 13-20 (2015).
201. Laplante, M. & Sabatini, D.M. mTOR Signaling in Growth Control and Disease. *Cell* **149**, 274-293 (2012).
202. Tsang, C.K., Qi, H.Y., Liu, L.F. & Zheng, X.F.S. Targeting mammalian target of rapamycin (mTOR) for health and diseases. *Drug Discovery Today* **12**, 112-124 (2007).
203. Abu-Khalaf, M.M. et al. Phase 1b study of the mammalian target of rapamycin inhibitor sirolimus in combination with nanoparticle albumin-bound paclitaxel in patients with advanced solid tumors. *Cancer* **121**, 1817-1826 (2015).
204. Perl, A. Activation of mTOR (mechanistic target of rapamycin) in rheumatic diseases. *Nature Reviews Rheumatology* **12**, 169-182 (2016).
205. Lisi, L. et al. Rapamycin reduces clinical signs and neuropathic pain in a chronic model of experimental autoimmune encephalomyelitis. *Journal of Neuroimmunology* **243**, 43-51 (2012).
206. Gu, Z.F. et al. Rapamycin reverses the senescent phenotype and improves immuno-regulation of mesenchymal stem cells from MRL/lpr mice and systemic lupus erythematosus patients through inhibition of the mTOR signaling pathway. *Aging-Us* **8**, 1102-1114 (2016).
207. Wu, W. et al. Intravitreal injection of rapamycin-loaded polymeric micelles for inhibition of ocular inflammation in rat model. *International Journal of Pharmaceutics* **513**, 238-246 (2016).
208. Nguyen, Q.D. et al. Intravitreal Sirolimus for Noninfectious Uveitis: A Phase III Sirolimus Study Assessing Double-masKed Uveitis TReAtment (SAKURA). *Ophthalmology* **123**, 2413-2423 (2016).
209. Yuan, R.R., Kay, A., Berg, W.J. & Lebwohl, D. Targeting tumorigenesis: development and use of mTOR inhibitors in cancer therapy. *Journal of Hematology & Oncology* **2**, 12 (2009).
210. Chan, S. et al. Phase II study of temsirolimus (CCI-779), a novel inhibitor of mTOR, in heavily pretreated patients with locally advanced or metastatic breast cancer. *Journal of Clinical Oncology* **23**, 5314-5322 (2005).
211. O'Donnell, A. et al. Phase I pharmacokinetic and pharmacodynamic study of the oral mammalian target of rapamycin inhibitor everolimus in patients with advanced solid tumors. *Journal of Clinical Oncology* **26**, 1588-1595 (2008).
212. Witzig, T.E. et al. A phase II trial of the oral mTOR inhibitor everolimus in relapsed aggressive lymphoma. *Leukemia* **25**, 341-347 (2011).
213. Zhu, A.X. et al. Phase 1/2 Study of Everolimus in Advanced Hepatocellular Carcinoma. *Cancer* **117**, 5094-5102 (2011).
214. Fleming, G.F. et al. Phase II trial of temsirolimus in patients with metastatic breast cancer. *Breast Cancer Research and Treatment* **136**, 355-363 (2012).
215. Zhang, Y.J. et al. The impact of everolimus versus other rapamycin derivative-eluting stents on clinical outcomes in patients with coronary artery

disease: A meta-analysis of 16 randomized trials. *Journal of Cardiology* **64**, 185-193 (2014).
216. Eisen, H.J. et al. Everolimus for the prevention of allograft rejection and vasculopathy in cardiac-transplant recipients. *New England Journal of Medicine* **349**, 847-858 (2003).
217. Cheng, L., Chen, J.L. & Mao, X.L. Everolimus vs. rapamycin for treating diabetic nephropathy in diabetic mouse model. *Journal of Huazhong University of Science and Technology-Medical Sciences* **31**, 457-462 (2011).
218. Fagone, P. et al. Comparative Study of Rapamycin and Temsirolimus Demonstrates Superimposable Anti-Tumour Potency on Prostate Cancer Cells. *Basic & Clinical Pharmacology & Toxicology* **112**, 63-69 (2013).
219. Waickman, A.T. & Powell, J.D. Mammalian Target of Rapamycin Integrates Diverse Inputs To Guide the Outcome of Antigen Recognition in T Cells. *Journal of Immunology* **188**, 4721-4729 (2012).
220. Waickman, A.T. & Powell, J.D. mTOR, metabolism, and the regulation of T-cell differentiation and function. *Immunological Reviews* **249**, 43-58 (2012).
221. Sakaguchi, S. Naturally arising CD4(+) regulatory T cells for immunologic self-tolerance and negative control of immune responses. *Annual Review of Immunology* **22**, 531-562 (2004).
222. Sakaguchi, S. et al. Immunologic tolerance maintained by CD25(+) CD4(+) regulatory T cells: their common role in controlling autoimmunity, tumor immunity, and transplantation tolerance. *Immunological Reviews* **182**, 18-32 (2001).
223. Sakaguchi, S. et al. Foxp3(+)CD25(+)CD4(+) natural regulatory T cells in dominant self-tolerance and autoimmune disease. *Immunological Reviews* **212**, 8-27 (2006).
224. Battaglia, M. et al. Induction of tolerance in type 1 diabetes via both CD4(+) CD25(+) T regulatory cells and T regulatory type 1 cells. *Diabetes* **55**, 1571-1580 (2006).
225. Han, R.R. et al. RAD001 (everolimus) attenuates experimental autoimmune neuritis by inhibiting the mTOR pathway, elevating Akt activity and polarizing M2 macrophages. *Experimental Neurology* **280**, 106-114 (2016).
226. Hennig, M. et al. Everolimus improves experimental autoimmune uveoretinitis. *Experimental Eye Research* **105**, 43-52 (2012).
227. Gammon, J.M., Tostanoski, L.H., Adapa, A.R., Chiu, Y.C. & Jewell, C.M. Controlled delivery of a metabolic modulator promotes regulatory T cells and restrains autoimmunity. *Journal of Controlled Release* **210**, 169-178 (2015).
228. Peine, K.J. et al. Treatment of Experimental Autoimmune Encephalomyelitis by Codelivery of Disease Associated Peptide and Dexamethasone in Acetalated Dextran Microparticles. *Molecular Pharmaceutics* **11**, 828-835 (2014).
229. Haddadi, A. et al. Delivery of rapamycin by PLGA nanoparticles enhances its suppressive activity on dendritic cells. *Journal of Biomedical Materials Research Part A* **84A**, 885-898 (2008).
230. Battaglia, M., Stabilini, A. & Tresoldi, E. in mTOR: Methods and Protocols. (ed. T. Weichhart) 279-293 (Humana Press, Totowa, NJ; 2012).

231. He, S.R. et al. Rapamycin/GABA combination treatment ameliorates diabetes in NOD mice. *Molecular Immunology* **73**, 130-137 (2016).
232. Manirarora, J.N. & Wei, C.H. Combination Therapy Using IL-2/IL-2 Monoclonal Antibody Complexes, Rapamycin, and Islet Autoantigen Peptides Increases Regulatory T Cell Frequency and Protects against Spontaneous and Induced Type 1 Diabetes in Nonobese Diabetic Mice. *Journal of Immunology* **195**, 5203-5214 (2015).
233. Northrup, L., Sullivan, B.P., Hartwell, B.L., Garza, A. & Berkland, C. Screening Immunomodulators To Skew the Antigen-Specific Autoimmune Response. *Molecular Pharmaceutics* **14**, 66-80 (2017).
234. Andorko, J.I., Hess, K.L., Pineault, K.G. & Jewell, C.M. Intrinsic immunogenicity of rapidly-degradable polymers evolves during degradation. *Acta Biomaterialia* **32**, 24-34 (2016).
235. Park, J. & Babensee, J.E. Differential functional effects of biomaterials on dendritic cell maturation. *Acta Biomaterialia* **8**, 3606-3617 (2012).
236. Park, J., Gerber, M.H. & Babensee, J.E. Phenotype and polarization of autologous T cells by biomaterial-treated dendritic cells. *Journal of Biomedical Materials Research Part A* **103**, 170-184 (2015).
237. Andorko, J.I., Pineault, K.G. & Jewell, C.M. Impact of Molecular Weight on the Intrinsic Immunogenic Activity of Poly(Beta Amino Esters). *Journal of Biomedical Materials Research Part A*, n/a-n/a (2016).
238. OptumRx 1-8 (2014).
239. Keselowsky, B.G., Xia, C.Q. & Clare-Salzler, M. Multifunctional dendritic cell-targeting polymeric microparticles Engineering new vaccines for type 1 diabetes. *Human Vaccines* **7**, 37-44 (2011).
240. Mohammad, M.G. et al. Immune cell trafficking from the brain maintains CNS immune tolerance. *Journal of Clinical Investigation* **124**, 1228-1241 (2014).
241. van Zwam, M. et al. Brain antigens in functionally distinct antigen-presenting cell populations in cervical lymph nodes in MS and EAE. *Journal of Molecular Medicine-Jmm* **87**, 273-286 (2009).
242. Vanderlugt, C.L. et al. Pathologic role and temporal appearance of newly emerging autoepitopes in relapsing experimental autoimmune encephalomyelitis. *Journal of Immunology* **164**, 670-678 (2000).
243. Cavone, L., Peruzzi, B., Caporale, R. & Chiarugi, A. Long-term suppression of EAE relapses by pharmacological impairment of epitope spreading. *British Journal of Pharmacology* **171**, 1501-1509 (2014).
244. Zubizarreta, I. et al. Immune tolerance in multiple sclerosis and neuromyelitis optica with peptide-loaded tolerogenic dendritic cells in a phase 1b trial. *Proceedings of the National Academy of Sciences of the United States of America* **116**, 8463-8470 (2019).
245. Willekens, B. et al. Tolerogenic dendritic cell-based treatment for multiple sclerosis (MS): a harmonised study protocol for two phase I clinical trials comparing intradermal and intranodal cell administration. *Bmj Open* **9**, 11 (2019).

246. Florez-Grau, G., Zubizarreta, I., Cabezon, R., Villoslada, P. & Benitez-Ribas, D. Tolerogenic Dendritic Cells as a Promising Antigen-Specific Therapy in the Treatment of Multiple Sclerosis and Neuromyelitis Optica From Preclinical to Clinical Trials. *Frontiers in Immunology* **9**, 10 (2018).
247. Zorina, Y., Stricker, J., Caggiano, A.O. & Button, D.C. Human IgM antibody rHIgM22 promotes phagocytic clearance of myelin debris by microglia. *Scientific Reports* **8**, 14 (2018).
248. Kremer, D., Gottle, P., Flores-Rivera, J., Hartung, H.P. & Kury, P. Remyelination in multiple sclerosis: from concept to clinical trials. *Current Opinion in Neurology* **32**, 378-384 (2019).
249. Ulery, B.D., Nair, L.S. & Laurencin, C.T. Biomedical Applications of Biodegradable Polymers. *Journal of Polymer Science Part B-Polymer Physics* **49**, 832-864 (2011).
250. Nair, L.S. & Laurencin, C.T. Biodegradable polymers as biomaterials. *Progress in Polymer Science* **32**, 762-798 (2007).
251. Fenton, O.S., Olafson, K.N., Pillai, P.S., Mitchell, M.J. & Langer, R. Advances in Biomaterials for Drug Delivery. *Advanced Materials* **30**, 29 (2018).
252. Bookstaver, M.L., Tsai, S.J., Bromberg, J.S. & Jewell, C.M. Improving Vaccine and Immunotherapy Design Using Biomaterials. *Trends Immunol* **39**, 135-150 (2018).
253. Ben-Akiva, E., Witte, S.E., Meyer, R.A., Rhodes, K.R. & Green, J.J. Polymeric micro- and nanoparticles for immune modulation. *Biomaterials Science* **7**, 14-30 (2019).
254. Dellacherie, M.O., Seo, B.R. & Mooney, D.J. Macroscale biomaterials strategies for local immunomodulation. *Nature Reviews Materials* **4**, 379-397 (2019).
255. Gosselin, E.A., Eppler, H.B., Bromberg, J.S. & Jewell, C.M. Designing natural and synthetic immune tissues. *Nature Materials* **17**, 484-498 (2018).
256. Holzer, M. et al. Physico-chemical characterisation of PLGA nanoparticles after freeze-drying and storage. *Eur J Pharm Biopharm* **72**, 428-437 (2009).
257. Chishti, N., Jagwani, S., Dhamecha, D., Jalalpure, S. & Dehghan, M.H. Preparation, Optimization, and In Vivo Evaluation of Nanoparticle-Based Formulation for Pulmonary Delivery of Anticancer Drug. *Medicina (Kaunas)* **55** (2019).
258. Shaikh, M.V., Kala, M. & Nivsarkar, M. Formulation and optimization of doxorubicin loaded polymeric nanoparticles using Box-Behnken design: ex-vivo stability and in-vitro activity. *Eur J Pharm Sci* **100**, 262-272 (2017).
259. Niu, L. & Panyam, J. Freeze concentration-induced PLGA and polystyrene nanoparticle aggregation: Imaging and rational design of lyoprotection. *J Control Release* **248**, 125-132 (2017).
260. Fonte, P. et al. Stability study perspective of the effect of freeze-drying using cryoprotectants on the structure of insulin loaded into PLGA nanoparticles. *Biomacromolecules* **15**, 3753-3765 (2014).

261. Fonte, P. et al. Co-encapsulation of lyoprotectants improves the stability of protein-loaded PLGA nanoparticles upon lyophilization. *Int J Pharm* **496**, 850-862 (2015).
262. Fonte, P. et al. Effect of the Freezing Step in the Stability and Bioactivity of Protein-Loaded PLGA Nanoparticles Upon Lyophilization. *Pharm Res* **33**, 2777-2793 (2016).
263. Lee, M.K., Kim, M.Y., Kim, S. & Lee, J. Cryoprotectants for Freeze Drying of Drug Nano-Suspensions: Effect of Freezing Rate. *Journal of Pharmaceutical Sciences* **98**, 4808-4817 (2009).
264. Izutsu, K., Yonemochi, E., Yomota, C., Goda, Y. & Okuda, H. Studying the morphology of lyophilized protein solids using X-ray micro-CT: effect of post-freeze annealing and controlled nucleation. *AAPS PharmSciTech* **15**, 1181-1188 (2014).
265. Hassett, K.J. et al. Stabilization of a recombinant ricin toxin A subunit vaccine through lyophilization. *Eur J Pharm Biopharm* **85**, 279-286 (2013).
266. Vlugt-Wensink, K.D. et al. Effect of excipients on the encapsulation efficiency and release of human growth hormone from dextran microspheres. *Eur J Pharm Biopharm* **67**, 589-596 (2007).
267. Jewell, C.M., López, S.C. & Irvine, D.J. In situ engineering of the lymph node microenvironment via intranodal injection of adjuvant-releasing polymer particles. *Proc Natl Acad Sci U S A* **108**, 15745-15750 (2011).
268. Singh, M., Chakrapani, A. & O'Hagon, D. Nanoparticles and microparticles as vaccine-delivery systems. *Expert Review of Vaccines* **6**, 797-808 (2007).
269. Kheddo, P. et al. The effects of arginine glutamate, a promising excipient for protein formulation, on cell viability: Comparisons with NaCl. *Toxicol In Vitro* **33**, 88-98 (2016).
270. Blobel, J. et al. Protein loop compaction and the origin of the effect of arginine and glutamic acid mixtures on solubility, stability and transient oligomerization of proteins. *Eur Biophys J* **40**, 1327-1338 (2011).
271. Sicotte, N.L. Neuroimaging in Multiple Sclerosis: Neurotherapeutic Implications. *Neurotherapeutics* **8**, 54-62 (2011).
272. Farrell, J.A.D. et al. High b-value q-space diffusion-weighted MRI of the human cervical spinal cord in vivo: Feasibility and application to multiple sclerosis. *Magnetic Resonance in Medicine* **59**, 1079-1089 (2008).
273. Tambalo, S. et al. Functional Magnetic Resonance Imaging of Rats with Experimental Autoimmune Encephalomyelitis Reveals Brain Cortex Remodeling. *Journal of Neuroscience* **35**, 10088-10100 (2015).
274. Zhang, J.Y., Jones, M.V., McMahon, M.T., Mori, S. & Calabresi, P.A. In vivo and ex vivo diffusion tensor imaging of cuprizone-induced demyelination in the mouse corpus callosum. *Magnetic Resonance in Medicine* **67**, 750-759 (2012).